The Role of Leucine-Rich Repeat Proteins Amigo1 and Slitrk1 in the Formation and Maintenance of Nervous System Circuits

Reesha Raja

Integrated Program in Neuroscience
Montreal Neurological Institute
McGill University
Montreal, Quebec, Canada

August 2020

A thesis dissertation submitted to the Department of Graduate and Postdoctoral Studies of McGill University in partial fulfillment of the requirements of the degree of Doctor of Philosophy in Neurological Sciences

Table of Contents

Abstract 6

Résumé 7

List of Figures 9

List of Abbreviations 10

Acknowledgements 12

Author Contributions 13

Chapter 1: General Introduction 14

I. Preface 14

II. Introduction Part 1 – Slitrk family members and their roles in synaptogenesis 15

1. Steps to synapse formation and the role of LRR-containing proteins 16

2. The Slitrks 18

3. Objectives for Manuscript 1 (Chapter 2) 24

III. Introduction part 2 26

1. Amigo1 26

2. Axon guidance and target selection in the mouse olfactory system 29

3. Rationale and objectives for Manuscript 2 (Chapter 3) 35

4. Mossy fiber projections of the Hippocampal Circuit 35

5. Objectives for Manuscript 3 (Chapter 4) 48

Chapter 2: Slitrk1 is localized to excitatory synapses and promotes their development 49

I. Preface 49

II. Acknowledgements 50

III. Abstract 50

IV. Introduction 51

V. Results 53

1. Slitrk1 is preferentially localized at excitatory synapses. 53
2. Overexpression of Slitrk1 and Slitrk2 in neurons increases synapse density. 56
3. Knockdown of Slitrk1 reduces synapse number in hippocampal neuron cultures. 59
4. The second leucine-rich repeat of Slitrk1 is necessary for its homophilic interaction at the cell surface. 62
VI. Discussion 67
VII. Materials and Methods 69
1. cDNA constructs 69
2. Antibodies 70
3. Cell culture 70
4. Slitrk1 knockdown 71
5. Transfection and immunocytochemistry 71
6. Image acquisition and quantification 72
7. Production of PTPδ-Fc protein 72
8. Cell surface binding assay 72
9. Crosslinking 73
10. Synaptosomal fractionation 73
11. Cell surface biotinylation 73
12. Immunoprecipitation and Western Blotting 74
Chapter 3: Amigo1 is expressed specifically in ventrolateral olfactory epithelium but is dispensable for olfactory receptor neuron targeting in the mouse olfactory system 75
I. Preface 75
II. Acknowledgements 75
III. Abstract 76
IV. Introduction 77
V. Results 79

1. Amigo1 is enriched in ventrolateral ORNs. 79
2. Insertion of a neomycin selection cassette in the *Amigo1* locus disrupts development of ventrolateral ORNs. 83
3. Defects to ventral glomeruli formation are caused by decreases in the numbers of ventrolateral ORN populations 94
4. Gene transcription is altered in the OE of *Amigo1*$^{neo/neo}$ mice. 100
VI. Discussion 107
1. Mechanisms underlying the loss of OR identity in ventrolateral ORNs in *Amigo1*$^{neo/neo}$ mice 107
2. Potential factors influencing region-specific effects on OR expression and ORN development. 109
VII. Materials and Methods 112
1. Animals 112
2. *In situ* hybridization and RT-PCR 113
3. Western Blot 115
4. Immunohistochemistry 115
5. Imaging and Image Analysis 116
6. RNASeq 117
Chapter 4: Amigo1 is required in the development and maintenance of hippocampal mossy fiber projections to CA3 118
I. Preface 118
II. Acknowledgements 118
III. Abstract 119
IV. Introduction 119
V. Results 121
1. Amigo1 is differentially expressed in populations of cells of various brain regions. 121

2. Loss of Amigo1 expression leads to altered development of the infrapyramidal mossy fiber bundle 125

3. Loss of Amigo1 expression leads to perturbed mossy fiber fasciculation and altered presynaptic terminal formation 128

VI. Discussion 134

VII. Materials and Methods 138

1. Animals 138

2. *In situ* hybridization 138

3. Immunohistochemistry 139

4. 5-Bromo-4-Chloro-3-Indolyl β-D-Galactopyranoside (X-Gal) Staining 140

5. Timm staining 140

6. Imaging and Image Analysis 141

Chapter 5: General Discussion 143

I. Summary 143

II. Slitrks in Synaptogenesis 144

1. A place for Slitrk1 in the network of synaptic adhesion molecules 144

III. Amigo1 in axonal fasciculation 148

1. Amigo1 as a cell adhesion molecule 149

2. Amigo1 as a regulator of neuronal activity 150

IV. Conclusion 153

References 154

Abstract

The functional assembly of the nervous system requires the organization of billions of neurons growing axons to connect to one another in remarkably precise patterns. These connections are formed by the orchestration of many developmental processes, from neurogenesis, to neurite outgrowth, axon guidance, target selection and synaptogenesis. Each of these individual processes are mediated by thousands of molecules expressed in precise locations and developmental time points, accuracy of which is crucial for proper nervous system functionality. One family of molecules involved in these processes are the leucine-rich repeat (LRR) containing proteins. The LRR domains are known to mediate homophilic or heterophilic protein interactions, providing the proteins with the ability to serve in diverse functions such as cell-cell interaction or adhesion. Importantly, several neurological disorders have been linked by genetic studies to mutations in the genes encoding LRR family members. Herein, we use both *in vitro* and *in vivo* methods to provide evidence for roles of two LRR proteins in multiple developmental processes crucial for proper nervous system development. First, we identify a role for Slitrk1 in excitatory synapse formation and characterize roles for its LRR domains in mediating protein interactions. Second, we show differential requirement for the LRR and Ig domain-containing Amigo1 in mouse nervous system development. While Amigo1 is dispensable for the targeting of olfactory sensory axons to their targets, it is crucial for proper targeting of hippocampal mossy fibers in fasciculated tracts. In addition to identifying a function for Amigo1 in axonal fasciculation, our *in vivo* analyses revealed potential off-target effects associated with the insertion of an antibiotic resistance selection gene in the mouse genome, thereby serving as a cautionary tale for the interpretation of phenotypes in genetically-targeted mouse models. Taken together, our results show that Slirtk1 and Amigo1 both contribute in spatially and temporally specific ways in nervous system development.

Résumé

Le développement du système nerveux nécessite l'organisation précise de milliards de neurones. Ces neurones communiquent via leur axone et leurs dendrites pour ainsi former un réseau bien précis. Cet assemblage complexe nécessite l'orchestration de différents processus développementaux incluant la neurogénèse, la croissance des neurites, la guidance axonale, le choix de la cible et finalement la formation de synapses. Chacun de ces processus est contrôlé par l'expression spatio-temporelle précise de milliers de molécules, et l'exactitude de ce code moléculaire est essentiel au bon fonctionnement du système nerveux. Une des familles de molécules impliquées dans ces processus sont les protéines à motifs LRR (leucine-rich repeat). Ces domaines LRR sont connus pour médier les interactions homophiliques et hétérophiliques entre protéines, ce qui permet à ces protéines d'avoir des fonctions d'intéractions et d'adhésions entre cellules. Il est intéressant de noter que des mutations dans certains gènes codants pour ces protéines-LRR ont été impliquées dans plusieurs maladies neurologiques d'origine génétique. Dans nos études, nous utilisons des méthodes *in vitro* et *in vivo* afin de démontrer la fonction de 2 protéines de cette famille dans des processus essentiels au développement du système nerveux. Premièrement, nous décrivons un rôle pour Slitrk1 dans la formation de synapses excitatrices et nous caractérisons un rôle spécifique pour chacun de ses motifs LRR dans la promotion d'intéractions entre protéines. Ensuite, nous démontrons qu'Amigo1 est important pour le développement du système nerveux chez la souris. Amigo1 semble essentiel pour la fasciculation et la guidance de certains axones provenant de neurones situés dans l'hippocampe, appelés les mossy fibers. Il n'est toutefois pas nécessaire pour guider les axones des neurones olfactifs vers leur cible, le bulbe olfactif. En plus d'identifier un rôle pour Amigo1 dans la fasciculation axonale, nos analyses *in vivo* ont révélées certains problèmes reliés à l'utilisation de modèles génétiques

provenant de la recombinaison homologue et de l'insertion de gènes de résistance aux antibiotiques dans le génome de la souris, servant ainsi de mise en garde pour l'interprétation de phénotypes chez des souris produites à l'aide de cette méthode. En résumé, nos résultats montrent que Slitrk1 et Amigo1 contribuent de façon spécifique au développement du système nerveux.

List of Figures

Chapter 1

Figure 1: Structures of Slitrk and Amigo1 25
Figure 2: Two-step targeting of olfactory sensory axons to the OB 34
Figure 3: Organization of the Hippocampal Circuit 37

Chapter 2

Figure 1: Localization of Slitrk1 at the synapse 55
Figure 2: Overexpression of Slitrk1 and Slitrk2 in cultured neurons increases the amount of presynaptic excitatory and inhibitory contacts. 57
Figure 3: Knockdown of Slitrk1 by shRNA in cultured neurons reduces synapse density 60
Figure 4: Slitrk1 molecules have the ability to interact at the cell surface 64
Figure 5: Determination of the LRR domain required for homophilic binding 65

Chapter 3

Figure 1: Amigo1 is expressed in the ventrolateral region of the olfactory epithelium 81
Figure 2: Knockout of Amigo1 ablates transcription of *amigo1* mRNA and production of Amigo1 protein 84
Figure 3: *Amigo1*$^{neo/neo}$ but not *Amigo1*$^{-/-}$ mutants show defects in the targeting of MOR28-positive axons to the olfactory bulb. 87
Figure 4: Presence of the neomycin cassette in *Amigo1*$^{neo/neo}$ animals disrupts glomerular size exclusively in ventral OB 90
Figure 5: Presence of the neomycin cassette in *Amigo1*$^{neo/neo}$ animals disrupts glomerular formation exclusively in ventral OB 92
Figure 6: The decrease in the size of ventral OB glomeruli is associated with a concomitant decrease in the size of ventrolateral ORN populations in the OE 95
Figure 7: The decrease in number of ORNs of ventrolateral populations is not due to alteration rates of proliferation, maturation, or cell death 98
Table 1: List of differentially expressed genes from RNA sequencing data 102
Table 2: List of olfactory receptor genes from RNA sequencing data with known zone indices 105
Table 3: Continuation of table 2 106

Chapter 4

Figure 1: Amigo1 is expression patterns are recapitulated by X-gal staining 122
Figure 2: Differential expression of Amigo1 is developmentally regulated in various brain structures 124
Figure 3: Loss of Amigo1 disrupts the length of infrapyramidal bundle during development, which is restored by 2 months 127
Figure 4: Loss of Amigo1 disrupts the mossy fiber fasciculation 130
Figure 5: Loss of Amigo1 results in the formation of ectopic mossy fiber boutons in CA3 ..132

List of Abbreviations

ADHD	Attention deficit hyperactivity disorder
AMIGO	Amphoterin-induced gene and ORF
BACE1	Beta-secretase 1
BCIP	5-bromo-4-chloro-3-indolylphosphate
BDNF	Brain-derived neurotrophic factor
CA	cornu ammonis
CAM	cell adhesion molecule
cAMP	cyclic adenosine monophosphate
CCAC	Canadian Council on Animal Care
CIHR	Canadian Institutes for Health Research
CHL1	Close homolog of L1
CNG	Cyclic nucleotide-gated
CNS	central nervous system
DCC	Deleted in colorectal carcinoma
DEPC	diethyl pyrocarbonate
DG	dentate gyrus
DIV	days *in vitro*
DM	dorsomedial
DNA	deoxyribonucleic acid
E	embryonic day
EC	entorhinal cortex
EGFP	Enhanced green fluorescent protein
FAK	Focal adhesion kinase
GABA	Gamma aminobutyric acid
GC	granule cells
GFP	Green fluorescent protein
GPC4	Glypican 4
GPCR	G-protein-coupled receptor
GPI	Glycosylphosphatidylinositol
HC	Hippocampus
HEK	Human embryonic Kidney
HSPG	Heparan sulfate proteoglycan
IPB	infrapyramidal bundle
IRIC	Institute for Research in Immunology and Cancer
KOMP	Knockout Mouse Project
LAMP	Limbic-associated membrane protein
LAR	Leukocyte common antigen-related protein
LMT	large mossy terminals
LMT-C	LMT complexes
LRR	leucine-rich repeat
LRRTMs	Leucine-rich repeat transmembrane neuronal proteins

MF	mossy fiber
MFB	mossy fiber bouton
MFS	mossy fiber sprouting
mIPSC	mini postsynaptic inhibitory current
MNI-ACC	Montreal Neurological Institute Animal Care Committee
NBF	neutral buffered formalin
NBT	nitro-bluetetrazolium chloride
NCAM	Neural cell adhesion molecule
NGL	Netrin-G ligand
Nrp1	Neuropilin-1
Nrp2	Neuropilin-2
OB	olfactory bulb
OCD	Obsessive-compulsive disorder (OCD)
OE	olfactory epithelium
OMP	Olfactory marker protein
OR	olfactory receptor
ORN	olfactory receptor neuron
P	postnatal day
PBS	phosphate-buffered saline
PFA	paraformaldehyde
PHH3	Phospho-histone H3
PSA-NCAM	Polysialic acid-neural cell adhesion molecule
PSD-95	Postsynaptic density protein 95
RGM	Repulsive guidance molecule A
RNA	ribonucleic acid
Robo-2	Roundabout-2
ROS	reactive oxidative species
RPTPs	Type IIa receptor-type protein tyrosine phosphatases
RT-PCR	reverse transcription polymerase chain reaction
SALMs	Synaptic adhesion-like molecule
shRNAs	short hairpin RNA
SPB	suprapyramidal bundle
SSC	saline sodium citrate
SynCAM	Synaptic cell adhesion molecule
TA	terminal arborization
TBST	tris buffered saline with tween
TE	thorny excrescence
TS	Gilles de la Tourette’s syndrome
VGAT	Vesicular GABA transporter
VGLUT	Vesicular glutamate transporter
VL	ventrolateral
X-gal	5-Bromo-4-Chloro-3-Indolyl β-D-Galactopyranoside
β-gal	β-galactosidase

Acknowledgements

Starting graduate school as a master's student and then transferring to the Ph.D. program were both daunting ideas for me. I would not have taken these steps were it not for my Professor, Dr. Jean-Francois Cloutier who believed in me from the beginning. JF, through my 10 years of being a part of the Cloutier lab, you have offered input, advice, and encouragement every step of the way. You have provided me with generous opportunities to grow as a scientist (and as a rock climber). I could not have asked for a better mentor! Thank you, JF.

I am indebted to my senior lab mates for everything that they have done for me. Emilie, a heartfelt thank you for being my strongest support through it all, from helping troubleshoot experiments, to always being positive and patient with me - I could not have done it without you, and I will miss you dearly! To Janet, having you first as a senior lab mate and role model and now as a friend, I have always been able to count on you for advice and support, and entertaining stories to keep me going. To Francois, thank you for teaching me so much science, for trusting me with the Slitrk project after you graduated, and for motivating me to "be a better version of me". To Jin, thank you for the knowledge you've passed on and for being a model of an amazing scientist!

Looking back at the friends I've made along the way, I want to especially mention Joseph Kam, Alex Brignall and our 'post-5p.m.-discussions'; Allen Scholl for weekly (*daily) coffees; Chris for the endless puns; Neelima for making sure I stay hydrated; Sab for appreciating my fashion sense; and Sydney for being such a cool 'mini' prep. To all former and current lab members for your endless support and motivation. My sincerest thank you. From designing Halloween costumes in lab, to heart-to-heart conversations and fun banter, I will cherish the many memorable moments.

From neighbouring labs, those who have made a lasting impression: Zahraa Chorghay, Sejal Davla, Karen Fung, Stephanie Harris, Camille Juzwik, Lawrie Shahbazian, Shannon Swikert. All the research technicians from the MP and BTRC labs who have shared their expertise along the way – you have been awesome.

My gratitude extends to my respected committee members, Dr. Tim Kennedy and Dr. Don Van Meyel who supported the ups and downs of my thesis projects, and to those who have imparted their knowledge and guidance, namely Mitra Cowan, Dr. Stefani Stifani, Dr. Keith Murai, Dr. Ed Ruthazer and Dr. Josephine Nalbantoglu.

To my roots: Mom and Dad, who lovingly keep me grounded, encourage me to shine and who find their happiness in me finding mine. To my brother Sheil, who has always been a source of inspiration and support not only through this endeavor, but through life. My late grandfather and my living grandparents, who have set the stage for strength and success. My cousins who are my forever-cheerleading squad, thank you for all the phone calls and reassurance! For the valuable friendships outside of lab, both old and new, that have supported me in this journey, I am forever grateful.

And finally (I have been waiting a decade to say this): *Adios, "Amigos"!*

Author Contributions

Chapter 1: General Introduction

Reesha Raja wrote all the material and prepared all figures

Chapter 2: Slitrk1 is localized to excitatory synapses and promotes their development

This chapter was published in Scientific Reports in 2016.

R.R., F.B., and J.-F.C. conceived the experiments.
R.R. and F.B. performed the experiments and analyzed the results.
T.E.K. and A.E.F provided reagents and technical insight.
R.R., F.B., and J.-F.C. wrote the manuscript and all authors provided comments.

Chapter 3: Amigo1 is expressed specifically in ventrolateral olfactory epithelium but is dispensable for olfactory receptor neuron targeting in the mouse olfactory system

R.R., E.D. and J.-F.C. conceived the experiments.
R.R. performed the experiments and analyzed the results.
E.D. maintained mouse colonies and bred mouse strains.
R.R. wrote the manuscript and J.-F.C. edited the manuscript. All authors provided comments.

Chapter 4: Amigo1 is required in the development and maintenance of hippocampal mossy fiber projections to CA3

R.R., T.E.K. and J.-F.C. conceived the experiments.
R.R. performed the experiments and analyzed the results.
E.D. maintained mouse colonies and bred mouse strains.
R.R. wrote the manuscript and J.-F.C. edited the manuscript. All authors provided comments.

Chapter 5: General Discussion

Reesha Raja wrote all the material

Chapter 1:

General Introduction

I. Preface

To create a functioning nervous system is a process that is at once complex yet ordered, random yet programmed. During development, a neural tube is formed from which neurons are generated based on stochastic levels of Notch signalling between cells. However, following this somewhat random process is a series of precise events: from neurogenesis, to neurite outgrowth, axon guidance, target selection and synaptogenesis. All these events come together in a highly complex and regulated manner to create one of the most intricate biological systems known: the nervous system. Both brain and periphery connect with one another by way of neurons that extend axons throughout the body and communicate via chemical signals. Each step of nervous system development requires the coordination of countless proteins working together with precise spatial and temporal accuracy. Failure to accurately perform these steps can compromise proper circuit formation and lead to neurodevelopmental disorders such as autism or epilepsy. Furthermore, failure of proteins to maintain correct circuitry can also lead to debilitating neurodegenerative disorders like Alzheimer's or Parkinson's. Many such disorders have been now shown to be linked to genetic mutations in genes that encode proteins involved in the processes of neural circuit formation like axon guidance and synapse formation or maintenance. It is therefore crucial to understand the normal function of these proteins in the healthy brain in order to discover potential therapeutic targets to treat neurological disorders.

One family of proteins implicated in neurodevelopmental processes are the leucine-rich repeat-containing transmembrane cell adhesion molecules (CAMs). The leucine-rich repeat (LRR) is a

protein-protein interaction motif, and CAMs containing this domain are involved in most aspects of nervous system development. Notably, LRR-containing CAMs have been implicated in multiple neurological diseases, highlighting the importance of studying proteins of this family as potential therapeutic targets for disease treatment (Winther and Walmod, 2014). My thesis will explore the function of two cell-surface LRR-containing proteins, Slitrk1 and Amigo1, in regulating various processes that occur during the development and maintenance of neural circuits. This introductory chapter is designed to provide the necessary background on these molecules as well as the model systems and processes used to study their function. The first section of the introduction will provide an overview of synaptogenesis and of the Slitrk family of LRR domain-containing proteins. The second section of the introduction will outline what is currently known about Amigo1 and will describe the two *in vivo* systems that I have used to study the function of Amigo1 in the mouse brain.

II. Introduction Part 1 – Slitrk family members and their roles in synaptogenesis

Brain function is completely reliant on communication between neurons in circuits, and there is strong evidence that defects in the formation, maintenance or plasticity of synapses are associated with behavioural phenotypes reminiscent of neuropsychiatric disorders (Aruga and Mikoshiba, 2003; Banerjee et al., 2014). This association is exemplified by the trans-synaptic Neurexin complex. *In vitro* studies of human neurons carrying *NEUREXIN* gene mutations linked to clinical presentations shed light on the function of Neurexin in synaptic transmission, and mouse *Neurexin1α* knockout studies provide further evidence for the association of these mutations with behavioural phenotypes reminiscent of those in psychiatric disorders (Etherton et al., 2009; Grayton et al., 2013; Dachtler et al., 2015; Esclassan et al., 2015; Pak et al., 2015; Südhof, 2017).

Similarly, mutations in several genes associated with Neurexin signalling, such as the Neuroligins, the Shanks and CASK, have also been implicated in conditions like intellectual disabilities and autism spectrum disorders (Südhof, 2017). Moreover, proteins of the leucine-rich repeat (LRR) superfamily are also linked to such disorders and to synapse development (Matsushima et al., 2005; Ko, 2012).

Accordingly, the Slitrk family of LRR domain-containing transmembrane proteins are involved in playing roles at the synapse, having differential effects on excitatory and inhibitory synapse formation and associated links to neuropsychiatric disorders. However, the detailed mechanisms of Slitrk function at the synapse are still being clarified, including the structure-function relationship and their localization to excitatory and inhibitory synapses.

1. Steps to synapse formation and the role of LRR-containing proteins

The formation of synapses in the central nervous system (CNS) requires a series of precise and coordinated events. Firstly, after cell fate determination and axon outgrowth, a neuron must identify its target cell, establish adhesive contact with that cell, initiate a program for differentiation of the pre and postsynaptic sides, and finally undergo synapse maturation. These processes require timely expression of molecules on both growing axons and developing dendrites and the correct signalling of intracellular pathways to initiate synapse differentiation (Batool et al., 2019). While various mechanisms of the timing of these events have been proposed, much evidence supports the idea that initial clustering of synaptic machinery is intrinsic to the growing axon and nascent synaptic terminal, while synapse specificity and promotion of mature functional synapses through recruitment of additional presynaptic molecules occurs with stabilization of the pre and postsynaptic sites by synaptic adhesion molecules (Kurshan and Shen, 2019)

Synaptic adhesion molecules play a major role in synapse formation, both in anchoring the contact between axon and dendrite and in promoting differentiation of the pre and postsynaptic sides into a functional synapse (Yamagata and Fukai, 2019). Specifically, synaptic adhesion molecules, such as members of the CAM superfamily or the LRR superfamily, interact in *trans* in synaptic adhesion complexes to allow stabilization of the presumptive synapse structure and allow for downstream signalling to mediate synapse differentiation (Kurshan and Shen, 2019; Yamagata and Fukai, 2019). The combinatorial expression of individual synaptic adhesion proteins hence confers synapse type specificity (Roppongi et al., 2020).

On the presynaptic side, Neurexins and type IIa receptor-type protein tyrosine phosphatases (RPTPs) mediate synapse formation by extracellular binding in *trans* to post synaptic adhesion molecules and by intracellular signalling via liprins and CASK to recruit presynaptic machinery (Han et al., 2016, 2018; Roppongi et al., 2020). Neurexins bind the scaffold protein CASK and link to synaptic vesicles through synaptotagmin binding (Hata et al., 1993; Biederer and Südhof, 2000; Graf et al., 2004). The members of the RPTP family, PTPδ, PTPσ, and leukocyte common antigen-related protein (LAR), interact with presynaptic liprin-α, a crucial organizer of the synaptic vesicle pool which also binds CASK (Spangler et al., 2013; Han et al., 2016). It is now thought that Neurexins and RPTPs can form complexes and act as hubs to mediate the differentiation of the presynaptic side (Südhof, 2017; Roppongi et al., 2020).

Postsynaptic adhesion molecules are more numerous and bind with different affinities to the multitudes of alternative splice forms of each of the Neurexin and RPTP family members (Südhof, 2017). These postsynaptic organizers are primarily of the LRR and CAM superfamilies such as the Neuroligins, Netrin-G ligand (NGL), Synaptic Adhesion-Like Molecules (SALMs), Leucine-Rich Repeat Transmembrane Neuronal proteins (LRRTMs) and Slitrks (Südhof, 2017). The

diversity of synaptic adhesion complexes can confer immense specificity in mediating levels of excitatory and inhibitory synapse formation. For example, the Neuroligins 1, 3 and 4 localize to glutamatergic synapses and bind presynaptic β-Neurexin to form excitatory synapses while Neuroligin 2 can localize to GABAergic synapses and mediate inhibitory synapse formation (Graf et al., 2004).

In addition to the prominent Neuroligin family of CAMs, LRR-domain containing proteins make for useful protein-protein interaction domains due to the curvature formed by the LRR motif tandem repeats (Ko, 2012), and can serve to provide structural stability at a developing synapse (Won et al., 2019). Over the years, LRR genes have been associated with neurodevelopmental and neuropsychiatric disorders, and their encoded proteins have become known as important players in neurodevelopmental processes, including synapse formation (Matsushima et al., 2005).

2. The Slitrks

Slitrk family members, structure

The Slitrks comprise a family of six LRR domain-containing transmembrane proteins. All Slitrk members contain two LRR motifs in their extracellular region, with high homology to the Slit family proteins which are secreted LRR-containing molecules involved in axon guidance (Brose and Tessier-Lavigne, 2000; Aruga and Mikoshiba, 2003). Each LRR module contains six LRR motif repeats capped by cysteine-rich domains (Aruga et al., 2003; Won et al., 2019). This structure suggests they are involved in protein-protein interactions. Indeed, it has been shown that Slitrks' most N-terminal LRR domain (LRR1) domain binds to the RPTP family in *trans* (Takahashi et al., 2012; Yim et al., 2013; Um et al., 2014). While less is known about the LRR2 domain, we and others have evidence to show that this second LRR domain of Slitrk1 mediates homophilic interactions in *cis* to allow for Slitrk dimerization at the surface (Figure 1A)(Um et al., 2014;

Beaubien et al., 2016). On their intracellular side, the Slitrks contain several conserved tyrosine residues that are putative tyrosine phosphorylation sites similar to those in the Trk neurotrophin receptor proteins, although they do not have a kinase activity. Nonetheless, it is possible that Slitrks could be involved in intracellular signalling modulated through the phosphorylation of their intracellular domain (Aruga and Mikoshiba, 2003). Interestingly, Slitrk1 has the shortest cytoplasmic tail of the family and does not contain the conserved tyrosine residues found in other Slitrk family members. This difference may contribute to the differential function of Slitrk1 in promoting neurite outgrowth *in vitro* in comparison to the other Slitrks which act to inhibit neurite outgrowth (Aruga and Mikoshiba, 2003).

Slitrks in neuropsychiatric disorders

Human genetic studies have revealed sequence variations in several Slitrks for specific neuropsychiatric disorders such as Gilles de la Tourette's syndrome (TS) and obsessive-compulsive disorder (OCD) (Katayama et al., 2010; Mah et al., 2010; Shmelkov et al., 2010; Proenca et al., 2011; Ozomaro et al., 2013; Zhang et al., 2015; Melo-Felippe et al., 2019; Liu et al., 2020). Gilles de la Tourette's syndrome is characterized by motor and vocal tics and tends to show comorbidity with OCD and attention deficit hyperactivity disorder (ADHD). Several human patient genetic studies of this complex disorder have found conflicting evidence linking mutations in *SLITRK1* to TS (Abelson et al., 2005; Deng et al., 2006; Geddes, 2006; Züchner et al., 2006; Speed et al., 2008; O'Roak et al., 2010; Proenca et al., 2011). For example, *de novo* mutations causing frameshifts or variations in the 3' untranslated region of *SLITRK1* were found in some patients, so *SLITRK1* was proposed as a candidate gene in TS etiology (Abelson et al., 2005). While not all further human patient studies of different populations were able to associate mutations in *SLITRK1* with TS (Pasquini et al., 2008; Zimprich et al., 2008; Miranda et al., 2009),

it should be noted that the rarity of this variation could make it more difficult to detect an association even with sample sizes up to one thousand (O'Rourke et al., 2009; Karagiannidis et al., 2012). Interestingly, Slitrk1 expression in corticostriatal and thalamocortical circuits is aligned with the etiology of TS being linked to these pathways (Stillman et al., 2009). Hence, further study of this gene is required for a more definitive linkage of Slitrk1 to TS (Miranda et al., 2009).

In support of the human patient data of rare variants of the *Slitrk* gene to neuropsychiatric disorders, some groups have studied the role of Slitrks *in vivo* using rodent models. *Slitrk1* null mice show a variety of neuropsychiatric-like phenotypes such as increased anxiety in an elevated plus maze and increased depression in a forced swim task, thus demonstrating a role for this protein in neuropsychiatric conditions (Katayama et al., 2010; Proenca et al., 2011).

Slitrk1 is not the only Slitrk member to show genetic variations in human neuropsychiatric patients and behavioural phenotypes in mutant mouse models. *Slitrk5* null mice also show increased anxiety and repetitive behaviours like excessive grooming. Excessive grooming was accompanied by overactivity in the orbitofrontal cortex, which has also been observed in human OCD patients (Mah et al., 2010; Shmelkov et al., 2010; Song et al., 2017). Alterations in striatal volume and decreased spine density were also found in *Slitrk5* null mice. All together, many features of OCD are represented in *Slitrk5* mice (Mah et al., 2010; Shmelkov et al., 2010). Slitrk2 was identified as a candidate gene mutated in human patients with schizophrenia, and knockdown of the *Slitrk2* gene in mice causes hyperactivity (Salesse et al., 2020). *Slitrk3* null mice have increased seizure susceptibility and decreased inhibitory marker staining in the hippocampus, correlating with reduced inhibitory transmission (Takahashi et al., 2012). In summary, the Slitrks represent a family of candidate genes involved in the etiology of neurological disorders with supporting evidence in rodent knockout models.

Expression of Slitrks in nervous system

Slitrk1, *Slitrk2* and *Slitrk4* are expressed during embryogenesis beginning around embryonic day (E) 11.5-E12.5, and by adulthood their expression is restricted to the CNS (Aruga et al., 2003). By E18, the Slitrks are expressed widely but in distinct patterns around the mouse brain, except for *Slitrk6*, which has an expression pattern restricted primarily to the thalamus. Importantly, *Slitrk1* is expressed highly and broadly throughout the brain, in both embryonic development and postnatally at day 10, with prominent expression in cortex, throughout hippocampus and in the anterior lobes of the cerebellum amongst other regions by postnatal day (P) 10 (Beaubien and Cloutier, 2009). The regional differences in expression patterns between the Slitrks could suggest they play different roles in CNS development at different developmental time points.

Overview of Slitrk function

The Slitrk family was discovered in a screen for genes misregulated in neural tube closure defects in mice. In the same study, Slitrk1 was found to induce neurite outgrowth in PC12 cells *in vitro* while Slitrk2 and 3 acted to suppress neurite outgrowth (Aruga and Mikoshiba, 2003). Since then, many publications have helped elucidate the function of Slitrks in the developing brain. Neurite outgrowth promotion by Slitrk1 was found to be mediated by interaction of the Slitrk1 intracellular region with 14-3-3 proteins, a regulator of multiple cellular processes (Kajiwara et al., 2009). Most prominently, the Slitrk family members have gained increased recognition as synaptic adhesion complexes that can work differentially to induce excitatory and inhibitory synapse formation. Over the years, both *in vitro and in vivo* evidence using genetic knockdown or overexpression models as well as human patient mutation studies have implicated Slitrks in synaptic development and in the etiology of neuropsychiatric disorders (Proenca et al., 2011; Ko, 2012; Won et al., 2019). As it is well established that changes to neural connections, or synapses, can underlie many

neuropsychiatric disorders (Jamain et al., 2003; Durand et al., 2007; Toro et al., 2010; Guilmatre et al., 2014), understanding the molecular role of Slitrks at the synaptic level will provide valuable perspective into mechanisms contributing to neuropsychiatric disorders.

Slitrk function at the synapse

The molecular evidence combined with human genetic studies of Slitrk mutations support a function for Slitrks in synapse formation in normal brain function and in the prevention of neuropsychiatric disorders. Over the last decade, we (Chapter 2) and others have demonstrated roles for several of the Slirtk family members at the developing synapse.

Slitrks are expressed postsynaptically and can induce presynaptic differentiation. Heterologous synapse formation assays in which COS cells are co-cultured with hippocampal neurons showed that all Slitrks can induce presynaptic clustering of inhibitory presynaptic machinery such as vesicular GABA transporter (VGAT), but only Slitrks 1, 2, 4, 5, and 6 could induce excitatory presynaptic differentiation (Takahashi et al., 2012). Thus, Slitrk3 was found to be an inducer of specifically inhibitory synapses. *Slitrk3* null mice showed a decrease in the presynaptic marker GAD65 in the hippocampus, which was accompanied by a decrease in mini inhibitory postsynaptic current (mIPSC) frequency (Takahashi et al., 2012). In contrast to the heterologous synapse formation system, overexpression of the Slitrk members 1 to 5 in hippocampal cultures showed more specificity in the induction of excitatory and inhibitory synapses between Slitrk family members. While overexpression of Slitrks 1, 2, 4 and 5 led exclusively to an increase in the number of excitatory synapses, Siltrk3 overexpression explicitly promoted inhibitory synapse formation (Yim et al., 2013). This discrepancy between these two studies could possibly be explained by different levels of overexpression of the Slitrk proteins in COS cells versus neurons. Furthermore, COS cell expression of Slitrks could test their synaptic induction capability while overexpression

in hippocampal neurons would more accurately mimic their specific endogenous localization and roles at excitatory or inhibitory synapses.

A screen for candidate trans-synaptic binding partners of Slitrks identified the RPTP family of type-IIa receptor protein tyrosine phosphatases as candidates (Takahashi et al., 2012; Yim et al., 2013). Their structure consists of three Ig-like domains and eight fibronectin type III-like domains extracellularly, followed by a transmembrane domain and two intracellular PTP domains (Pulido et al., 1995). Interestingly, single amino acid mutations of Slitrk1 linked to human patients with schizophrenia or Tourette's syndrome were studied in co-culture assays and shown to disrupt its interaction with PTP and its synapse-inducing function (Kang et al., 2016). Differential trans-synaptic binding of Slitrk family members to the RPTPs appears to determine the nature of the synapse, whether excitatory or inhibitory, that is formed. The RPTP family is comprised of 3 members: leukocyte common antigen relater (LAR), PTPδ and PTPσ. The three members have known functions in synapse formation at both excitatory and inhibitory synapses via trans-synaptic interactions with various synaptogenic molecules such as the SALMs, NGL, ILRAPL1, TrkC and IL1RacP (Um and Ko, 2013; Han et al., 2016). With numerous interacting proteins and various splice forms mediating differential downstream signalling processes, including interaction with liprin-α (Pulido et al., 1995; Han et al., 2016), the RPTP family can contribute greatly to synapse specificity. Cell aggregation assays demonstrated that the Slitrks can bind both PTPδ and PTPσ, but PTPδ and PTPσ knockdown experiments identified a requirement for PTPσ in Slitrk-mediated excitatory synapse formation and for PTPδ in Slitrk3-induced inhibitory synapse formation (Yim et al., 2013). In addition to cell aggregation and co-culture studies, the crystal structure of the Slitrk-PTP interaction has been elucidated (Um et al., 2014; Yamagata et al., 2015). These studies determined the precise binding sites between the pre and postsynaptic counterparts of this adhesion

complex and identify the PTPδ and PTPσ splice variants that interact with Slitrks. Specifically, the Slitrk LRR1 domain interacts with the Ig1-2 domain of PTPδ and σ, but only with those PTP splice forms containing a critical arginine residue within mini exon B (meB). This meB is a lengthened linker between Ig2 and Ig3 such that the Ig3 domain does not interfere with Slitrk LRR1 binding to PTP Ig1-2 (Um et al., 2014; Yamagata et al., 2015). These results provide further indication that alternative splice forms of the PTP family confer binding specificity to postsynaptic partners and allow for accurate excitatory and inhibitory synapse development.

3. Objectives for Manuscript 1 (Chapter 2)

Our studies aimed to address some of the unresolved questions of the role of Slitrk1 in synapse formation. Firstly, we generated a Slitrk1-specific antibody to determine the relative localization of endogenous Slitrk1 to excitatory versus inhibitory synapses. We also sought to resolve the discrepancy between two studies providing conflicting data regarding the ability of Slitrk1 to induce excitatory and inhibitory synapses when overexpressed (Takahashi et al., 2012; Yim et al., 2013). Finally, while the first LRR domain of Slitrk1 was shown to be required for binding to presynaptic RPTP (Um et al., 2014; Yamagata et al., 2015), we identified a potential role for the second LRR domain whose requirement is yet unknown. Our results shed light on a possible mechanism whereby Slitrks undergo lateral interactions and clustering to promote synapse formation as is the case with Neuroligins (Shipman and Nicoll, 2012; Um et al., 2014).

Figure 1: Structures of Slitrk1 and Amigo1

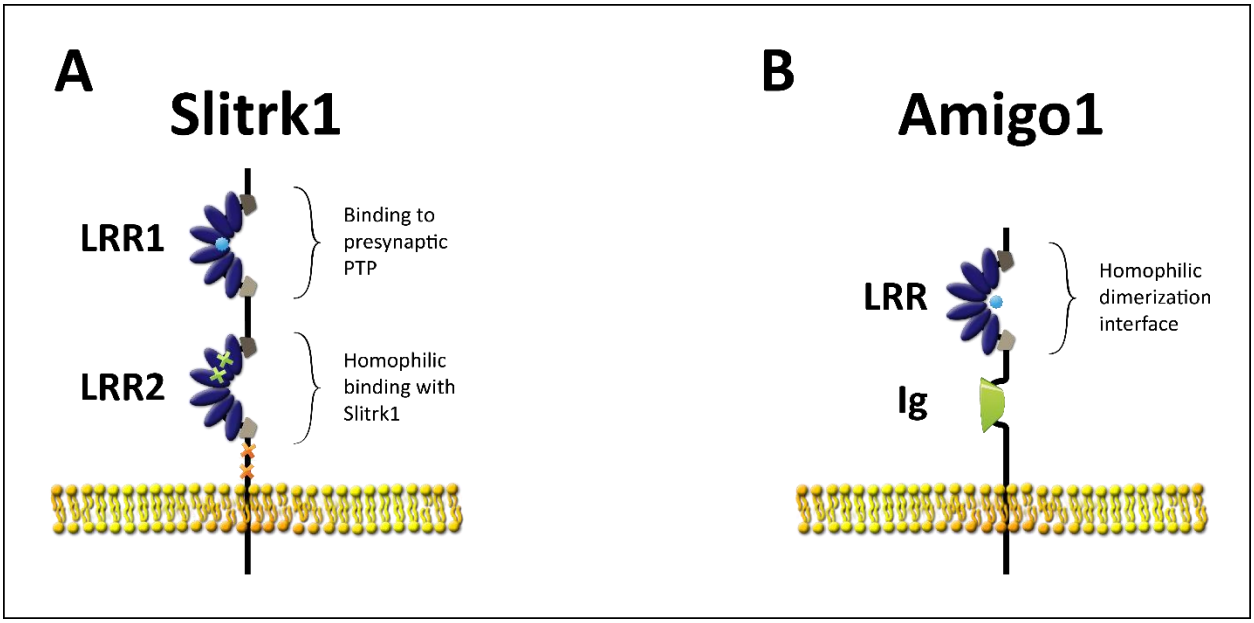

(A) Structure of Slitrk1 protein. Slitrk1 is a transmembrane protein containing two extracellular LRR domains. Each domain contains six leucine-rich repeat modules (*purple*) and flanking amino (*dark grey*) and carboxy (*light grey*) terminus cysteine-rich regions. The N-terminal-most LRR domain (LRR1) is required for binding to its presynaptic partner PTPσ while its LRR2 domain mediates homophilic dimerization. Blue badge indicates area known to be involved in lateral clustering (Um et al., 2014). X's indicate general locations of mutated residues associated with the human disease TS (*green*) and the obsessive hair-pulling disorder trichotillomania (TTM, *orange*)

(B) Structure of Amigo1 protein. Amigo1 is a transmembrane protein containing one extracellular LRR (*purple*) and one Ig (*green*) domain. The LRR domain contains six leucine-rich repeat modules (*purple*) and flanking amino (*dark grey*) and carboxy (*light grey*) terminus cysteine-rich regions. Blue badge indicates that the concave side of the LRR domain is important for dimerization of the protein.

III. Introduction part 2

Precise synapse formation is only one of the crucial developmental processes underlying nervous system development. This step must be preceded by accurate guidance and targeting of axons to their synaptic partners, and it must also be followed by the establishment of mechanisms to maintain synaptic integrity and allow for synaptic plasticity. These other steps also rely on LRR-containing proteins, which can act as guidance molecules or mediate axonal fasciculation important for axonal targeting and can promote transmission at synapses for maturation and maintenance of neural connectivity (Kim et al., 2006; Wang et al., 2008; Yamagishi et al., 2011; Bando et al., 2012; Winther and Walmod, 2014).

Manuscripts 2 and 3 of my thesis aim to understand the *in vivo* roles for Amigo1, an LRR-containing surface receptor, in axon target selection and in the maintenance of neural circuits. In Chapter 3, we use the mouse olfactory system as a model for studying axon guidance and the role of Amigo1 as a cell adhesion molecule involved in regulating axon target selection during development. Conversely, we turned to the hippocampal circuit in Chapter 4 as a good model to examine the role of Amigo1 in the maintenance of neural circuits, where we specifically study mossy fiber projections from the dentate gyrus, which can be compromised due to changes in axon targeting and neural activity.

1. Amigo1

Amigo1 was identified in 2003 as a gene whose transcript is upregulated in an assay of amphoterin-induced hippocampal neurite outgrowth (Kuja-Panula et al., 2003; Chen et al., 2012). It is a member of the Amphoterin induced gene and ORF (AMIGO) family of three cell-surface adhesion proteins, AMIGO (Amigo1), AMIGO2 and AMIGO3, expressed in various tissues, however, of the three members, Amigo1 has the most nervous system-specific expression (Kuja-Panula et al.,

2003). While there is differing evidence regarding Amigo1's subcellular localization to axons or dendrites, western blot analysis examining temporal expression shows that it is upregulated during development, and expression levels are sustained throughout life (Kuja-Panula et al., 2003; Chen et al., 2012).

Amigo1 Function in Cell Adhesion

Amigo1 encodes for a transmembrane protein with an extracellular region containing an LRR domain with six LRRs and a single Ig domain (Figure 1B), but no known functional domain encoded by its short intracellular region (Kuja-Panula et al., 2003). Leucine-rich repeats and Ig domains are typical features of cell adhesion molecules, and they are well-known to be involved in protein-protein interactions. Many extracellular Ig- and LRR-containing transmembrane proteins play important roles in nervous system development, including axon fasciculation and target recognition. A few *in vitro* studies support a role for Amigo1 in various functions typical of cell adhesion molecules such as cell adhesion, neurite outgrowth and axon fasciculation (Kuja-Panula et al., 2003; Kajander et al., 2011; Zhao et al., 2014). Crystal structure analysis revealed that Amigo1 forms homomeric dimers via the LRR domain, and it is thought that dimerization is necessary for its expression at the cell surface as well as its function in cell-cell adhesion (Kajander et al., 2011). *In vitro* data has provided evidence for Amigo1 in homophilic interactions, and both homophilic and heterophilic interactions occur between the three family members as shown by co-immunoprecipitation (Kuja-Panula et al., 2003). Protein-protein interactions in cell adhesion are important for developmental processes such as axon pathfinding and synapse stabilization (Chen et al., 2006). Indeed, Amigo1 has been demonstrated to promote hippocampal neurite extension *in vitro* (Kuja-Panula et al., 2003). In addition to a role for CAMs in cellular interactions, other Ig domain containing CAMs such as Neural cell adhesion molecule (NCAM) and L1 influence cell

survival (Loers et al., 2005; Chen et al., 2006; Ditlevsen et al., 2007). Similarly, it has been demonstrated that Amigo1 can protect SH-SY5Y cells in culture from factors that induce apoptosis, thus indicating a role for Amigo1 in cell survival as well (Chen et al., 2012).

Amigo1 Function in Neuronal Activity

Intriguingly, apart from canonical roles for CAMs in neurite outgrowth and fasciculation, Amigo1 acts as an auxiliary subunit of the voltage-gated potassium channel, Kv2.1, and can modulate the gating and current flow through the channel (Peltola et al., 2011). Specifically, knockdown of Amigo1 affects the channel gating properties such that the channels need stronger depolarization to open (Peltola et al., 2011). Furthermore, not only were these results were confirmed in *Amigo1* null mice, but these mice also have decreased levels of Kv2.1 protein (Peltola et al., 2016). Delayed rectifier currents through Kv2.1 play a critical role in the repolarization of an action potential and are known to regulate intrinsic neuronal excitability in an activity-dependent manner (Du et al., 2000; Mohapatra et al., 2009). Loss-of-function studies of Kv2.1 demonstrate a role for these channels in regulating action potential width and repetitive firing, thus contributing to membrane excitability (Palacio et al., 2017). The alteration in gating properties of Kv2.1 with loss of Amigo1 could lead to a broadening of the action potential (Palacio et al., 2017) and in turn, cause increased neuronal activity or hyperexcitability. Thus, while Amigo1 is structurally a canonical cell adhesion molecule, there is evidence to suggest that it also acts to affect neuronal activity by mediating ion channel dynamics.

In summary, the LRR and Ig domain-containing structure identifies Amigo1 as a cell adhesion molecule with various proposed functions, including neurite outgrowth, cell adhesion and ion channel physiology (Kuja-Panula et al., 2003; Chen et al., 2006; Kajander et al., 2011; Peltola et al., 2011; Zhao et al., 2014).

2. Axon guidance and target selection in the mouse olfactory system

Once a neuron is born, it begins to extend its axon which will sample the environment using receptors expressed on its leading edge, or growth cone, to detect guidance cues in the surrounding tissue. Generally, secreted ligands from a distance or membrane-linked ligands in the proximity of a growing axon can be detected by receptors expressed on the growth cone in specific ligand-receptor pairs. A ligand-receptor binding event can trigger either attraction or repulsion of the growth cone towards or away from the source of the ligand. In this way, the array of receptors on a growing axon will bind the appropriate ligand cues in the environment to allow the axon to grow to its correct target zone (Bellon and Mann, 2018). Once the target zone is reached, guidance cues that act at a shorter range as well as axon-axon interactions allow for specific target neuron selection (Stoeckli, 2018). Good examples of where axon guidance is crucial for proper nervous system development are the sensory systems. Whether it be a spatial map of the visual field, a tonotopic map of sound pitch, or a somatotopic map of touch, order must be maintained from the sensory neuron in the periphery to the second order neurons in the brain for an accurate representation of the organism's environment.

The mouse main olfactory system is commonly used to study mechanisms of axon guidance and circuit formation. It consists of the main olfactory epithelium (OE), housing the primary sensory neurons, and the main olfactory bulb (OB), where the projection neurons reside (Ressler et al., 1994a). Primary sensory neurons, called olfactory receptors neurons (ORNs), extend dendritic cilia expressing olfactory receptors (ORs) to the surface of the epithelium to detect odorant molecules from the environment. These neurons project a single axon towards the OB to form synapses with dendrites of mitral and tufted projection neurons as well as interneurons in neuropil structures termed glomeruli (Reed, 1992; Vassar et al., 1994; Mori et al., 1999). Interestingly, each ORN

expresses one receptor gene from a gene family encoding for over 1000 ORs via stochastic activation of one OR gene in a mono-allelic fashion and subsequent negative feedback to other OR genes (Buck and Axel, 1991; Serizawa et al., 2000, 2003; Zhang and Firestein, 2002). Neurons expressing a given OR are spatially restricted to one of the distinct yet overlapping regions along the dorsomedial-ventrolateral axis of the OE, and they are randomly distributed within that region (Reed, 1992; Vassar et al., 1994; Miyamichi et al., 2005). Classically, the OE could be divided into four of these overlapping regions, however a more recent study has shown an even more precise definition of up to nine spatially restricted regions along the dorsomedial to ventrolateral and anterior to posterior axes (Zapiec and Mombaerts, 2020). In a remarkable instance of targeting specificity, neurons from an individual OR population project and converge their axons into one medial and one lateral glomerulus at stereotypic locations on the surface of the OB (Ressler et al., 1994a; Vassar et al., 1994; Mombaerts et al., 1996; Mori and Sakano, 2011). There is a strong correlation between the regional positioning of the neuron in the OE and its projection site along the dorsal-ventral axis the OB. Thus, a map is formed whereby each glomerulus is innervated by a homogenous population of ORN axons whose cell bodies are spatially distributed in a particular region of the OE. Interestingly, each OR is tuned to recognize a variety of odorant molecules with different affinities, and multiple ORs can recognize the same odorant molecule (Malnic et al., 1999; Meister and Bonhoeffer, 2001; Mori and Sakano, 2011). The range of odor molecules greatly outnumbers the number of ORs, hence, an odor can be represented in the brain as the pattern of activation of a set of glomeruli in the OB (Imamura et al., 1992; Vassar et al., 1994).

Olfactory map formation during development: Establishing coarse topography

The OE and OB share a sense of direct mapping along one axis, where the dorsomedial (DM)-ventrolateral (VL) position of an OR subpopulation correlates with the dorsal-ventral positioning

of its target glomerulus in the OB. In contrast, the anterior-posterior location of a glomerulus is determined by neuronal activity rather than spatial positioning in the OE (Mori and Sakano, 2011).

Along the dorsal-ventral axis of the OB, axons target glomeruli with the help of two sets of ligand-receptor pairs: Slits and Roundabout-2 (Robo-2), and Semaphorin (Sema) 3F and Neuropilin-2 (Nrp2), both of which function by repulsive signalling. The Robo-2 receptor is expressed in a DM-high to VL-low manner in the OE. During development, dorsomedial Robo2-positive ORNs project their axons to the dorsal bulb first, since they are repelled by Slits expressed in the ventral OB, and they secrete Sema3F in this dorsal region. Late-arriving, ventrolateral axons express Nrp2 and are repelled away from Sema3F to target more ventral areas of the bulb (Cho et al., 2007, 2012; Takeuchi et al., 2010). Thus, the combination of these guidance ligands and receptors help to establish a dorsal to ventral topography in the OB (Figure 2A).

While dorsal-ventral patterning of glomeruli in the OB is determined by anatomical locations of ORNs in the OE, topography along the anterior-posterior axis is controlled by levels of OR activity. ORs are G-protein-coupled receptors (GPCRs) that signal odor-binding events by interacting with the G-protein G_{olf} to initiate cyclic adenosine monophosphate (cAMP) signaling (Jones and Reed, 1989; Buck and Axel, 1991). In the absence of ligand binding during early development, the ORs generate a baseline level of cAMP via interaction with G_s and activation of adenylyl cyclase III, and this level of activity varies by OR type (Nakashima et al., 2013). The baseline level of GPCR activity and cAMP signalling together regulate the differential expression of Neuropilin-1 (Nrp1) in subsets of ORNs (Imai et al., 2006). ORNs producing low levels of cAMP express low levels of Nrp1 and project to anterior regions of the OB while those generating high levels of cAMP highly express Nrp1 and project to the posterior OB (Imai et al., 2006).

In summary, general topography in the olfactory bulb is established both by dorsal-ventral patterning based on anatomical locations of ORNs within the OE, and by anterior-posterior patterning, driven by differential cAMP activity between ORN populations (Imai et al., 2006; Imai and Sakano, 2009; Mori and Sakano, 2011). After coarse sorting of axons to their destination, axons use other cues, such as cell adhesion molecules, to segregate and converge onto appropriate glomeruli.

Olfactory map formation during development: Refinement of the glomerular map

Studies examining the mechanisms by which ORNs converge their axons into individual glomeruli have provided growing evidence for axon-axon interactions in regulating the process of discrete map formation (St John et al., 2003; Imai and Sakano, 2011). Similar to ORN activity-dependent expression of axon guidance molecules involved in anterior-posterior targeting, neuronal activity also modulates the expression of cell adhesion molecules involved in axon-axon interactions to allow axons to recognize one another and converge onto appropriate glomeruli (Figure 2B) (Serizawa et al., 2006; Imai and Sakano, 2011). However, rather than intrinsic baseline GPCR activity, the expression of cell adhesion molecules is based on ligand-dependent activation of ORs, canonical signalling through G_{olf}, and subsequent cyclic nucleotide-gated (CNG) channel activity (Serizawa et al., 2006; Nakashima et al., 2013). Kirrel2, and EphA are positively regulated by neuronal activity while Kirrel3, ephrin-A5 and BIG-2 are negatively regulated by neuronal activity (Serizawa et al., 2006; Kaneko-Goto et al., 2008). In Kirrel 2 or 3 transgenic mouse lines, which express different levels of Kirrel 2 or 3 within a single OR type, axons expressing the same receptor but different levels of Kirrel segregate into two neighbouring glomeruli in the OB. Therefore, levels of Kirrel appear to instruct coalescence of homotypic axons for specific glomerular targeting in a dose-dependent manner (Serizawa et al., 2006; Imai and Sakano, 2011). A more recent study

demonstrated a requirement for Kirrel2 in the targeting of ORN axons and showed variability in the requirement for Kirrels in axonal coalescence between ORN populations (Vaddadi et al., 2019). In addition, EphA5 and ephrin-A5 may play a role in local sorting of axons via contact-mediated repulsion between heterotypic axons (Serizawa et al., 2006). Finally, BIG-2 is another cell adhesion molecule involved in local axon sorting in the OB, and its expression also correlates with neural activity (Kaneko-Goto et al., 2008). Loss of BIG-2 expression results in the innervations of ectopic glomeruli by specific OR populations, and BIG-2-AP binding assays suggest that BIG-2 has a heterophilic binding partner also expressed in ORN axons (Kaneko-Goto et al., 2008). Further studies of these CAMs in mediating the precise targeting of specific ORN populations is necessary, as implicated by the varied requirement of Kirrels between ORN populations (Vaddadi et al., 2019). As such, there are likely other CAMs that are necessary to specify coalescence of subsets of ORNs.

Figure 2: Two-step targeting of olfactory sensory axons to the OB

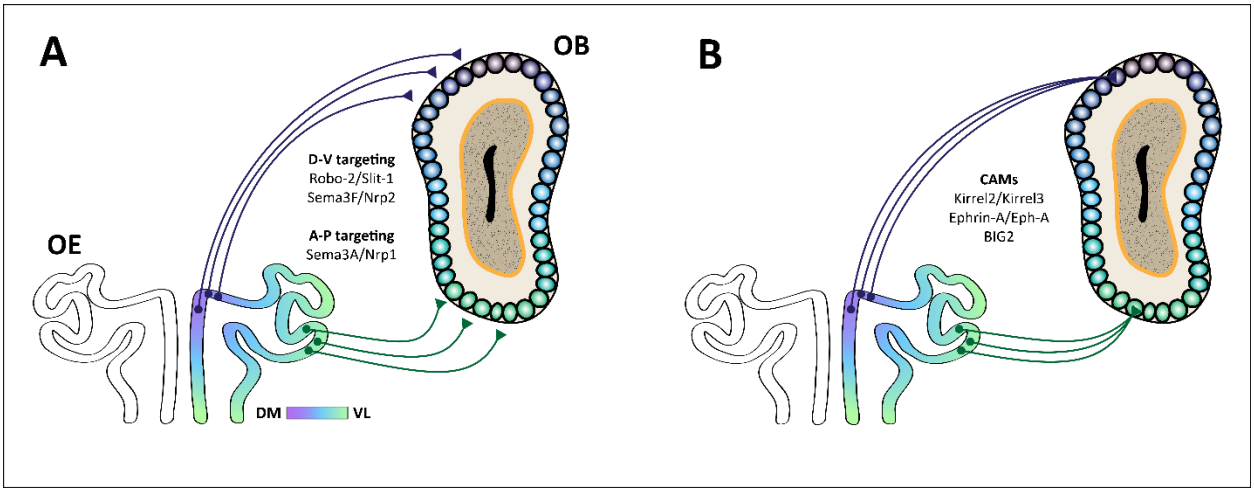

Depiction of a coronal section of OE and a coronal section of OB and the targeting of two populations of ORN axons to the bulb.

(A) ORNs are expressed in populations organized along the dorsomedial (DM) to ventrolateral (VL) axis. They are guided by axon guidance molecules to regions along dorsoventral (D-V) and anterior-posterior (A-P) axes of the olfactory bulb.

(B) Once they reach their general target zone, the expression of CAMs on the ORN axons allow them to coalesce into appropriate glomeruli

3. Rationale and objectives for Manuscript 2 (Chapter 3)

Thus far, only a few sets of adhesion molecules have been shown to play a putative role in refined glomerular map formation. These few molecules are unlikely to be sufficient to sort the axons of over 1000 types of ORN populations into their proper glomerular targets. Hence, we were interested in identifying other cell adhesion molecules that may facilitate local axon sorting or play a role in the targeting of ORN axons to the OB to allow for accurate neuronal wiring and odor processing. Based on its structure as a CAM and its known roles in neurite outgrowth and fasciculation, we chose to examine the function of Amigo1 in the precisive formation of the olfactory glomerular map, and these results will be described in Chapter 3.

4. Mossy fiber projections of the Hippocampal Circuit

The hippocampal formation

The hippocampus is a vastly studied brain structure located on the medial aspect of the brain's hemispheres. It is known to be crucial for memory formation and learning, both for long- and short-term memory. As such, high levels of plasticity also make this structure more vulnerable to degenerative conditions such as ischemia, epilepsy, and neurodegenerative diseases, such as Alzheimer's (Khalaf-Nazzal and Francis, 2013; Bartsch and Wulff, 2015). It is therefore of interest to many researchers to study the mechanisms involved in the formation and maintenance of proper hippocampal circuitry. The hippocampal formation is composed of the dentate gyrus (DG) and the cornu ammonis (CA) subfields, CA1-CA3. These structures, along with the adjacent entorhinal cortex (EC), form the well-known trisynaptic circuit (Schultz and Engelhardt, 2014; Knierim, 2015). In this circuit, cells of the entorhinal cortex receive input from surrounding brain regions and project excitatory output to the dendrites of granule cells located in the thin granule cell layer of the DG. Granule cells then project axons in the form of mossy fiber bundles to the proximal

apical and basal dendrites of pyramidal cells in area CA3 (Figure 3A). The synapses formed at this junction are large structures composed of the mossy fiber boutons (presynaptic terminals) and the elaborate multi-headed postsynaptic dendritic spiny structures called thorny excrescences (TEs, Figure 3B) (Amaral et al., 2007). CA3 pyramidal cells in turn project their axons, termed the Schaffer collaterals, to CA1 pyramidal cells, which finally project back to deep layers of the entorhinal cortex for output back to cortex (Figure 3A) (Vago and Wallenstein, 2014). Within this circuit, the mossy fiber projections from the dentate gyrus to CA3 provide an invaluable model to study the mechanisms of axonal guidance to lamina-specific target structures, and the large highly plastic mossy fiber terminals allow for the study of synapse formation and maintenance.

Figure 3: Organization of the Hippocampal Circuit

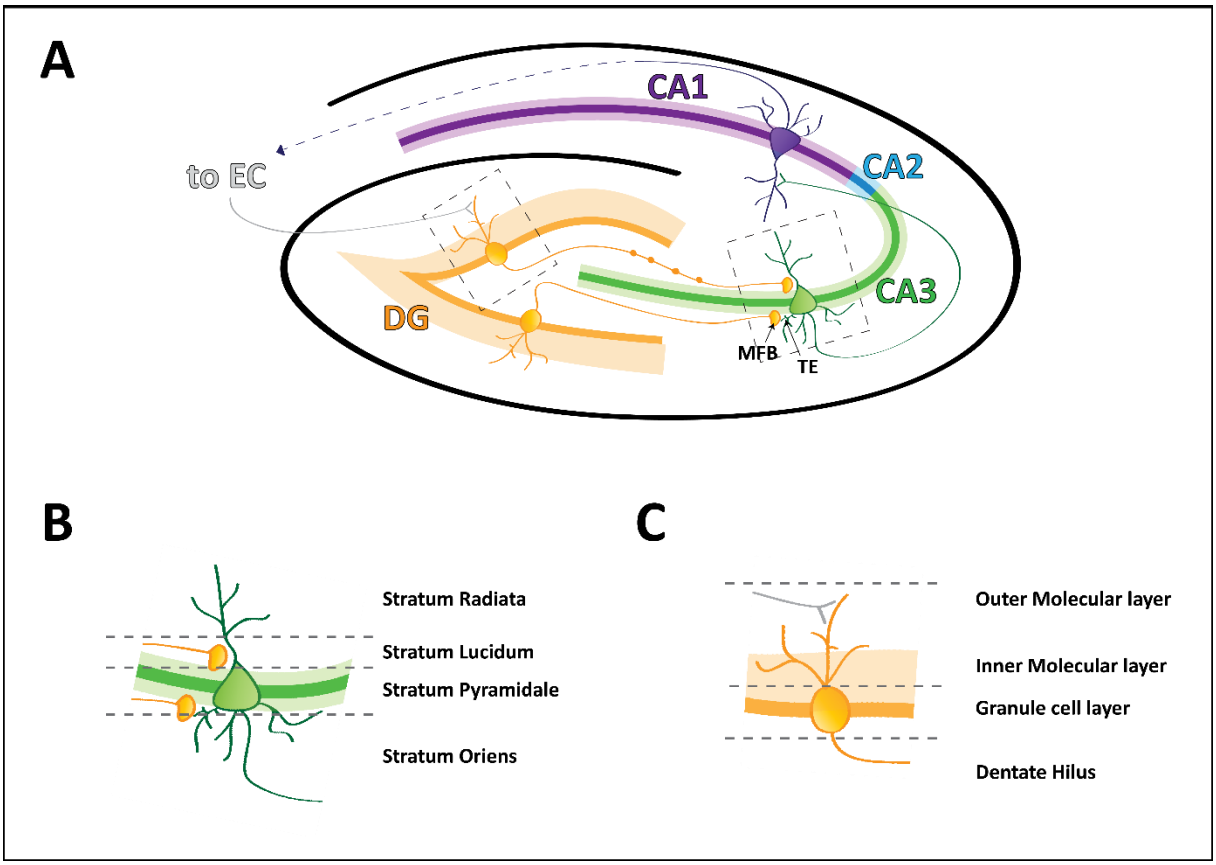

(A) Diagram of the flow of information through the hippocampal trisynaptic circuit. Dentate gyrus (DG) granule cells (*orange*) receive information from entorhinal cortex (EC, *grey*) and send their axons towards CA3. These axons form large terminals called mossy fiber boutons (MFBs) onto the proximal apical and basal dendrites of CA3 pyramidal neurons (*green*). They synapse specifically onto large complexes of spine heads called thorny excrescences (TEs) of the proximal CA3 neuron dendrites. CA3 pyramidal cells then send their axons to CA1 (*purple*) which relay information back to CA3.
(B) Laminar organization of the CA3 subfield. Mossy fiber boutons synapse on the proximal apical dendrites in stratum lucidum and on the proximal basal dendrites in stratum oriens. CA3 pyramidal cells project distal dendrites into stratum radiata.
(C) Laminar organization of the dentate gyrus. Granule cells reside in the granule cell layer and project dendrites into the inner and outer molecular layers. Entorhinal axons (*grey*) synapse onto dendrites of the outer molecular layer. Granule cell axons project through the dentate hilus before traversing to CA3.
Not shown: dentate hilar cells receiving mossy fiber input also synapse back onto granule cell dendrites in the inner molecular layer.

Development of the hippocampus

Neurogenesis in the different subfields of the hippocampus (HC) does not occur at equal rates. CA1 and CA3 neurons are generated from E10 to E15 (Angevine, 1965; Stanfield and Cowan, 1979; Khalaf-Nazzal and Francis, 2013). Neurogenesis of dentate gyrus granule cells, on the other hand, begins at E10, with most cells being generated in the first post natal week. Uniquely, neurogenesis of granule cells continues throughout adult life in rodents (Bayer, 1980a, 1980b; Amaral and Dent, 1981; Reznikov, 1991). It is thought that adult granule cell neurogenesis can contribute to learning and memory (Deng et al., 2010). Rates of adult neurogenesis can be modulated by environmental factors such as environmental enrichment and exercise (Kempermann et al., 1997; van Praag et al., 1999). How it contributes to the cognitive improvements with these environmental factors remains unclear (van Praag et al., 1999; Meshi et al., 2006; Deng et al., 2010), however neural activity plays a role in regulating survival and integration of newly born granule cells into existing circuitry (Ramirez-Amaya et al., 2006; Kee et al., 2007; Deng et al., 2010). Furthermore, adult born dentate granule neurons that experience neural activity when young tend to have enhanced responses to neural activity when older (Jessberger and Kempermann, 2003; Trouche et al., 2009), suggesting that plasticity and learning is thought to be localized more to newer born dentate granule cells while mature granule cells could preserve existing information (Deng et al., 2010).

Axon Guidance

Once generated, granule cells of the dentate gyrus project axons, termed mossy fibers (MFs), to CA3 pyramidal cells. MFs project to CA3 in two to three bundles in the developing HC that travel above, within or below the pyramidal cell layer. The infrapyramidal bundle (IPB), travelling below the pyramidal layer, arises from granule cells in the lower (infrapyramidal) dentate gyrus blade. In proximal CA3, the suprapyramidal bundle (SPB) arises from axons of granule cells located in the

suprapyramidal and crest of the dentate blade, but distally the infrapyramidal bundle crosses over the pyramidal cell layer to join the SPB (Claiborne et al., 1986). There exists as well an intrapyramidal bundle in some genetic mouse strains that travels within the pyramidal CA3 layer proximally, but distally also joins the SPB (Blaabjerg and Zimmer, 2007).

The initial polarization of granule cells relies on local environmental cues, orienting their dendrites towards the dentate molecular layer and axons towards the dentate hilus (Figure 3C) (Kim et al., 2004). Peak development of the mossy fiber tract occurs within the first 3 postnatal weeks (Gaarskjaer, 1986), and their highly cell-specific targeting requires specific recognition of the individual CA3 cells (Kim et al., 2003). Furthermore, the guidance mechanisms of mossy fiber projections are developmentally regulated within this period (Nguyen et al., 1996). Evidence using *in vitro* explant co-cultures discovered that early in development (P0), diffusible cues from CA3 could attract MFs, with contact-dependent cues allowing for final targeting, a mechanism requiring precise orchestration of localization and timing of ligand and receptor expression (Skutella and Nitsch, 2001; Koyama et al., 2004b). Moreover, newly generated granule cells (GCs) can project their mossy fiber axons to the CA3 using already established MF projections to guide them (Nguyen et al., 1996; Koyama et al., 2004b).

Repellant cues are crucial to prevent the outgrowth of DG axons to non-CA3 areas. The Robo1 and 2 receptors respond to the Slit family of ligands and are prominent axon guidance molecules regulating the development of many CNS pathways. In the hippocampus, Slit2 expressed by entorhinal neurons repel the axons of DG neurons away from the entorhinal cortex and dendritic molecular layer (Ba-Charvet et al., 1999). Additionally, the Slit2 ligand may also function to repel mossy fiber axons from crossing the midline to contralateral hippocampus (Ba-Charvet et al., 1999). Elegant hippocampal slice culture experiments have demonstrated that blockage of cAMP

signalling in DG cells allows for growth of their axons into the CA3 region (Mizuhashi et al., 2001). These results imply that a repellant cue could act on DG axons and signal downstream through cAMP to mediate growth cone retraction (Mizuhashi et al., 2001).

Several groups have demonstrated the importance of the Neuropilin-Semaphorin family of axon guidance molecules in mediating mossy fiber attraction towards CA3. Neuropilin-1 and -2 are strongly expressed in the hippocampus both in development and in adult, and secreted class 3 Semaphorins can repel Neuropilin-expressing hippocampal axons (Chédotal et al., 1998; Skutella, 1999). Sema3A has been shown to repel Neuropilin-1 expressing cells of DG, CA3 and CA1, and its expression in the DG was hypothesized to prevent mossy fiber innervation of the DG molecular layer. Sema3A mutant animals however fail to show misguidance of these axons, suggesting other mechanisms of guidance of mossy fibers towards CA3 (Catalano et al., 1998; Steup et al., 2000). In contrast, Neuropilin-2 is highly expressed in dentate gyrus and in CA3, and loss of Neuropilin-2 in *Nrp2* null mice results in an increase in mossy fibers projecting deep into stratum pyramidale of CA3 and into stratum oriens, creating a longer infrapyramidal mossy fiber bundle that extends further towards CA1 (Chédotal et al., 1998; Chen et al., 2000; Giger et al., 2000). These results were shown to be mediated by Neuropilin's strong binding partner, Sema3F, and the expression of Sema3F in CA3 was thus suggested to restrict Neuropilin-2-expressing granule cell axons to stratum lucidum (Chédotal et al., 1998; Giger et al., 2000).

Apart from long range axon guidance cues, contact-dependent cues can instruct the more precise layer-specific targeting of DG axons. One mechanism demonstrates that Plexin-A2 expression in CA3 proximal pyramidal cell dendrites attenuates the effects of Sema6A repulsion to allow axons to be guided to the stratum pyramidale. This model suggests that the balance between repulsive

and attractive cues regulates MF trajectory to the correct layer of CA3 (Suto et al., 2007; Tawarayama et al., 2010, 2018).

While guidance cues contribute to the directed growth of axons to CA3, cell adhesion molecules can promote fasciculation to help axons coalesce into the thin target layer. For example, Limbic system-associated membrane protein (LAMP) is expressed in DG axons and CA3 pyramidal cells (Keller et al., 1989; Zacco et al., 1990). In rats treated with LAMP antibody to block endogenous LAMP-mediated homophilic adhesion, MF axon trajectories became diffuse and aberrantly projected into stratum pyramidale, oriens and radiatum, implicating LAMP as an important mediator of mossy fiber fasciculation in CA3 (Pimenta et al., 1995).

Additionally, several molecules involved in axon guidance and neurite outgrowth and synapse formation have recently been shown to be targets of Beta-Secretase 1 (BACE1)-mediated cleavage, including the cell adhesion molecules L1 and Close homolog of L1 (CHL1) (Hemming et al., 2009; Zhou et al., 2012). It was hypothesized that BACE1-mediated cleavage would cause deficiency in the function of these guidance and cell adhesion molecule substrates. Indeed, *BACE1* null mice show defects in guidance of olfactory receptor neurons to the OB as well as of mossy fiber projections to CA3 (Rajapaksha et al., 2011; Cao et al., 2012; Hitt et al., 2012). Specifically, loss of BACE1 causes premature crossover of infrapyramidal MF axons to the suprapyramidal bundle and shortened IPBs. Interestingly, this phenotype mimics that seen in *CHL1* null mice, confirming that CHL1 cleavage by BACE1 is important for proper neurite development exemplified in olfactory and hippocampal systems (Hitt et al., 2012).

Finally, the environment itself can support MF outgrowth. For example, digestion of KSPGs in the extracellular matrix resulted in a failure of axons to fasciculate upon exiting the dentate gyrus and entering stratum lucidum in hippocampal slices, suggesting that KSPGs contribute to

coalescence of mossy fibers (Butler et al., 2004). Furthermore, initially projecting MF axons serve as guidance scaffolds to mediate contact-dependent guidance of subsequently arriving MF axons (Koyama et al., 2004b). Polysialic acid-neural cell adhesion molecule (PSA-NCAM) is an Ig superfamily molecule important for cell-cell interactions. Mossy fibers express high levels of PSA-NCAM and removal of the PSA or of NCAM results in significant defasciculation of MF axons and ectopic mossy fiber bouton formation (Muller et al., 1994; Cremer et al., 1997, 2000; Seki and Rutishauser, 1998; Seki and Arai, 1999).

Synapse formation

Once they reach CA3, MFs form a unique type of synaptic structure composed of the mossy fiber bouton (MFB; also called large mossy terminal, LMT) and the postsynaptic thorny excrescences (TEs), which are elaborate clustered spines on the proximal dendrites of glutamatergic pyramidal cells. Interestingly, each mossy fiber forms only 11 to 18 mossy fiber boutons onto individual CA3 pyramidal cells (Blaabjerg and Zimmer, 2007). The mossy fiber boutons also extend filopodia to synapse onto GABAergic interneurons to regulate feedforward inhibition (Torborg et al., 2010). The MFB can grow up to 100 times larger than a typical presynaptic terminal (Williams et al., 2011), encompassing both excitatory and inhibitory neuron targets, yet there is still very little information regarding the molecular mechanisms controlling the formation of these two synapse types. Cell adhesion molecules have started to emerge as players in this process. Synapse formation between the mossy fibers and CA3 pyramidal dendrites was identified to be regulated by the cell adhesion molecule Cadherin-9. Expression analysis found that both *in vivo* and *in vitro*, Cadherin-9 was expressed exclusively in the DG and CA3 cell types of the hippocampus, and knockdown studies discovered a requirement in *trans* for Cadherin-9 in preferential synapse formation between the MF terminals and CA3 pyramidal cell dendrites (Williams et al., 2011).

Thus, this cell adhesion molecule is shown to regulate the differentiation of this specific synapse in the developing HC. Additional Cadherins such as Cadherin-8 and N-Cadherin also regulate mossy fiber targeting to CA3 pyramidal cell dendrites. While Cadherin-8 is important for growth of MF axons, N-cadherin plays a strong role in dendritic elaboration of CA3 pyramidal cells, and both Cadherins interact with β-catenin ultimately regulating the formation of mossy fiber terminals (Bekirov et al., 2008). Recently, the homophilic adhesion molecule Kirrel3 was found to be an essential target-specific cue in inhibitory synapse formation (Martin et al., 2015; Taylor et al., 2020). Specifically, Kirrel3 regulates the development of synapses between MF terminals and GABAergic interneurons. Kirrel3 is expressed in both DG neurons as well as GABAergic CA3 interneurons but not CA3 pyramidal cells, and knockout of the *Kirrel3* gene causes reductions in mossy fiber filopodia size and number, resulting in fewer GABAergic synapses and higher CA3 pyramidal cell excitability (Martin et al., 2015, 2017). Adult *Kirrel3* null mice show a variety of altered behaviours, including hyperactivity, which may be attributable to an excitatory versus inhibitory imbalance as seen at the neuronal level in the hippocampus (Choi et al., 2015; Hisaoka et al., 2018; Völker et al., 2018).

The heparan sulfate proteoglycan (HSPG) Glypican 4 (GPC4) is another synaptic organizing protein found to be expressed in the hippocampal circuit. At the EC-DG synapse, glycosylphosphatidylinositol (GPI)-anchored GPC4 binds in *cis* to the presynaptic LAR and in *trans* to postsynaptic LRRTM4 to mediate synaptogenesis in the dentate gyrus molecular layer (DeWit et al., 2013; Siddiqui et al., 2013; Ji et al., 2015). More recently, it was found that GPC4 in the mossy fiber terminal binds to the postsynaptic orphan receptor GPR158 on CA3 pyramidal cells, and this interaction is required for the input specific regulation of excitatory MF-CA3 synapse organization (Condomitti et al., 2018).

Maturation, Maintenance and Plasticity of mossy fiber projections

Hippocampal mossy fiber terminals exhibit a strong amount of plasticity even in adult animals, with neural activity being important in regulating structural plasticity of synapses (Chierzi et al., 2012).

IPB axons undergo significant pruning in the 3rd and 4th postnatal week, by a mechanism involving Semaphorins, Neuropilin-2, and Plexin-As, resulting in a shortened IPB by adulthood (Chen et al., 2000; Bagri et al., 2003; Liu et al., 2005; Suto et al., 2007). Draxin, a repellant axon guidance cue and an inhibitor of dentate granule cell apoptosis (Zhang et al., 2010) was recently shown to also mediate the balance between projections of mossy fibers along the infra-and supra pyramidal bundle. *Draxin* null mice show a significant reduction in the length of the infrapyramidal bundle due to more immediate crossover of infrapyramidal axons to the suprapyramidal tract (Tawarayama et al., 2018).

Individual large mossy terminals (LMTs) and LMT complexes (LMT-C), containing a central terminal with additional surrounding small satellite terminals, get larger with age and experience (Galimberti et al., 2006), with one LMT-C of a mossy fiber providing the largest increase in total LMT volume. Hippocampal-dependent learning tasks show correlation between performance and mossy fiber projection size (Pleskacheva et al., 2000; Ramirez-Amaya et al., 2006). As well, environmental enrichment causes an increase in the complexity of LMT-Cs and TE lengths (Galimberti et al., 2006) while long-term stress can cause reductions in mossy fiber terminal complexity (Sandi et al., 2003; Galimberti et al., 2006). With age and experience, there is a large shift in the distribution of LMT sizes to results in many small LMTs with a concomitant increase in the size of one LMT-C complex, comprising one large core LMT and many connected satellite LMTs. This characteristic complex has been termed Terminal Arborization (TA) in adult animals

by Galimberti and colleagues in 2010, and most mature mossy fibers possess a single TA per mossy fiber. It was found that the TA position of each mossy fiber was positioned along the proximo-distal CA3 axis in a topographic manner relative to the position of the GC body in the DG (Galimberti et al., 2010). This topography is mediated by EphA4 expressed in a gradient form along the DG blades. Furthermore, EphA4 signalling and PSA-NCAM were both shown to regulate plasticity of TAs during a critical period in juvenile mice, allowing the selection of one prominent TA per mossy fiber neuron (Galimberti et al., 2010; Khalaf-Nazzal and Francis, 2013). EphA4 regulates TE spine morphology by binding ephrin-A3 and inhibiting integrin function (Murai et al., 2003; Bourgin et al., 2007; Klein, 2009).

Contact mediated cues are also important for continuous maintenance of the circuit even with the addition of adult born GC axons. As such, cell adhesion molecules allowing newly born granule cells to extend axons along existing fiber tracts may continue to be important throughout adulthood to maintain correct circuit trajectory (Koyama et al., 2004b).

Mossy Fiber Sprouting/epilepsy

The high degree of plasticity in the hippocampus is conducive for learning and memory, but also makes it vulnerable to the abnormal remodelling of the circuit known as mossy fiber sprouting (MFS), a common phenomenon in models of temporal lobe epilepsy (Koyama et al., 2004b). In epilepsy, there tends to be pathologically increased levels of mossy fiber sprouting whereby granule cell axons sprout new branches outside stratum lucidum of CA3 or even back into the inner molecular layer of the DG where they synapse back onto granule cell dendrites (Okazaki et al., 1999). This recurrent excitatory pathway of sprouted mossy fibers is thought to contribute to seizure susceptibility (Koyama and Ikegaya, 2005). Mechanisms underlying MFS are not fully known, but it has been suggested to be triggered by seizure activity, granule cell deafferentation,

or neuron loss in the hilus of the dentate gyrus (Buckmaster, 2012). These triggers presumably lead to a disruption of molecular mechanisms of axon growth and guidance, resulting in pathological synaptic reorganization (Koyama and Ikegaya, 2005). Furthermore, establishment of aberrant circuitry could be exacerbated by the projection of newborn GC axons that follow the existing sprouted trajectories (Koyama et al., 2004b).

The mechanisms of mossy fiber sprouting are beginning to be better understood, and the possibility of focusing on mossy fiber sprouting as a therapeutic target of temporal lobe epilepsy continues to be investigated (Koyama and Ikegaya, 2005).

Brain-derived neurotrophic factor (BDNF) signalling through the Trk receptor has been identified as a probable mechanism underlying mossy fiber sprouting. Seizure induction causes increases in BDNF, and BDNF overexpression can activate mossy fiber branching (Scharfman et al., 2002; Danzer et al., 2009), while heterozygous *BDNF* knockout mice showed decreased sprouting levels after seizure induction (Vaidya et al., 1999). Thus, it was initially suggested that BDNF is both necessary and sufficient to cause axonal branching which can lead to mossy fiber sprouting (Koyama et al., 2004a). Subsequent studies challenged these results, with either transgenic overexpression of *BDNF* or BDNF infusion unable to induce mossy fiber sprouting. Hence, while not sufficient (Vaidya et al., 1999; Qiao et al., 2001), BDNF might be required for DG cell axonal branching leading to mossy fiber sprouting (Koyama et al., 2004a). Subsequently, it was found that Netrin-1 signalling through Unc5 also plays a role in sprouting of mossy fibers. Under normal conditions, Deleted in Colorectal Carcinoma (DCC)-expressing DG axons are repelled away from Netrin-1 expression in the DG. However, neuronal hyperactivity causes upregulation of Unc5 on DG cell axons, thereby strengthening attraction to Netrin-1 in the DG molecular layer instead of repulsion (Muramatsu et al., 2010).

Another example of mossy fiber sprouting came from cultured hippocampal slices, in which recombinant repulsive guidance molecule A (RGMa) application inhibited mossy fiber sprouting normally induced by hyperexcitability, suggesting that this guidance molecule also controls axonal branching of mossy fibers (Shibata et al., 2013). In a pentylenetetrazole kindling model, RGMa levels were reduced with concomitant increases in focal adhesion kinase (FAK) phosphorylation and Ras activation which mediate cytoskeletal changes involved in neurite outgrowth. These changes correlated with the progression of mossy fiber sprouting (Song et al., 2015b). Conversely, administration of RGMa in the pentylenetetrazole kindling model restored FAK phosphorylation, diminished mossy fiber sprouting, and suppressed seizure activity (Chen et al., 2017; Song et al., 2019).

Importantly, the misguidance and sprouting of mossy fiber axons has been shown to correlate with alterations to neuronal activity, which may link to changes in cognition or memory formation. Cognitive impairments observed in conditions such as schizophrenia are suggested to involve abnormal hippocampal neural transmission (Tamminga et al., 2010). For example, the alpha-isoform of calcium/calmodulin-dependent protein kinase II (CAMKIIα) is an important regulator of neurotransmitter release important for maintaining proper neural transmission (Hinds et al., 2003). *CAMKIIα* heterozygote mice have working memory deficits and hyperlocomotion reminiscent of impairments in psychiatric conditions (Yamasaki et al., 2008). These heterozygous mice display an increased number of mossy fiber axons projecting aberrantly into stratum oriens, likely caused by the reduction in Semaphorin expression observed in CA3 (Nakahara et al., 2015, 2018). These findings provide good examples of neuronal activity-induced disruptions to axon guidance mechanisms.

Together, these studies provide ample evidence that both development and maintenance of hippocampal circuitry is vital for normal brain function. Further studying the role of axon guidance and cell adhesion molecules will help elucidate the complex mechanisms of mossy fiber circuit formation and maintenance.

5. Objectives for Manuscript 3 (Chapter 4)

Cell adhesion functions and neural activity regulation are common requirements of MF projection formation and maintenance and thus make Amigo1 a good candidate for regulating the projections of this part of the HC circuit. In Chapter 4, we characterize the expression of Amigo1 in various brain regions, including the hippocampus, and we investigate a function for Amigo1 in the regulation of mossy fiber projections. We chose to examine its role in both the development and maintenance of these projections using an *Amigo1* null mouse model.

Chapter 2:

Slitrk1 is localized to excitatory synapses and promotes their development

François Beaubien[1,2,*] , **Reesha Raja**[1,2,*] , Timothy E. Kennedy[1,3], Alyson E. Fournier[1,3] & Jean-François Cloutier[1,3]

1 Montreal Neurological Institute, Montreal, Quebec, Canada.
2 Integrated Program in Neuroscience, McGill University, Montreal, Quebec, Canada
3 Department of Neurology and Neurosurgery, McGill University, Montreal, Quebec, Canada
⁎These authors contributed equally to this work.

I. Preface

This chapter was published in Scientific Reports in 2016. In this manuscript, we study the role of Slitrk1 in synaptogenesis using an *in vitro* approach, where we grow hippocampal neurons in culture, followed by overexpression or knockdown of Slitrk1 in order to assess its ability and necessity in regulating the formation of excitatory or inhibitory synapses. I am co-first author on this manuscript with Dr. François Beaubien, a former graduate student who initiated and contributed to this study. A version of this story was first submitted for publication to The Journal of Biochemistry following its inclusion in the Doctoral Thesis of Dr. François Beaubien. The manuscript underwent major revisions for publication in Scientific Reports, including all new figures and datasets that I have generated. Thus, I have acquired and performed the analysis of all data included in the final published manuscript. Some overlap in the text of the introduction and methods sections exist between the published paper and the early version of the manuscript included in Dr. Beaubien's thesis.

II. Acknowledgements

We thank Dr. Keith Murai and members of the Cloutier lab for critical comments on the manuscript. We thank Dr. Emma Jones, Carolin Madwar, Ricardo Sanz, and Andrew Kaplan for technical insight and help. J.-F.C. held a Canada Research Chair in developmental neurobiology and is an FRQ-S Senior Scholar. R.R. held a Vanier Studentship from the Canadian Institutes for Health Research (CIHR). This research was supported by CIHR and the Brain and Behavior Research Foundation (NARSAD).

III. Abstract

Following the migration of the axonal growth cone to its target area, the initial axo-dendritic contact needs to be transformed into a functional synapse. This multi-step process relies on overlapping but distinct combinations of molecules that confer synaptic identity. Slitrk molecules are transmembrane proteins that are highly expressed in the central nervous system. We found that two members of the Slitrk family, Slitrk1 and Slitrk2, can regulate synapse formation between hippocampal neurons. Slitrk1 is enriched in postsynaptic fractions and is localized to excitatory synapses. Overexpression of Slitrk1 and Slitrk2 in hippocampal neurons increased the number of synaptic contacts on these neurons. Furthermore, decreased expression of Slitrk1 in hippocampal neurons led to a reduction in the number of excitatory, but not inhibitory, synapses formed in hippocampal neuron cultures. In addition, we demonstrate that different leucine rich repeat domains of the extracellular region of Slitrk1 are necessary to mediate interactions with Slitrk binding partners of the LAR receptor protein tyrosine phosphatase family, and to promote dimerization of Slitrk1. Altogether, our results demonstrate that Slitrk family proteins regulate synapse formation.

IV. Introduction

One of the key steps in the development of the nervous system is the formation of new connections between different neurons. This process, referred to as synaptogenesis, also plays a critical role in the mature brain where the dynamic modification of circuitry has a profound effect on functions such as learning and memory. Multiple families of cell adhesion molecules have been implicated in various aspects of synapse formation, such as the formation of initial contacts and synapse maturation. Members of the Neuroligin (Ichtchenko et al., 1995; Scheiffele et al., 2000), Neurexin (Ichtchenko et al., 1995; Graf et al., 2004), LRRTM (DeWit et al., 2009; Ko et al., 2009; Linhoff et al., 2009), synaptic cell adhesion molecule (SynCAM) (Biederer et al., 2002; Robbins et al., 2010), Netrin G-ligand (NGL) (Kim et al., 2006), SALM (Mah et al., 2010), and EphB (Kayser et al., 2006) families of cell surface proteins are examples of such molecules involved in these processes. It has been suggested that defects in neural connectivity or synaptic patterning underlie many neurodevelopmental disorders including autism and schizophrenia (Wright and Washbourne, 2011). For example, familial forms of autism-spectrum disorders have been linked to mutations in Neuroligin and Neurexin (reviewed by Bourgeron, 2009) as well as in SynCAM and Cadherin (Zhiling et al., 2008; Wang et al., 2009). Another family of transmembrane proteins that has been implicated in the etiology of brain disorders is the Slitrks. *SLITRK1* was proposed as a susceptibility gene for Gilles de la Tourette Syndrome (Abelson et al., 2005; Zimprich et al., 2008; Miranda et al., 2009) and for the OCD spectrum disorder trichotillomania (Züchner et al., 2006; Chattopadhyay and Chatterjee, 2012), while variants of the *SLITRK2* gene have been found in patients with schizophrenia (Piton et al., 2011). Mutations in Slitrk6 have been associated with myopia and deafness, and Slitrk family members may also associate with bipolar disorder (Smith et al., 2009; Greenwood et al., 2013; Tekin et al., 2013).

The Slitrks form a family of six structurally similar proteins that contain two leucine-rich repeat (LRR) domains in their extracellular portion and a cytoplasmic region that varies in size between members of the family (Aruga and Mikoshiba, 2003). LRR domains are protein-protein interaction regions commonly found in synaptogenic proteins (Ko and Kim, 2007). Despite some overlap in their expression, the Slitrks display mostly distinct patterns of expression in the developing murine nervous system suggesting they may play specific roles in different regions of the brain (Beaubien and Cloutier, 2009). In keeping with this possibility, gene ablation studies in mice for different Slitrk family members have yielded distinct phenotypes. While ablation of *Slitrk1* leads to increased anxiety-like behaviour (Katayama et al., 2010), *Slitrk5* mutant mice display obsessive compulsive-like behaviors (Shmelkov et al., 2010), and *Slitrk3* mutant mice exhibit increased susceptibility to seizures (Takahashi et al., 2012). In contrast, *Slitrk6*-knockout mice display specific defects in development of the inner ear, including disorganized innervation and neuronal loss (Katayama et al., 2009). Based on the structure of Slitrks and the nature of phenotypes observed in some Slitrk mutant mice, Slitrks were proposed to regulate synapse formation in the central nervous system. Recent evidence has shown that Slitrk3 is specifically required for the formation of inhibitory synapses both *in vitro* and *in vivo*, and that other members of the Slitrk family can promote excitatory synapse formation (Linhoff et al., 2009; Takahashi et al., 2012; Yim et al., 2013).

Here we have examined the function of two members of the Slitrk family, Slitrk1 and Slitrk2, in synapse formation. We show that Slitrk1 is preferentially localized to excitatory synapses. Overexpression of Slitrk1 or Slitrk2 can promote the formation of both excitatory and inhibitory synapses in cultures of hippocampal neurons. However, inhibition of Slitrk1 expression reduces the number of excitatory, but not inhibitory, synapses formed between hippocampal neurons in

culture. We also demonstrate that the first LRR domain of Slitrk1 mediates interactions with the receptor tyrosine phosphatase PTPδ, while the second LRR domain is necessary for dimerization of Slitrk1 at the cell surface. Taken together, our results demonstrate that Slitrk1 and Slitrk2 contribute to synapse formation and suggest that dimerization of Slitrk family members could be implicated in this process.

V. Results

1. Slitrk1 is preferentially localized at excitatory synapses.

The Slitrks are predominantly expressed in neural tissues at embryonic ages and postnatally (Aruga and Mikoshiba, 2003; Aruga et al., 2003; Beaubien and Cloutier, 2009). More specifically, their localization at the synapse has been recently suggested based on the presence of tagged recombinant versions of these proteins at synaptic sites in cultured neurons. While Slitrk3 was localized to inhibitory synapses, other members of the Slitrk family appear localized to excitatory synapses (Shmelkov et al., 2010; Takahashi et al., 2012; Yim et al., 2013). To examine whether endogenous Slitrk1 is found at excitatory or inhibitory synapses, dissociated hippocampal neuron cultures were immunostained with an antibody against the Slitrk1 extracellular N-terminal region (Slitrk1-N) that does not recognize other Slitrk family members (Fig. 1a,b,e). In confocal images of these neurons, Slitrk1 signal was detected in a punctate pattern on hippocampal processes with a majority of these puncta colocalizing with VGLUT1- and PSD-95-positive excitatory synapses (Fig. 1a). A large proportion of VGLUT1- and PSD-95-positive clusters (57.23 ± 4.76%) were apposed to Slitrk1-positive puncta, while only 16.74 ± 4.09% of VGAT- and Gephyrin-positive clusters overlapped with Slitrk1 puncta (Fig.1a–c). To further characterize the localization of Slitrk1 at the synapse, we examined its distribution in subcellular fractions generated from 3-4-week-old mouse hippocampi using a specific antibody against the intracellular domain of Slitrk1

(Slitrk1-C). These analyses revealed that a portion of Slitrk1 protein is found in synaptic membrane fractions (Fig. 1d). As previously described, expression of Slitrk1 in an heterologous cell system leads to the detection of two closely migrating bands that likely represent differentially glycosylated forms of Slitrk1 (Fig. 1e) (Kajiwara et al., 2009). The Slitrk1-C and Slitrk1-N antibodies we have generated detect both forms of Slitrk1 proteins, but not other members of the Slitrk family (Fig. 1e). Taken together, our results indicate that Slitrk1 is localized to synapses and may thus play a role in synaptogenesis.

Figure 1: Localization of Slitrk1 at the synapse.

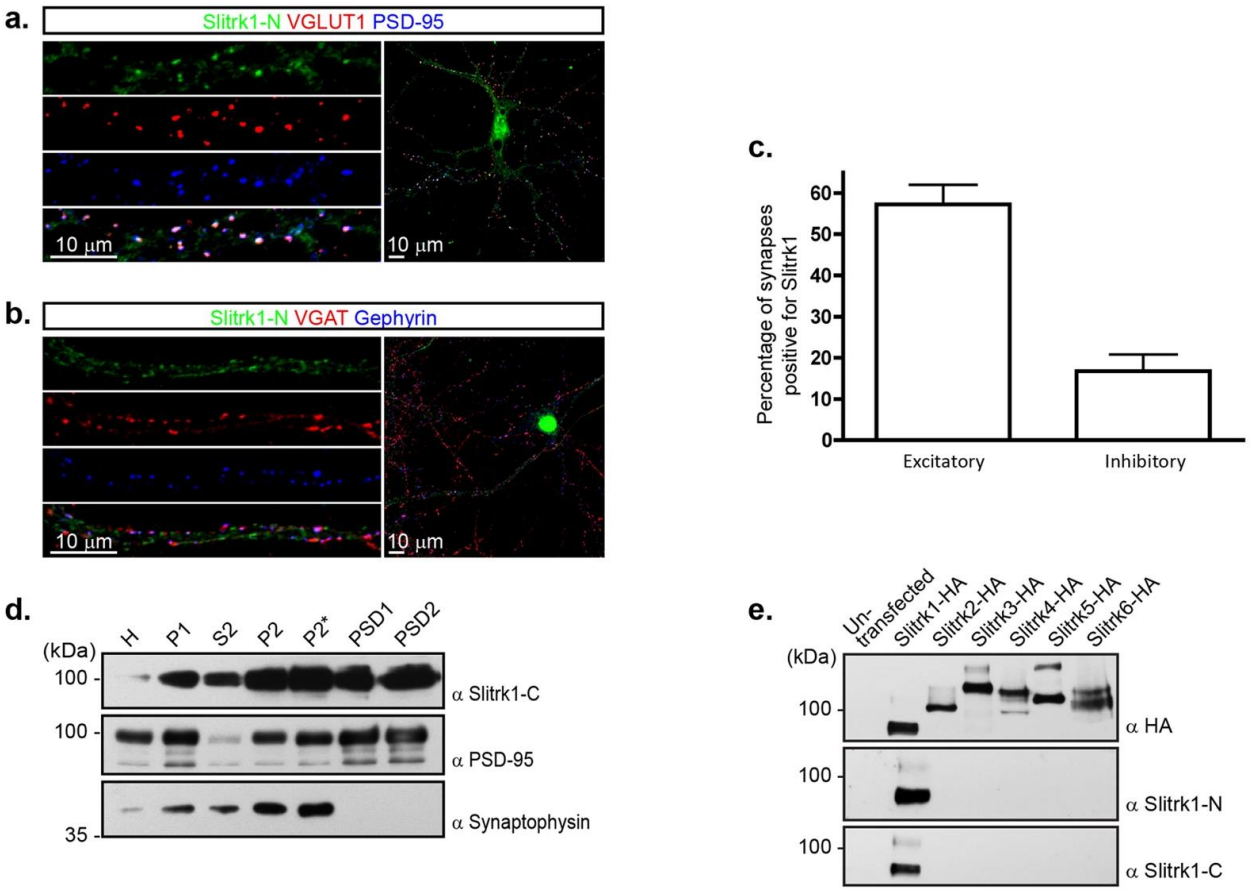

(a,b) Subcellular localization of Slitrk1 in dissociated hippocampal neurons. Neurons at DIV15 were fixed and stained for Slitrk1-N (N-terminal antibody, *green*) with pre- (*red*) and post-synaptic (*blue*) excitatory **(a)** or inhibitory **(b)** markers. Slitrk1 staining is punctate and colocalizes mostly with excitatory synaptic puncta, as well as some inhibitory synaptic puncta. **(c)** Quantification of average number of Slitrk1-positive synapses per neuron. Mean ± s.e.m.: Excitatory, 57.23 ± 4.76, n = 6 neurons; Inhibitory, 16.74 ± 4.09, n = 5 neurons. Endogenous Slitrk1 localizes mainly to excitatory synapses in cultured hippocampal neurons. **(d)** Distribution of Slitrk1 in subcellular fractions of hippocampi isolated from 3-4-week old mouse brain. Note that Slitrk1 is detected in synaptic fractions including P2, P2* and the postsynaptic densities (PSD). PSD-95 and synaptophysin were probed for comparison. H, homogenate; P1, crude nuclear fraction; S2, supernatant after P2 precipitation; P2, crude synaptosomes; P2*, purified synaptosomes; PSD1, pellet after the first Triton X-100 extraction; PSD2, pellet after the second Triton X-100 extraction. **(e)** Characterization of Slitrk1 antibodies. Lysates of HEK293T cells expressing HA-tagged Slitrk family proteins were immunoblotted with Slitrk1-C (C-terminal antibody), Slitrk1-N and HA antibodies. Slitrk1 antibodies specifically recognize Slitrk1.

2. Overexpression of Slitrk1 and Slitrk2 in neurons increases synapse density.

To determine whether Slitrk1 and another Slitrk family member, Slitrk2, can promote synaptic differentiation in neurons, we overexpressed Slitrk1 or Slitrk2 in hippocampal neurons. Cultured hippocampal neurons were transfected at 13 days *in vitro* (DIV) with two different amounts of vector DNA (1μg or 2μg) expressing either EGFP, or EGFP-tagged Slitrk1 or Slitrk2. Cultures were immunostained two days later with antibodies against markers of glutamatergic excitatory synapses, VGLUT1 and PSD-95, or against markers of inhibitory GABAergic synapses, VGAT and Gephyrin, and the number of synapses was quantified. In agreement with previously published observations (Yim et al., 2013), overexpression of either Slitrk1 or Slitrk2 induced a robust increase in excitatory synaptic differentiation in contacting axons, as measured by the number of VGLUT1-PSD-95 clusters (Fig. 2a,c). In contrast to previous observations where overexpression of Slitrk1 and Slitrk2 did not have an effect on inhibitory presynaptic differentiation (Yim et al., 2013), we observed a significant increase in the number of inhibitory synaptic contacts as measured by the number of VGAT-Gephyrin-positive clusters (Fig. 2b,d, *grey bars*) on hippocampal dendrites. However, this effect appeared to be dependent on high levels of overexpression of Slitrk1 or Slitrk2 as transfecting these neurons with smaller amounts EGFP-tagged Slitrk1- or Slitrk2-expressing vectors led to increased numbers of excitatory, but not inhibitory, synapses (Fig. 2b,d, *white bars*). Hence, overexpression of either Slitrk1 or Slitrk2 can promote the formation of excitatory synapses in dissociated hippocampal cultures. Furthermore, they are capable of promoting inhibitory synapse formation when expressed at high enough levels.

Figure 2: Overexpression of Slitrk1 and Slitrk2 in cultured neurons increases the amount of presynaptic excitatory and inhibitory contacts.

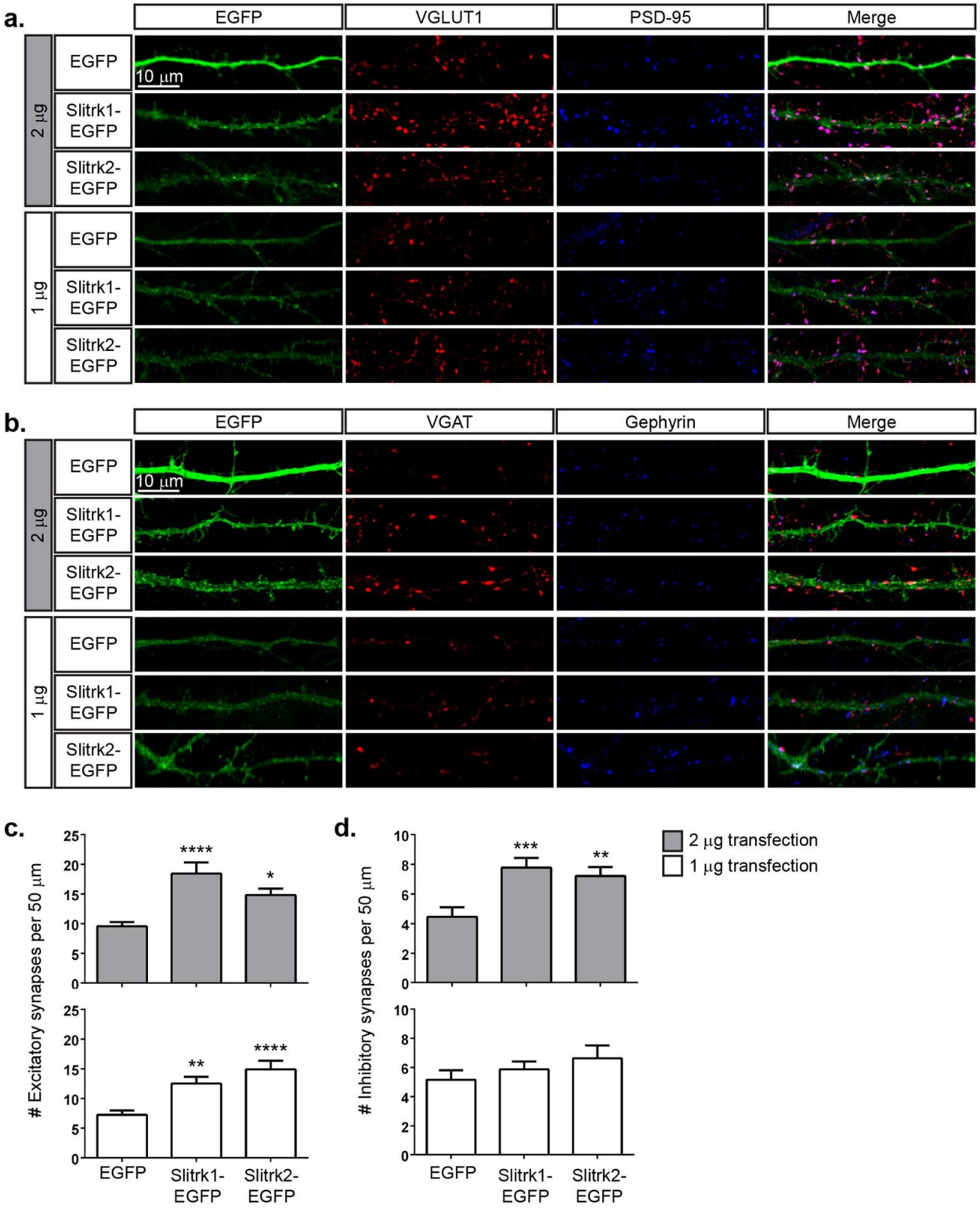

(a,b) Cultured hippocampal neurons were transfected with either 1 or 2 μg of EGFP alone, Slitrk1 EGFP, or Slitrk2 EGFP at 13 DIV and immunostained for VGLUT1/PSD-95 **(a)** or VGAT/Gephyrin **(b)** at 15 DIV. **(c,d)** Quantification of the results from **(a,b)** respectively. **(c)** Average number of excitatory synapses per 50 μm, for 2 μg and 1 μg transfections Mean ± s.e.m. (Vector EGFP 2 μg, 9.58 ± 0.710, n = 36; Slitrk1 EGFP 2 μg, 18.47 ± 1.859, n = 36; Slitrk2 EGFP 2 μg, 14.83 ± 1.069, n = 36; From 3 separate experiments; ****$p < 0.0001$ *$p < 0.05$, One-way ANOVA and Vector EGFP 1 μg, 7.26 ± 0.745, n = 23; Slitrk1 EGFP 1 μg, 12.52 ± 1.142, n = 23; Slitrk2 EGFP 1 μg, 14.92 ± 1.473, n = 24; From 2 separate experiments; **$p < 0.01$ ****$p < 0.0001$ One-way ANOVA). **(d)** Average number of inhibitory synapses per 50 μm, for 2 μg and 1 μg transfections Mean ± s.e.m. (Vector EGFP 2 μg, 4.47 ± 0.642, n = 36; Slitrk1 EGFP 2 μg, 7.78 ± 0.649, n = 36; Slitrk2 EGFP 2 μg, 7.22 ± 0.600, n = 36; From 3 separate experiments; ***$p < 0.001$ **$p < 0.01$ One-way ANOVA and Vector EGFP 1 μg, 5.171 ± 0.646, n = 35; Slitrk1 EGFP 1 μg, 5.889 ± 0.533, n = 36; Slitrk2 EGFP 1 μg, 6.64 ± 0.876, n = 36; From 3 separate experiments; ns, $p > 0.05$ One-way ANOVA).

3. Knockdown of Slitrk1 reduces synapse number in hippocampal neuron cultures.

To test whether endogenous Slitrk1 is required for excitatory or inhibitory synapse formation, we used RNA interference to knock down expression of Slitrk1 in hippocampal neurons. We generated two lentiviral vectors expressing individual shRNAs targeting Slitrk1 and infected dissociated hippocampal neuron cultures. These two independent shRNA constructs reduced the expression of endogenous Slitrk1 by 82.7% and 70.5% in hippocampal neurons (Fig. 3a,b). Knockdown of Slitrk1 significantly reduced the number of VGLUT1- and PSD-95-positive excitatory synapses (Fig. 3c,e) but did not affect the number of VGAT- and Gephyrin-positive inhibitory synapses (Fig. 3d,f), indicating that Slitrk1 specifically contributes to excitatory synapse differentiation.

Figure 3: Knockdown of Slitrk1 by shRNA in cultured neurons reduces synapse density.

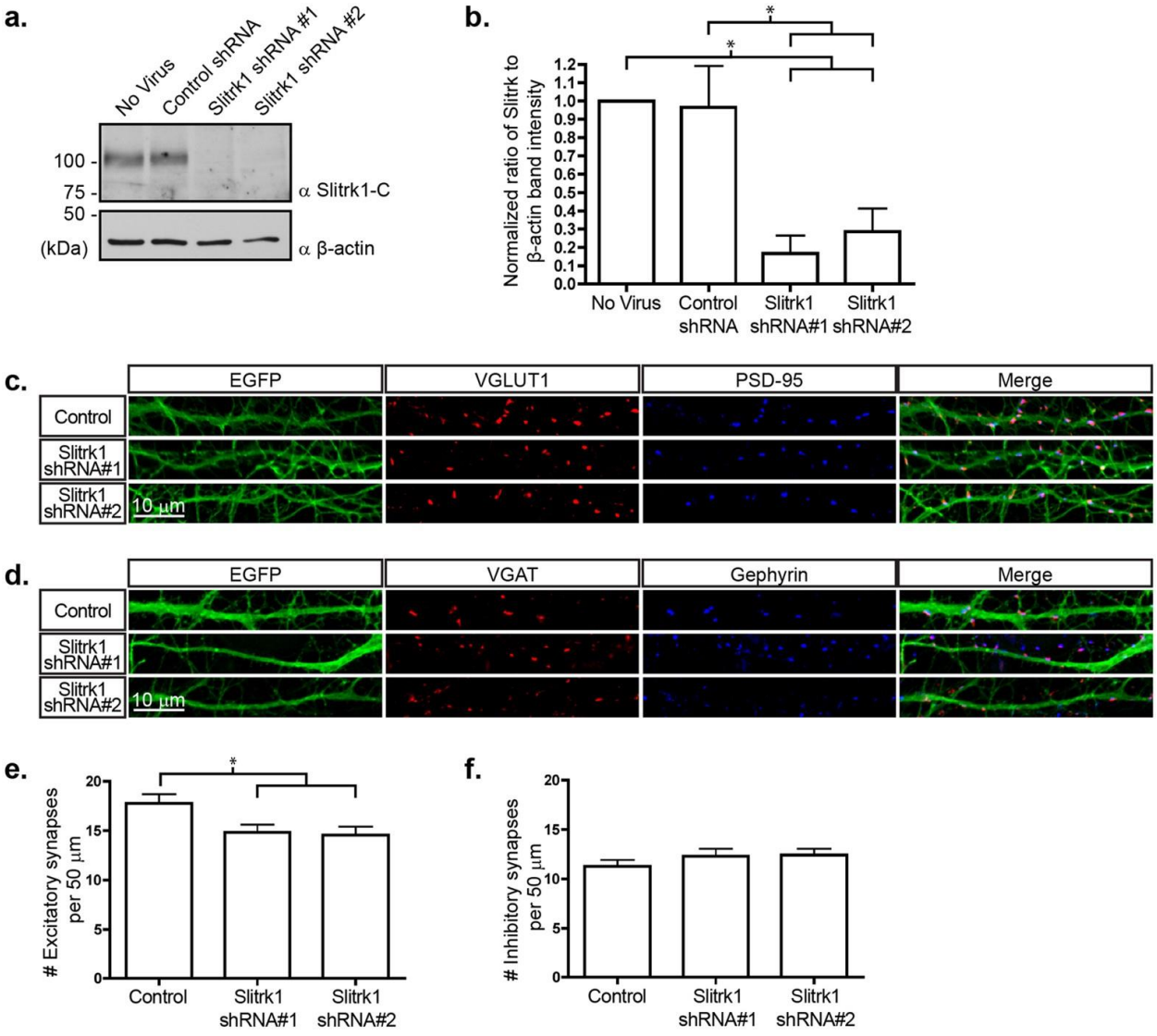

Hippocampal neurons in culture were infected at 3 DIV with Slitrk1-shRNA lentivirus. At 10–11 DIV, cell lysates were immunoblotted for Slitrk1 to test knockdown. **(a)** Western blot analysis of Slitrk1 knockdown efficiency by shRNA #1 and #2. **(b)** Quantification of knockdown efficiency. Ratio of Slitrk1 to β-Actin band intensity normalized to untreated cells. Mean ± s.e.m. (Untreated, 1 ± 0.00; Control shRNA, 0.966 ± 0.226; Slitrk1 shRNA #1, 0.167 ± 0.098; Slitrk1 shRNA #2, 0.285 ± 0.128; From 3 separate experiments; *$p < 0.05$, One-way ANOVA). **(c,d)** Cultured hippocampal neurons were infected with Control, Slitrk1 shRNA #1 or Slitrk1 shRNA #2 at 3 DIV and immunostained at 10–11 DIV for VGLUT and PSD-95 (**c**) or VGAT and Gephyrin **(d)** to label excitatory or inhibitory synaptic puncta, respectively. **(e)** Average number of excitatory synapses per 50 μm, Mean ± s.e.m. (Control siRNA, 17.76 ± 0.96 $n = 75$; Slitrk1 siRNA #1, 14.84 ± 0.781 $n = 80$; Slitrk1 siRNA #2, 14.56 ± 0.857 $n = 73$; From 5 separate experiments; *$p < 0.05$, One-way ANOVA). **(f)** Average number of inhibitory synapses per 50 μm, Mean ± s.e.m. (Control siRNA,

11.28 ± 0.649 n = 47; Slitrk1 siRNA #1, 12.31 ± 0.760 n = 36; Slitrk1 siRNA #2, 12.42 ± 0.629 n = 33; Done in 3 separate experiments; One-way ANOVA).

4. The second leucine-rich repeat of Slitrk1 is necessary for its homophilic interaction at the cell surface.

The extracellular region of Slitrk1 contains two leucine-rich repeats, which are domains that can mediate protein-protein interactions and dimerization of cell surface receptors (Bella et al., 2008; Kajander et al., 2011). To examine whether Slitrk1 molecules can interact in *cis* at the cell surface, we used a chemical cross-linking approach to promote the maintenance of *cis*-interacting complexes at the plasma membrane. V5-tagged Slitrk1 was expressed in HEK293T cells, and native plasma membrane complexes were preserved through covalent cross-linking. The SDS-PAGE migration of Slitrk1 corresponded to two bands at molecular weights of approximately 85 and 120kDa. While the band migrating at 120kDa represents the mature form of Slitrk1 expressed at the surface (Fig. 4a), the lower molecular weight band likely represents an immature form of Slitrk1 (Kajiwara et al., 2009). After cross-linking, the majority of Slitrk1 immunoreactivity appeared as a single band corresponding to an approximate molecular weight of 260kDa, suggesting that it may be composed of Slitrk1 homodimers (Fig. 4a, *arrowhead*). Furthermore, V5- and Myc-tagged Slitrk1 molecules can be co-immunoprecipitated from lysates of HEK293T cells expressing these two proteins (Fig. 4b). Taken together, these two results indicate that Slitrk1 molecules have the ability to interact with each other at the cell surface, possibly forming homodimers.

Since leucine-rich repeats have been implicated in the dimerization of cell surface receptors, we examined the requirement of the two LRR domains of Slitrk1 for this interaction. V5-tagged Slitrk1 molecules containing deletions of either the first (Slitrk1ΔLRR1) or second (Slitrk1ΔLRR2) LRR domains (Fig. 5a) were expressed in HEK293T cells with a Myc-tagged full-length Slitrk1 to perform co-immunoprecipitation experiments. Both Slitrk1 deletion proteins were expressed at the cell surface at similar levels to the wild-type Slitrk1 (Fig. 5b). While deletion of

the first LRR domain did not affect the co-immunoprecipitation of this mutant with Slitrk1, we observed a robust decrease in the interaction of Slitrk1ΔLRR2 with Slitrk1, indicating that the second LRR contributes to Slitrk1-Slitrk1 interactions (Fig. 5c). Interestingly, removal of the second LRR did not affect the binding of Slitrk1 to PTPδ in a cell binding assay, indicating that improper folding of this deletion mutant is unlikely to account for the lack of interaction with full length Slitrk1 (Fig. 5d). In contrast, removal of the first LRR prevented Slitrk1 binding to PTPδ, confirming this previously published observation (Fig. 5d) (Yim et al., 2013). Taken together, these results demonstrate that Slitrk1 can form homodimers at the cell surface and that the LRR2 domain is necessary for this interaction to take place.

Figure 4: Slitrk1 molecules have the ability to interact at the cell surface.

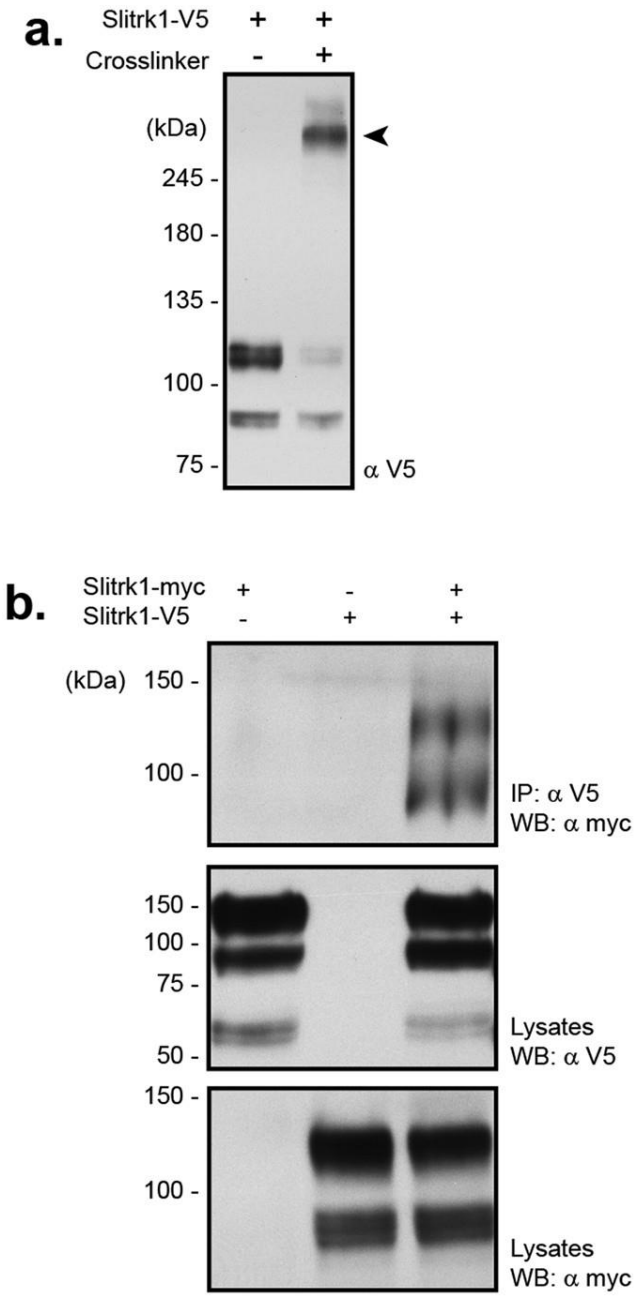

(a) Slitrk1 exists in a complex at the cell surface. Western blot of cross-linked (+) or mock-treated (−) HEK293T cells transfected with Slitrk1-V5. Cross-linked sample reveals a protein complex containing Slitrk1-V5 that migrates above 245kDa (*arrowhead*). **(b)** Slitrk1 forms homophilic complexes. HEK293T cells were transfected with either Slitrk1-V5 alone, Slitrk1-myc alone, or co-transfected with both tagged vectors. Protein lysates were immunoprecipitated with V5 antibodies and western blots were performed using myc and V5 antibodies. These results indicate that Slitrk1 can form homophlic complexes when expressed in HEK293T cells. IP, Immunoprecipitation; WB, Western Blot.

Figure 5: Determination of the LRR domain required for homophilic binding

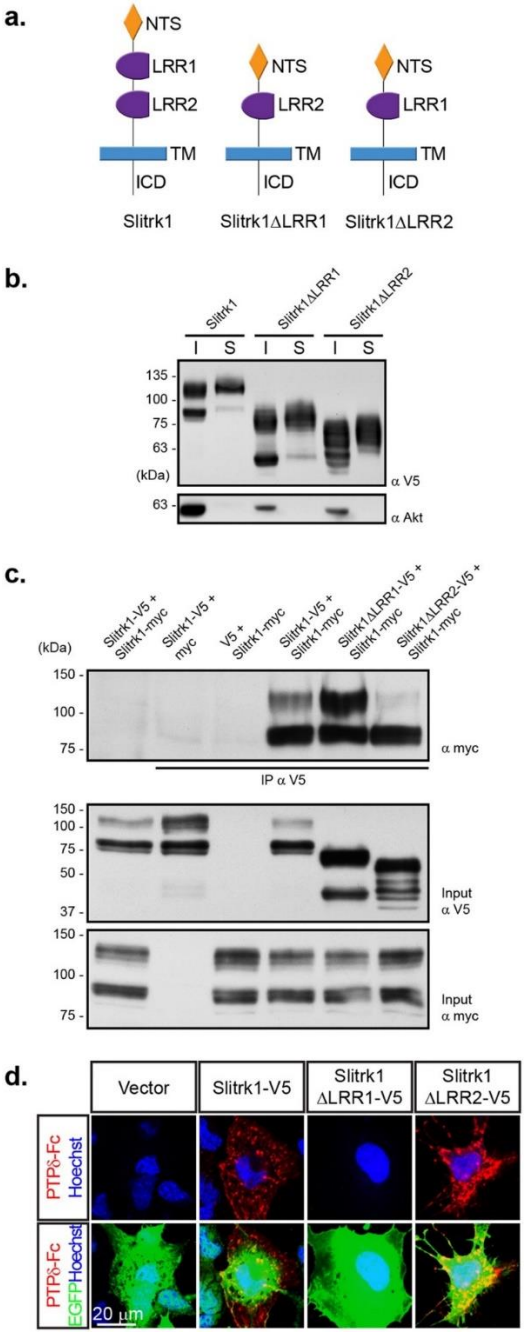

(a) Diagram of Slitrk1 mutant constructs. Mutants, Slitrk1ΔLRR1 and SlitrkΔLRR2, are missing the coding region for leucine-rich repeat domain 1 and 2, respectively. Full length and mutant constructs are C-terminally V5-tagged. NTS, n-terminal sequence; LRR, Leucine-rich repeat domain; TM, Transmembrane domain; ICD, intracellular domain. **(b)** Expression of full length and mutant V5-tagged Slitrk1 protein at the cell surface. COS cells were transfected with Slitrk1-V5 or mutant variants. Cell-surface proteins were isolated by incubating cells with biotin, followed by immunoprecipitation with avidin-conjugated beads. Biotinylated cell surface Slitrk1-V5 was

detected by blotting with a V5 antibody. The intracellular protein Akt was not detected in these immunoprecipitates. Expression of the Slitrk1 mutants at the cell surface is similar to that of full length Slitrk1. I, Input; S, Surface protein. **(c)** Analysis of interaction between Slitrk1 full length and mutant constructs by co-immunoprecipitation. HEK293T cells were either transfected with Slitrk1-myc or Slitrk1-V5 alone, or co-transfected with Slitrk1-myc and one of the Slitrk1-V5 full length or mutant constructs. Lysates were immunoprecipitated with V5 antibodies and blotted with myc and V5 antibodies. These results indicate that the LRR2 domain of Slitrk1 is required for homophilic Slitrk1 interactions. **(d)** Cell surface binding assay performed on COS cells transfected with V5-tagged Slitrk1 variants. Cells were treated with purified PTPδ-Fc protein and analyzed by immunofluorescence for PTPδ-Fc binding (red) and V5 (green). These results demonstrate that the LRR1 is required for the binding of PTPδ to Slitrk1.

VI. Discussion

Members of the Slitrk family of proteins have been implicated in the etiology of multiple neuropsychiatric disorders (Abelson et al., 2005; Züchner et al., 2006; Zimprich et al., 2008; Miranda et al., 2009; Smith et al., 2009; Piton et al., 2011; Chattopadhyay and Chatterjee, 2012; Greenwood et al., 2013). Here, we show that Slitrk1 is present in postsynaptic density fractions isolated from mouse hippocampi and that Slitrk1 is preferentially localized to excitatory synapses in hippocampal neurons, supporting a role for these proteins in regulating synapse formation. We also demonstrate that overexpression of Slitrk1 or Slitrk2 in hippocampal neurons promotes the formation of both excitatory and inhibitory synapses, which is consistent with the previously reported observation that Slitrk1 can promote presynaptic clustering of both VGLUT1 and VGAT in a mixed-culture assay (Takahashi et al., 2012). However, considering that Slitrk1 is preferentially localized at excitatory synapses (Fig. 1a–c) and that its overexpression has been shown to specifically enhance the formation of excitatory synapses (Yim et al., 2013), it is somewhat surprising that we also observe an increase in inhibitory synapse formation in our experiments. It is therefore likely that the enhanced number of inhibitory synapses we observe in these neuronal cultures results from high overexpression of Slitrk1 in our system leading to its ectopic localization to inhibitory synapses. In keeping with this possibility, transfecting hippocampal neurons with lower amounts of EGFP-tagged Slitrk1 vector promotes formation of excitatory synapses but not inhibitory synapses (Fig. 2). Decreased expression of Slitrk1 in hippocampal neurons reduced the number of excitatory, but not inhibitory, synapses formed, demonstrating that endogenous Slitrk1 specifically contributes to excitatory synapse formation (Fig. 3). Taken together, our observations and previously published results indicate that Slitrk1 has

the potential to promote presynaptic differentiation of both excitatory and inhibitory synapses, but that its localization restricts its effect to excitatory synapses.

Slitrk3 has been identified as a specific inducer of inhibitory presynaptic differentiation by binding to the receptor protein tyrosine phosphatase, PTPδ, on the presynaptic side of the cleft (Takahashi et al., 2012). Ablation of *Slitrk3* in mice leads to specific reductions in both inhibitory synapse density and synaptic transmission in the hippocampus (Takahashi et al., 2012). In contrast to the specific role that Slitrk3 plays in regulating inhibitory synapse formation, other Slitrk family members have been shown to modulate excitatory synapse formation by interacting with PTPσ (Yim et al., 2013). Our results demonstrate for the first time that endogenous Slitrk1 proteins are localized to excitatory synapses and confirm that Slitrk1 contributes to the formation of these synapses *in vitro*.

The presence of two LRR domains in the extracellular region of Slitrk molecules suggests that protein-protein interactions play a critical role in their functions. Indeed, the most N-terminal LRR domain (LRR1) of Slitrk1 is essential to mediate its interaction in *trans* with RPTPs and for its ability to promote synapse formation (Fig. 5d) (Um et al., 2014). Interestingly, this domain is also necessary for the interaction of another Slitrk family member, Slitrk5, with a cell surface receptor in *cis* to regulate its cell surface expression. The LRR1 domain of Slitrk5 was recently shown to mediate interactions with the receptor tyrosine kinase TrkB and to regulate its trafficking inside the cell. The binding of BDNF to TrkB promotes an interaction between Slitrk5 and TrkB, outcompeting PTPδ binding (Song et al., 2015a). In contrast to the LRR1 domain, binding partners for the second LRR2 domain of Slitrks remain to be identified. Our observation that Slitrk1 molecules can form complexes at the cell surface through interactions between their LRR2 domains when expressed in HEK293T cells suggests that other Slitrk family members may also

be capable of forming homodimers at the surface. While it remains unclear whether dimerization of Slitrk1 is required for its function at the synapse, dimerization and lateral interactions of other synaptogenic proteins have been implicated in their ability to promote synapse formation (Fogel et al., 2011; Shipman and Nicoll, 2012). For example, the dimerization of Neuroligin is necessary for its synaptogenic activity and has been proposed to regulate the trans-synaptic clustering of Neurexin in the presynaptic terminal during synapse assembly (Shipman and Nicoll, 2012). While dimerization of Slitrk1 does not appear to be necessary for its binding to PTPδ (Fig. 5d), it may serve to promote the lateral assembly of LAR-RPTP-Slitrk complexes that has been proposed to take place at the synapse (Um et al., 2014). Future studies should shed light on the role of Slitrk1 dimerization through LRR2 for its function at the synapse.

VII. Materials and Methods

1. cDNA constructs

Full-length human *Slitrk1* (aa 1–696) and human *Slitrk2* (aa 1–845) were sub-cloned into the pEGFP-N1 vector (Clontech). For C-terminal V5- or MYC-tagged Slitrk1 constructs, full-length human *Slitrk1* (aa 1–696) was sub-cloned into the pcDNA3.1 MYC-His A vector and the pcDNA3.1 V5-His A vector (Invitrogen), respectively. *Slitrk1* mutants lacking either of the LRR domains (*Slitrk1ΔLRR1* (Δ aa 18–264) and *Slitrk1ΔLRR2* (Δ aa 304–599)) were also each sub-cloned into the pcDNA3.1 V5-His A vector. For knockdown of Slitrk1 in hippocampal neurons, shRNA sequences targeting nucleotides against rat Slitrk1 (Target #1: nucleotides 1222–1242; Target #2: nucleotides 2214–2234) were cloned into pcDNA6.2/GW-EmGFP-miR plasmid (gifted by Dr. Peter S. McPherson). PTPδ-Fc and HA-tagged Slitrk1 to Slitrk6 constructs were gifted to us by Dr. Hideto Takahashi and Dr. Ann Marie Craig, respectively.

2. Antibodies

A rabbit polyclonal antibody recognizing the intracellular portion of Slitrk1 (referred to as Slitrk1-C) was generated against the peptide DGSHRVYDCGSHS (aa 680–693 of the mouse sequence) and purified against the same epitope. Another Slitrk1 rabbit polyclonal antibody (namely Slitrk1-N) was obtained from an animal immunized with the complete extracellular portion of the protein (aa 2–600). The other antibodies were obtained commercially; Akt (rabbit, New England Biolabs); β-Actin (mouse, Abcam); Gephyrin (mouse, SynapticSystems); GFP (rabbit, Invitrogen); HA (mouse, Sigma); myc (goat, Abcam); PSD-95 (mouse, NeuroMab); Synaptophysin (Mouse, SynapticSystems); V5 (rabbit, Invitrogen); VGAT (guinea pig, SynapticSystems); VGLUT1 (guinea pig, SynapticSystems).

3. Cell culture

All procedures involving the use of animals were approved by the animal care committee of the Montreal Neurological Institute and performed in accordance with the approved guidelines. Embryonic day (E) 18-19 rat embryos were obtained from Sprague Dawley females (Charles River). Cultures of hippocampal neurons were prepared from the embryos according to previously described protocols (Kaech and Banker, 2006). Briefly, hippocampi were isolated from the embryos, Cells were trypsinized for 15–20 minutes in 0.25% Trypsin-EDTA (gibco, Life Technologies), washed in Neurobasal media (Invitrogen, Life Technologies) supplemented with L-Glutamine (gibco, Life technologies), Pen/Strep (gibco, Life technologies), and B-27 (gibco, Life Technologies), triturated using flamed glass pasteur pipettes, and then plated onto Poly-L-lysine-coated (Sigma) coverslips (Fisherbrand, 12CIR-1D) in 24-well plates and grown at 37°C, 5% CO2.

4. Slitrk1 knockdown

Lentiviral shRNA vectors targeting Slitrk1 contained the following nucleotide sequences: Slitrk1shRNA#1, 5′-AGCACCCTACCTGCTAATGTA-3′; Slitrk1shRNA#2, 5′-TAAGCTCAG TCTGCACAATAA-3′. Lentiviral vectors and virus was produced according to Allaire et al. (Allaire et al., 2010). Oligonucleotide sequences targeting Slitrk1 were cloned into the lentiviral expression vector pRRLsinPPTeGFP. HEK293T cells were then transfected with this vector, together with pMD2.g and pRSV-Rev and pMDLg/pRRE which encode necessary viral genes. Media was collected at 24, 36, and 48hrs post-transfection and concentrated by centrifugation. Hippocampal neurons were infected at 3 DIV with control or shRNA lentivirus and were either fixed for immunostaining or lysed at 10–11 DIV. Knockdown efficiency was verified by Western blotting of hippocampal neuron lysates with the Slitrk1-C antibody.

5. Transfection and immunocytochemistry

HEK cells and cultured hippocampal neurons were transfected using Lipofectamine2000 Reagent (Invitrogen, Life Technologies). For HEK cell transfections, DNA to Lipofectamine2000 ratios were used as recommended by manufacturer's guidelines. Cultured neurons were transfected at 13 DIV for 15 minutes with 1 or 2μg DNA and 0.5μL Lipfectamine2000 per well. Cells were fixed with 4% paraformaldehyde/4% sucrose (vol/vol) at 15 DIV, and permeabilized with 0.2% Triton X-100 (vol/vol) in phosphate-buffered saline (1×PBS, pH= 7.4). All cells undergoing immunocytochemistry were blocked in 5% FBS diluted in 1×PBS and then incubated with the appropriate primary antibodies overnight at 4°C, followed by Alexa-488-, Alexa-546-, Alexa-647-conjugated species-specific secondary antibodies (1:400; Invitrogen). Coverslips were mounted onto microscope slides using Fluoromount-G (Southern Biotech).

6. Image acquisition and quantification

Images were acquired using a confocal microscope with a 63× oil objective (LSM710; Zeiss). The settings were kept constant for all scanning in each experiment. The number of pre- and post-synaptic puncta were counted along 50μm lengths of axons. All values are presented as mean± s.e.m., and significance of the quantification was determined by ANOVA followed by Tukey's multiple comparisons test.

7. Production of PTPδ-Fc protein

Soluble PTPδ-Fc was purified as previously described (Takahashi et al., 2012). HEK293T cells were first transfected with the PTPδ-Fc plasmid. Secreted protein was purified by affinity chromatography using protein G-sepharose 4 Fast Flow beads (GE Healthcare), eluted with 100mM Glycine, pH 2.7 (immediately neutralized with 1M Tris pH 9.0), and concentrated using Amicon Ultra centrifugal filter units (30kDa cutoff, Millipore).

8. Cell surface binding assay

COS cells were grown on Poly-L-Lysine-coated coverslips and transfected with Slitrk1-V5 full length or mutant variants (Slitrk1ΔLRR1-V5 and Slitrk1ΔLRR2-V5), or the V5 vector alone as a control. Binding was performed as previously described (Takahashi et al., 2012). Cells were grown for 48 hours, then washed with extracellular solution (168mM NaCl, 2.4mM KCl, 20mM HEPES pH 7.4, 10mM D-glucose, 2mM $CaCl_2$, 1.3mM $MgCl_2$) with 200 ug/mL BSA (ECS/BSA). Cells were then treated with purified PTPδ-Fc for 1 hour at room temperature and fixed for 12 minutes in 4% paraformaldehyde (PFA) in 1×PBS. After blocking in 3% BSA, 5% FBS in 1×PBS, cells were incubated with Alexa546-conjugated Donkey anti-Human IgG for one hour at room temperature, stained for nuclei using Hoechst 33342 (1:7500, Molecular probes), and mounted onto microscope slides using Fluoromount-G (Southern Biotech).

9. Crosslinking

HEK293T cells were transfected with full length V5-tagged Slitrk1 plasmid. 48 hours post-transfection, cells were treated with 1.0mM bis[sulfosuccinimidyl] suberate (BS3, Thermo Scientific) for 30 minutes at 4°C. Cross-linker reaction was quenched with 15mM Tris pH 8.0 for 15 minutes at RT. Cells were then lysed in lysis buffer (1% SDS, 5mM EDTA, 50mM Tris, 150mM NaCl), sonicated and run on an SDS-page gel for Western Blotting analysis using the V5 antibody.

10. Synaptosomal fractionation

PSD fractionation was performed on hippocampi isolated from 3-4-week-old mouse brain as described (Fallon et al., 2002) with some minor modifications: a purified P2 pellet was incubated in 0.5% Triton X-100, 40mM Tris-HCl (pH 8.0) and then centrifuged at 32,000×*g* to generate the PSD1 fraction. This fraction was then further extracted with 0.5% Triton X-100, 40mM Tris-HCl (pH 8.0), and subsequently centrifuged at 200,000×*g* to isolate the PSD2 fraction. Samples were subject to Western Blotting analysis.

11. Cell surface biotinylation

COS cells were transfected with the different plasmids for 48 hours, washed 3 times with 1× PBS, incubated with EZ-Link Sulfo-NHS-LC-Biotin 1mg/ml (Thermo Scientific Pierce) at 4°C for 30 minutes, and washed 3 times with 1×PBS + 100mM glycine to quench the biotin reagent. The cells were then lysed, and surface proteins were isolated using streptavidin agarose beads (Thermo Scientific Pierce) prior to running samples on an SDS-page gel for Western Blotting analysis.

12. Immunoprecipitation and Western Blotting

For immunoprecipitation, HEK293T cells were doubly transfected with Slitrk1-myc (full length Slitrk) as well as Slitrk1-V5 or V5-tagged Slitrk1 variants. 750μg cell lysates were incubated with anti-V5 for 2 hours at 4°C and then incubated with Protein A/G Plus Agarose beads (Santacruz) for 2 hours at 4°C. Beads were then washed and immunoprecipitate was eluted using sample buffer and β-mercaptoethanol and heated for 10 minutes at 95°C. Samples were run alongside initial protein lysate (input) on an SDS-page gel. Proteins were transferred onto PVDF membranes, blocked with 5% milk in 1×TBST (Tris Buffered Saline with Tween) before probing with antibodies.

Chapter 3:

Amigo1 is expressed specifically in ventrolateral olfactory epithelium but is dispensable for olfactory receptor neuron targeting in the mouse olfactory system

Reesha Raja[1,2], Emilie Dumontier[1], Alina Phen[1], Jean-François Cloutier[1,2,3]

1 Montreal Neurological Institute, Montreal, Quebec, Canada.
2 Integrated Program in Neuroscience, McGill University, Montreal, Quebec, Canada
3 Department of Neurology and Neurosurgery, McGill University, Montreal, Quebec, Canada

I. Preface

This chapter is in preparation for submission for publication. As discussed in Chapter 1, the process of axon guidance is complex, requiring integration of many guidance cues to allow for proper establishment of neuronal circuitry in a system consisting of billions of neurons (Stoeckli, 2018). However, mechanisms regulating the targeting of specific populations of neurons at a more precise level are still being elucidated. The main objective of this project was to identify new molecules and mechanisms of circuit formation in the main olfactory system of mouse. Here, we identify Amigo1 to be differentially expressed within the olfactory epithelium and find it dispensable for targeting of olfactory receptor neurons to the olfactory bulb.

II. Acknowledgements

We thank Dr. Donald Van Meyel and Dr. Timothy Kennedy and members of the Cloutier lab for helpful discussions on the development of this project.

We are grateful to Patrick Gendron (Institute for Research in Immunology and Cancer of the Université de Montréal) for bioinformatic analysis on the RNA sequencing data. We are thankful

to Dr. Heiki Rauvala and Dr. Zhihua Zou for cDNA clones and to Dr. Stefano Stifani for sharing antibody.

This work was supported by CIHR. J.-F.C. held an FRQ-S Senior Scholar Award. R.R. held a Vanier Studentship from CIHR.

III. Abstract

During development, billions of neurons connect to one another in a highly specified and precisely organized manner. Sensory systems provide a good example of this organization, whereby the composition of the outside world is represented in the brain by neuronal maps. Establishing correct patterns of neural circuity is crucial, as inaccurate map formation would lead to severe disruptions in sensory processing. In rodents, olfactory stimuli modulate a wide variety of behaviours, including predator avoidance and food foraging. The formation of the olfactory glomerular map is dependent on cues that guide olfactory receptor neuron axons to the olfactory bulb and on cell adhesion molecules that promote their sorting into specific synaptic units in this structure. Here, we investigate the role of the cell adhesion molecule Amigo1 in the precise targeting of olfactory receptor neurons to their targets on the olfactory bulb using a genetic loss-of-function approach in mice. We demonstrate that Amigo1 is expressed in a subpopulation of olfactory receptor neurons but is not required for proper axonal targeting of these neuronal processes. Interestingly, we observed that insertion of a neomycin resistance cassette in the Amigo1 locus, as part of the process of generating the Amigo1 null mouse line, leads to off-target effects, including altered expression of several additional genes and disruptions to the targeting of axons projecting from specific subsets of olfactory receptor neurons. Our results highlight the necessity of removing antibiotic resistance cassettes from genetic loss-of-function mouse models to prevent the study of phenotypes caused by off-target effects of the gene targeting procedure.

IV. Introduction

The nervous system is made up of an immensely complex network of neurons that must develop and connect to one another in intricate and precise patterns. The formation of these connections is essential for the establishment of sensory neural maps that provide a representation of the outside world. The development of olfactory maps is especially important for the interpretation of environmental and social cues necessary for survival in rodents. The mouse main olfactory system comprises the main olfactory epithelium (OE), housing primary olfactory receptor neurons (ORNs), expressing a single olfactory receptor gene from a repertoire of over 1000 genes (Buck and Axel, 1991; Chess et al., 1994; Ishii et al., 2001; Zhang and Firestein, 2002; Serizawa et al., 2003; Godfrey et al., 2004). Axons of ORNs expressing a given olfactory receptor (OR) project to the olfactory bulb (OB) where they coalesce into a small number of neuropil structures termed glomeruli, within which they synapse with dendrites of second order mitral and tufted cells for further codification of the olfactory signal and for higher order processing (Ressler et al., 1994a, 1994b; Vassar et al., 1994; Mombaerts et al., 1996). Most mature ORNs express a single type of OR, and each OR is expressed in a subset of cells located within a given subregion of the OE, which has been historically divided into four semi-overlapping regions along the dorsomedial to ventrolateral axis (Ressler et al., 1994b; Vassar et al., 1994; Sullivan et al., 1996; Miyamichi et al., 2005). More recently, the division of the OE has been shown to be more complex, with the classification of OR expression into nine zones (Zapiec and Mombaerts, 2020). Nevertheless, the mechanisms modulating OR gene choice and zonal expression remain poorly understood. Newly differentiated immature ORNs can express multiple ORs until a functional OR protein elicits the expression of downstream signalling molecules and activates negative feedback to repress gene expression of other ORs (Dalton et al., 2013). Islands of epigenetically marked OR enhancer

sequences in the genome can regulate the probability of a given OR or cluster of OR genes to be expressed and may contribute to zonal expression of ORs within the OE (Lomvardas et al., 2006; Degl'Innocenti and D'Errico, 2017; Monahan et al., 2019). From regulation of single OR gene expression in each ORN, to ORN maturation, axon guidance towards the bulb, and finally target selection of the appropriate glomerulus, a complex system of signalling molecules is necessary to ensure accuracy in map formation. Indeed, axons from over 1000 types of different ORN populations must self-organize and coalesce into roughly 2000 glomeruli on the OB. While several families of axon guidance molecules direct ORN axons to broad regions of the OB, cell adhesion molecules (CAMs) promote coalescence of these axons into specific glomeruli.

A few cell adhesion molecules belonging to the leucine-rich repeat (LRR) and Ig families of CAMs are implicated in ORN axon sorting into glomeruli at the level of the OB, such as Kirrels (Öztokatli et al., 2012; Vaddadi et al., 2019), ephrins (Cutforth et al., 2003; Serizawa et al., 2006), protocadherins (Hasegawa et al., 2008; Lee et al., 2008), and BIG-2 (Kaneko-Goto et al., 2008). These few molecules alone, however, are likely insufficient to regulate the organization of such a complex map. In an effort to identify additional molecules involved in accurate olfactory map development, we examined the involvement of the CAM Amigo1 in mouse olfactory system development. Amigo1 is one of three members of the Amigo family, which is a part of the LRR-domain containing super family of adhesion molecules. Of the three Amigo family members, Amigo1 expression is most restricted to the nervous system and it can promote axonal fasciculation and neurite outgrowth *in vitro* (Kuja-Panula et al., 2003). It has also been implicated in the regulation of axonal fasciculation of catecholaminergic neurons in zebrafish (Zhao et al., 2014). Interestingly, Amigo1 can regulate neuronal activity through association with the voltage-gated potassium channel Kv2.1, and it has been proposed to promote cell survival (Kajander et al., 2011;

Peltola et al., 2011, 2016; Chen et al., 2012; Bishop et al., 2018). The evidence for roles of Amigo1 in homophilic and heterophilic interactions, neurite outgrowth, and cell survival has led us to hypothesize that Amigo1 is involved in regulating the growth and targeting of ORN axons from the OE to the OB.

Here, we show that Amigo 1 expression is enriched in the ventrolateral region of the OE during development, but the mRNA expression of other Amigo family members could not be detected. While loss of Amigo1 expression in mice did not affect the development of the olfactory system, the targeted insertion of a neomycin expression cassette within the *Amigo1* allele selectively disrupted the development of ORNs in the ventrolateral region of the OE. Mice containing the neomycin cassette insertion showed reduced numbers of ORNs positive for ventrolaterally-expressed ORs, such as MOR28, and smaller glomeruli in the ventral part of the OB. These defects were specific to the ventrolateral region as ORN development in other regions of the OB was unaffected. These region-specific defects were associated with misregulation of gene expression in these mice, including several ORs, likely caused by the presence of the neomycin selection cassette in the *Amigo1* allele. Our results provide evidence that genomic insertion of a neomycin-resistance cassette can have region-specific effects on the development of ORNs and provides an additional cautionary tale of the effects of neomycin cassette-induced gene misregulation in the study of gene function through gene-targeting.

V. Results

1. Amigo1 is enriched in ventrolateral ORNs.

To begin to examine the function of Amigo1 in olfactory system development, we characterized the expression of Amigo family members in the main olfactory system of the mouse. *In situ* hybridization experiments using cRNA probes against *amigo1, amigo2* and *amigo3* were

performed on coronal sections of the olfactory epithelium (OE). While *amigo2* and *amigo3* had very low to no expression in the epithelium (Figure 1D,G), *amigo1* appeared to have enriched expression in the ventrolateral region of the OE at embryonic day (E) 16.5, when ORN axons are projecting to the OB (Figure 1A). This pattern of enriched expression persisted into early postnatal development at postnatal day (P) 7 (Figure 1J). To assess whether the enriched *amigo1* expression correlated with previously described zones of the OE (Miyamichi et al., 2005), we compared the expression of *amigo1* at P7 with the localization of region-specific ORN populations. The enriched expression of *amigo1* in the ventrolateral OE correlated with the expression of *mor28*, an OR gene expressed by a subpopulation of ORNs in the ventrolateral-most region, often referred to as zone 4, but did not correlate with the more intermediate region OR population *p2* (Figure 1J-L), indicating that Amigo1 may specifically regulate the development of ventrolateral ORNs.

Figure 1: Amigo1 is expressed in the ventrolateral region of the olfactory epithelium

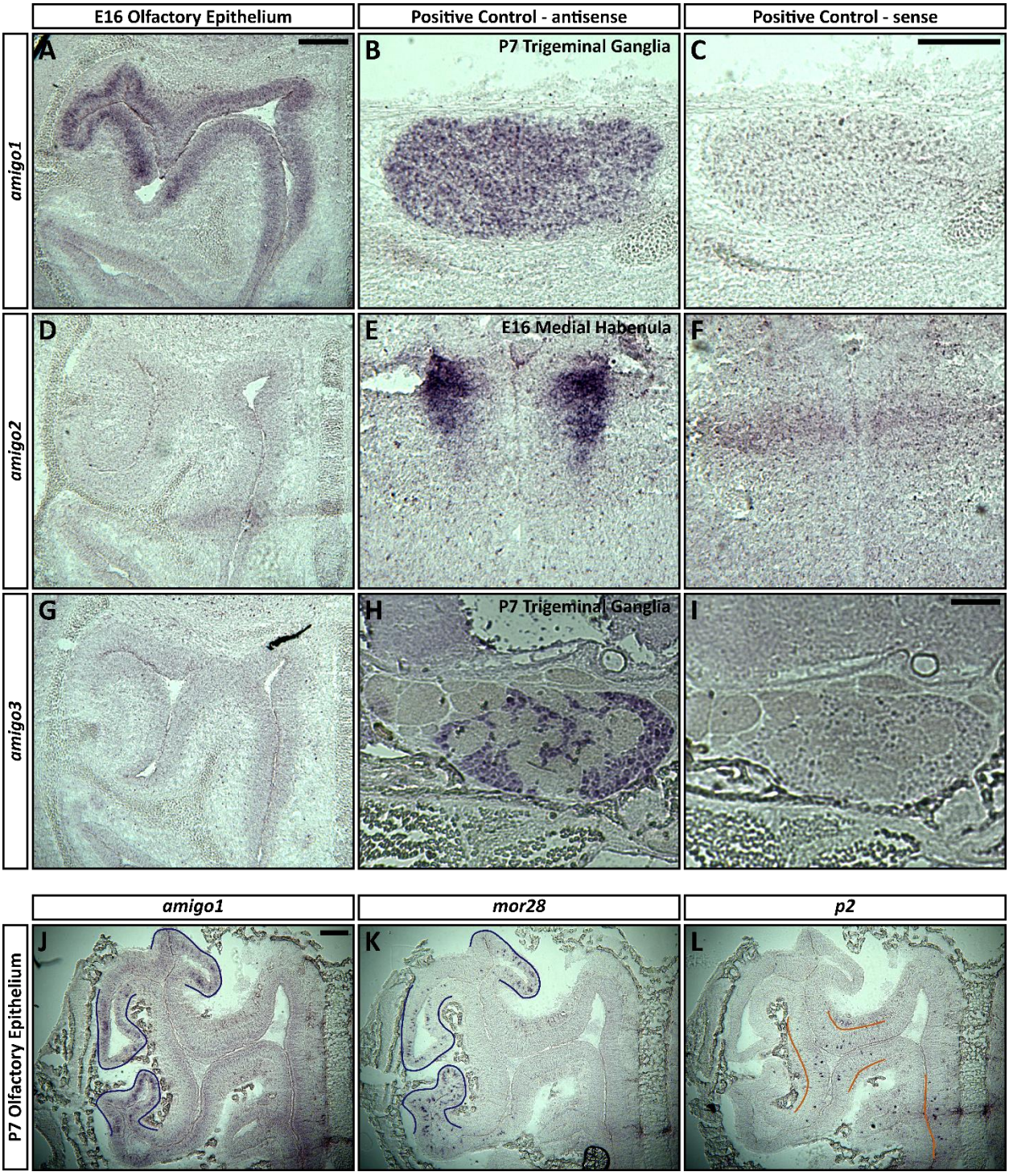

(A-I) Expression of Amigo family members in the olfactory epithelium of E16 by *in situ* hybridization using probes targeting *amigo1* **(A-C)**, *amigo2* **(D-F)**, and *amigo3* **(G-I)** mRNA. **(A,D,G)** Coronal sections of E16 olfactory epithelium showing enriched expression of *amigo1* but not *amigo2* or *amigo3* in the OE. Scale bars: 200µm

(B,E,H) Positive control regions for antisense *in situ* probes showing an area of high expression (trigeminal ganglia at P7 for *amigo1* **(B)** and *amigo3* **(H)**, and the medial habenula at E16 for *amigo2* **(E)**). Antisense probes detect the high levels of expression of *amigo1-3* in these tissues. Scale bars: 200μm.
(C,F,I) Sense probes for the same regions as a negative control show no non-specific staining.
(J-L) Comparison of *amigo1* pattern of expression to OR gene expression. *In situ* hybridization on coronal sections of P7 OE using probes against *amigo1* **(J)**, *mor28* **(K)** and *p2* **(L)** mRNA. *Amigo1* is expressed in a region of the OE that correlates with the localization of cells expressing *mor28*, but not with the region of *p2*-positive cells. Scale bars: 100μm

2. Insertion of a neomycin selection cassette in the *Amigo1* locus disrupts development of ventrolateral ORNs.

In vitro and zebrafish *in vivo* evidence have suggested that Amigo1 can promote axon fasciculation, indicating that it may regulate the projection of ventrolateral ORN axons to the OB (Kuja-Panula et al., 2003; Zhao et al., 2014). To determine whether Amigo1 plays a role in axonal fasciculation and glomerular targeting in the mouse olfactory system, we generated an *Amigo1* null mouse and examined the projection of MOR28-expressing ORN axons to the OB in these mice. The null allele was generated using embryonic stem (ES) cells containing the modified *Amigo1* allele, *Amigo1*$^{\text{tm1(KOMP)Vlcg}}$ created by the trans-NIH Knock-Out Mouse Project (KOMP) (Figure 2A).

The resulting knockout allele comprised a replacement of the Amigo1 coding region with a *lacZ* gene and a neomycin selection cassette (termed *Amigo1*^{neo}), which completely ablated expression of Amigo1 (Fig. 2D). *Amigo1*^{neo} mice were crossed with a reporter mouse line expressing tau-GFP in a specific population of ORNs located in the ventrolateral region of the OE *(MOR28-IRES-tau-GFP)* to visualize axonal projections of these neurons (Figure 2B).

Figure 2: Knockout of Amigo1 ablates transcription of *amigo1* mRNA and production of Amigo1 protein

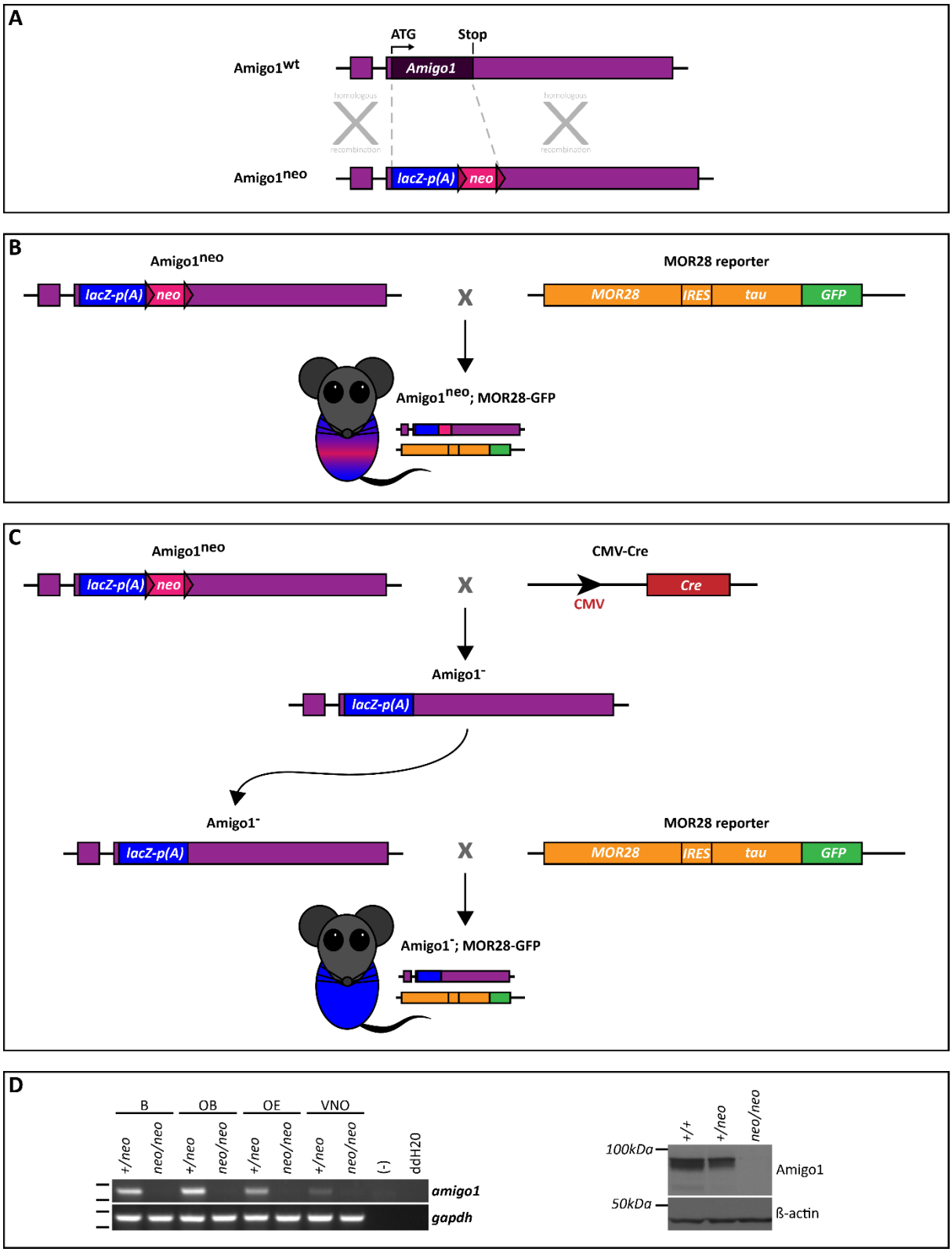

(A) Knockout strategy used by the KOMP repository. The *Amigo1* coding region is replaced by a *lacZ* gene cassette followed by a floxed *neomycin* resistance gene cassette. The modified allele (*Amigo1*$^{tm1(KOMP)Vlcg}$) is referred to as *Amigo1*^{neo}
(B) Mice containing the *Amigo1*^{neo} allele were crossed with a reporter mouse line which expresses the fusion protein tau-GFP in cells that express the *mor28* OR gene (*MOR28-GFP*).
(C) Mice containing the *Amigo1*^{neo} allele were crossed with a CMV-Cre mouse line to excise the floxed neomycin cassette from the *Amigo1*^{neo} allele, resulting in the complete *Amigo1*$^{-}$ allele containing only the *lacZ* gene cassette. These mice were then crossed to the *MOR28-GFP* line to allow expression of tau-GFP in MOR28-expressing cells of *Amigo1* mutant mice.
(D) Characterization of ablation of Amigo1 expression by RT-PCR and Western Blot. [**Left**] RT-PCR amplifying *amigo1* mRNA sequence from cDNA prepared from adult Amigo1$^{+/neo}$ and Amigo1$^{neo/neo}$ tissue. *Gapdh* was used as a control. B: Brain; OB: olfactory bulb; OE: Olfactory epithelium; VNO: Vomeronasal organ. [**Right**] Western Blot of whole brain lysate from wild type, heterozygous and homozygous *Amigo1* mutants. Blots were probed with Amigo1 antibody to confirm the knockout and with β-actin antibody as a loading control.

We assessed glomerular targeting of axons from the MOR28-positive neurons to the OB and found that adult *Amigo1*$^{neo/neo}$ mice had a drastic reduction in the size of the MOR28 glomeruli when compared to control animals, as observed by GFP fluorescence in a whole-mount preparation of the ventral side of the OB (Figure 3A). While the MOR28 glomeruli were smaller, their location appeared unchanged in *Amigo1*$^{neo/neo}$ mice. As the presence of a neomycin selection cassette in a genomic allele has previously been shown to cause unexpected misregulation of gene expression outside the targeted locus (Fiering et al., 1993; Pham et al., 1996), we excised the floxed neomycin cassette by crossing the *Amigo1*^{neo} mice with a mouse expressing Cre in the germline (CMV-Cre), resulting in *Amigo1*$^{-/-}$ mice (Figure 2C). Interestingly, we found that the MOR28 glomeruli had normal volumes in adult *Amigo1*$^{-/-}$ mice, suggesting that the glomerular phenotype observed in the *Amigo1*$^{neo/neo}$ mice is likely caused by the presence of the neomycin cassette within the *Amigo1* locus, rather than from the loss of Amigo1 protein (Figure 3B). We therefore decided to investigate the glomerular phenotype observed in the *Amigo1*^{neo} line further as a method to potentially uncover novel genes or mechanisms underlying ORN development.

Figure 3: *Amigo1*$^{neo/neo}$ but not *Amigo1*$^{-/-}$ mice show defects in the targeting of MOR28-positive axons to the olfactory bulb.

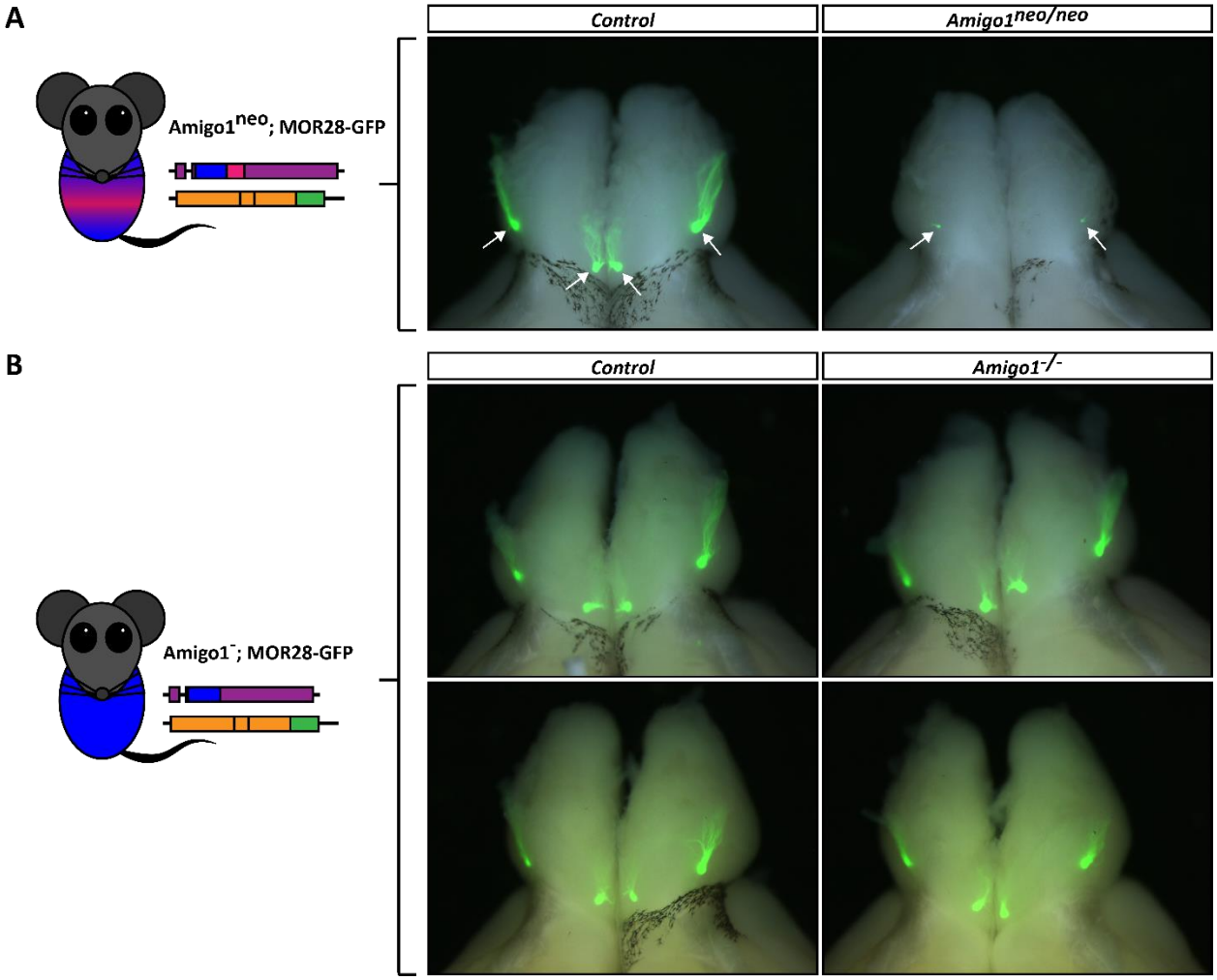

(A) Ventral views of the olfactory bulb to examine MOR28-positive glomeruli visible by endogenous fluorescent signal from the tau-GFP in MOR28-positive axons. Neomycin-containing *Amigo1* mutants show a drastic reduction in the size of the glomerular target. Arrows point to the MOR28-positive glomeruli

(B) Ventral views of the olfactory bulb to examine MOR28-positive glomeruli visible by endogenous fluorescent signal from the tau-GFP in MOR28-positive axons. Neomycin-lacking *Amigo1* mutants show no obvious defects in their MOR28 glomeruli.

To determine whether the ORN targeting defects observed are specific to the ventrolateral region of the OE or are more widespread, we examined the axonal projections of two additional populations of ORNs that project to dorsal or intermediate regions of the OB using reporter mice (MOR174-9-IRES-tau-GFP and P2 P2-IRES-tau-lacZ, respectively) crossed to the *Amigo1*^{neo} line. Sections of OB from adult control and *Amigo1*$^{neo/neo}$ animals were stained for GFP and β-galactosidase (β-gal) to label the MOR174-9, P2 and MOR28 glomeruli, and glomerular volumes were measured. While we observed a robust decrease in the size of both the medial and the lateral MOR28-positive glomeruli in the *Amigo1*$^{neo/neo}$ mice, the size of MOR174-9- and P2-positive glomeruli remained unchanged when compared to controls (Figure 4A-G). To assess whether reduced size is a general hallmark of glomeruli in the ventral region of the OB in *Amigo1*$^{neo/neo}$ mice, we measured the area of glomeruli surrounding the MOR28-GFP glomerulus on sections of adult OB, which allowed us to get an estimate of the average size of glomeruli in this region of the OB. As observed for MOR28-positive glomeruli, the average size of glomeruli in the ventral region of the OB was reduced in *Amigo1*$^{neo/neo}$ mice (Figure 4J,M,N). In contrast the average size of glomeruli surrounding the MOR174-9 and P2-positive glomeruli in the dorsal and intermediate regions of the OB, respectively, was unchanged in these mice (Figure 4H-I, K-L, N). These findings demonstrate that reduced glomerular size is observed throughout the ventral part of the OB, yet it is restricted to this region, suggesting that presence of the neomycin resistance cassette in the *Amigo1* locus specifically affects the development and/or maintenance of ventrolateral ORNs in the OE. To assess whether improper glomerular development underlies the defects observed in *Amigo1*$^{neo/neo}$ mice, we analyzed the size of MOR28-GFP glomeruli at an early developmental time point, P7, when MOR28 glomeruli have recently formed and are being refined (Zou et al., 2004; Kerr and Belluscio, 2006). We found a similar reduced size of the MOR28 but

not of the MOR174-9 or P2 glomeruli in these mice, indicating that the defects are due to an effect on development, rather than on maintenance, of the glomeruli (Figure 5A-I). Taken together, these results support a notion that the development of glomeruli in the ventral-most zone are specifically affected in *Amigo1*$^{neo/neo}$ mice.

Figure 4: Presence of the neomycin cassette in *Amigo1*$^{neo/neo}$ animals disrupts glomerular size exclusively in ventral OB

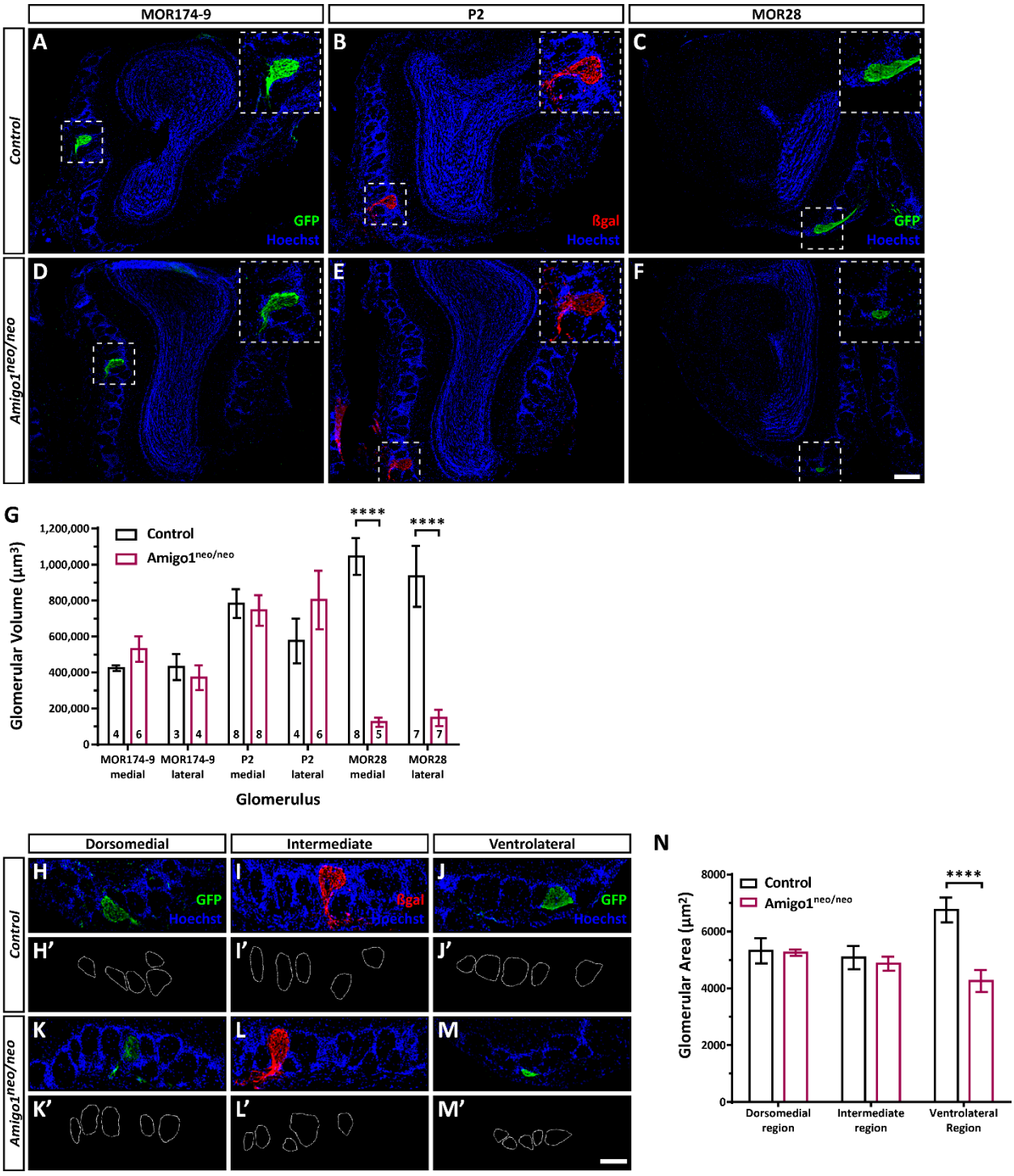

(A-F) Representative coronal sections of OB stained with GFP and β-gal antibodies to show MOR174-9-**(A,D)**, P2- **(B,E)** and MOR28- **(C,F)** positive glomeruli from control **(A-C)** and *Amigo1*$^{neo/neo}$ **(D-F)** mice. Insets show magnified (2x) glomeruli from the same section as shown

by the outlined boxes. MOR28 glomeruli but not MOR174-9 or P2 glomeruli appear smaller in size in the *Amigo1*$^{neo/neo}$ OBs. Scale bar: 200μm

(G) Quantification of glomerular volume estimated by calculating the sum of the area of each section containing a labelled glomerulus, multiplied by the section thickness. Data shown as average ± s.e.m. (MOR174-9 medial (units: μm^3): control 423944.7 ± 15134.45 n=4 OBs, *Amigo1*$^{neo/neo}$ 530975 ± 70866.38 n=6 OBs; MOR174-9 lateral: control 430499.4 ± 71451.94 n=3 OBs, *Amigo1*$^{neo/neo}$ 371522 ± 68387.36 n=4 OBs; P2 medial: control 783145.1± 79701.2 n=8 OBs, *Amigo1*$^{neo/neo}$ 745176 ± 85432.9 n=8 OBs; P2 lateral: control 575237.8 ± 125103.1 n=4 OBs, *Amigo1*$^{neo/neo}$ 802952 ± 162159 n=6 OBs; MOR28 medial: control 1044657 ± 102565.1 n=8 OBs, *Amigo1*$^{neo/neo}$ 124447 ± 26242.75 n=5 OBs; MOR28 lateral: control 933811.8 ± 169297.5 n=7 OBs, *Amigo1*$^{neo/neo}$ 147536 ± 45577 n=7 OBs) 2-way ANOVA with Sidak's multiple comparisons test for genotype, **** $p < 0.0001$.

(H-M) Representative coronal sections of OB stained with GFP and β-gal antibodies, and Hoechst used for measuring glomeruli surrounding MOR174-9 **(H,K)**, P2 **(I,L)** and MOR28- **(J,M)** positive glomeruli from control **(H-J)** and *Amigo1*$^{neo/neo}$ (K-M) mice. Ventrolateral glomeruli adjacent to the MOR28 glomeruli but not glomeruli adjacent to MOR174-9 or P2 appear smaller in size in the *Amigo1*$^{neo/neo}$ OBs. **(H',I', J', K', L', M')** Traces of surrounding glomeruli of the corresponding antibody-stained panels. Scale bar: 100μm

(N) Quantification of average area of glomeruli in dorsomedial, intermediate and ventral regions of the OB. Data shown as average ± s.e.m (Dorsomedial glomeruli (units: μm^2): control 5319.7 ± 443.2 n=8 OBs, *Amigo1*$^{neo/neo}$ 5252 ± 114.69 n=8 OBs; Intermediate: control 5079 ± 407 n=7 OBs, *Amigo1*$^{neo/neo}$ 4864.9 ± 245.16 n=9 OBs; Ventrolateral: control 6756.4 ± 435.02 n=12 OBs, *Amigo1*$^{neo/neo}$ 4256.5 ± 391.38 n=7 OBs) 2-way ANOVA with Sidak's multiple comparisons test for genotype, **** $p < 0.0001$.

Figure 5: Presence of the neomycin cassette in *Amigo1*$^{neo/neo}$ animals disrupts glomerular formation exclusively in ventral OB

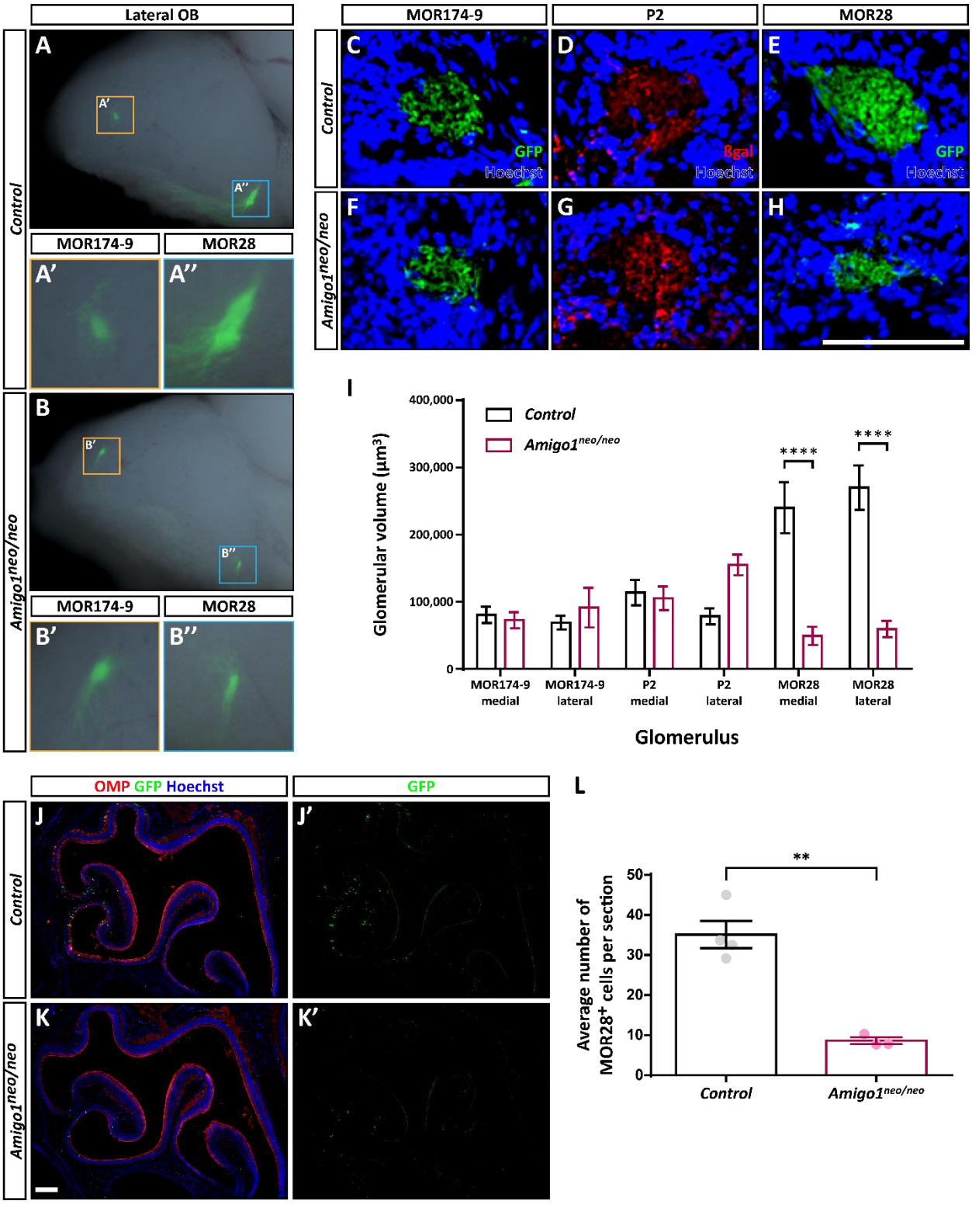

(A,B) Lateral view of control and *Amigo1*$^{neo/neo}$ OBs at P7 to showing MOR174-9- and MOR28-positive glomeruli visible by endogenous fluorescent signal from tau-GFP in the axons. Glomerular size deficits for the MOR28 glomeruli are also seen at this age. (**A', B'**) Zoom-in of the lateral MOR174-9 glomerulus. **(A", B")** Zoom-in of the lateral MOR28 glomerulus.
(C-H) Representative images of sections of OB stained with GFP and βgal antibodies to show MOR174-9-**(C,F)**, P2- **(D,G)** and MOR28- **(E,H)** positive glomeruli from P7 control **(C-E)** and *Amigo1*$^{neo/neo}$ **(F-H)** mice. MOR28 glomeruli but not MOR174-9 or P2 glomeruli appear smaller in size in the *Amigo1*$^{neo/neo}$ OBs even at P7. Scale bar: 100μm
(I) Quantification of glomerular volume estimated by calculating the sum of the area of each section containing a labelled glomerulus, multiplied by the section thickness. Data shown as average ± s.e.m (MOR174-9 medial (units: μm^3): control 80643.5 ± 12153.36 n=8 OBs, *Amigo1*$^{neo/neo}$ 72589.6 ± 12053.1 n=5 OBs; MOR174-9 lateral: control 77374.4 ± 9391.94 n=9 OBs, *Amigo1*$^{neo/neo}$ 91209.1 ± 29484.04 n=3 OBs; P2 medial: control 113601.9 ± 18892.41 n=7 OBs, *Amigo1*$^{neo/neo}$ 105162.8 ± 17385.84 n=4 OBs; P2 lateral: control 78386.21 ± 11873.382 n=6 OBs, *Amigo1*$^{neo/neo}$ 154924.5 ± 15270.48 n=4 OBs; MOR28 medial: control 286126.5 ± 33997.19 n=15 OBs, *Amigo1*$^{neo/neo}$ 69685.1 ± 18090.44 n=10 OBs; MOR28 lateral: control 336692.5 ± 32529.08 n=15 OBs, *Amigo1*$^{neo/neo}$ 78145.66 ± 11152.10 n=11 OBs) 2-way ANOVA with Sidak's multiple comparisons test for genotype, **** $p < 0.0001$
(J-K) Representative coronal sections of P7 OE stained with GFP and OMP antibodies, and Hoechst used for counting GFP-positive MOR28 cells **(J', K')** Single channel image showing GFP-positive puncta. There appear to be far fewer GFP-positive MOR28 cells in *Amigo1*$^{neo/neo}$ OE **(K)** compared to controls **(J).** Scale bar: 200μm
(L) Quantification of average number of MOR28-positive cells per section in the OE from control and *Amigo1*$^{neo/neo}$ mutant animals. Data shown as average ± s.e.m (Control: 35.11 ± 3.433 n=4 OEs, *Amigo1*$^{neo/neo}$ 8.64 ± 0.84 n=3 OEs) Unpaired t-test, ** $p < 0.01$

3. Defects to ventral glomeruli formation are caused by decreases in the numbers of ventrolateral ORN populations

We next sought to determine why ventral OB glomeruli are smaller in the OBs of *Amigo1*$^{neo/neo}$ mice. We considered the possibilities that either outgrowth or guidance of ORN axons is affected, so that fewer axons were reaching their final glomerular target, or that there were fewer ORNs expressing ventrolateral ORs in the OE (Bressel et al., 2016). Counts of MOR28-GFP-positive cells in the OE of control and *Amigo1*$^{neo/neo}$ mice at P7 revealed a drastic reduction in the number of MOR28-positive cells in the OE of mutant mice compared to controls (Figure 5J-L). Using an *in situ* hybridization approach, we examined the size of other OR populations throughout the OE of *Amigo1*$^{neo/neo}$ mice. We found that while several populations of ORNs in the ventrolateral regions of the OE were reduced in numbers, ORN populations in other regions of the OE appeared unchanged in the *Amigo1*$^{neo/neo}$ mutants compared to controls (Figure 6A-O). To further confirm that the specific decrease in the number of ORNs expressing ventrolateral-specific ORs is due to a defect in early development of the olfactory map rather than in its maintenance, we counted cells expressing *mor174-9*, *i7* and *mor28* in newborn mice (P0). Once again, we found a specific effect in the ventrolateral OR population sizes in the *Amigo1*$^{neo/neo}$ mice (Figure 6Q-W). Together, these results confirm that the presence of the neomycin cassette in the *Amigo1*$^{neo/neo}$ animals causes a developmental defect leading to a reduction in the size of the ORN populations expressing ventrolateral ORs and consequently, the formation of smaller glomeruli in the ventral region of the OB.

Figure 6: The decrease in the size of ventrally located OB glomeruli is associated with a concomitant decrease in the size of ventrolateral ORN populations in the OE

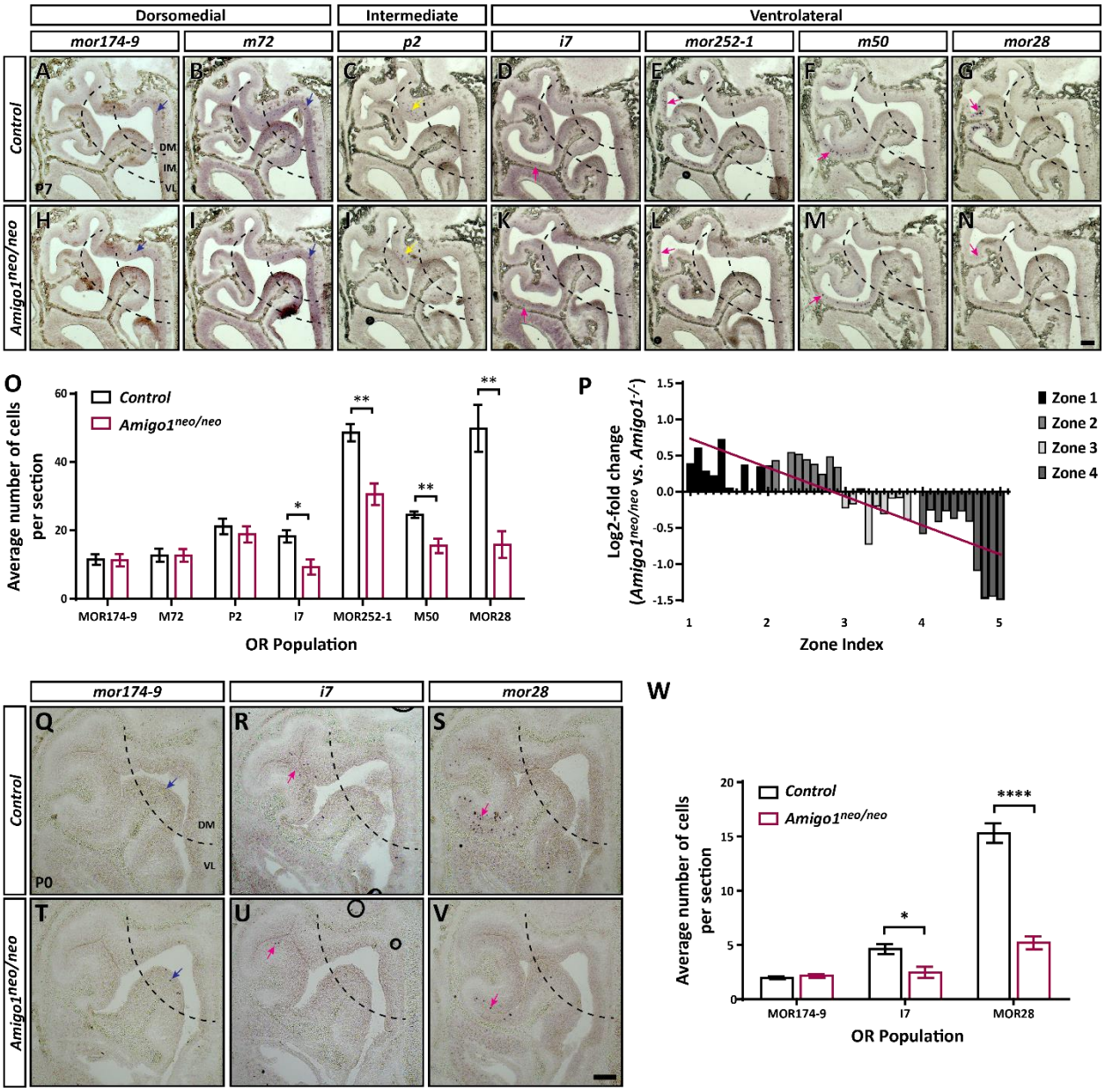

(A-N) Representative coronal sections of P7 control and *Amigo1*$^{neo/neo}$ OE stained by *in situ* hybridization with probes against different OR genes to count the number of positive cells of each ORN population. ORN populations from dorsomedial (*mor174-9*: **A-B**; *m72*: **H-I**), intermediate (*p2*: **C,J**), and ventrolateral (*i7*: **D,K**; *mor252-1*: **E,L**; *m50*: **F,M**; *mor28*: **G,N**) regions were counted. Dotted lines represent approximate divisions of these regions. DM: dorsomedial; IM: intermediate; VL: ventrolateral. Examples of positively stained cells are indicated by arrows of different colours according to OE region (*blue*: dorsomedial, *yellow*: intermediate; *pink*: ventrolateral). Scale bar: 200µm

(O) Quantification of data from **(A-N)**. Graph displays average number of positive cells per section in the OE from control and *Amigo1*$^{neo/neo}$ mutant animals for each ORN population. Data shown as

average ± s.e.m (MOR174-9: control 11.47 ± 1.53 n=7 OEs, *Amigo1*$^{neo/neo}$ 11.30 ± 1.85 n=5 OEs; M72: control 12.74 ± 1.94 n=5 OEs, *Amigo1*$^{neo/neo}$ 12.75 ± 1.81 n=5 OEs; P2: control 21.15 ± 2.29 n=6 OEs, *Amigo1*$^{neo/neo}$ 18.88 ± 2.41 n=6 OEs; I7: control 18.27 ± 1.74 n=4 OEs, *Amigo1*$^{neo/neo}$ 9.34 ± 2.20 n=4 OEs; MOR252-1: control 48.58 ± 2.51 n=6 OEs, *Amigo1*$^{neo/neo}$ 30.57 ± 3.16 n=6 OEs; M50: control 26.62 ± 0.94 n=4 OEs, *Amigo1*$^{neo/neo}$ 15.52 ± 2.10 n=4 OEs; MOR28: control 49.85 ± 6.87 n=6 OEs, *Amigo1*$^{neo/neo}$ 15.88 ± 3.90 n=5 OEs) Unpaired Student's t-tests * $p < 0.05$, ** $p < 0.01$

(P) Graph representing log2-fold change of expression of ORs between *Amigo1*$^{neo/neo}$ and *Amigo*$^{-/-}$ mRNA extracted from P7. Data from RNA Sequencing results. Data from ORs with known zone indices from Miyamichi et al., 2005 were used for this plot. Positive values represent increases in gene expression in *Amigo1*$^{neo/neo}$ and negative values represent downregulation of genes in the neomycin-containing tissue. Linear regression line: $Y = 0.4002X + 1.113$. $R^2 = 0.6857$. Zone indices (ZI) and zonal identity as follows: ZI 1 ≤ Zone 1 < ZI 2 ≤ Zone 2 < ZI 3 ≤ Zone 3 < ZI 4 ≤ Zone 4 ≤ ZI 5.

(Q-V) Representative coronal sections of P0 control and *Amigo1*$^{neo/neo}$ OE stained by *in situ* hybridization with probes against different OR genes to count the number of positive cells of each ORN population. ORN populations from dorsomedial (*mor174-9*: **Q,T**), and ventrolateral (*i7*: **R,U**; *mor28*: **S,V**) regions were counted. Dotted lines represent approximate divisions of these regions. DM: dorsomedial; VL: ventrolateral. Examples of positively stained cells are indicated by arrows of different colours according to OE region (*blue*: dorsomedial, *pink*: ventrolateral). Scale bar: 200μm

(W) Quantification of average number of positive cells per section in the OE from control and *Amigo1*$^{neo/neo}$ mutant animals for each ORN population. Data shown as average ± s.e.m (MOR174-9: control 1.96 ± 0.1 n=6 OEs, *Amigo1*$^{neo/neo}$ 2.15 ± 0.17 n=6 OEs; I7: control 4.62 ± 0.45 n=6 OEs, *Amigo1*$^{neo/neo}$ 2.48 ± 0.50 n=6 OEs; MOR28: control 15.30 ± 0.89 n=6 OEs, *Amigo1*$^{neo/neo}$ 5.20 ± .59 n=6 OEs) Unpaired Student's t-tests * $p < 0.05$, **** $p < 0.0001$

A decrease in the size of the OR populations within the ventrolateral region of the OE could suggest an alteration in the total number of ORNs in this zone, due to cell proliferation or survival defects. Alternatively, ORNs in this region of the OE may be produced and survive normally but fail to express an olfactory receptor. Given that the total epithelial thickness is related to the number of neuronal cells (Mackay-Sim et al., 1988), if there is a decrease in the total number of ORNs in the ventrolateral region of the OE, we would expect to observe a decrease in either the thickness of the mature olfactory marker protein (OMP) layer or total OE thickness in this region relative to other parts of the OE. Immunohistochemical analysis of OMP staining in the OE at P7, however, revealed that there was no difference in the thickness of the OMP layer nor a difference in the total thickness of the OE by Hoechst staining in any region of the OE between control and neomycin-containing *Amigo1* mutants (Figure 7A-G). Furthermore, we could not detect significant changes in the number of proliferating cells or of cells undergoing apoptosis in the ventrolateral region of the OE in newborn *Amigo1*$^{neo/neo}$ mice (Figure 7H-M). Taken together, our results indicate that the presence of a neomycin resistance cassette within the *Amigo1* locus disrupts the development of ventrolateral ORNs in the OE, possibly by altering expression of specific sets of ORs.

Figure 7: The decrease in number of ORNs of ventrolateral populations is not due to an alteration in rates of proliferation, maturation, or cell death

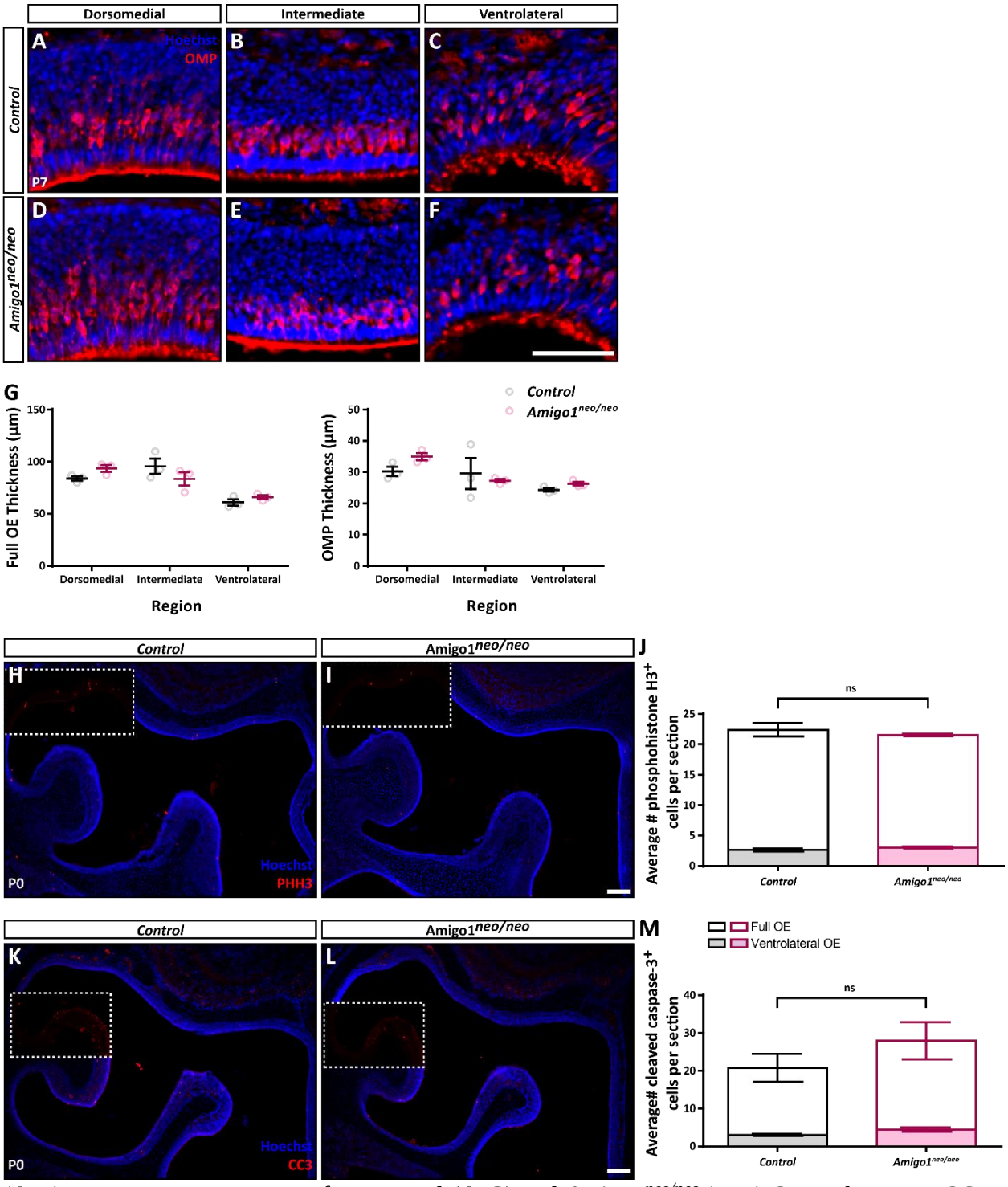

(A-F) Representative images of P7 control (**A-C**) and *Amigo1*$^{neo/neo}$ (**D-F**) OE with mature OSNs labelled using an OMP antibody and cell nuclei stained with Hoechst. Defined areas of dorsomedial **(A,D)**, intermediate **(B,E)**, and ventrolateral **(C,F)** OE were used to measure the thickness of the OE and of the OMP layers. Scale bar: 50µm

(G) Quantification of **(A-F)** showing average OE thickness **[left]** and average OMP layer thickness **[right]** in 3 different regions of the OE. Data shown as average in μm ± s.e.m. (Full OE thickness: DM control 83.75 ± 2.06 n=3 OEs, *Amigo1*$^{neo/neo}$ 93.56 ± 3.27 n=3 OEs; IM control 95.68 ± 7.40 n=3 OEs, *Amigo1*$^{neo/neo}$ 83.38 ± 6.45 n=3 OEs; VL control 60.93 ± 3.09 n=3 OEs, *Amigo1*$^{neo/neo}$ 65.88 ± 1.91 n=3 OEs. OMP layer thickness: DM control 30.19 ± 1.53 n=3 OEs, *Amigo1*$^{neo/neo}$ 34.93 ± 1.15 n=3 OEs; IM control 29.57 ± 4.99 n=3 OEs, *Amigo1*$^{neo/neo}$ 27.21 ± 0.57 n=3 OEs, VL control 24.31 ± 0.57 n=3 OEs, *Amigo1*$^{neo/neo}$ 26.29 ± 0.61 n=3 OEs) 2-way ANOVA with Sidak's multiple comparisons test for genotype. No significant changes detected.
(H,I) Example OE section from control **(H)** and *Amigo1*$^{neo/neo}$ **(I)** P0 mice stained for the proliferation marker Phosphohistone-H3 (PHH3). Boxed areas show OE without Hoechst to see individual PHH3-positive cells. Scale bar: 100μm
(J) Quantification from **(H,I)** showing average number of PHH3-positive cells per section of P0 OE. White bars display the average number of stained cells throughout the OE while shaded areas define the subset of stained cells in the ventrolateral region. Data shown as average ± s.e.m. (Full OE: control 22.39 ± 1.11 n=3 OEs, *Amigo1*$^{neo/neo}$ 21.51 ± 0.20 n=3 OEs. Ventrolateral OE: control 2.62 ± 0.25 n=3 OEs, *Amigo1*$^{neo/neo}$ 3.04 ± 0.13 n=3 OEs) 2-way ANOVA with Sidak's multiple comparisons test for genotype. ns = non significant
(K,L) Example OE section from control **(K)** and *Amigo1*$^{neo/neo}$ **(L)** P0 mice stained for the marker of apoptosis Cleaved Caspase-3 (CC3). Boxed areas show OE without Hoechst to see individual CC3-positive cells. Scale bar: 100μm
(M) Quantification from **(K,L)** showing average number of CC3-positive cells per section of P0 OE. White bars display the average number of stained cells throughout the OE while shaded areas define the subset of stained cells in the ventrolateral region. Data shown as average ± s.e.m. (Full OE: control 20.79 ± 3.69 n=5 OEs, *Amigo1*$^{neo/neo}$ 28 ± 4.40 n=5 OEs. Ventrolateral OE: control 3.01 ± 0.23 n=3 OEs, *Amigo1*$^{neo/neo}$ 4.46 ± 0.50 n=3 OEs) 2-way ANOVA with Sidak's multiple comparisons test for genotype. ns = non significant

4. Gene transcription is altered in the OE of *Amigo1*$^{neo/neo}$ mice.

There is evidence that the presence of a neomycin cassette in a specific gene locus can cause or modify phenotypes independently of the gene of interest that is knocked-out (Kim et al., 1992; Fiering et al., 1993, 1995; Rijli et al., 1994; Hug et al., 1996; Olson et al., 1996; Meier et al., 2010; Maguire et al., 2014; Han et al., 2016; Pan et al., 2016). It has been proposed that insertion of the neomycin cassette with its own exogenous promoter at the locus of the gene of interest acts to modify the regulation of additional clusters of genes surrounding the insertion locus at both short and long ranges (Pham et al., 1996; West et al., 2016). To determine whether the presence of a neomycin cassette in the *Amigo1* locus could alter gene expression in the OE, we performed RNA sequencing (RNAseq) analyses on cDNA generated from the OE of *Amigo1*$^{-/-}$ and *Amigo1*$^{neo/neo}$ animals at P7. Comparing gene expression in these two samples allows us to identify genes that are misregulated due to the presence of the neomycin cassette in the *Amigo1* locus, rather than due to loss of Amigo1 expression. Such genes could represent candidate genes important for the regulation of ORN development and OR gene expression.

RNAseq analyses revealed that several genes differed in expression between the two groups of mutant mice, including multiple genes that are located near the *Amigo1* locus, such as *psma5*, *cyb561d1*, and *atxn7l2* (Table 1). To note, *Amigo2* and *Amigo3* levels were unchanged between the mutant groups, suggesting no compensatory change in the expression of other Amigo family members with the presence of the neomycin cassette. Other groups of genes that were misregulated were found in clusters around the genome. Gene ontology analysis suggested that several differentially expressed genes in the *Amigo1*$^{neo/neo}$ mice may be involved in modulating oxidoreductase activity, such as *Cyb561d1*, *Gpx3*, *Atxn7l2*, *Carns1*, *Ggt7* and *Aldh1l2*. *Gpx3*, for example, is a major reactive oxidative species (ROS) scavenger that is downregulated 2-fold in

Amigo1$^{neo/neo}$ (Brigelius-Flohé, 2006; An et al., 2018). While changes in oxidative stress could affect survival of ORNs, our observation that there is no change in the survival rates of ORNs in *Amigo1*$^{neo/neo}$ mice make it unlikely that alterations in expression of these genes underlie the specific defects in development of ventrolateral ORNs observed in these mice.

Table 1: List of differentially expressed genes from RNA sequencing data.

pvalue	padj	Significance	Amigo1-/- mean (log2)	Amigo1-/-sd	Amigo1neo/neo mean (log2)	Amigo1neo/neo.sd	log2FoldChange (unshrunken)	Change (Amigo1^{neo} - Amigo1)	EnsemblID	Gene	Location	Amigo1$^{neo/neo}$ A1.1.1.20180703.4	Amigo1$^{neo/neo}$ A1.1.1.20180703.8	Amigo1$^{neo/neo}$ A1.1.1.20180703.9	Amigo1$^{-/-}$ A1.5.1.20180601.12	Amigo1$^{-/-}$ A1.5.1.20180601.2	Amigo1$^{-/-}$ A1.5.1.20180601.7
0.0000	0.0001		5.3605	0.2737	1.7803	0.4390	3.5802		ENSMUSG00000090129.9	Olfr287	chr15:98206971-98221056	2.326704	4.377387	2.439435	45.49411	32.50085	45.18436
0.0000	0.0000		8.3719	0.0712	5.3298	0.4112	3.0422		ENSMUSG00000048796.7	Cyb561d1	**chr3:108195687-108201212**	29.47158	40.49083	52.44785	334.6344	345.1815	313.3437
0.0002	0.0435		5.1740	0.5141	2.9848	0.7768	2.1892		ENSMUSG00000081836.3	Olfr1192-ps1	chr2:88410649-88419151	3.877839	12.03781	8.538023	41.45019	23.5351	46.16663
0.0001	0.0286		5.5286	0.1147	3.3411	0.8085	2.1875		ENSMUSG00000030226.12	Lmo3	chr6:138362918-138581968	7.755678	18.60389	6.098588	43.47215	43.70804	50.09571
0.0000	0.0000		6.6972	0.3961	4.6042	0.1743	2.0929		ENSMUSG00000048997.17	Atxn7l2	**chr3:108202222-108210934**	24.81817	26.26432	20.7352	122.3286	75.08818	119.8368
0.0001	0.0197		5.5864	0.4697	3.5387	0.5257	2.0477		ENSMUSG00000053863.3	Mepe	chr5:104325329-104338611	15.51136	12.03781	7.318305	67.73567	44.82876	35.36168
0.0000	0.0150		5.7529	0.6582	3.8793	0.2446	1.8736		ENSMUSG00000057447.2	Olfr1205	chr2:88829737-88837104	13.96022	12.03781	17.07605	53.58195	33.62157	84.47511
0.0000	0.0066		7.7063	0.4277	5.8459	0.9525	1.8604		ENSMUSG00000038173.15	Enpp6	chr8:46986887-47096762	105.4772	62.37776	28.0535	293.1842	180.4358	170.9148
0.0000	0.0009		7.0509	0.7620	5.2053	0.3980	1.8456		ENSMUSG00000109449.3	Olfr1280	chr2:111314017-111326003	26.36931	41.58517	43.90983	142.5482	75.08818	215.1169
0.0002	0.0454		6.7660	0.0903	4.9240	0.9646	1.8420		ENSMUSG00000044952.5	Kctd21	chr7:97332327-97350213	65.1477	20.79259	19.51548	101.098	114.3133	110.0141
0.0000	0.0040		6.8784	0.8528	5.1471	0.1211	1.7312		ENSMUSG00000074483.2	Bglap	**chr3:88383501-88384464**	37.22726	36.11344	31.71266	231.5144	78.45034	88.40419
0.0001	0.0412		5.8159	0.3703	4.1718	0.4239	1.6441		ENSMUSG00000013483.14	Card14	chr11:119307768-119345375	12.40909	19.69824	21.95492	66.72469	41.46661	62.8652
0.0000	0.0161		6.8333	0.6001	5.2077	0.6617	1.6257		ENSMUSG00000095156.2	Olfr1281	chr2:111326520-111332852	21.7159	53.62299	41.4704	133.4494	70.6053	155.1985
0.0000	0.0000		8.6494	0.4773	7.0768	0.3450	1.5725		ENSMUSG00000057564.6	Olfr1508	chr14:52458829-52467495	103.9261	140.0764	167.1013	366.9858	303.7149	578.5563
0.0000	0.0012		7.0315	0.3055	5.5419	0.3463	1.4897		ENSMUSG00000060404.3	Olfr1369-ps1	chr13:21111483-21119095	34.90055	54.71733	51.22814	133.4494	104.2269	159.1275
0.0000	0.0011		8.0509	0.5308	6.7310	0.2468	1.3199		ENSMUSG00000099486.3	Olfr1228	chr2:89247964-89254062	86.8636	113.8121	119.5323	277.0086	179.3151	373.2621
0.0000	0.0150		7.2662	0.4766	5.9638	0.4030	1.3024		ENSMUSG00000072662.2	Mansc4	chr6:147075060-147087032	46.53407	62.37776	81.72108	166.8117	106.4683	203.3296
0.0000	0.0098		9.6915	0.5593	8.5319	0.4889	1.1596		ENSMUSG00000067279.2	Ppp1r3c	chr19:36731737-36736653	263.6931	519.8147	368.3547	538.8524	1148.737	911.5454
0.0000	0.0006		16.4311	0.2960	15.2842	0.5134	1.1469		ENSMUSG00000029661.16	Col1a2	chr6:4504814-4541544	52377.97	45476.67	26674	107727	89543.21	71517.02
0.0000	0.0012		16.3569	0.3553	15.2355	0.5117	1.1214		ENSMUSG00000001506.10	Col1a1	chr11:94936224-94953042	49063.97	45581.73	25670.18	105948.7	86025.28	64863.14
0.0000	0.0005		10.0154	0.3354	8.9293	0.3233	1.0861		ENSMUSG00000032265.14	Fam46a	chr9:85320439-85327348	628.9855	413.663	443.9772	1352.691	915.6275	893.8646
0.0000	0.0066		9.5082	0.3157	8.4229	0.4699	1.0853		ENSMUSG00000046186.8	Cd109	chr9:78615546-78716253	484.7299	327.2096	253.7013	916.959	708.2945	593.2903
0.0000	0.0042		11.0311	0.4286	9.9769	0.4326	1.0542		ENSMUSG00000018339.11	Gpx3	chr11:54902453-54910377	1203.681	1191.743	712.3151	2945.996	1799.875	1726.828
0.0000	0.0079		8.2813	0.1884	7.2459	0.3978	1.0354		ENSMUSG00000042638.14	Gucy2c	chr6:136697284-136781765	110.1306	171.8124	182.9576	282.0635	294.7491	360.4926
0.0001	0.0395		7.7127	0.2492	6.7266	0.3464	0.9861		ENSMUSG00000028351.5	Brinp1	chr4:68761514-68954397	138.8266	88.64208	95.13797	234.5474	171.47	227.8864
0.0000	0.0008		9.7384	0.3025	8.7693	0.2563	0.9691		ENSMUSG00000020218.11	Wif1	chr10:121033960-121100650	485.5055	480.4182	354.9378	1062.54	837.1771	699.3754
0.0000	0.0066		8.5181	0.2732	7.5547	0.2627	0.9634		ENSMUSG00000022479.15	Vdr	chr15:97854425-97910630	229.5681	178.3785	161.0027	438.7654	372.0787	300.5742
0.0000	0.0129		8.3511	0.0427	7.3962	0.4010	0.9549		ENSMUSG00000044647.16	Csrnp3	chr2:65845767-66031546	190.7897	203.5485	121.9718	333.6234	329.4914	315.3083
0.0000	0.0001		9.4559	0.2257	8.5207	0.1631	0.9351		ENSMUSG00000046794.9	Ppp1r3b	chr8:35375739-35388139	395.5396	387.3987	322.0054	601.5332	822.6078	698.3931
0.0001	0.0412		7.4827	0.1568	6.5931	0.2019	0.8896		ENSMUSG00000046410.10	Kcnk6	chr7:29221926-29232515	90.74144	112.7177	86.59995	161.7568	200.6087	174.8438
0.0000	0.0042		15.2491	0.2841	14.3855	0.3646	0.8636		ENSMUSG00000018593.13	Sparc	chr11:55394500-55423183	25679.83	23804.23	16038.07	48607.92	36427.85	33355.88
0.0001	0.0244		9.4057	0.1236	8.5521	0.4096	0.8536		ENSMUSG00000005124.9	Wisp1	chr15:66891320-66923201	503.3435	366.6061	285.4139	713.752	710.5359	613.918
0.0001	0.0339		8.4965	0.2727	7.6749	0.2579	0.8217		ENSMUSG00000020256.14	Aldh1l2	chr10:83487450-83534140	166.7471	235.2845	215.89	300.2611	438.2012	356.5636
0.0002	0.0432		9.2019	0.4077	8.3819	0.2610	0.8200		ENSMUSG00000028238.6	Atp6v0d2	chr4:19876841-19922605	402.5197	327.2096	280.535	790.5865	572.6874	449.8791
0.0002	0.0454		10.8599	0.3265	10.0689	0.3836	0.7910		ENSMUSG00000050931.7	Sgms2	**chr3:131318985-131491411**	1444.883	990.3837	864.7797	2335.364	1849.186	1485.19
0.0000	0.0042		10.8401	0.1503	10.0550	0.3109	0.7851		ENSMUSG00000044533.15	Rps2	chr17:24718116-24721929	1272.707	837.1752	1128.239	2060.377	1687.803	1770.048
0.0000	0.0174		9.1068	0.1787	8.3528	0.2382	0.7539		ENSMUSG00000054555.11	Adam12	chr7:133883199-134232146	393.2129	308.6058	286.6336	589.4014	593.9811	477.3826
0.0001	0.0357		10.5701	0.0409	9.8830	0.3443	0.6870		ENSMUSG00000027230.9	Creb3l1	chr2:91982328-92024502	747.6474	1204.876	933.0839	1474.009	1558.92	1527.428
0.0001	0.0290		10.6598	0.2528	9.9940	0.2265	0.6659		ENSMUSG00000026365.15	Cfh	chr1:140084708-140183764	1221.519	940.0438	922.1065	1853.127	1720.304	1327.045
0.0002	0.0432		9.0393	0.0577	8.3766	0.2375	0.6627		ENSMUSG00000028619.15	Tceanc2	chr4:107134155-107179116	400.9686	307.5114	296.3914	507.512	521.1344	549.0882
0.0001	0.0412		8.4086	0.0327	7.7538	0.1212	0.6548		ENSMUSG00000005360.14	Slc1a3	chr15:8634124-8710764	195.4431	227.6241	224.428	342.7223	330.6121	344.7763
0.0000	0.0150		9.8151	0.1368	9.1651	0.2028	0.6500		ENSMUSG00000013846.9	St3gal1	chr15:67102875-67113992	487.8322	629.2493	614.7376	884.6076	997.44	827.0703
0.0000	0.0143		12.6147	0.1842	11.9678	0.2462	0.6468		ENSMUSG00000026042.16	Col5a2	chr1:45374321-45503282	4802.316	3909.006	3422.527	6753.347	6748.97	5411.319
0.0000	0.0066		9.3831	0.1047	8.7396	0.1027	0.6435		ENSMUSG00000030157.5	Clec2d	chr6:129180615-129186534	393.9885	437.7387	451.2955	615.6869	680.2765	709.1981
0.0001	0.0197		9.6844	0.0538	9.0536	0.2134	0.6308		ENSMUSG00000037370.13	Enpp1	chr10:24637914-24712159	615.0253	531.8525	457.3941	843.1574	837.1771	787.7796
0.0000	0.0019		11.4452	0.1646	10.8516	0.0560	0.5936		ENSMUSG00000043019.12	Edem3	chr1:151755371-151822051	1767.519	1875.71	1901.54	2444.55	2951.974	3002.796
0.0001	0.0339		10.1956	0.1620	9.6782	0.0184	0.5174		ENSMUSG00000003721.14	Insig2	chr1:121304353-121332589	818.2241	829.5148	808.6727	1308.208	1177.876	1045.134
0.0000	0.0143		10.7629	0.0732	10.2529	0.1071	0.5099		ENSMUSG00000032300.7	1700017B05Rik	chr9:57253117-57262612	1299.076	1123.894	1242.892	1699.458	1675.475	1840.772
0.0002	0.0454		9.6886	0.0801	9.2033	0.0270	0.4853		ENSMUSG00000027601.13	Mtfr1	**chr3:19187327-19220817**	577.0225	598.6076	591.563	844.1684	858.4708	774.0278
0.0002	0.0462		10.7576	0.1214	10.3104	0.0320	0.4471		ENSMUSG00000001542.6	Ell2	chr13:75707484-75772356	1280.463	1237.706	1290.461	1579.151	1761.77	1863.364
0.0000	0.0150		11.4239	0.0400	11.8481	0.0362	-0.4242		ENSMUSG00000040473.15	Cfap69	chr5:5579278-5664239	3761.504	3583.985	3715.26	2800.415	2781.625	2660.966
0.0001	0.0371		10.0918	0.0871	10.5465	0.0398	-0.4547		ENSMUSG00000028521.17	Slc35d1	chr4:103170649-103215164	1536.4	1495.972	1453.903	1122.188	1136.409	1017.63
0.0000	0.0098		12.0814	0.1001	12.5610	0.0751	-0.4797		ENSMUSG00000021134.17	Srsf5	chr12:80945504-80950507	5994.364	5761.735	6387.661	4689.937	4119.763	4210.986
0.0001	0.0357		13.0791	0.0882	13.5717	0.1968	-0.4925		ENSMUSG00000068009.11	Bpifb6	chr2:153900388-153912795	10707.49	14049.22	11995.92	8095.929	9129.378	8766.749
0.0002	0.0462		9.4738	0.1518	9.9887	0.0556	-0.5149		ENSMUSG00000037703.14	Lzts3	chr2:130632839-130642803	972.5621	1047.29	1028.222	653.0932	687.0008	799.5668
0.0002	0.0443		9.3920	0.1474	9.9276	0.1052	-0.5356		ENSMUSG00000068749.9	Psma5	**chr3:108256926-108279974**	920.599	1057.139	947.7205	749.1363	611.9126	660.0846
0.0000	0.0176		10.4502	0.1744	10.9942	0.0723	-0.5440		ENSMUSG00000027603.15	Ggt7	chr2:155490379-155518237	1934.266	2051.9	2136.945	1245.528	1385.209	1585.382
0.0000	0.0004		10.6173	0.0592	11.1918	0.0358	-0.5745		ENSMUSG00000075289.4	Carns1	chr19:4164324-4175479	2285.598	2400.997	2330.88	1529.613	1537.627	1646.282
0.0001	0.0211		8.8422	0.0953	9.4284	0.1091	-0.5862		ENSMUSG00000078851.4	Hist3h2a	chr11:58954685-58956830	632.0878	729.9292	707.4362	475.1607	424.7525	477.3826
0.0000	0.0138		12.8210	0.2365	13.4769	0.2217	-0.6559		ENSMUSG00000023943.7	Sult1c1	chr17:53961615-53990674	9864.447	11213.77	13396.16	8104.017	7796.843	5995.769
0.0002	0.0454		9.2518	0.2545	9.9209	0.2424	-0.6691		ENSMUSG00000034156.16	Tspoap1	chr11:87760541-87785928	1148.616	820.76	964.7966	610.632	509.9272	725.8966
0.0000	0.0075		8.2918	0.0794	9.0185	0.1878	-0.7267		ENSMUSG00000055430.4	Nap1l5	chr6:58905233-58907076	465.3407	499.0221	598.8813	328.5685	294.7491	316.2905
0.0000	0.0155		10.7212	0.2134	11.4597	0.3571	-0.7385		ENSMUSG00000028248.15	Pnisr	chr4:21847583-21876475	3651.373	2230.278	2741.925	1773.259	1428.917	1896.761
0.0000	0.0012		7.9963	0.1057	8.8113	0.1275	-0.8150		ENSMUSG00000033585.5	Ndn	chr7:62346569-62350262	483.9543	407.0969	458.6138	237.5803	253.2825	275.0353
0.0001	0.0361		9.7548	0.3438	10.6034	0.4668	-0.8486		ENSMUSG00000085396.7	Firre	chrX:50555744-50635321	2193.306	1153.441	1486.836	986.7166	655.6207	995.0383
0.0002	0.0435		7.7401	0.1412	8.6454	0.5559	-0.9053		ENSMUSG00000074415.12	2610203C20Rik	chr9:41327260-41655483	618.1276	296.5679	348.8392	237.5803	196.1258	208.241
0.0000	0.0016		8.9708	0.0556	9.9322	0.4698	-0.9614		ENSMUSG00000028393.10	Alad	chr4:62509169-62519918	682.4997	1057.139	1290.461	484.2595	497.5993	522.567
0.0001	0.0375		6.0382	0.0851	7.0803	0.2939	-1.0420		ENSMUSG00000069733.11	Ube2u	chr4:100478849-100550147	107.8039	141.1707	161.0027	67.73567	67.24314	60.90066
0.0000	0.0161		8.6661	0.3464	9.7191	0.6572	-1.0530		ENSMUSG00000097767.8	Miat	chr5:112213228-112229395	1304.505	525.2864	872.0981	494.3693	310.4392	435.1451
0.0000	0.0143		6.0190	0.0902	7.0831	0.1032	-1.0641		ENSMUSG00000048425.3	Olfr686	chr7:105201858-105207485	146.5823	131.3216	128.0703	60.65881	63.88099	68.75881
0.0001	0.0357		5.2803	0.3337	6.5549	0.2539	-1.2746		ENSMUSG00000029797.13	Sspo	chr6:48448229-48501250	91.51701	112.7177	79.28164	29.31842	42.58732	45.18436

Padj (column 2) from bioinformatics analysis was used to identify genes expressed at significantly different levels between *Amigo1*$^{neo/neo}$ and *Amigo1*$^{-/-}$ mice. Bars in column 3 are a visual representation of p-value with larger bar representing smaller p-value. Columns 8 and 9 contain values and bars representing log2-fold change between the two groups. Positive values (red cells) represent genes downregulated in the *Amigo*$^{neo/neo}$ group while negative values (green cells) represent overexpressed genes in the neomycin-containing samples. Gene names highlighted in blue are of genes around the Amigo1 locus on chromosome 3. Gene names highlighted in brown have gene ontology terms related to oxidative stress or oxidation-reduction. Gene names highlighted in yellow are olfactory receptor genes.

Since a reduced number of ORNs expressing ventrolateral ORs is observed in *Amigo1*$^{neo/neo}$ mice, we examined more closely ORs expression in our RNAseq data set. Interestingly, out of the 68 protein-coding differentially expressed genes, 9 were ORs. Amongst these, 5 are known to be expressed in the ventrolateral region of the OE and show decreased expression in *Amigo1*$^{neo/neo}$ mice. To further examine the relationship between the spatial location and changes in expression levels of OR expression in these mice, we plotted ORs with previously described zone indices (Miyamichi et al., 2005; Zapiec and Mombaerts, 2020) against their fold change in expression between the *Amigo1*$^{-/-}$ and *Amigo1*$^{neo/neo}$ mice, regardless of the significance of the change. We observed a clear trend from dorsomedial to ventrolateral showing a decrease in the expression levels of ORs located in the ventrolateral OE in *Amigo1*$^{neo/neo}$ tissue (Figure 6P, Table 2 & 3). This lower level of expression correlates with *in situ* data from which we find a significant decrease in the number of cells expressing OR genes in this region of the OE. Together, the RNA sequencing and *in situ* hybridization data provide evidence that several ventrolateral ORs are downregulated, and that the downregulation seen by RNA sequencing is likely related to a decrease in the total number of cells expressing those ORs.

Table 2: List of olfactory receptor genes from RNA sequencing data with known zone indices.

pvalue	padj	Amigo1-/- mean (log2)	Amigo1-/- sd	Amigo1neo/neo mean (log2)	Amigo1neo/neo sd	log2FoldChange (unshrunken)	Change	EnsemblID	Gene	MOR	Zone Index (Miyamichi)	Zone	Location	A1.1.1.20180704	A1.1.1.20180708	A1.1.1.20180709	A1.5.1.20180612	A1.5.1.20180602	A1.5.1.20180607
0.1848	0.9109	5.9453	0.5025	6.4343	0.0908	-0.4890		ENSMUSG00000037924.6	Olfr16	23	1	1	chr1:172950409-172958357	92.29257	84.26469	81.72108	46.50509	90.77824	54.02478
0.0380	0.5914	6.4799	0.5063	7.1543	0.3632	-0.6745		ENSMUSG00000066747.6	Olfr878	163-1	1	1	chr9:37917840-37922474	167.5227	160.869	106.1154	82.90037	130.0034	64.82974
0.2827	0.9721	4.5671	0.4726	5.0908	0.3489	-0.5237		ENSMUSG00000047868.6	Olfr770		1	1	chr10:129132578-129138998	27.14487	31.73605	43.90983	16.17568	31.38013	24.55672
0.3869	0.9991	5.2296	0.2471	5.5580	0.1299	-0.3284		ENSMUSG00000094496.2	Olfr792	108-2	1	1	chr10:129539162-129542534	51.18748	42.67952	46.34927	42.46117	39.22517	30.45033
0.6319	0.9991	4.4877	0.5666	4.2494	0.4240	0.2383		ENSMUSG00000043692.6	Olfr399	255-1	1	1	chr11:74053127-74056615	23.26704	13.13216	20.7352	15.1647	33.62157	20.62764
0.1048	0.8009	4.2750	0.5744	5.0585	0.8915	-0.7835		ENSMUSG00000059069.5	Olfr749	S1	1	1	chr14:50736171-50745094	44.98294	49.2456	15.85633	25.2745	22.41438	11.78723
0.0511	0.6500	5.5307	0.4368	6.2509	0.3008	-0.7201		ENSMUSG00000095030.2	Olfr1513	223-10	1	1	chr14:52347495-52356408	68.24997	96.3025	65.86475	37.40626	65.00171	39.29075
0.4183	0.9991	5.3564	0.4765	5.7174	0.1705	-0.3610		ENSMUSG00000094140.2	Olfr1512	223-5	1	1	chr14:52371332-52379168	48.08521	49.2456	59.76616	34.37332	59.39811	32.41487
0.1815	0.9078	5.1164	0.5627	5.7003	0.6528	-0.5839		ENSMUSG00000063867.2	Olfr1511	223-9	1	1	chr14:52389794-52397379	50.41191	82.076	32.93237	53.58195	29.1387	25.53899
0.4059	0.9991	5.4365	0.4830	5.7841	0.1282	-0.3476		ENSMUSG00000063106.6	Olfr1510	223-6	1	1	chr14:52409131-52414373	60.49429	52.52864	51.22814	46.50509	57.15667	29.46806
0.1891	0.9149	6.8711	0.3854	7.2376	0.0968	-0.3666		ENSMUSG00000048101.6	Olfr19	M12	1	1	chr16:16672228-16676405	162.0937	142.2651	147.5858	105.1419	158.0214	95.28007
0.3671	0.9991	5.8278	0.2852	6.1140	0.3655	-0.2862		ENSMUSG00000075208.6	Olfr1019	180-1	1	1	chr2:85839621-85845483	78.33235	80.98165	51.22814	48.52705	70.6053	52.06024
0.6135	0.9991	4.9848	0.8826	5.3836	0.2483	-0.3988		ENSMUSG00000080713.2	Olfr1174-p	174-18	1	1	chr2:88310284-88315135	42.65623	48.15125	34.15209	17.18666	59.39811	29.46806
0.7912	0.9991	4.9250	0.5044	5.0809	0.2346	-0.1559		ENSMUSG00000044824.8	Olfr545	S50	1	1	chr7:102491466-102499573	39.55396	28.45301	32.93237	23.25254	44.82876	25.53899
0.6799	0.9991	5.3297	0.4978	5.1579	0.3816	0.1718		ENSMUSG00000061165.9	Olfr160	M72	1	1	chr9:37708964-37716250	47.30964	32.8304	28.0535	38.41724	57.15667	28.48579
0.0207	0.4852	7.3790	0.4306	7.9808	0.1914	-0.6019		ENSMUSG00000051118.9	Olfr77	143-1	1.1	1	chr9:19916865-19929124	293.1646	239.6619	228.0872	126.3725	228.6267	158.1453
0.9839	0.9997	5.7529	0.3263	5.7723	0.1943	-0.0193		ENSMUSG00000048356.6	Olfr1496	127-1	1.2	1	chr19:13777878-13782920	53.51418	62.37776	47.56898	47.51607	69.48458	46.16663
0.2110	0.9388	4.8221	0.4300	5.3684	0.5028	-0.5463		ENSMUSG00000061561.5	Olfr373	282-1	1.2	1	chr8:72083177-72103084	53.51418	27.35867	46.34927	22.24156	39.22517	24.55672
0.0701	0.7146	3.2207	0.2418	4.3382	0.2440	-1.1175		ENSMUSG00000051952.5	Olfr371	141-3	1.3	1	chr8:85225988-85231509	20.16476	16.4152	23.17463	8.087841	7.845034	10.80496
0.3366	0.9965	8.3481	0.3419	8.5671	0.1441	-0.2190		ENSMUSG00000054141.5	Olfr24	132-1	1.3	1	chr9:18751507-18763996	379.2527	342.5305	418.3631	297.2282	425.8732	272.0884
0.0066	0.3134	6.1852	0.1477	6.9063	0.2191	-0.7211		ENSMUSG00000094449.3	Olfr972	171-17 (171-1,43,18 = ZI 1-1.9)	1.4	1	chr9:39866422-39874651	140.3778	117.0951	103.676	79.86743	65.00171	72.68789
0.9322	0.9991	5.8567	0.3459	5.8967	0.2720	-0.0400		ENSMUSG00000044897.3	Olfr821	109-1	1.5	1	chr10:130030348-130035071	58.16759	49.2456	71.96334	43.47215	67.24314	64.82974
0.4666	0.9991	5.0094	0.0661	5.2521	0.5511	-0.2428		ENSMUSG00000049528.7	Olfr429	105-1	1.7	1	chr1:174084331-174091343	48.86077	24.07563	45.12955	33.36234	31.38013	30.45033
0.0496	0.6450	5.5880	0.2335	6.2371	0.4682	-0.6491		ENSMUSG00000045306.3	Olfr734	242-1	1.7	1	chr14:50316506-50326761	93.06814	51.43429	87.81966	39.42822	51.55308	53.04251
0.4795	0.9991	5.9577	0.1279	6.1557	0.2635	-0.1980		ENSMUSG00000051493.7	Olfr974	171-1	1.7	1	chr9:39937501-39945170	86.08803	68.94384	59.76616	55.60391	65.00171	64.82974
0.2210	0.9438	6.1234	0.1437	6.4650	0.1182	-0.3416		ENSMUSG00000111190.2	Olfr947-ps	171-43	1.9	1	chr9:39287813-39299548	91.51701	79.8873	92.69853	61.66979	73.96746	72.68789
0.6856	0.9991	3.9856	0.2851	4.2217	0.2058	-0.2361		ENSMUSG00000044025.6	Olfr790	112-1	2	2	chr10:129498492-129503342	15.51136	18.60389	20.7352	12.13176	16.81079	17.68084
0.0029	0.2220	7.2880	0.1593	7.8943	0.1231	-0.6063		ENSMUSG00000050763.4	Olfr1395	277-1	2	2	chr11:49142274-49150453	217.9346	237.4732	258.5801	138.5043	172.5907	158.1453
0.3291	0.9929	5.1365	0.4775	5.5720	0.1221	-0.4355		ENSMUSG00000095218.2	Olfr1338	259-9	2	2	chr4:118751975-118758737	48.86077	42.67952	50.00842	25.2745	49.31164	33.39714
0.8153	0.9991	5.8173	0.1883	5.8964	0.0374	-0.0791		ENSMUSG00000043087.5	Olfr855	148-1	2	2	chr9:19582617-19586030	59.71872	60.18907	57.32673	52.57097	65.00171	51.07798
0.2172	0.9421	5.0504	0.4097	5.5546	0.2787	-0.5042		ENSMUSG00000059623.6	Olfr39	144-1	2	2	chr9:20282351-20287578	57.39202	44.86821	39.03096	32.35136	43.70804	24.55672
0.0463	0.6303	7.2554	0.0697	7.6766	0.2817	-0.4211		ENSMUSG00000075066.7	Olfr32	227-7	2.1	2	chr2:90136273-90142296	250.5084	169.6237	200.0337	144.5702	153.5385	159.1275
0.0054	0.2903	7.3317	0.3322	7.9725	0.1754	-0.6408		ENSMUSG00000052625.8	Olfr851	155-1	2.1	2	chr9:19493295-19502815	288.5112	233.0958	234.1858	123.3396	177.0736	189.5779
0.1855	0.9119	5.7894	0.3094	6.2277	0.3573	-0.4383		ENSMUSG00000101918.2	Olfr1225	233-11	2.1	2	chr2:89168380-89174669	85.31246	55.81168	86.59995	45.49411	69.48458	52.06024
0.4053	0.9991	7.1047	0.2898	7.3099	0.2834	-0.2052		ENSMUSG00000052182.4	Olfr849	151-1	2.1	2	chr9:19440266-19446923	193.1164	130.2272	157.3436	113.2298	169.2286	134.5708
0.0058	0.2974	5.8797	0.2391	6.7657	0.6282	-0.8859		ENSMUSG00000056564.7	Olfr324	102-2 (102-1=ZI 2.3)	2.3	2	chr11:58595114-58600783	148.1335	65.6608	130.5098	64.70273	63.88099	48.13117
0.2888	0.9774	7.6964	0.0786	7.8913	0.1935	-0.1948		ENSMUSG00000051706.3	Olfr1325	102-1	2.3	2	chrX:74592679-74597578	276.1022	224.3411	214.6703	220.3937	200.6087	200.3828
0.1011	0.7948	2.3668	0.3875	3.5590	0.9222	-1.1922		ENSMUSG00000051793.4	Olfr284	160-4	2.4	2	chr15:98340022-98340987	12.40909	5.471733	20.7352	6.065881	3.362157	4.911344
0.5004	0.9991	6.6548	0.2227	6.8351	0.0763	-0.1803		ENSMUSG00000101391.3	Olfr1217	233-4	2.4	2	chr2:89021336-89032065	107.0284	116.0007	118.3126	91.99919	119.9169	91.351
0.5954	0.9991	6.3535	0.3882	6.5288	0.1995	-0.1753		ENSMUSG00000075104.3	Olfr1219	233-6	2.4	2	chr2:89072241-89083513	107.8039	85.35904	84.16051	62.68077	107.589	79.56377
0.0310	0.5596	4.7593	0.0988	5.6150	0.6883	-0.8557		ENSMUSG00000075377.2	Olfr362	158-1	2.5	2	chr2:37101706-37117910	72.90338	28.45301	54.88729	27.29646	28.01798	24.55672
0.0026	0.2075	6.2584	0.2510	7.0671	0.1990	-0.8087		ENSMUSG00000075166.2	Olfr1104	207-1	2.5	2	chr2:87020703-87027080	156.6647	124.7555	121.9718	69.75763	93.01968	67.77654
0.0063	0.3110	6.8537	0.2865	7.5050	0.1057	-0.6514		ENSMUSG00000068806.5	Olfr1259	232-9	2.5	2	chr2:89940532-89948664	196.9942	171.8124	175.6393	94.02115	140.0899	115.9077
0.0022	0.1938	6.2167	0.2998	7.1823	0.6307	-0.9656		ENSMUSG00000049648.4	Olfr273	262-8	2.5	2	chr4:52852154-52859236	231.8948	97.39685	134.1689	94.02115	66.12243	64.82974
0.0087	0.3430	4.3351	0.7676	5.6854	0.4476	-1.3503		ENSMUSG00000043385.4	Olfr267	262-1	2.5	2	chr4:58782704-58787716	66.69883	36.11344	54.88729	20.2196	11.20719	33.39714
0.0043	0.2674	7.3808	0.1804	7.9918	0.2435	-0.6110		ENSMUSG00000051051.7	Olfr523	104-4 (104-1 =ZI 2.5)	2.5	2	chr7:140173217-140178758	222.588	239.6619	307.3688	172.8776	183.7979	144.3935
0.6707	0.9991	4.1065	0.2700	4.2707	0.6650	-0.1642		ENSMUSG00000043529.4	Olfr266	122-2	2.5	2	**chr3:106820485-106826287**	22.49147	10.94347	26.83379	20.2196	16.81079	13.75176
0.4685	0.9991	5.4684	0.2151	5.1675	0.2727	0.3009		ENSMUSG00000051392.5	Olfr1402	217-1	2.5	2	**chr3:97407450-97422020**	44.20737	31.73605	31.71266	42.46117	51.55308	38.30848
0.4646	0.9991	3.4297	0.8236	4.0100	0.5860	-0.5803		ENSMUSG00000110970.2	Olfr156	262-6, 37B	2.5	2	chr4:43820132-43823895	22.49147	9.84912	17.07605	20.2196	6.724314	7.85815
0.1131	0.8121	5.1025	0.2789	5.6831	0.8928	-0.5806		ENSMUSG00000111611.1	Olfr157	262-12, 37C	2.5	2	chr4:43830542-43840201	83.76133	25.16997	62.2056	41.45019	28.01798	33.39714
0.0954	0.7854	4.9573	0.6435	5.7315	0.7592	-0.7742		ENSMUSG00000071000.3	Olfr155	262-14, 37A	2.5	2	chr4:43851565-43857595	69.80111	28.45301	73.18305	49.53803	20.17294	28.48579
0.1126	0.8120	4.6109	0.2688	5.2752	0.6266	-0.6643		ENSMUSG00000051593.4	Olfr272	262-7	2.5	2	chr4:52910207-52919178	60.49429	25.16997	36.59153	19.20862	26.89726	26.52126
0.7642	0.9991	6.0390	0.1558	5.9370	0.2087	0.1019		ENSMUSG00000073898.3	Olfr713	263-1, P3	2.5	2	chr7:107031174-107040994	67.4744	51.43429	64.64503	61.66979	73.96746	60.90066
0.2687	0.9651	5.1189	0.6235	4.4155	0.9373	0.7033		ENSMUSG00000049674.7	Olfr714	263-2, P4	2.5	2	chr7:107070981-107077802	34.90055	26.26432	9.75774	24.26352	56.03595	29.46806
0.1937	0.9199	7.1834	0.1532	7.4656	0.1435	-0.2822		ENSMUSG00000073897.5	Olfr17	P2, 263-5	2.5	2	chr7:107093220-107099808	157.4403	182.7559	190.2759	130.4164	161.3835	144.3935
0.7832	0.9991	7.8876	0.1223	7.8328	0.1887	0.0548		ENSMUSG00000056883.5	Olfr533	252-3	2.5	2	chr7:140463370-140468128	201.6476	261.5488	223.2083	228.4815	221.9024	260.3012
0.4352	0.9991	6.1751	0.4371	5.9318	0.2605	0.2433		ENSMUSG00000054498.6	Olfr308	104-1	2.5	2	chr7:86318218-86325630	73.67895	51.43429	58.54644	50.54901	88.53681	82.51058
0.0066	0.3134	7.6254	0.2635	8.2018	0.2118	-0.5764		ENSMUSG00000046650.4	Olfr1440	215-1	2.6	2	chr19:12387279-12401584	345.1277	284.5301	258.5801	202.196	233.1096	162.0743
0.0500	0.6455	6.2824	0.1574	6.8304	0.4901	-0.5480		ENSMUSG00000048173.5	Olfr1324	128-2	2.6	2	chrX:50420998-50428498	164.4204	105.0573	84.16051	74.81253	87.41609	70.72335
0.8510	0.9991	6.5901	0.2589	6.5968	0.4765	-0.0067		ENSMUSG00000049028.7	Olfr873	145-2	2.6	2	chr9:20298532-20303599	141.1533	80.98165	78.06192	77.84547	107.589	105.1028
0.5611	0.9991	4.9191	0.7214	5.1598	0.9380	-0.2407		ENSMUSG00000046210.6	Olfr735	243-1	2.7	2	chr14:50342612-50348872	54.28975	16.4152	48.7887	17.18666	47.0702	32.41487
0.6246	0.9991	5.3639	0.2039	5.5346	0.2098	-0.1706		ENSMUSG00000049806.4	Olfr466	209-1	2.8	2	chr13:65150240-65156152	54.28975	41.58517	42.69011	40.4392	47.0702	35.36168
0.0054	0.2903	6.4850	0.4190	7.2694	0.1308	-0.7844		ENSMUSG00000046493.5	Olfr1352	139-1	2.8	2	chr10:78981050-78987903	165.9715	157.5859	139.0478	65.71371	117.6755	91.351
0.0363	0.5884	6.0292	0.4798	6.7802	0.8993	-0.7510		ENSMUSG00000048153.6	Olfr49	118-1	2.8	2	chr14:54278253-54284939	214.8323	62.37776	97.5774	95.03213	56.03595	51.07798
0.5139	0.9991	5.0623	0.3696	4.6938	0.5454	0.3685		ENSMUSG00000046450.3	Olfr71	262-4	2.8	2	chr4:43704562-43710255	38.77839	22.98128	18.29576	40.4392	35.86301	24.55672
0.6961	0.9991	4.4340	0.6911	4.7028	0.4450	-0.2688		ENSMUSG00000056184.5	Olfr283	160-1	2.9	2	chr15:98377699-98380946	34.90055	18.60389	25.61407	15.1647	36.98373	16.69857
0.4534	0.9991	4.5326	0.5149	4.9414	0.2632	-0.4088		ENSMUSG00000044039.4	Olfr1288	245-9	2.9	2	chr2:111474101-111479994	33.34942	33.92475	24.39435	34.37332	19.05222	17.68084
0.0000	0.0143	6.0190	0.0902	7.0831	0.1032	-1.0641		ENSMUSG00000048425.3	Olfr686	35-1	2.9	2	chr7:105201858-105207485	146.5823	131.3216	128.0703	60.65881	63.88099	68.75881
0.1216	0.8353	4.8735	0.2492	5.4242	1.0517	-0.5507		ENSMUSG00000091983.6	Olfr457	257-1	2.9	2	chr6:42468015-42476335	90.74144	20.79259	40.25068	31.34038	23.5351	32.41487
0.8127	0.9991	5.6029	0.2561	5.4851	0.3778	0.1178		ENSMUSG00000073969.3	Olfr556	41-1	2.9	2	chr7:102664899-102673270	59.71872	36.11344	40.25068	51.55999	39.22517	55.00705

Icons in column 2 represent whether the gene is significantly differentially expressed between the two groups based on the p-value. A red "x" indicates no significance. A green "✓" indicates a differentially expressed gene. Columns 7 and 8 contain values and bars representing log2-fold change between the two groups. Positive values (red cells) represent genes downregulated in the *Amigo*$^{neo/neo}$ group while negative values (green cells) represent overexpressed genes in the neomycin-containing samples. Alternate OR gene names are indicated in column 11 along with zone index and zone in columns 12 and 13, respectively. This table contains OR genes with zone indices smaller than 3. Table is continued on next page (table 3)

Table 3: (continuation of table 2)

pvalue	padj	Amigo1-/- mean (log2)	Amigo1-/- sd	Amigo1neo/neo mean (log2)	Amigo1neo/neo sd	log2FoldChange (unshrunken)	Change	EnsemblID	Gene	MOR	Zone Index (Miyamichi)	Zone	Location	A1.1.1.2018070.4	A1.1.1.2018070.8	A1.1.1.2018070.9	A1.5.1.2018060.12	A1.5.1.2018060.2	A1.5.1.2018060.7
0.1099	0.8108	8.9416	0.1163	9.1725	0.0316	-0.2309		ENSMUSG00000059043.2	Olfr15	256-17	3	3	chr16:3830878-3844747	590.9827	566.8716	572.0475	454.9411	487.5128	534.3542
0.0049	0.2823	6.5060	0.3241	5.6233	0.2345	0.8827		ENSMUSG00000042849.11	Olfr1414	103-2 (103-1 = ZI 3.0)	3	3	chr1:92506366-92518661	58.94316	44.86821	43.90983	95.03213	70.6053	110.0141
0.4898	0.9991	7.5726	0.0701	7.7050	0.0951	-0.1324		ENSMUSG00000049168.9	Olfr449	103-1	3	3	chr6:42834384-42839516	194.6675	222.1524	208.5717	180.9654	199.488	189.5779
0.6993	0.9991	6.3181	0.1274	6.3964	0.3507	-0.0783		ENSMUSG00000046881.7	Olfr374	130-1	3	3	chr8:72107040-72118200	110.9062	71.13253	74.40277	71.77959	85.17465	81.52831
0.8676	0.9991	5.9634	0.2521	5.8960	0.2830	0.0674		ENSMUSG00000052012.6	Olfr796	269-1	3.1	3	chr10:129605492-129612570	72.90338	49.2456	57.32673	50.54901	67.24314	69.74108
0.6533	0.9991	3.8866	0.3045	4.0478	0.6764	-0.1612		ENSMUSG00000075088.2	Olfr1239	231-3	3.1	3	chr2:89417030-89420407	27.92044	12.03781	12.19718	11.12078	15.69007	16.69857
0.1017	0.7965	5.7478	0.2366	5.1463	0.1611	0.6015		ENSMUSG00000051046.7	Olfr214	119-1	3.1	3	chr6:116554235-116560611	39.55396	33.92475	31.71266	44.48313	61.63955	55.00705
0.7368	0.9991	4.7586	0.1637	4.8932	0.2293	-0.1346		ENSMUSG00000042774.8	Olfr1353	139-2	3.2	3	chr10:78963309-78971338	33.34942	30.64171	24.39435	24.26352	30.25941	25.53899
0.8323	0.9991	7.7688	0.1198	7.7011	0.2808	0.0677		ENSMUSG00000053391.5	Olfr211	253-9	3.2	3	chr6:116489091-116498221	259.0397	192.605	179.2985	215.3388	237.5924	201.3651
0.5229	NA	2.6324	0.7268	1.9086	0.9813	0.7238		ENSMUSG00000075100.4	Olfr1223	233-10	3.3	3	chr2:89143508-89151560	4.653407	5.471733	1.219718	3.03294	6.724314	8.840419
0.4158	0.9991	4.4887	0.1751	3.9910	0.5409	0.4977		ENSMUSG00000057464.4	Olfr1415	103-12	3.4	3	chr1:92489101-92496101	20.16476	9.84912	18.29576	19.20862	22.41438	24.55672
0.0602	0.6887	5.6142	0.5503	6.3373	0.1680	-0.7231		ENSMUSG00000049041.6	Olfr398	157-1	3.4	3	chr11:73979967-73990407	70.57667	88.64208	82.94079	32.35136	50.43236	69.74108
0.0018	0.1716	7.5926	0.5273	6.7816	0.1364	0.8110		ENSMUSG00000054938.7	Olfr1346	103-6 (103-12,15 = 3.4,4.0)	3.4	3	chr7:6467101-6478112	98.49712	112.7177	118.3126	196.1301	132.2449	275.0353
0.1463	0.8697	5.2045	0.6059	4.4956	0.5490	0.7089		ENSMUSG00000046300.4	Olfr1412	208-4	3.5	3	chr1:92585779-92591375	31.79828	22.98128	14.63661	22.24156	44.82876	48.13117
0.6016	NA	1.6635	1.0126	0.6375	1.5701	1.0260		ENSMUSG00000111456.1	Olfr1245	231-12	3.5	3	chr2:89573406-89578447	3.877839	0	1.219718	1.01098	5.603595	2.946806
0.6681	0.9991	4.7765	0.4034	4.9493	0.4764	-0.1728		ENSMUSG00000060974.3	Olfr530	252-2	3.5	3	chr7:140371872-140376331	44.20737	27.35867	23.17463	23.25254	22.41438	37.32621
0.8289	0.9991	6.8935	0.1476	6.9469	0.1038	-0.0534		ENSMUSG00000062712.3	Olfr531	251-3	3.5	3	chr7:140399045-140402918	118.6619	133.5103	117.0929	105.1419	125.5205	125.7304
0.9482	0.9991	6.1654	0.1043	6.1725	0.2416	-0.0071		ENSMUSG00000057997.6	Olfr541	253-3	3.5	3	chr7:140697267-140705606	70.57667	85.35904	60.98588	65.71371	72.84674	75.6347
0.6307	0.9991	4.2306	0.3320	3.9125	0.4635	0.3181		ENSMUSG00000074955.3	Olfr1305	245-8	3.6	3	chr2:111867657-111877149	20.94033	10.94347	13.41689	14.15372	19.05222	22.59218
0.5739	0.9991	6.7024	0.1515	6.8473	0.1511	-0.1449		ENSMUSG00000063230.5	Olfr535	253-7	3.6	3	chr7:140484216-140497104	101.5994	120.3781	123.1915	108.1749	91.89896	111.9786
0.9905	0.9997	6.2298	0.0273	6.1516	0.5342	0.0782		ENSMUSG00000048067.8	Olfr1349	232-8	3.7	3	chr7:6513269-6522950	106.2528	64.56645	51.22814	73.80155	76.2089	73.67016
0.9344	NA	0.6200	0.0678	0.2365	1.0861	0.3835		ENSMUSG00000094266.1	Olfr340	136-1	3.8	3	chr2:36452587-36453525	1.551136	1.094347	0	1.01098	1.120719	0.982269
0.4007	0.9991	5.1044	0.2825	5.4390	0.2445	-0.3345		ENSMUSG00000063549.4	Olfr322	216-1	4	4	chr11:58658782-58669528	41.88066	51.43429	36.59153	27.29646	40.34589	35.36168
0.1430	0.8679	8.8651	0.2780	8.6051	0.1609	0.2600		ENSMUSG00000044985.6	Olfr124	SR1, 256-3	4	4	chr17:37799888-37808617	400.9686	343.6248	426.9011	439.7764	397.8553	577.574
0.1332	0.8509	4.2192	0.6331	3.1666	0.8243	1.0526		ENSMUSG00000108827.3	Olfr1310	245-3	4	4	chr2:112004574-112012708	9.306814	4.377387	14.63661	19.20862	11.20719	27.50353
0.4988	0.9991	6.0618	0.2194	6.2726	0.0885	-0.2109		ENSMUSG00000075112.2	Olfr1211	233-21	4	4	chr2:88926876-88938111	76.78122	72.22688	81.72108	68.74665	56.03595	75.6347
0.3929	0.9991	7.4917	0.3353	7.2920	0.2515	0.1997		ENSMUSG00000075068.3	Olfr140	235-1	4	4	chr2:90049380-90063594	184.5851	130.2272	158.5633	181.9764	141.2106	224.9395
0.8636	0.9991	7.6691	0.3207	7.6329	0.2930	0.0362		ENSMUSG00000036647.5	Olfr6	m50, 103-16	4	4	chr7:106953251-106963937	223.3635	156.4916	221.9886	209.2729	160.2628	249.4963
0.2369	0.9506	5.6778	0.2753	5.2009	0.4165	0.4769		ENSMUSG00000070417.6	Olfr2	103-15, i7	4	4	chr7:106995399-107006072	46.53407	26.26432	39.03096	51.55999	41.46661	60.90066
0.6106	0.9991	8.3400	0.5299	7.9757	0.8594	0.3643		ENSMUSG00000050030.5	Olfr728	246-1	4.1	4	chr14:50133758-50142680	299.3692	129.1329	409.8251	230.5035	307.077	478.3649
0.0970	0.7894	7.3650	0.2126	7.7188	0.1282	-0.3538		ENSMUSG00000045341.2	Olfr167	272-1	4.1	4	chr16:19509558-19522266	231.1192	193.6994	207.352	173.8886	138.9692	183.6843
0.0126	0.3942	8.2360	0.5144	7.5340	0.4787	0.7020		ENSMUSG00000059488.3	Olfr727	246-2 (246-1 = ZI 4.1)	4.1	4	chr14:50123186-50128746	127.1931	240.7563	206.1323	380.1285	199.488	359.5104
0.2558	0.9577	7.3290	0.0801	7.0402	0.2701	0.2888		ENSMUSG00000051313.12	Olfr1262	234-1	4.1	4	chr2:90000145-90008291	162.8692	118.1894	117.0929	154.68	155.78	170.9148
0.1310	0.8482	6.5792	0.4315	6.1666	0.0817	0.4127		ENSMUSG00000061295.5	Olfr1261	234-3	4.2	4	chr2:89991221-89996189	67.4744	71.13253	75.62249	115.2517	67.24314	110.9964
0.6289	0.9991	6.9881	0.1307	6.8770	0.1255	0.1111		ENSMUSG00000072707.3	Olfr31	274-1	4.3	4	chr14:14322828-14331791	120.213	106.1516	125.6309	124.3506	116.5548	139.4822
0.2611	0.9600	4.9296	0.2065	4.3368	0.5868	0.5927		ENSMUSG00000109528.2	Olfr1309	245-5	4.3	4	chr2:111979857-111990281	12.40909	21.88693	28.0535	28.30744	26.89726	35.36168
0.8706	0.9991	5.3579	0.4204	5.2675	0.5146	0.0904		ENSMUSG00000050504.3	Olfr1323	216-1	4.3	4	chrX:50005448-50019359	49.63634	25.16997	43.90983	51.55999	29.1387	44.20209
0.1020	0.7971	8.1304	0.3625	7.7649	0.2657	0.3655		ENSMUSG00000075097.3	Olfr1226	233-2	4.4	4	chr2:89188839-89200048	222.588	178.3785	257.3604	277.0086	218.5402	361.4749
0.3965	0.9991	7.4376	0.6246	7.2240	0.3736	0.2137		ENSMUSG00000075069.3	Olfr1264	236-1	4.5	4	chr2:90018526-90025577	196.2187	117.0951	143.9267	190.0643	107.589	252.4431
0.0479	0.6366	9.6416	0.3179	9.3250	0.0284	0.3166		ENSMUSG00000052508.10	Olfr536	252-1	4.5	4	chr7:140500849-140507396	637.5168	630.3437	654.9883	865.399	621.9991	944.9426
0.2882	0.9774	5.9874	0.3849	5.5809	0.3947	0.4065		ENSMUSG00000075073.3	Olfr1256	231-1	4.6	4	chr2:89825311-89841555	65.1477	40.49083	40.25068	62.68077	48.19092	82.51058
0.0004	0.0697	6.7028	0.3578	5.6168	0.2015	1.0860		ENSMUSG00000035626.4	Olfr1509	244-3	4.7	4	chr14:52442990-52452574	43.4318	56.90603	46.34927	97.05409	84.05393	136.5354
0.0516	NA	1.5052	1.4889	-1.0000	0.0000	2.5052		ENSMUSG00000075427.14	Olfr288	286-3	4.8	4	chr15:98186013-98195542	0	0	0	1.01098	1.120719	8.840419
0.0925	0.7788	6.8551	0.2993	6.4163	0.1905	0.4388		ENSMUSG00000042894.11	Olfr1260	232-2	4.8	4	chr2:89974340-89981586	72.90338	93.01946	90.2591	120.3066	91.89896	138.4999
0.0000	0.0000	8.6494	0.4773	7.0768	0.3450	1.5725		ENSMUSG00000057564.6	Olfr1508	244-2	4.9	4	chr14:52458829-52467495	103.9261	140.0764	167.1013	366.9858	303.7149	578.5563
0.0000	0.0011	8.0509	0.5308	6.7310	0.2468	1.3199		ENSMUSG00000099486.3	Olfr1228	233-1	4.9	4	chr2:89247964-89254062	86.8636	113.8121	119.5323	277.0086	179.3151	373.2621
0.0072	0.3152	8.9894	0.9820	7.2701	0.7226	1.7193		ENSMUSG00000059887.7	Olfr1507	244-1, MOR28, SP1	5	4	chr14:52488791-52495749	122.5397	273.5867	108.5549	983.6837	252.1618	527.4783
0.0000	0.0001	5.3605	0.2737	1.7803	0.4390	3.5802		ENSMUSG00000090129.9	Olfr287	286-1 (248-11 = ZI 5.0)	5	4	chr15:98206971-98221056	2.326704	4.377387	2.439435	45.49411	32.50085	45.18436
0.0007	0.1032	7.6395	0.4540	6.6628	0.4143	0.9767		ENSMUSG00000059460.6	Olfr286	286-2	5	4	chr15:98224308-98234450	118.6619	72.22688	119.5323	217.3607	140.0899	258.3367
0.0147	0.4301	5.9059	0.5165	5.0272	0.0274	0.8787		ENSMUSG00000074965.5	Olfr1277	248-11	5	4	chr2:111264946-111274106	31.79828	32.8304	31.71266	70.76861	39.22517	75.6347
0.0000	0.0009	7.0509	0.7620	5.2053	0.3980	1.8456		ENSMUSG00000109449.3	Olfr1280	248-1 (248-11 = ZI 5.0)	5	4	chr2:111314017-111326003	26.36931	41.58517	43.90983	142.5482	75.08818	215.1169
0.0000	0.0161	6.8333	0.6001	5.2077	0.6617	1.6257		ENSMUSG00000095156.2	Olfr1281	248-14P, 248-18 (248-11 = ZI 5.0)	5	4	chr2:111326520-111332852	21.7159	53.62299	41.4704	133.4494	70.6053	155.1985
0.0027	0.2125	5.2985	0.4637	3.9220	0.0959	1.3764		ENSMUSG00000096703.3	Olfr1286	248-21 (248-11 = ZI 5.0)	5	4	chr2:111417842-111423115	13.96022	14.22651	15.85633	43.47215	26.89726	50.09571
0.0106	0.3664	6.9177	0.1511	7.4850	0.1585	-0.5673		ENSMUSG00000094858.3	Olfr1297	248-4 (248-11 = ZI 5.0)	5	4	chr2:111615233-111626497	179.1562	199.1711	159.783	109.1859	118.7962	134.5708

List of olfactory receptor genes from RNA sequencing data with known zone indices. Icons in column 2 represent whether the gene is significantly differentially expressed between the two groups based on the p-value. A red "x" indicates no significance. A green "✓" indicates a differentially expressed gene. Columns 7 and 8 contain values and bars representing log2-fold change between the two groups. Positive values (red cells) represent genes downregulated in the *Amigo*$^{neo/neo}$ group while negative values (green cells) represent overexpressed genes in the neomycin-containing samples. Alternate OR gene names are indicated in column 11 along with zone index and zone in columns 12 and 13, respectively. This table contains OR genes with zone indices 3 or higher.

VI. Discussion

We have identified Amigo1 as a cell adhesion molecule preferentially expressed in ORNs of the ventrolateral region of the developing OE. Insertion of a neomycin resistance cassette in the *Amigo1* locus to ablate Amigo1 expression specifically altered the development of ventrolateral ORNs, leading to reduced numbers of ORNs that express ventrolateral ORs. In contrast, loss of Amigo1 expression in the absence of the neomycin resistance cassette was not sufficient to adversely affect the development of ventrolateral ORNs, indicating that Amigo1 is not necessary for their proper development. These results represent a new example of the potential deleterious effect insertion of a neomycin resistance cassette in the genome can have on very selective cell populations that normally specifically express the original gene-of-interest, and how such effects can lead to misinterpretation of protein function. Hence, they highlight the importance of removing selection cassettes in mouse models generated by this strategy.

While unexpected, the defects we observed in the *Amigo1*$^{neo/neo}$ animals became of interest to study in the development of the mouse main olfactory system map. We made use of this neomycin-containing mouse line to attempt to uncover novel mechanisms contributing to zonal OR identity and ORN development. Our results provide the first instance to postulate that ORNs in *Amigo1*$^{neo/neo}$ mice might not be attaining an OR identity due to misregulation of OR gene expression.

1. Mechanisms underlying the loss of OR identity in ventrolateral ORNs in *Amigo1*$^{neo/neo}$ mice

OR genes reside in gene clusters around the genome (Sullivan et al., 1996; Niimura et al., 2014). The expression of a single OR in mature ORNs appears to be regulated by both epigenetic mechanisms and OR signalling. The expression of multiple ORs or switching of OR genes can

occur until a functional OR gene is more strongly expressed, its signalling promoting type 3 adenylyl cyclase expression, thereby eliciting a feedback mechanism causing repression of other OR gene loci (Dalton et al., 2013). OR gene choice also depends on the silencing of all OR loci in newly born ORNs followed by the demethylation of epigenetic marks from a single OR allele (Magklara et al., 2011; Clowney et al., 2012). OR elements which are regulatory sequences similar to enhancers can influence the probability of a given OR gene to be transcribed (Lomvardas et al., 2006; Degl'Innocenti and D'Errico, 2017; Monahan et al., 2019). For example, the H element is a genetic region that regulates a cluster of OR genes known as the MOR28 cluster. Knockout of the H cluster reduces the size of the ORN population expressing ORs from its neighbouring MOR28 cluster (Fuss et al., 2007; Markenscoff-Papadimitriou et al., 2014). Furthermore, DNA footprinting and 4C chromatin capture have revealed enrichments in multiple enhancer elements around specific OR gene locus, suggesting interchromosomal enhancer interactions being important for stable OR gene expression (Markenscoff-Papadimitriou et al., 2014; Monahan et al., 2019). It is possible that the presence of the neomycin cassette in the Amigo1 locus can cause disruptions to enhancer interactions and chromatin structure important for controlling OR gene choice. Insertion of a neomycin resistance gene cassette in several genes has been shown on multiple occasions to cause misregulation of gene expression of genes both locally and at long range, and to affect co-regulation of genes in clusters (Fiering et al., 1995; Pham et al., 1996; Müller, 1999; Coleman et al., 2015; West et al., 2016). These effects have been suggested in part to be due to the exogenous promoter in the neomycin cassette (West et al., 2016). Our RNA sequencing data comparing gene expression in the OE *Amigo1*$^{neo/neo}$ and *Amigo1*$^{-/-}$ mice identified trends for ORs within a cluster to be similarly either upregulated or downregulated in the samples isolated from *Amigo1*$^{neo/neo}$ mice.

This observation suggests that the neomycin cassette may be interfering with enhancer interaction networks and thus modifying OR gene expression.

Our observation that there is a reduced number of ORNs expressing ventrolateral ORs in *Amigo1*$^{neo/neo}$ mice suggests that OR gene choice is indeed affected in these ORNs. Since the survival of ORNs and the thickness of the OE is unaffected in these mice, it is possible that many ORNs in the ventrolateral region of the OE remain without an OR identity and do not express an OR. This prospect is quite surprising as much evidence points towards a mechanism whereby immature ORNs express multiple ORs or undergo OR gene switching until stabilization of the expression of a single OR takes over (Lewcock and Reed, 2004; Serizawa et al., 2004; Shykind et al., 2004; Lomvardas et al., 2006; Young et al., 2011). It remains to be confirmed whether many individual cells in the ventrolateral region of *Amigo1*$^{neo/neo}$ OE indeed lack OR expression completely or just express low levels of multiple OR genes, below the detection sensitivity of our ISH probes. To establish whether these cells are indeed not expressing any OR, or instead expressing low levels of multiple ORs, single cell reverse transcription polymerase chain reaction (RT-PCR) or RNAseq could be performed on cells isolated from the ventrolateral region of the OE of *Amigo1*$^{neo/neo}$ mice (Malnic, 2013).

2. Potential factors influencing region-specific effects on OR expression and ORN development.

The insertion of the neomycin-resistance cassette in the *Amigo1* locus may specifically alter expression of clusters of OR expressed in the ventrolateral region of the OE, as suggested by our RNAseq data. However, it remains possible that there are fundamental differences in the development of ORNs across the OE that modulate their sensitivity to the effects exerted by the insertion of the neomycin cassette in the *Amigo1* locus. Differences in properties of ORNs across

the dorsomedial to ventrolateral regions of the OE have been identified over the years. Class I ORs are phylogenetically different from class II ORs and are expressed exclusively in the most dorsomedial region of the OE (Zhang et al., 2004; Miyamichi et al., 2005; Niimura and Nei, 2005, 2007; Tsuboi et al., 2006). It is also known that the generation of ORNs proceeds in a graded manner from dorsomedial to ventrolateral. Cells expressing ventrolateral ORs, such as I7 and MOR28, are produced at late embryonic stages, with highest rates of production of MOR28-positive ORNs at P0 (Ihara et al., 2017). Furthermore, ORN turnover rates are lower in dorsomedial versus ventrolateral OE (Vedin et al., 2009). These differences may be attributable to levels of retinoic acid signalling in the OE, which have been shown to have an effect on ORN progenitor cell fate (Paschaki et al., 2013), ORN survival (Hägglund et al., 2006) and recovery after trauma (Peluso et al., 2012). The retinoic acid inactivating enzyme, Cyp26B1 is normally expressed in a dorsomedial to ventrolateral gradient in the OE, which results in different levels of retinoic acid signalling in ORNs depending on their zonal location. Genetic overexpression of Cyp26B1 in all ORNs alters OR expression and ORN turnover, and reduce BACE1 expression, which is required for normal ORN axon guidance and glomerular formation (Rajapaksha et al., 2011; Login et al., 2015b, 2015a). Retinoic acid metabolism is also involved in regulating levels of guidance molecules such as Neuropilin-1 and Kirrel2 as well as altering CNG channel activity important for neuronal survival (Öztokatli et al., 2012). It is thus possible that the inherent differences between dorsomedial and ventrolateral ORN turnover or retinoic acid signalling might contribute to the sensitivity of ventrolateral neurons to the gene expression changes caused by the presence of the neomycin cassette in the *Amigo1* locus.

Our RNAseq analyses also showed that several genes implicated in oxidative stress pathways are misregulated in the OE of *Amigo1*$^{neo/neo}$ mice, raising the possibility of increased oxidative stress

in the OE. A recent study suggested that ORNs located in different regions of the OE have different sensitivities to oxidative stress, which can affect their development (Tuerdi et al., 2018). Hence, it is possible that different cellular mechanisms regulate oxidative stress in dorsal and ventral zones of the OE and that these intrinsic differences could cause ventral neurons to be more susceptible to changes in expression levels of oxidation-related genes caused by the presence of the neomycin cassette. Further studies looking specifically at oxidative stress markers, such as 8-OHdG (Vaishnav et al., 2007; Tuerdi et al., 2018), by immunohistochemistry could help elucidate whether ventrolateral cells of the OE exhibit higher levels of oxidative stress in the *Amigo1*$^{neo/neo}$ mice. It also remains to be investigated whether changes in oxidative stress in ORNs can influence OR gene expression.

Finally, we must also consider the possibility that the loss of Amigo1 expression in ventrolateral ORNs, where we have shown it is specifically expressed, combined with the presence of the neomycin cassette in the *Amigo1* locus, may render ventrolateral ORNs more susceptible to the changes in gene expression observed in *Amigo1*$^{neo/neo}$ mice, causing significant defects in OR identity and axonal projections. Both spontaneous and evoked activity are required for proper establishment and maintenance of the olfactory sensory map and contribute greatly to promotion of cell survival and OR stabilization (Song and Poo, 2001; Yu et al., 2004; Zou et al., 2004; Imai et al., 2006; Kerr and Belluscio, 2006; Serizawa et al., 2006; Kaneko-Goto et al., 2008). Furthermore, Amigo1 has been implicated in the regulation of neuronal activity through the Kv2.1 voltage-gated potassium channel in cortical and hippocampal neurons and could also modulate neuronal activity by altering channel gating properties in ORNs (Kajander et al., 2011; Peltola et al., 2011, 2016). Loss of Amigo1 expression in ventrolateral ORNs of the *Amigo1*$^{neo/neo}$ mice could alter neural activation, which, combined with the misregulation of OR gene caused by the presence

of the neomycin cassette in the *Amigo1* locus, could preclude these neurons from stabilizing OR gene choice and establishing correct axonal projections to the OB. Unfortunately, the presence of the neomycin resistance cassette in the *Amigo1* gene coding region makes it difficult to separate the direct effects of the cassette insertion on ORN development from the combined effects of the cassette insertion and loss of Amigo1 expression.

Future studies aimed at examining how ventrolateral OR gene expression is affected in the *Amigo1*$^{neo/neo}$ mice should provide additional insight in identifying key enhancer interaction networks that can specifically regulate expression of these genes during the development and maturation of ORNs.

VII. Materials and Methods

1. Animals

Animals were housed and handled in strict accordance with the guidelines set by the Canadian Council on Animal Care (CCAC), and protocols and procedures were approved by the Montreal Neurological Institute Animal Care Committee (MNI-ACC). For *in situ* hybridization experiments using embryonic tissue, animals were acquired from timed-pregnant CD1 female mice purchased from Charles River Laboratories. Embryonic day corresponds to the number of days since the date of vaginal plug. For postnatal analysis, day of birth was considered P0. Embryonic stem cells containing the targeted disruption of the *Amigo1* gene (Amigo1$^{tm1(KOMP)Vlcg}$) were purchased from the KOMP Repository (Knockout Mouse Project, US Davis). The whole coding region of *Amigo1* (GRCm38 Chr3:108,187,190-108,188,665) was replaced with the ZEN-Ub1 cassette containing the lacZ gene and a floxed neomycin coding sequence under the control of the human ubiquitin C protomer (http://velocigene.com/komp/detail/10669). Embryonic stem cells were injected in to CD1 blastocysts to produce chimeras. Heterozygotes produced by germline transmission were

crossed to *CMV-Cre* mice to remove the neomycin selection cassette (https://www.jax.org/strain/006054). *Amigo1*^{neo} and *Amigo1*$^{-}$ mouse lines are maintained in a C57Bl/6 mice background. *MOR174-9-ires-tau-GFP* (Cho et al., 2011), *P2-IRES-tau-lacZ* (Mombaerts et al., 1996), and *MOR28-IRES-tau-GFP* (Shykind et al., 2004) mice have been described previously. All analyses included male and female mice.

2. *In situ* hybridization and RT-PCR

Digoxigenin-labeled cRNA probes were prepared by *in vitro* transcription using the DIG labeling mix (Roche). pBluescript vector containing cloned *Amigo1* cDNA was a kind gift from Dr. Heiki Rauvala, and pBluescript containing *m50* cDNA was a kind gift from Dr. Zhihua Zou. DNA fragments of the coding sequences for olfactory receptor probes were PCR amplified from C57Bl/6 genomic DNA and cloned into the pBluescript vector. mRNA sequences of *amigo2* and a*migo3* were PCR amplified from wild type cDNA and cloned into the pBluescript vector. Primer sets used for cloning are as follows:

Gene	Template
Amigo2	F: 5'-TAATACGACTCACTATAGAAGCTTATCCAATAGGCTGAAGTCGGTA-3' R : 5'-AATTAACCCTCACTAAAGGGCTCGAGCCGTTGTAAAACACACGAAAG-3'
Amigo3	F: 5'-TAATACGACTCACTATAGAAGCTTGGGTCTTCAAGAACTGCTCTGT-3' R: 5'-AATTAACCCTCACTAAAGGGCTCGAGGTGGAACTGGCTGATTCAGAG-3'
MOR174-9	F: 5' AGATGGAAATCACAGTGGGG-3' R: 5'-CACAGAGGCCACTTTTACGG-3'
M72	F: 5'-CCGAATCGAGGGCTAACTAACAG-3' R: 5'-CACTCGAGCAGTGCGGTCTTCACC-3'
P2	*F: 5'-TGTCAGGGAATTTATC-3'* *R: 5'-AGCCTTCACCTCATTA-3'*
I7	F: 5'-CTGCGGGCACTACTAT-3' R: 5'-TGGTATTGGCGTCCTG-3'
MOR252-1	F: 5'-TTTCCCGGGTTTCCCCGTTGATGACTTTG-3' R: 5'-ATACCGCGGAGAGATCCTAGGCCCCCATA-3'
MOR28	F: 5'-GGAAAAGGCTGTCCTCATCA-3' R: 5'-GGGTTCAGCAGAGGGGTTAT-3'

In situ hybridization staining was performed as described previously (Pasterkamp et al., 1998). Briefly, sections were fixed for 20 minutes in 4% paraformaldehyde (PFA) followed by washes in 1× phosphate-buffered saline (PBS) treated with Diethyl pyrocarbonate (DEPC). Sections were then deacetylated in 0.25% acetic anhydride in 0.1M triethanolamine and underwent prehybridization in hybridization buffer (50% formamide, 5×Denhardt's solution, 5×Saline Sodium Citrate (SSC), 250 µg/ml bakers' yeast tRNA) before hybridizing with DIG-labelled probes for incubation overnight at 60^{o}C. The following day, stringency washes in 5×SSC, 2×SSC, and 50% formamide in 0.2×SSC were done at 60^{o}C and in 0.2×SSC at room temperature. Sections were then blocked in Blocking Reagent (Roche) at room temperature and probed with an AP-conjugated α-Digoxigenin antibody (Fab fragments, 1:3000, Roche) for 2.5-3 hours at room temperature before visualization of antibody binding using a colorimetric enzymatic reaction with NBT/BCIP stock solution (nitro-bluetetrazolium chloride (NBT) 5-bromo-4-chloro-3-indolylphosphate (BCIP), Roche)

For RT-PCR, 2.5µg of total RNA from tissue samples of adult *Amigo1*$^{+/neo}$ and *Amigo1*$^{neo/neo}$ were treated with DNaseI (Amplification Grade, Invitrogen) and reverse transcribed using SuperScriptII Reverse transcriptase (Invitrogen) along with dNTPs (PCR Grade, Invitrogen), OligodT (Invitrogen), 5× First Strand Buffer (Invitrogen) and dithiothreitol. The following primer sets for PCR were used:

Gene	Template
amigo1	F: 5'-AGATAGCCTCAGCTCTTCT-3' R: 5'-GTATCAGAAAAGACCGAGCT-3'
gapdh	F: 5'-GCCTCCTGCACCACCAACTG-3'; R: 5'-CCGACGCCTGCTTCACCACCTTCT-3'

3. Western Blot

Mouse brain homogenates from *Amigo1*$^{+/+}$, *Amigo1*$^{+/neo}$ and *Amigo1*$^{neo/neo}$ animals were prepared using HEPES-sucrose buffer (20mM HEPES, 320mM sucrose pH 7.4) with protease inhibitors (1µg/mL aprotinin, 1µg/mL leupeptin, 1mM PMSF). After centrifugation (1000x*g* 10 minutes at 4°C), supernatants were loaded onto an SDS-PAGE gel and transferred to PVDF membrane (Immobilon-P, Millipore). Membranes were blotted with α-Amigo1 (1:5, monoclonal mouse clone L86/37, supernatant, NeuroMab) and α-β-actin (1:20,000 donated from Dr. Stefano Stifani) antibodies to show relative amount of Amigo1 protein compared to the control β-actin.

4. Immunohistochemistry

Mouse tissue was fixed by transcardial perfusion with 4% PFA in 1×PBS followed by a 30-minute post fix for adults or fixed by immersion of embryonic and postnatal brains in 4% PFA in 1×PBS. Tissue was cryoprotected in a 30% sucrose solution in 1×PBS and then embedded in OCT (TissueTek, Cedarlane) for storage at -80°C. 20µm cryostat sections of tissue samples were collected onto Superfrost® Plus microscope slides (Fisherbrand). Sections were rehydrated in 1×PBS, blocked with 10% fetal bovine serum (FBS) and 0.5% Triton ×100 for 1 hour at room temperature and incubated overnight at 4°C with primary antibodies. After rinsing with 1×PBS, primary antibodies were detected with Alexa-Fluor conjugated secondaries for 1 hour at room temperature, and the cell nuclei were stained for 5 minutes with Hoechst 33342 (1:20,000, Molecular Probes).

The primary antibodies used were as follows: α-GFP (1:1000, mouse, Molecular probes A11120), α-β-galactosidase (β-gal) (1:1000, rabbit, MP Biochemicals (Cappel), 559762), α-OMP (1:1000, goat, WAKO 544-10001), α-Cleaved caspase 3 (1:1000, rabbit, D175, Cell Signalling 9661S), α-Phosphohistone H3 (PHH3) (1:1000, rabbit, Ser10, D2C8, Cell Signalling 9701S)

The secondary antibodies used were: Donkey α-Mouse Alexa-Fluor-488 (1:500 IgG (H+L), Invitrogen), Donkey α-Rabbit 546 (1:500 IgG (H+L), Invitrogen), Donkey α-goat Alexa-Fluor-546 (1:500 IgG (H+L), Invitrogen)

5. Imaging and Image Analysis

Images of wholemount preparations were taken on the Zeiss Stereoscope Discovery.V20 with the Zeiss AxioCam MRc camera.

Immunohistochemical sections were imaged using the Zeiss Axiocam 503 mono on the Zeiss Axio Imager.M1 microscope.

The volume measurement of glomeruli was taken by measuring the area of GFP or β-gal signal in each section containing the labelled glomerulus. The sum of the area of all sections in μm^2, multiplied by the section thickness (20μm) gave an estimate of the total glomerular volume in μm^3.

In situ hybridization or GFP immunofluorescence was used to quantify the number of cells for each olfactory receptor population. 20μm coronal sections of the entire olfactory epithelium were collected onto alternating slides. Each slide was probed for a different marker (either cRNA OR probes for *in situ* hybridization or GFP antibody for the MOR28-GFP population), and the number of cells on each section was counted for each probe. Results were presented as the average number of positive cells per section.

Similar methods were used to analyse the number of apoptotic cleaved caspase3-positive and proliferating PHH3-positive cells in the OE at P0.

To measure the thickness of the mature olfactory receptor neuron layer in different zones, sections of coronally sliced olfactory epithelium at P7 containing endoturbinates I and II and ectoturbinate 1 (Barrios et al., 2014) were collected and stained for OMP. The thickness of the full OE and of

the OMP layer was measured at specific dorsomedial to ventrolateral locations corresponding undoubtedly to dorsomedial, intermediate, and ventrolateral regions of the OE. All results presented as average ± s.e.m

6. RNAseq

Total RNA was collected from 3 *Amigo1*$^{neo/neo}$ OE and 3 *Amigo1*$^{-/-}$ OE using the RNeasy mini kit (QIAGEN) and sent for RNA sequencing and Bioinformatics at the Genomics Platform at the Institute for Research in Immunology and Cancer (IRIC) where it was processed using Nextseq 500, 0.5 Flowcell High Output, 75 cycles Single-End reads. Sequences were trimmed for adaptor sequences and low-quality reads using Trimmomatic version 0.35 and then mapped to mouse reference genome GRCm38 using STAR version 2.5.1b. Read counts from STAR were used to obtain gene expression levels and DESeq2 version 1.18.1 was used to normalize the read counts and perform sample clustering and identify differentially expressed genes (DEGs).

From sequencing and normalized read count data, OR genes with known zone indices (Miyamichi et al., 2005; Zapiec and Mombaerts, 2020) were plotted in order of zone index against log2 fold change between the two groups.

Chapter 4:

Amigo1 is required in the development and maintenance of hippocampal mossy fiber projections to CA3

Reesha Raja[1,2] Emilie Dumontier[1], Timothy E. Kennedy[1,2], Jean-François Cloutier[1,2]

1 Montreal Neurological Institute, McGill University, Montreal, Quebec, Canada
2 Integrated Program in Neuroscience, McGill University, Montreal, Quebec, Canada
3 Department of Neurology and Neurosurgery, McGill University, Montreal, Quebec, Canada

I. Preface

This chapter is a manuscript in preparation for submission for publication. In characterizing the expression of Amigo1 in the olfactory system, we became interested in the expression pattern of Amigo1 in other brain regions and whether this protein plays a role in axonal development in these regions. Over the last 10 years, roles for Amigo1 in fasciculation and neural excitability have been proposed. Furthermore, cell adhesion molecules and neuronal activity have been implicated in the proper development of hippocampal mossy fiber projections, making Amigo1 an excellent candidate to investigate its potential role in regulating proper targeting of these projections. We provide evidence that proper fasciculation and prevention of ectopic synapse formation are controlled in part by Amigo1.

II. Acknowledgements

We thank Dr. Donald Van Meyel and members of the Cloutier lab for helpful discussions on the development of this project.

We are grateful to Dr. Stephanie Harris and Celina Cheung for technical insights.

This work was supported by CIHR. J.-F.C. held an FRQ-S Senior Scholar Award. R.R. held a Vanier Studentship from CIHR.

III. Abstract

Memory-encoding and learning are functions strongly associated with the hippocampus. The hippocampal formation is known as a brain region associated with high levels of plasticity which can mediate learning, and the generation of new granule cells integrated into the hippocampal circuit is thought to play a role in memory formation. Thus, understanding the complex mechanisms underlying both the formation and maintenance of hippocampal circuity is important for understanding the problems underlying neurological disorders associated with memory. Specifically, the mossy fibers projections from the hippocampal dentate gyrus can undergo synaptic reorganization. Here, we provide evidence that the cell adhesion molecule Amigo1, which can regulate neural excitability, contributes to the development and maintenance of mossy fiber projections in the mouse. We show that loss of Amigo1 expression leads to the defasciculation of mossy fiber bundles during development and to the formation of ectopic mossy fiber boutons in the adult hippocampus.

IV. Introduction

During development of various systems within the brain, cells must connect to one another in precise manners, and they often make use of various cell adhesion molecules (CAMs) to target precisely. Gradients or differential patterns of expression of axon guidance molecules and cell adhesion molecules underlie a common mechanism by which axons can sense their environment and gain orientation. The organization of a multitude of brain subregions rely on regional and spatial differences in the expression of CAMs that control axonal fasciculation and synapse formation and maintenance (Dufour et al., 2003; Price et al., 2006; Walz et al., 2006; Cho et al.,

2009; Demyanenko et al., 2011; Imai and Sakano, 2011; Schwarting and Henion, 2011; Petrovic and Schmucker, 2015). The hippocampus, specifically the mossy fiber projections to CA3, provides a well-established system to study the projection of axonal tracts and the formation and maintenance of synapses (Henze et al., 2000). The projections of mossy fibers to CA3 are oriented along the proximo-distal CA3 axis rather than septo-temporally, which allows visualization of full axonal projections of individual mossy fibers in transverse hippocampal slices. The synapses formed by each mossy fiber onto excitatory pyramidal cells are few (10-15) and yet very large in size, making them easily identifiable by various staining techniques, such as the Timm staining method (Galimberti et al., 2006). Finally, as a brain structure majorly involved in memory formation, it is also of large benefit to understand the complex mechanisms of the development, maintenance, and plasticity of the hippocampus as they contribute to the etiology of neurological brain disorders involving memory defects.

As observed in other regions of the brain, CAMs have been implicated in regulating circuitry formation and maintenance in the hippocampus. For example, Limbic-associated membrane protein (LAMP) is an Ig superfamily member that has been shown to be involved in proper targeting of mossy fiber projections (Pimenta et al., 1995). NCAM is highly expressed on axons projecting from dentate gyrus granule cells, and its ablation leads to defasciculation and premature termination of mossy fibers (Cremer et al., 1997). The post-translational modification of NCAM with polysialic acid (PSA) has also been proposed to modulate synaptic plasticity as removal of PSA causes decreases in plasticity and increases in the number of ectopic mossy fiber boutons (Seki and Rutishauser, 1998; Galimberti et al., 2010). Finally, the CAM Kirrel3 has been implicated particularly in target-specific selection and synapse formation at the mossy fiber terminal (Martin et al., 2015, 2017).

Our examination of the spatio-temporal patterns of expression of Amigo1 in the brain has revealed that Amigo1 is expressed in specific populations of cells in several regions of the brain, including in the olfactory epithelium (Chapter 3) and in the developing cortex and cerebellum. Interestingly, we have found that Amigo1 expression in the hippocampus is restricted to the dentate gyrus during development, suggesting a role for Amigo1 in the dentate granule cells and their projections to CA3. We find that genetic loss of Amigo1 causes changes to the organization of mossy fiber bundles during development and leads to ectopic mossy fiber terminal formation in distal CA3 in ageing animals.

V. Results

1. Amigo1 is differentially expressed in populations of cells of various brain regions.

To examine the expression of Amigo1 in the developing brain, we used heterozygous gene-targeted Amigo1 animals in which the *Amigo1* allele is replaced by the *lacZ* gene. In this mouse, β-galactosidase (β-gal) is expressed in the cells in which the *Amigo1* promoter is active. We first characterized this mouse line to verify that the expression of β-gal protein, detected by X-gal staining, could represent the expression of Amigo1 as seen by *in situ* hybridization and immunohistochemistry in specific regions of the nervous system. X-gal staining in *Amigo1*$^{+/-}$ mice recapitulated the patterns of expression observed by *in situ* hybridization in the olfactory epithelium and trigeminal ganglia (Figure 1A-D), as well as Amigo1 protein expression in the developing cortex of wild-type animals (Figure 1E-F). These results indicate that expression of the *lacZ* gene in these animals mimics endogenous Amigo1 expression and could be used as a reliable reporter for Amigo1 expression in the developing brain.

Figure 1: Amigo1 is expression patterns are recapitulated by X-gal staining

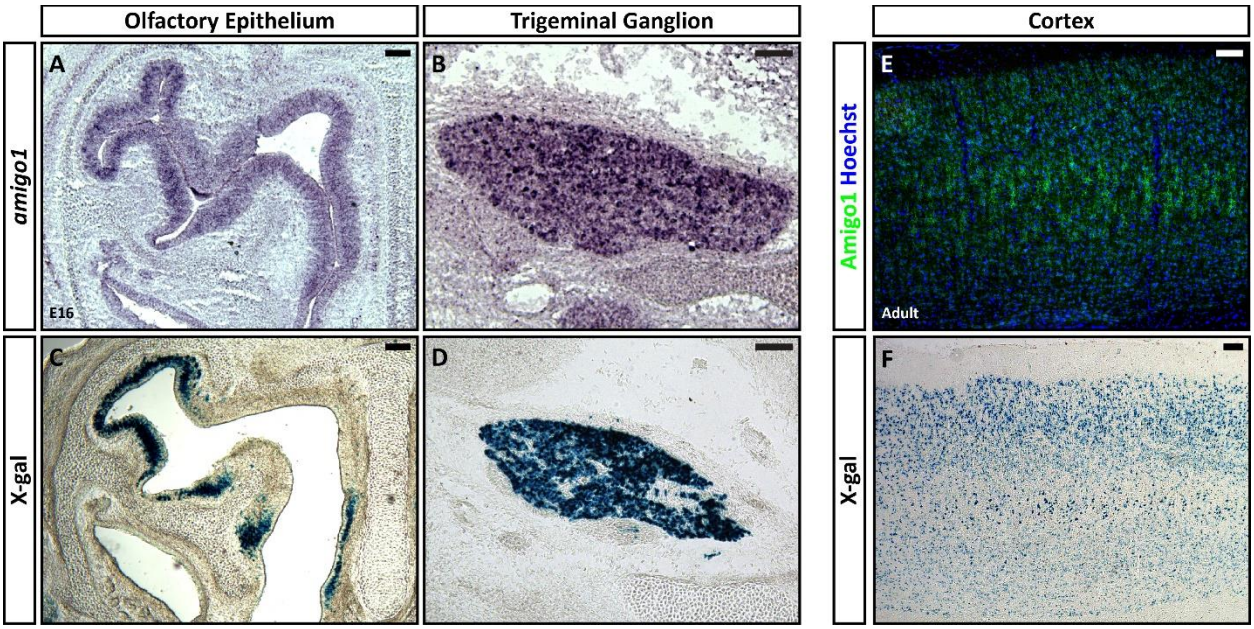

(A,B) Representative expression of *amigo1* on coronal sections of the olfactory epithelium (OE) **(A)** and trigeminal ganglion (TG) **(B)** of wild type embryonic day (E) 16 mice by *in situ* hybridization using probes targeting *amigo1* mRNA (**A,B**). Scale bars: 100µm
(C,D) Representative expression of *amigo1* on coronal sections of the olfactory epithelium (OE) **(C)** and trigeminal ganglion (TG) **(D)** of E16 *Amigo1*$^{+/-}$ mice by X-gal staining. X-gal staining recapitulates the pattern of Amigo1 expression in these structures. Scale bars: 100µm
(E,F) Expression of Amigo1 protein in wild type adult cortex by immunohistochemistry using an antibody against Amigo1 **(E)**, recapitulated by representative X-gal staining of Adult *Amigo1*$^{+/-}$ cortex **(F)**. Scale bars: 100µm

We used this approach to investigate the expression pattern of Amigo1 during development in three regions of the nervous system: the hippocampus, cortex, and cerebellum. In early development at embryonic day (E) 16 and postnatal day (P) 0, very few cells of the hippocampus were positive for β-gal (Figure 2A-B). In contrast, β-gal expression was specifically observed in the dentate gyrus by P7 and was maintained at later ages (Figure 2C-D). The expression of Amigo1 in the cortex also evolved over developmental time points. At early stages, from E16 into P7, expression was restricted to the more basal layers of cortex (Figure 2E-G). At E16, some cells of layer 1 were also detected to be X-gal-positive. However, by P21, X-gal staining was detected throughout the width of cortex, with stronger staining in the more superficial layer 2/3 (Figure 2H). Overall, the frequency of cells in the superficial-most layer 1 seemed to decrease with age. Finally, X-gal staining in the cerebellum looked rather intriguing since Amigo1 seemed to be expressed specifically in the Purkinje cells of lobe X, with fewer labeled cells in lobe IX and extremely sparse expression in the rest of the cerebellum. This pattern of expression was especially notable at P7 but persisted into P21 (Figure 2J-K). At P0, the cerebellum is not yet developed, however staining was detected in the deep cerebellar nuclei (Figure 2I). These results exemplify how specific brain regions have Amigo1 enrichment in subsets of cells and that these expression patterns of Amigo1 change over development, suggesting that Amigo1 could function differently in both development and in the more mature brain.

Figure 2: Differential expression of Amigo1 is developmentally regulated in various brain structures

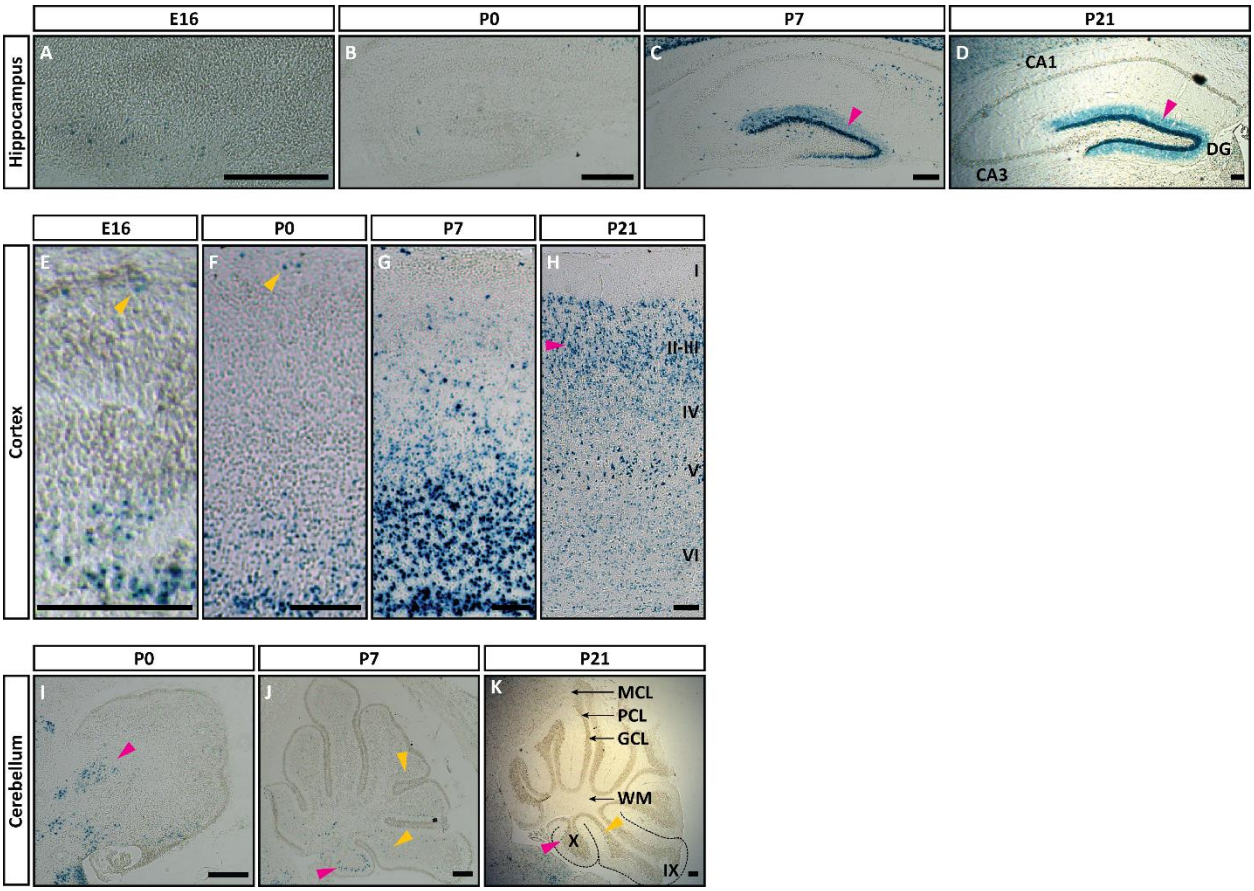

(A-D) X-gal staining representative of Amigo1 expression at developmental time points E16 **(A)**, P0 **(B)**, P7 **(C)** and P21 **(D)** in the hippocampus cut transversely to show the structures in the hippocampal circuit, dentate gyrus (DG), cornu ammonis (CA) subfields, CA1 and CA3 as shown in **(D)**. Amigo1 is enriched in the DG in the first postnatal week (*pink arrowheads*). Scale bars: 200µm.

(E-H) X-gal staining representative of Amigo1 expression at developmental time points E16 **(E)**, P0 **(F)**, P7 **(G)** and P21 **(H)** in the cortex. Amigo1 is enriched in basal layers during development and sparsely in the apical-most layer (*yellow arrowheads*, **E,F**) and upregulated in the upper layers of cortex by P21 (*pink arrowheads*, **H**). Roman numerals I-VI in **(H)** define cortical layers. Scale bars: 100µm

(I-K) X-gal staining representative of Amigo1 expression at developmental time points P0 **(I)**, P7 **(J)** and P21 **(K)** in the cerebellum. Newborn animals show Amigo1 expression in the deep cerebellar nuclei (*pink arrowhead*, **I**). During early postnatal development, Amigo1 is expressed in many Purkinje cells of lobe X of the cerebellum which is maintained into P21 (*pink arrowheads*, **J, K**). Sparse labelling of Purkinje cells is also detected in other lobes postnatally (*yellow arrowheads*, **J, K**) MCL: Molecular cell layer; PCL: Purkinje cell layer; GCL: Granule cell layer; WM: White matter. Roman numerals IX and X in **(K)** and dotted outlines show the IX^{th} and X^{th} lobes of the cerebellum, respectively. Scale bars: 200µm. Arrowheads point to key areas of Amigo1 expression (*pink*: prominent expression; *yellow*: sparser expression)

2. Loss of Amigo1 expression leads to altered development of the infrapyramidal mossy fiber bundle

The restricted expression of Amigo1 in the dentate gyrus (DG) of the hippocampus during development led us to investigate its role in the mossy fiber projections to the CA3 region using mice carrying a germline deletion of the *Amigo1* gene. Several decades of research into the circuity and function of the hippocampus gave way to the development of numerous histochemical techniques to visualize mossy fibers. For example, neuropeptides such as dynorphin are specifically expressed by mossy fibers (Khachaturian et al., 1982; McGinty et al., 1983; Blaabjerg and Zimmer, 2007), however rely on the accessibility of good antibodies. Anterograde tracing techniques and the Golgi staining method have also been used (West et al., 1982; Frotscher and Zimmer, 1983), but these methods do not stain all mossy fibers. Alternatively, the Timm sulfide silver method (Laurberg and Zimmer, 1981) stains the chelatable zinc that are present at high levels in mossy fiber terminals. It is a relatively simple, yet very sensitive, method to label the population of mossy fiber projections (Blaabjerg and Zimmer, 2007). We thus employed Timm staining to visualize mossy fiber projections in the hippocampi of control and *Amigo1*$^{-/-}$ mice.

Mossy fibers travel through the dentate hilus and then through CA3 to synapse with the proximal apical and basal dendrites of pyramidal cells. In this way, they form the suprapyramidal bundle (SPB) in stratum lucidum and infrapyramidal bundle (IPB) in stratum oriens, respectively. More distally, the infrapyramidally projecting axons will cross over the pyramidal cell layer to join the suprapyramidal tract in stratum lucidum. By the fourth postnatal week, hippocampal circuitry is generally established, and the ratio of axons traversing suprapyramidally versus infrapyramidally is refined (Amaral and Dent, 1981; Bagri et al., 2003). We thus examined the projections of mossy fiber bundles in hippocampi of control and *Amigo1*$^{-/-}$ animals at one month of age to test our

hypothesis that the loss of Amigo1 would affect the development of the two separate mossy fiber bundles. We examined mid-septotemporal sagittal sections in Timm-stained hippocampi and found a decrease in the length ratio between the IPB and SPB (Figure 3J), caused by a decrease in the length of the IPB in the mutant animals (Figre 3A-C, K). To then assess whether this defect was exclusive to development or persisted into adulthood and ageing, we examined the IPB to SPB ratio in mice of 2 and 5 months of age (Figure 3D-I, L-M). Interestingly, lengths of IPB and SPB and their ratios were similar between control and mutant animals both at 2 and 5 months, suggesting that this defect was due to a role for Amigo1 in pruning or in activity- or adhesion-dependent guidance solely during development (Bagri et al., 2003; Römer et al., 2011; Tawarayama et al., 2018).

Figure 3: Loss of Amigo1 disrupts the length of infrapyramidal bundle during development, which is restored by 2 months

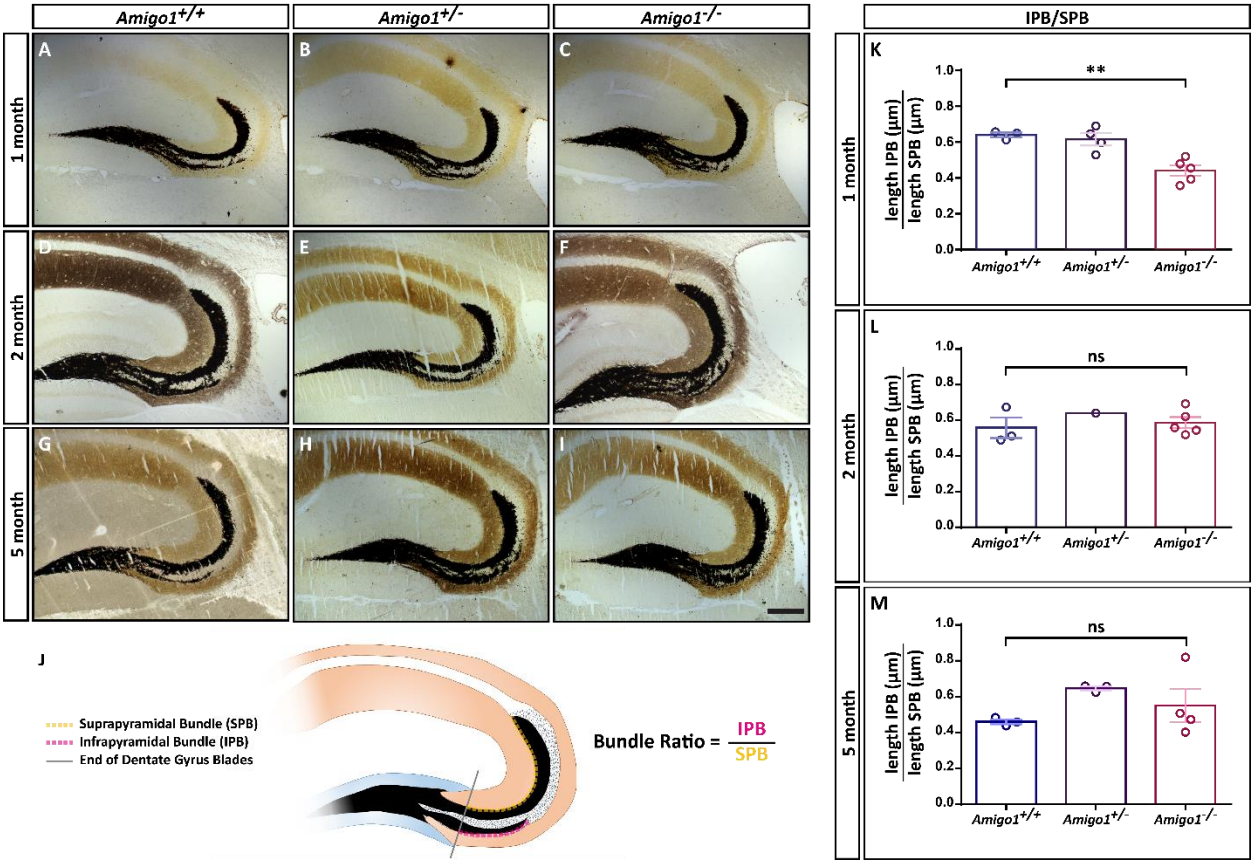

(A-I) Timm-stained mossy fibers reveal projections of dentate gyrus axons to CA3 along suprapyramidal and infrapyramidal bundles in control **(A,D,G)**, *Amigo1*$^{+/-}$ **(B,E,H)**, and *Amigo1*$^{-/-}$ **(C,F,I)** mice at 1 **(A-C)**, 2 **(D-F)**, and 3 **(G-I)** months of age. Scale bar: 200µm

(J) Diagram depicting strategy used to measure bundle ratios. Dotted *pink* and *yellow* lines show where the infrapyramidal and suprapyramidal bundles were traced, respectively. The *grey* line joins the two tips of the dentate gyrus blades and serves at the starting point of bundle length measurements. The ratio of bundle lengths was calculated as the length of the infrapyramidal bundle divided by the length of the suprapyramidal bundle. SPB: Suprapyramidal bundle. IPB: infrapyramidal bundle.

(K-M) Quantification of IPB/SPB length ratios in control and heterozygous and homozygous *Amigo1* mutants at 1 **(K)**, 2 **(L)**, and 5 **(M)** months of age. Data shown as average ± s.e.m. (1 month **(K)**: *Amigo1*$^{+/+}$ 0.64 ± 0.014 n=3 HCs; *Amigo1*$^{+/-}$ 0.62 ± 0.034 n=4 HCs; *Amigo1*$^{-/-}$ 0.44 ± 0.030 n=5 HCs. 1-way ANOVA with Dunnett's multiple comparisons test for each mean with *Amigo1*$^{+/+}$; 2 months **(L)**: *Amigo1*$^{+/+}$ 0.56 ± 0.058 n=3 HCs; *Amigo1*$^{+/-}$ 0.64 n=1 HC; *Amigo1*$^{-/-}$ 0.59 ± 0.031 n=5 HCs. Unpaired Student's t-test between *Amigo1*$^{+/+}$ and *Amigo1*$^{-/-}$. Additional *Amigo1*$^{+/-}$ animals will be needed for statistical assessment; 5 months **(M)**: *Amigo1*$^{+/+}$ 0.46 ± 0.013 n=3 HCs; *Amigo1*$^{+/-}$ 0.65 ± 0.012 n=3 HCs; *Amigo1*$^{-/-}$ 0.55 ± 0.093 n=4 HCs. 1-way ANOVA with Dunnett's multiple comparisons test for each mean with *Amigo1*$^{+/+}$) ** $p < 0.01$, ns = non significant

3. Loss of Amigo1 expression leads to perturbed mossy fiber fasciculation and altered presynaptic terminal formation

In our analysis of the stained hippocampi, however, we noticed that the organization of the supra and infrapyramidal axon mossy fiber axon bundles seemed more disorganized in the *Amigo1*$^{-/-}$ mice. In the proximal CA3 of *Amigo1*$^{-/-}$ mice, more fibers appeared to be projecting between the two main bundles. Measurement of the staining intensity of a 20μm track between the two bundles along the CA3 pyramidal area (Figure 4J) revealed increases in Timm staining in the *Amigo1*$^{-/-}$ mice when compared to controls, inferring that more axons are traversing the inter-bundle space and suggesting that Amigo1 is required for normal fasciculation of mossy fiber bundles (Figure 4A-M). Furthermore, the thickness of the suprapyramidal bundle was unchanged in the mutant animals, implying that the defasciculation could be due to aberrant projection of the more plastic infrapyramidal axons (Schwegler et al., 1981; Crusio et al., 1989). Importantly, this defect was present at all ages analysed (Figure 4N-P).

In the more distal regions of CA3, individual mossy fiber boutons (MFBs) in the pyramidal cell layer adjacent to the suprapyramidal bundle could be identified as small Timm-stained puncta, which were not visible in more proximal CA3 due to the high density of fiber bundles. To quantify these individual boutons, we divided CA3 into 6 regions beginning from the tip of the suprapyramidal DG blade and ending at the CA3-CA2 border. We then analysed the numbers of MFBs in the pyramidal layer of the three distal-most areas of CA3, regions 4, 5, and 6 (Figure 5J). In wild-type 5-month-old animals, a low density of MFBs was observed in all three regions of the CA3, while a significant increase in MFB density was observed in regions 4 and 5 of hippocampi from the age-matched mice lacking either *Amigo1*$^{+/-}$ or *Amigo1*$^{-/-}$ mice, suggesting that lower levels of Amigo1 expression are not sufficient to prevent ectopic MFB formation in the ageing hippocampus (Figure 5G-I, M). Interestingly, these effects could be observed in mutant animals

as early as 2 months of age but not in animals of one month of age (Figure 5A-F, K-L). Thus, we conclude that Amigo1 is required for both the development and maintenance of normal fasciculation of mossy fiber bundles and for the prevention of ectopic mossy fiber bouton formation in adult mice.

Figure 4: Loss of Amigo1 disrupts the mossy fiber fasciculation

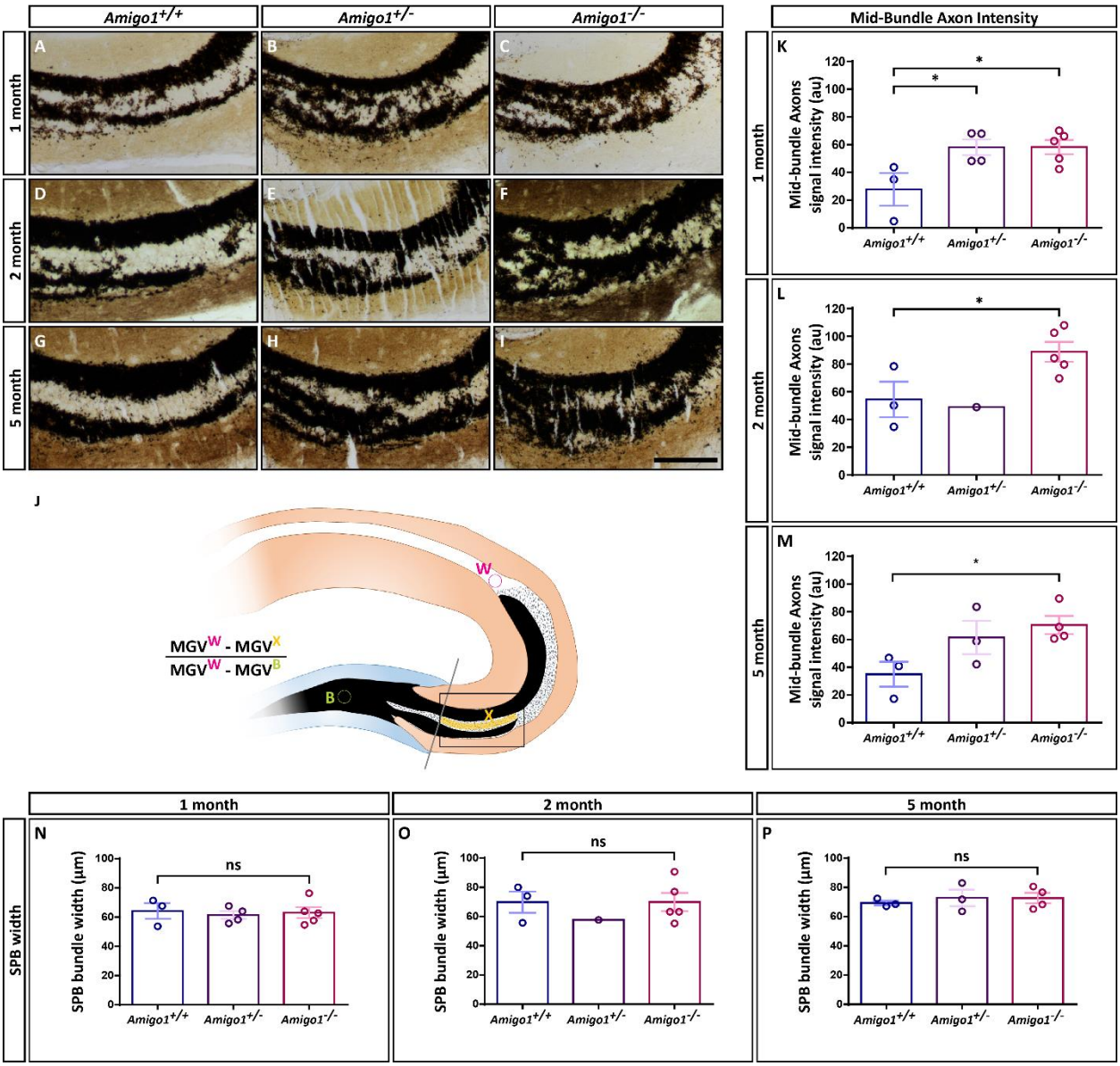

(A-I) Zoom-in images of Timm-stained mossy fibers projecting into proximal CA3 along suprapyramidal and infrapyramidal bundles in control **(A,D,G)**, *Amigo1*$^{+/-}$ **(B,E,H)**, and *Amigo1*$^{-/-}$ **(C,F,I)** mice at 1 **(A-C)**, 2 **(D-F)**, and 3 **(G-I)** months of age. Area of zoom in is depicted by box in **(J)** Scale bar: 100µm.

(J) Diagram depicting strategy used to measure inter-bundle Timm stain intensity. Transparent thick yellow line **(X)** depicts the mid-bundle trace used for analysis. The grey line joins the two tips of the dentate gyrus blades and serves at the starting point of mid-bundle trace. The staining intensity measured with mean grey value (MGV) was normalized to background using an unstained region (*pink circle*, "W") and to the dark positively-stained region in the dentate hilus (*green circle*, labelled "B"). MGV: Mean grey value

(K-M) Quantification of Timm staining intensity between intrapyramidal and suprapyramidal bundles in control and heterozygous and homozygous *Amigo1* mutants at 1 **(K)**, 2 **(L)**, and 5 **(M)**

months of age. Data shown as average ± s.e.m in arbitrary units (au). (1 month **(K)**: *Amigo1*$^{+/+}$ 27.83 ± 11.76 n=3 HCs; *Amigo1*$^{+/-}$ 58.20 ± 5.698 n=4 HCs; *Amigo1*$^{-/-}$ 58.30 ± 5.195 n=5 HCs. 1-way ANOVA with Dunnett's multiple comparisons test for each mean with *Amigo1*$^{+/+}$; 2 months **(L)**: *Amigo1*$^{+/+}$ 54.42 ± 12.78 n=3 HCs; *Amigo1*$^{+/-}$ 48.91 n=1 HC; *Amigo1*$^{-/-}$ 88.81 ± 7.17 n=5 HCs. Unpaired Student's t-test between *Amigo1*$^{+/+}$ and *Amigo1*$^{-/-}$. Additional *Amigo1*$^{+/-}$ animals will be needed for statistical assessment; 5 months **(M)**: *Amigo1*$^{+/+}$ 34.95 ± 9.003 n=3 HCs; *Amigo1*$^{+/-}$ 61.47 ± 12.04 n=3 HCs; *Amigo1*$^{-/-}$ 70.49 ± 6.591 n=4 HCs. 1-way ANOVA with Dunnett's multiple comparisons test for each mean with *Amigo1*$^{+/+}$) * $p < 0.05$.
(N-P) Quantification of the width of the suprapyramidal bundle between control and heterozygous and homozygous *Amigo1* mutants at 1 **(N)**, 2 **(O)**, and 5 **(P)** months of age. Data shown as average ± s.e.m in (μm). (1 month **(N)**: *Amigo1*$^{+/+}$ 64.22 ± 5.383 n=3 HCs; *Amigo1*$^{+/-}$ 61.42 ± 2.713 n=4 HCs; *Amigo1*$^{-/-}$ 63.07 ± 3.720 n=5 HCs. 1-way ANOVA with Dunnett's multiple comparisons test for each mean with *Amigo1*$^{+/+}$; 2 months **(O)**: *Amigo1*$^{+/+}$ 69.89 ± 7.319 n=3 HCs; *Amigo1*$^{+/-}$ 57.67 n=1 HC; *Amigo1*$^{-/-}$ 69.93 ± 6.245 n=5 HCs. Unpaired Student's t-test between *Amigo1*$^{+/+}$ and *Amigo1*$^{-/-}$. Additional *Amigo1*$^{+/-}$ animals will be needed for statistical assessment; 5 months **(P)**: *Amigo1*$^{+/+}$ 69.38 ± 1.601 n=3 HCs; *Amigo1*$^{+/-}$ 72.84 ± 5.607 n=3 HCs; *Amigo1*$^{-/-}$ 72.75 ± 3.58 n=4 HCs. 1-way ANOVA with Dunnett's multiple comparisons test for each mean with *Amigo1*$^{+/+}$.)
ns = non significant.

Figure 5: Loss of Amigo1 results in the formation of ectopic mossy fiber boutons in CA3

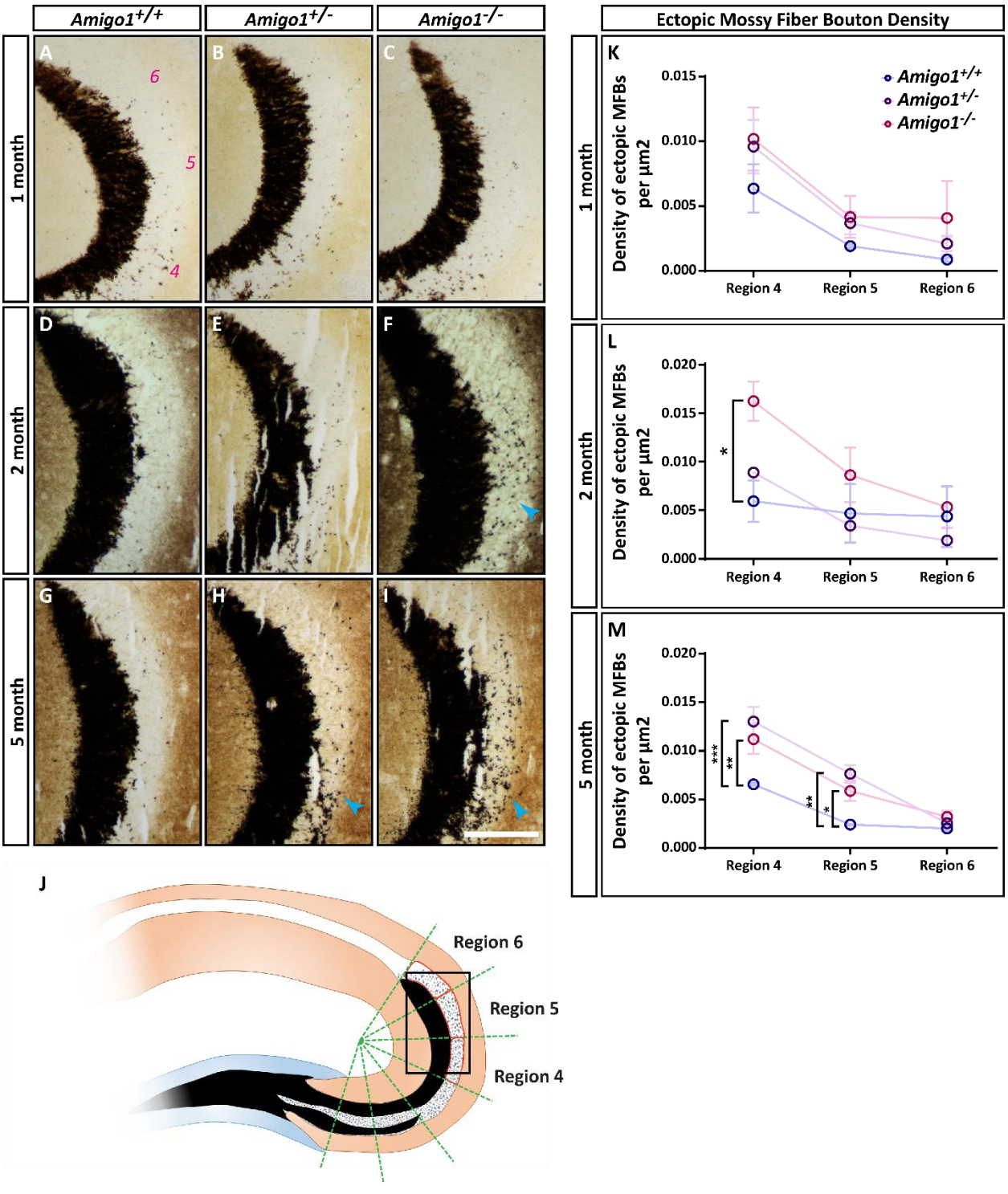

(A-I) Zoom-in images of Timm-stained mossy fibers projecting into distal CA3 and forming mossy fiber boutons in control **(A,D,G)**, *Amigo1*$^{+/-}$ **(B,E,H)**, and *Amigo1*$^{-/-}$ **(C,F,I)** mice at 1 **(A-C)**, 2 **(D-F)**, and 3 **(G-I)** months of age. Area of zoom-in is depicted by box in **(J)** Regions are indicated in *pink* text **(A)**. Scale bar: 100µm.

(J) Diagram depicting strategy used to measure ectopic mossy fiber bouton density. The suprapyramidal dentate gyrus blade and the beginning of CA2 were used as delimiters to split CA3 into 6 parts radially (*dotted green lines*). The number of mossy fibers in regions 4, 5, and 6, were counted in the pyramidal cell layer (*red outlines*), and density of synapses per μm^2 were calculated for each region. Black box shows located of images in **(A-I)**.
(K-M) Quantification of Timm staining intensity between intrapyramidal and suprapyramidal bundles in control and heterozygous and homozygous *Amigo1* mutants at 1 **(K)**, 2 **(L)**, and 5 **(M)** months of age. Data shown as average ± s.e.m. (1 month **(K)**: Region 4: $Amigo1^{+/+}$ 0.0064 ± 0.0011 n=3 HCs; $Amigo1^{+/-}$ 0.0096 ± 0.0012 n=4 HCs; $Amigo1^{-/-}$ 0.0102 ± 0.0028 n=5 HCs; Region 5: $Amigo1^{+/+}$ 0.0019 ± 0.0004 n=3 HCs; $Amigo1^{+/-}$ 0.0037 ± 0.0005 n=4 HCs; $Amigo1^{-/-}$ 0.0042 ± 0.0014 n=5 HCs; Region 6: $Amigo1^{+/+}$ 0.0009 ± 0.0001 n=3 HCs; $Amigo1^{+/-}$ 0.0021 ± 0.00314 n=4 HCs; $Amigo1^{-/-}$ 0.0041 ± 0.0026 n=5 HCs; 2-way ANOVA with Tukey's multiple comparisons test. 2 month **(L)**: Region 4: $Amigo1^{+/+}$ 0.0059 ± 0.0012 n=3 HCs; $Amigo1^{+/-}$ 0.0089 n=1 HC; $Amigo1^{-/-}$ 0.0162 ± 0.0014 n=5 HCs; Region 5: $Amigo1^{+/+}$ 0.0047 ± 0.0015 n=3 HCs; $Amigo1^{+/-}$ 0.0034 n=1 HC; $Amigo1^{-/-}$ 0.0086 ± 0.0015 n=5 HCs; Region 6: $Amigo1^{+/+}$ 0.0044 ± 0.0016 n=3 HCs; $Amigo1^{+/-}$ 0.0019 n=1 HC; $Amigo1^{-/-}$ 0.0053 ± 0.0012 n=5 HCs; 2-way ANOVA with Tukey's multiple comparisons test; Additional $Amigo1^{+/-}$ animals will be needed for statistical assessment. 5 month **(M)**: Region 4: $Amigo1^{+/+}$ 0.0066 ± 0.0009 n=3 HCs; $Amigo1^{+/-}$ 0.0130 ± 0.0012 n=3 HCs; $Amigo1^{-/-}$ 0.0112 ± 0.0009 n=4 HCs; Region 5: $Amigo1^{+/+}$ 0.0024 ± 0.0003 n=3 HCs; $Amigo1^{+/-}$ 0.0076 ± 0.0011 n=3 HCs; $Amigo1^{-/-}$ 0.0059 ± 0.0008 n=4 HCs; Region 6: $Amigo1^{+/+}$ 0.0020 ± 0.0003 n=3 HCs; $Amigo1^{+/-}$ 0.0025 ± 0.0004 n=3 HCs; $Amigo1^{-/-}$ 0.0032 ± 0.0004 n=4 HCs; 2-way ANOVA with Tukey's multiple comparisons test) * $p < 0.05$; ** $p < 0.01$; *** $p < 0.001$; ns = non significant

VI. Discussion

Mossy fibers are unique projections in that they form few but large synapses onto post-synaptic CA3 cells, with each terminal providing strong excitatory information to both postsynaptic excitatory pyramidal cells and inhibitory interneurons. The combination of firing frequency of the mossy fibers and level of the feedforward inhibition provided by the inhibitory interneurons allow for a small number of mossy fiber terminals to elicit transmission of information through the hippocampal network (Henze et al., 2002; Galimberti et al., 2006). At a higher level, this synapse is thought to play a key role in memory formation and learning, especially with concepts such as pattern separation (GoodSmith et al., 2017). Therefore, understanding the molecular mechanisms regulating formation, maintenance and plasticity of these synapses can help in elucidating deficits in memory and learning that are dependent on accurate information passage within the hippocampal circuit. In this study, we identify a role for the cell adhesion molecule Amigo1 in the precise development of mossy fiber tracts to CA3, and in the maintenance of these fibers in adult and ageing mice.

In normal IPB development, the IPB begins as a long bundle extending to the apex of CA3. Around 3-4 weeks of age, the IPB is dramatically pruned by Semaphorins in CA3 acting on the Plexin-A3 receptor to induce mossy fiber retraction (Bagri et al., 2003). The disruption of normal mossy fiber projections along the IPB in our 1-month-old *Amigo1*$^{-/-}$ mice could be due to enhanced pruning of this IPB bundle, but experiments would need to test whether loss of Amigo1 affects the expression of these signalling molecules involved in pruning. Importantly, whether the IPB is indeed pruned away or just does not form properly needs to be determined by experiments looking at bundle lengths in even younger animals. Conversely, Amigo1 could act as an axon guidance molecule attracting a subset of mossy fibers to the infrapyramidal bundle. For example, the reduced IPB

lengths seen in *Draxin* knockout mice were attributed to loss of repulsive or attractive cues within CA3 lamina (Tawarayama et al., 2018). However, a similar mechanism seems unlikely for the *Amigo1* mice since members of the Amigo1 family (that can bind homo- or heterophilically to Amigo1) are not expressed in CA3 at this age (data not shown + Hitti and Siegelbaum, 2014; Bishop et al., 2018). Finally, the length of the infrapyramidal bundle is known to be plastic, changing between genetic backgrounds and with spatial learning tasks (Schwegler et al., 1981; Crusio et al., 1989; Blaabjerg and Zimmer, 2007). It is thus possible that changes in intrinsic neural activity can explain the altered bundle length in the *Amigo1*$^{-/-}$ animals as described below. Importantly, anatomical-behavioural correlations have been shown whereby the length of the IPB correlates positively with spatial learning ability. As such, shorter IPBs in the young *Amigo1*$^{-/-}$ mice could impair their learning performance on spatial tasks as shown by studies by Crusio's group, and it would be important to test these behavioural paradigms our mice (Crusio et al., 1987, 1993; Jamot et al., 1994).

In contrast, the length of the infrapyramidal bundles were unchanged in older *Amigo1*$^{-/-}$ mice. The absence of these defects in mice 2 months and older could be explained by compensatory mechanisms of other molecules involved in guiding projections to the IPB and SPB.

In all age groups, we found evidence of defasciculation of mossy fiber axons. Whether this defasciculation is caused by impaired targeting of the bundles in early development or by re-routing of existing fibers remains to be determined by examining these bundles in the first few postnatal weeks. The axons that are defasciculated could also be from more newly generated granule cells. Studies have provided strong evidence that newly born neurons preferentially innervate the infrapyramidal bundle and contribute to the high levels of plasticity within that bundle (Schwegler et al., 1981; Crusio et al., 1989; Römer et al., 2011). Since there are no

differences in the thickness of the suprapyramidal bundle, the model that it is the younger neurons that are misguided in *Amigo1* null animals is an attractive one and can be tested by examining staining of PSA-NCAM-positive mossy fibers, which specifically label adult-born granule cell axons and dendrites (Seki and Arai, 1999).

The increase in crossover of axons between infra and suprapyramidal bundles in our *Amigo1*$^{-/-}$ animals is reminiscent of defects seen in mice deficient for the cell adhesion molecule CHL1 (Montag-Sallaz et al., 2002; Heyden et al., 2008). *CHL1*- and *BACE1*-deficient mice both show similar mossy fiber fasciculation defects, and the defects in *BACE1* mice were suggested to be representative of the effect of loss of CHL1 since BACE1-mediated CHL1 cleavage is necessary for its adhesive function in this system (Montag-Sallaz et al., 2002; Heyden et al., 2008; Hitt et al., 2012; Ou-Yang et al., 2018). The similarity of this phenotype leads us to infer that Amigo1 has a role in axonal adhesion of dentate mossy fibers. However, we cannot rule out the possibility of a role for Amigo1 in the regulation of neural activity. Recently, it was found that BACE1 mediates the expression of the voltage-gated potassium channel, Kv3.4, important in repolarization of the action potential (Hartmann et al., 2018). BACE1 levels gradually decline in the adult central nervous system except for high expression in the mossy fibers (Willem et al., 2006; Hartmann et al., 2018). It enhances surface levels of Kv3.4 in mossy fibers and targets this channel to the presynaptic terminal where it can have a stronger impact on synaptic transmission (Hartmann et al., 2018). BACE1 has been shown to regulate neural excitability through alteration of ion channel dynamics, likely by cleavage of auxiliary subunits (Kim et al., 2007, 2011; Sachse et al., 2013; Lehnert et al., 2016). Interestingly, Amigo1 is a cell adhesion molecule that is also an auxiliary subunit of the voltage-gated potassium channel, Kv2.1, a crucial component of the delayed rectifier current in an action potential (Murakoshi and Trimmer, 1999; Peltola et al., 2011). Amigo1

extensively co-localizes with Kv2.1, and *Amigo1* null mice have decreased Kv2.1 expression (Peltola et al., 2016; Bishop et al., 2018). Experiments *in vivo* using *Amigo1* null mice and *in vitro* administering RNAi against Amigo1 have both demonstrated altered gating properties of the Kv2.1 channel such that stronger depolarization is required to activate current through the channel, making neurons more prone to hyperexcitation (Peltola et al., 2011, 2016). Thus, it is highly plausible that the similarity in phenotypes between *BACE1* null and *Amigo1* null mice could also be attributed to modifications in neural excitability rather than adhesion. Furthermore, it has been suggested that increases in the sprouting of mossy fibers could be due to an increase in intrinsic neuronal excitability (Sutula et al., 1988; Qiao et al., 2013) triggering changes in axon guidance events or channel and receptor composition at the synapse which may explain the ectopic formation of mossy fiber boutons in *Amigo1*$^{-/-}$ mice. Examination of Timm-stained mossy fibers to determine whether similar defects exist in *Kv2.1*$^{-/-}$ mice could reinforce this notion. Furthermore, *Kv2.1* null mice are hyperactive, show behavioural deficits in spatial learning and have increased seizure progression (Speca et al., 2014), providing good rationale for testing these behaviours in our *Amigo1* null animals. Taken together, our results lend support to the idea that loss of Amigo1 in mice causes changes in axon stabilization or guidance leading to aberrant mossy fiber growth and ectopic synapse formation, triggered either by loss of cell adhesion or by modulation of intrinsic neuronal activity. Similarity in phenotypes to other mouse models lead us to believe that the hippocampal mossy fiber deficits in the *Amigo1* null mice could be associated with changes in behaviour in terms of learning and hyperactivity or seizure susceptibility.

In conclusion, we demonstrate a role for Amigo1 in the development and maintenance of mossy fiber projections. These findings provide a strong base to further elucidate mechanisms of Amigo1 function as a cell adhesion molecule and/or regulator of neural activity and to further understand

how these functions contribute to the formation, maintenance, and plasticity of mossy fibers within the hippocampal circuit.

VII. Materials and Methods

1. Animals

Animals were housed and handled in strict accordance with the guidelines set by the Canadian Council on Animal Care (CCAC), and protocols and procedures were approved by the Montreal Neurological Institute Animal Care Committee (MNI-ACC). For *in situ* hybridization experiments using embryonic tissue, animals were acquired from timed-pregnant CD1 female mice purchased from Charles River Laboratories. Embryonic day corresponds to the number of days since the date of vaginal plug. For postnatal analysis, day of birth was considered P0. Embryonic stem cells containing the targeted disruption of the *Amigo1* gene (Amigo1$^{tm1(KOMP)Vlcg}$) were purchased from the KOMP Repository (Knockout Mouse Project, US Davis). The whole coding region of *Amigo1* (GRCm38 Chr3:108,187,190-108,188,665) was replaced with the ZEN-Ub1 cassette containing the *lacZ* gene and a floxable neomycin coding sequence under the control of the human ubiquitin C protomer (http://velocigene.com/komp/detail/10669). Embryonic stem cells were injected in to CD1 blastocysts to produce chimeras. Heterozygotes produced by germline transmission were crossed to *CMV-Cre* mice to remove the neomycin selection cassette (https://www.jax.org/strain/006054).

2. *In situ* hybridization

Digoxigenin-labeled cRNA probes were prepared by *in vitro* transcription using the DIG labeling mix (10x conc., Roche) of *Amigo1* cDNA in the pBluescript vector, a kind gift from Dr. Heiki Rauvala. *In situ* hybridization staining was performed as described previously (Pasterkamp et al., 1998). Briefly, sections were fixed for 20 minutes in 4% paraformaldehyde (PFA) followed by

washes in 1×phosphate-buffered saline (PBS) treated with DEPC. Sections were then deacetylated in 0.25% acetic anhydride in 0.1M triethanolamine and underwent prehybridization in hybridization buffer (50% formamide, 5×Denhardt's solution, 5×SSC, 250 μg/ml bakers' yeast tRNA) before hybridizing with DIG-labelled probes for incubation overnight at 60^{o}C. The following day, stringency washes in 5×SSC, 2×SSC, and 50% formamide in 0.2×SSC were done at 60^{o}C and in 0.2×SSC at room temperature. Sections were then blocked in Blocking Reagent (Roche) at room temperature and probed with an AP-conjugated α-Digoxigenin antibody (Fab fragments, 1:3000, Roche) for 2.5-3 hours at room temperature before visualization of antibody binding using a colorimetric enzymatic reaction with NBT/BCIP stock solution (nitro-bluetetrazolium chloride (NBT) 5-bromo-4-chloro-3-indolylphosphate (BCIP), Roche)

3. Immunohistochemistry

Adult mice were fixed by transcardial perfusion with 4% PFA in 0.1M sodium phosphate buffer, pH 7.4. Brains were dissected out of the head and cryoprotected in a 30% sucrose solution before embedding in OCT (TissueTek, Cedarlane) for storage at -80°C. 20μm cryostat sections of tissue samples were collected onto Superfrost® Plus microscope slides (Fisherbrand). Sections were rehydrated in 1×PBS, blocked with 10% fetal bovine serum (FBS) and 0.5% Triton×100 for 1 hour at room temperature and incubated overnight at 4°C with primary antibody against Amigo1 (1:300, purified monoclonal mouse clone L86/37, NeuroMab). After rinsing with 1×PBS, primary antibody was detected with an IgG-specific Alexa-Fluor-conjugated secondary antibody (1:500 Goat α-Mouse IgG2b, Alexa-Fluor-488; Invitrogen) for 1 hour at room temperature, and the cell nuclei were stained for 5 minutes with Hoechst 33342 (1:20,000, Molecular Probes).

4. 5-Bromo-4-Chloro-3-Indolyl β-D-Galactopyranoside (X-Gal) Staining

For X-Gal staining, tissue was immersion-fixed in 4% PFA in 1×PBS for 7 minutes (E16) or 45 minutes (P0, P7 tissue). P21 mice were perfused with 10-15mL of 4% PFA in 1×PBS, and brain was dissected out. All tissue was cryoprotected in 1×PBS containing 30% sucrose before embedding in OCT (TissueTek, Cedarlane). 20μm sections mounted on Superfrost® Plus microscope slides (Fisherbrand) were incubated in Buffer A (0.1M PO_4 buffer, pH 7.4, 2mM $MgSO_4$, 5mM EGTA) and then Buffer B (0.1M PO_4 buffer, pH 7.4, 2mM $MgSO_4$, 0.01% Na Deoxycholate, 0.02% NP-40). Sections were subsequently kept in X-gal reaction solution (Buffer B with 5mM $K_3Fe(CN)_6$, 5mM $K_4Fe(CN)_6$ and 1mg/mL X-gal (Bioshop)) at 37^oC until the development of the colour reaction became saturated (Mombaerts et al., 1996), after which slides were dehydrated in an ethanol series (70%-100%) and Xylene and then coverslipped with Permount (Fisher Scientific).

5. Timm staining

Timm staining was performed based on a previously described protocol (Sloviter, 1982). Animals were transcardially perfused first with a 0.37% sulfide perfusate (0.0487M $Na_2S{\cdot}9H_2O$ (Sigma), 0.0862M $NaH_2PO_4{\cdot}H_2O$ (Sloviter, 1982)) and subsequently with 10% neutral buffered formalin (NBF). Brains dissected out of the skull were post fixed in 10% NBF and then dehydrated in a series of graded EtOH solutions (70% to 100%), Xylene and final clearing in chloroform before cutting brain down the midline into two hemispheres and incubating in Paraffin wax at 60^oC, followed by embedding in fresh Paraffin. Thus, each half-brain was separately embedded so that the flat surface of the midline served to align the sagittal plane of sectioning. 10μm sagittal sections were cut using a rotary microtome, floated on a warm water bath (~53^oC) and then collected onto glass slides to dry. Sections chosen for staining from each control-mutant pair were processed

simultaneously using a slide rack immersed into the different staining solutions. Slides were deparaffinized in Xylene, rehydrated with an ethanol series and water before developing at room temperature for 45 minutes and then at 60^{o}C for 12 minutes in the Timm's solution (30mL Gum Arabic solution [500g Gum Arabic and 1L milli-Q water], 5mL citrate buffer [5.1g citric acid, monohydrate, 4.7g sodium citrate, dihydrate in 20mL milli-Q water], 15mL hydroquinone [0.85g hydroquinone in 15mL milli-Q water], 250µL silver nitrate solution [0.17g silver nitrate in 1mL milli-Q water]). Slides were finally once again dehydrated with ethanol and Xylene and coverslipped with Permount (Fisher Scientific).

6. Imaging and Image Analysis

All analyses were done using the ImageJ software (National Institutes of Health).

Three sagittal sections from the midpoint of the hippocampus along the septo-temporal axis (medial-lateral) were chosen for analysis. The centroid of the curvature in the dentate fissure was used as the focal point to divide CA3 into six parts. The distal end of CA3 was determined anatomically by the end of the mossy fiber staining and the change in layer thickness at the CA2 border. The proximal end of CA3 was cut off at the level of the tip of the suprapyramidal dentate blade. These two boundaries were then used to divide CA3 into six equal parts radially from the focal point (Figure 5J). The 3 most distal regions labelled 4, 5 and 6 were used for analysis. The number of mossy fiber boutons (black puncta) were counted using the "Find Maxima" function in ImageJ for each of these 3 areas in the pyramidal cell layer, which was delimited by the brown staining of stratum oriens (basally) and black mossy fiber staining of stratum lucidum (apically)

For the tracing of intra and suprapyramidal bundles, a line was first made to join the two tips of the dentate gyrus blades. The IPB was traced along the border between stratum pyramidal and stratum oriens starting from this line. This line also served as the starting point to trace the SPB

along the border between stratum lucidum and stratum radiatum. The ratio of the length of the IPN to the length of the SPB was used for statistical analysis (Figure 3J).

To measure the level of crossover between infra and suprapyramidal layers, the mean gray value of a 20μm-thick line traversing the clearest CA3 pyramidal path from the end of the dentate blades to the limit of the infrapyramidal bundle was measured. This value was normalized to background staining levels of stratum pyramidal of CA3 and to strongest staining levels in the dentate hilus (Figure 4J).

Chapter 5:

General Discussion

I. Summary

The primary objective of this thesis was to examine the roles of Leucine-Rich Repeat (LRR) domain containing proteins in the processes of nervous system development, from axon guidance to synapse formation and maintenance. While several major families of proteins have been implicated in generalized mechanisms underlying these processes, the more fine-tuned and intricate complexities of subsystems within the brain call for a much more complex integration of a range of protein functions and families (Batool et al., 2019). Differential expression of many proteins within the families of membrane-associated or secreted guidance cues, transmembrane cell adhesion molecules, and intracellular signalling proteins can confer a much more nuanced modulation of cellular processes for the development of neural networks amongst the multitudes of neuronal subpopulations. The molecular mechanisms underlying target cell identification and synapse development and plasticity remain to be fully understood (Harris and Littleton, 2015). The results presented in this thesis identify the role of two LRR proteins, Slitrk1 and Amigo1, in two specific developmental processes: synapse formation and axon fasciculation.

Chapter 2 of this thesis examines the role of Slitrk1 in the development of synapses. We used *in vitro* techniques to overexpress and downregulate Slitrk1 expression in dissociated hippocampal neurons to identify the sufficiency and necessity of Slitrk1 in the formation of excitatory synapses. Furthermore, we provided evidence for a structure-function mechanism whereby Slitrk1 dimerization at the cell surface requires its second LRR domain while binding to its presynaptic binding partner requires its first extracellular LRR domain.

In Chapters 3 and 4 of this thesis, we turned to study the role of Amigo1 in the development of neuronal circuits *in vivo* using the mouse olfactory system and hippocampal system as models. In Chapter 3, we showed that while Amigo1 has expression restricted to the most ventrolateral region of the olfactory epithelium, it is dispensable for the targeting of olfactory receptor neurons from this region to their specific glomeruli at the surface of the olfactory bulb. In contrast, we show in Chapter 4 that Amigo1 expression in the dentate gyrus during development is essential for the formation of the infrapyramidal mossy fiber bundle. In adult, Amigo1 is required for the maintenance of axonal fasciculation of the mossy fibers and in the prevention of their ectopic bouton formation in the hippocampal trisynaptic circuit.

Together, our results provide novel insight into the roles these two LRR-domain containing proteins play in specific neuronal processes. While many molecules several molecules have already been found to play roles in excitatory synapse formation, in mossy fiber fasciculation and bouton formation, the identification of additional players in this process can provide a starting point towards understanding the integration of signalling between ensembles of proteins and the more subtle modulations required for the development and maintenance of numerous circuits within the brain.

II. Slitrks in Synaptogenesis

1. A place for Slitrk1 in the network of synaptic adhesion molecules

The formation of synapses is not restricted to the developmental period. Brain plasticity requires the retraction of non-functional synapses and the development of new synapses constantly throughout life to enable learning and adaptation in response to changing environments and behaviours. Some major regulators of synapse development such as the Neurexins and Neuroligins have been shown to be important mediators of synaptogenesis, however additional genes are

required to modulate the major pathways to enable synapse specification. Thus, a model whereby a myriad of interactions between cells and their signalling pathways act cooperatively to regulate the synaptogenic program is emerging (Batool et al., 2019). Our data, combined with several additional studies from other labs in the field, have contributed to defining the role of Slitrks in modulating synaptic development.

Specification of synapses by cooperative function of synaptogenic proteins could be mediated by differential spatial and temporal patterns of expression of these molecules between neuron populations. As well, binding interactions between different combinations of proteins and their splice forms can impart information on neuronal identity and promote diversification of synapse types. We and others have independently shown multiple lines of evidence that the Slitrks are mediators of synapse formation. Together, these data suggest that the Slitrk proteins are good candidates to contribute to synapse specificity due to: (1) their differential patterns of expression throughout the brain, and (2) their differential binding abilities to presynaptic partners.

Differential patterns of Slitrk expression in the brain

The broad but differential patterns of expression of Slitrks in the brain could speak to the idea that different populations of neurons express different combinations of Slitrk family members and other synaptogenic proteins, and that the combinatorial molecular code provides instruction for the specific development, maturation, and plasticity of synapses. For example, in the cerebellum of 10-day old mice, *Slitrk1, 3, 4, 5* and *6* but not *Slitrk2* are expressed in the Purkinje cell layer. Interestingly, *Slitrk1* is expressed inner granule cells of the anterior cerebellar lobe while Slitrk5 on the other hand has enriched expression in the molecular layer of the posterior lobe. *Slitrk2* and *4* are enriched in the granule cell layers as well, while *Slitrk6* mRNA is restricted to the Purkinje cells (Beaubien and Cloutier, 2009). Moreover, *Slitrk6* expression is strikingly restricted to limited

regions in the central nervous system compared to the broader expression patterns of the other Slitrks. It is most highly upregulated in the thalamus and hypothalamus. Finally, a recent study demonstrated opposing requirements for Slitrk2 and Slitrk5 in dopaminergic synapse formation, whereby Slitrk2 promotes excitatory synapse formation while Slitrk5 promotes inhibitory synapse formation onto dopaminergic neurons (Salesse et al., 2020). Together, the differential expression data and evidence of differential requirements of Slitrks within brain structures highlights the importance of precise protein expression at both spatial and temporal levels. More studies of the differential expression of the Slitrks in excitatory and inhibitory neuron populations can provide an additional layer of understanding of their function not only at the synapse, but in the overall modulation of excitatory and inhibitory circuits.

Slitrk interactions at the synapse

The Slitrks, with differential expression patterns throughout the nervous system, can also work in combination with other spatiotemporally-regulated synaptogenic proteins to confer synapse type. As such, the Slitrks have been shown to bind differentially to their presynaptic binding partners, the type IIa receptor protein tyrosine phosphatases (RPTPs) (Takahashi et al., 2012; Yim et al., 2013). All Slitrks function to promote excitatory synapse formation through PTPσ except for Slitrk3 which binds instead to PTPδ to regulate inhibitory synapse formation (Takahashi et al., 2012; Yim et al., 2013). We and others have identified the N-terminal LRR domain (LRR1) of Slitrk1 as the interface binding to presynaptic PTP (Um et al., 2014; Beaubien et al., 2016). Furthermore, just as the postsynaptic family members show differential binding to presynaptic partners, members of the RPTP family of presynaptic transmembrane proteins are prominent synaptogenic adhesion molecules have varying binding affinities to various postsynaptic partners (Han et al., 2018). Specifically, PTPδ was shown to interact with Slitrk1 and 2 only if it contained the splicing insert meB (Um et al., 2014; Yamagata et al., 2015). In this way, splicing variants can

confer a more precise molecular code for the specificity of synapse type by regulation through different levels and binding affinities to post-synaptic molecules (Li et al., 2015; Yamagata et al., 2015; Choi et al., 2016; Won et al., 2017; Won and Kim, 2018). In addition to binding in *trans* to mediate signalling between presynaptic and postsynaptic sides, it is expected that Slitrks are important for activating intracellular signalling pathways. Such a model has been shown for PTPσ where a combination of extracellular and intracellular signalling components is required for excitatory synapse development (Han et al., 2018). Similarly, many postsynaptic adhesion molecules like Neuroligins, NGL-2 and SALMs also bind to intracellular scaffolding proteins to mediate downstream signalling (reviewed in Jang et al., 2017). Recently, Slitrk2 was shown to bind the scaffold proteins PSD-95 and Shank3, and this interaction was crucial for excitatory synapse development and regulation of spine density (Han et al., 2019; Loomis et al., 2020). The other Slitrks do not bind PSD-95, however, further supporting a notion that differential intracellular signalling between Slitrk members can also promote diversity in synapse development (Han et al., 2019). Binding of Slitrks to other postsynaptic adhesion molecules can also be a method by which combinatorial CAM expression confers synaptic identity. Presynaptic Neurexins, for example, use coreceptors to transduce their trans-synaptic signalling cascades (Gokce and Südhof, 2013). Lateral assembly of SynCAM trans-synaptic complexes also been shown to increase adhesion at the synaptic cleft (Fogel et al., 2011). The Slitrk3 LRR2 domain binds to Neuroligin 2, an interaction that is required for differentiation of GABAergic synapses (Li et al., 2017). Similarly, our studies show that the LRR2 domain is involved Slitrk1 homophilic interaction at the surface, and we posit that this lateral interaction is important for clustering of the Slitrk/PTP complexes. As such, further experiments could test the model that homophilic or heterophilic lateral interactions of Slitrks and other synaptic adhesion molecules can cooperatively

bind to distinct postsynaptic scaffolding molecules and recruit neurotransmitters and other intracellular signalling molecules for synapse diversification and regulation of spine formation and density.

Finally, future studies looking at the synaptogenic role of Slitrk1 *in vivo* in specific regions of the brain would help elucidate combinatorial mechanisms by which synaptic adhesion molecules work together to orchestrate synapse specificity. For example, FLRT2, LRRTM1 and Slitrk1 are all expressed in CA1 and have been shown to differently affect transmission at input synapses (Schroeder et al., 2018). While the current *in vitro* knockdown studies of Slitrks demonstrated a role for Slitrks in synapse development, shRNA experiments to downregulate Slitrks in mature cultures would help identify a role for Slitrks in synapse maintenance. Moreover, *in vivo* studies using conditional knockout approaches to knockout Slitrk1 in spatially or temporally restricted areas can provide more precise insight into the spatiotemporal requirements for Slitrk1 in nervous system development and can complement the data showing behavioural changes associated with Slirtk1 deficiency (Katayama et al., 2010).

III. Amigo1 in axonal fasciculation

Our data demonstrate that Amigo1 contributes to promoting axonal fasciculation in the hippocampus but is dispensable for the fasciculation and coalescence of ORN axons in the main olfactory system. These observations suggest that Amigo1 may have differential roles in the development of circuits in specific brain regions. Alternatively, a contribution of Amigo1 to axonal fasciculation in the olfactory system may be masked by the expression of additional cell adhesion molecules, such as Kirrels, that compensate for the loss of Amigo1 in these cells. Although other Amigo family members are not expressed in ORNs, loss of Amigo1 could alter their expression in ORNs leading to compensation. However, an examination of the expression of a*migo2* and *amigo3*

mRNA in the olfactory epithelium of *Amigo1*$^{-/-}$ mice did not reveal any change in their expression (data not shown). The modulation of axon fasciculation by Amigo1 in the hippocampus can be attributed to its putative role in cell adhesion or in neural excitability, as discussed in the following sections.

1. Amigo1 as a cell adhesion molecule

Thus far, *in vitro* studies have shown a role for Amigo1 in cell adhesion through its LRR domains (Kajander et al., 2011). The only *in vivo* data to support this notion was reported by Zhao et al. in 2014 where morpholino knockdown of Amigo1 or the application of the Amigo1 ectodomain to block endogenous homophilic interactions caused fiber tract fasciculation defects in zebrafish central nervous system (Zhao et al., 2014). Here, we report the first example of fasciculation defects in a full *Amigo1* knockout model. Crystal structure data have proposed that dimerization of Amigo1 allows its cell surface expression and, through the LRR interface, can be involved in cell-cell adhesion (Kajander et al., 2011), leading us to believe that the defasciculation defects seen in the *Amigo1*$^{-/-}$ mice in mossy fiber projections could be due to a role for Amigo1 in cell adhesion. Furthermore, we found Amigo1 to have differential expression patterns in other subregions of the brain, including cerebellum, where it seems to be enriched specifically in lobe X. As far as we can tell, this finding is the first to identify a molecule with this type of specific enhancement in the flocculonodulus of the cerebellum. Examining whether loss of Amigo1 affects fasciculation of the projection of Purkinje cells or of other cell populations in the brain where it is highly expressed will help elucidate the more regulated functions for Amigo1 at different developmental time points. Our findings provide a basis for further studies into the role of Amigo1 in cell adhesion *in vivo*. Point mutations specifically targeting the LRR interaction interface could be introduced by

Cripsr-Cas9 technology, for example, to determine whether the effect of Amigo1 on mossy fiber fasciculation could be attributed to cell adhesion.

2. Amigo1 as a regulator of neuronal activity

While the loss of fasciculation could be due to loss of cell adhesion in the hippocampus of *Amigo1* null mice, Amigo1 may instead influence fasciculation through a distinct mechanism. For example, Sema3D was shown to regulate axon fasciculation by an indirect mechanism involving the regulation of expression of another cell adhesion molecule, L1 (Wolman et al., 2007). Therefore, we must consider the possibility that Amigo1 affects axonal fasciculation through its role in modulating neuronal activity.

Amigo1 is an auxiliary subunit of the voltage-gated potassium (Kv) channel Kv2.1 (Peltola et al., 2011). The Kv2.1 channel is a potent suppressor of neural activity and mediates the delayed rectifier current of an axon potential (Misonou et al., 2006). Currents through Kv channels thus play an important role in mitigating neuronal excitability (Du et al., 2000; Misonou et al., 2005b). Importantly, the Kv2.1 phosphorylation level regulates its voltage-dependent activation, providing a mechanism for homeostatic plasticity (Surmeier and Foehring, 2004; Misonou et al., 2005a, 2006). Kainate-induced seizures and ischemia both can elicit dephosphorylation and de-clustering of Kv2.1, resulting in diffuse localization and suppressed neuronal activity (Misonou et al., 2004, 2006). Amigo1 was shown to act as an auxiliary subunit of Kv2.1 and affect the channel dynamics by regulating its voltage-dependent activation (Peltola et al., 2011). Loss of Amigo1 protein caused downregulation of Kv2.1 and shifted the current density curve such that neurons deficient for Amigo1 in culture required stronger depolarization to elicit potassium current (Peltola et al., 2011, 2016). These studies together define a function for Amigo1 in the proper expression of Kv2.1 and identify its ability to alter neuronal excitability through this channel. Intrinsic neuronal excitability

is thought to influence axonal growth and sprouting during development as well as control refinement of circuits (Catalano and Shatz, 1998). For example, intrinsic activity in olfactory receptor neurons regulate the expression of axon guidance and cell adhesion molecules (Imai et al., 2006; Serizawa et al., 2006; Nakashima et al., 2013). Thus, changes to neural activity caused by loss of Amigo1 could instigate modifications to axon guidance and cell adhesion signals causing the defasciculation defects that we observed in hippocampal mossy fiber projections. Furthermore, altered levels of neural activity could also mediate synaptic changes leading to the destabilization of mossy fiber terminals and/or sprouting of ectopic boutons seen in the pyramidal cell layer of CA3.

The Kv2.1 gene, *KCNB1,* has been associated with strong susceptibility to schizophrenia, and schizophrenia-related behaviours such as hyperactivity accompanied the electrophysiological changes to neuronal excitability via the Kv2.1 channel in *Amigo1* null mice (Peltola et al., 2016). These mice were characterized for a multitude of behavioural tests, including spatial memory tasks. Pre-pulse inhibition of startle response was reduced in *Amigo1* null mice, similar to *BACE1*$^{-/-}$ mice, which show similar mossy fiber fasciculation defects as our *Amigo1* mutant mice (Hitt et al., 2012; Peltola et al., 2016; Weber et al., 2017; Ou-Yang et al., 2018). In a patrolling task testing behavioural flexibility and working memory, *Amigo1* null mice performed worse than wild type littermates. However, the *Amigo1* null mice tested for behaviour by Peltola and colleagues in 2016 seem to have been generated without the removal of the neomycin gene on the targeted allele (Peltola et al., 2016, Supplemental Figure 1). Presence of the neomycin gene insertion can have off-target effects, as we have described in Chapter 2, so it would be important to confirm these behavioural deficits in our *Amigo1*$^{-/-}$ animals, or to examine whether Timm-stained mossy fibers in the *Amigo1*$^{neo/neo}$ mice have similar phenotypes to those in *Amigo1*$^{-/-}$

animals. Furthermore, the *Amigo1* mice tested by Peltola et al began behavioural testing at only 2 months of age. Considering that changes to the IPB are related to spatial memory and learning tasks, it would be worth examining spatial learning paradigms such as the Morris Water Maze or Radial Maze in both our young (1-month old) and ageing (>5-month old) *Amgio1*$^{-/-}$ animals to determine any behavioural outcomes of defasciculated and ectopic mossy fibers (Blaabjerg and Zimmer, 2007; Peltola et al., 2016). Importantly, *Kv2.1*$^{-/-}$ mice also show behavioural deficits that fit with what we would expect for our *Amigo1* null animals with hippocampal connectivity problems. *Kv2.1*$^{-/-}$ mice are hyperactive and show deficits in the Morris Water Maze spatial learning task. Furthermore, they have accelerated seizure progression, which could be a result of a lack of homeostatic regulation of neuronal hyperexcitability due to loss of this channel (Speca et al., 2014). Finally, the triple transgenic mouse model of Alzheimer's disease exhibits a reduction in functional Kv2.1 channels with concomitant current density changes (Frazzini et al., 2016), implicating this channel in the pathology of this memory disease. The strong link between Amigo1 and Kv2.1 in the regulation of neuronal excitability and the alteration in Kv2.1 channel functioning with loss of Amigo1 lead us to believe that we would see similar behavioural deficits in our *Amigo1*$^{-/-}$ animals as in the *Kv2.1* null mice and that these deficits could be at least in part attributed to the changes in mossy fiber projections observed.

Finally, mossy fiber sprouting, comprising the sprouting of abnormal axon collaterals and synaptic reorganization of mossy fibers, including their targeting back onto granule cell dendrites in the dentate molecular layer, is a common hallmark of epileptic brains (Scheibel et al., 1974). Seizure-induction using kindling models to promote mossy fiber sprouting and neural hyperexcitability have widely been used as models to study the epileptic brain (Cavazos and Sutula, 1990; Kokaia et al., 1995; Buckmaster, 2012). While there is no detectable mossy fiber sprouting in the inner

molecular layer, the evidence of increased plasticity and synaptic reorganization with the ectopic mossy fiber boutons and defasciculation in the *Amigo1*$^{-/-}$ mice makes it worth testing whether these mice are more susceptible to seizure induction or seizure progression as seen with the *Kv2.1*$^{-/-}$ mice (Speca et al., 2014). Furthermore, Golgi staining of individual CA3 pyramidal cells to visualize the size and distribution of thorny excrescences, the excitatory post-synaptic counterpart of mossy fiber boutons, or ultrastructural analysis of inhibitory interneurons in the pyramidal layer of CA3 at various proximo-distal levels would help elucidate whether an increase in mossy fiber bouton density is accompanied by concomitant increase in excitatory or inhibitory post-synaptic sites.

IV. Conclusion

Although many questions remain to be addressed, our results contribute to the understanding of LRR proteins in the processes of neural circuit development, from axon targeting to synapse formation and maintenance. Our data from studying Amigo1 in the olfactory system define the importance of examining both expression pattern and function within a system to determine its requirement, however conclusions made from one model might not always be translatable to other systems, as we found for the hippocampus. This notion speaks to the idea that the formation of different nervous system circuits is extremely complex, and that molecules expressed differentially both in space and time likely act synergistically in highly orchestrated manners for proper development, with certain players being more important than others in a subsystem-dependent manner. Further study of this important LRR superfamily of molecules will offer insight into how malfunctions of these proteins can lead to debilitating neurological diseases and also help in directing the development of strategies for their treatment.

References

Abelson JF et al. (2005) Sequence variants in SLITRK1 are associated with Tourette's syndrome. Science (New York, NY) 310:317–320.

Allaire PD, Marat AL, Dall'Armi C, Paolo GD, McPherson PS, Ritter B (2010) The Connecdenn DENN Domain: A GEF for Rab35 Mediating Cargo-Specific Exit from Early Endosomes. Molecular Cell 37.

Amaral DG, Dent JA (1981) Development of the mossy fibers of the dentate gyrus: I. A light and electron microscopic study of the mossy fibers and their expansions. Journal of Comparative Neurology 195:51–86.

Amaral DG, Scharfman HE, Lavenex P (2007) The dentate gyrus: fundamental neuroanatomical organization (dentate gyrus for dummies). In: Progress in Brain Research (Scharfman HE, ed), pp 3–790 The Dentate Gyrus: A Comprehensive Guide to Structure, Function, and Clinical Implications. Elsevier.

An BC, Choi Y-D, Oh I-J, Kim JH, Park J-I, Lee S (2018) GPx3-mediated redox signaling arrests the cell cycle and acts as a tumor suppressor in lung cancer cell lines Ahmad A, ed. PLOS ONE 13:e0204170.

Angevine JB (1965) Time of neuron origin in the hippocampal region. An autoradiographic study in the mouse. Exp Neurol Suppl: 2:1-70.

Aruga J, Mikoshiba K (2003) Identification and characterization of Slitrk, a novel neuronal transmembrane protein family controlling neurite outgrowth. Molecular and cellular neurosciences 24:117–129.

Aruga J, Yokota N, Mikoshiba K (2003) Human SLITRK family genes: Genomic organization and expression profiling in normal brain and brain tumor tissue. Gene 315:87–94.

Ba-Charvet KTN, Brose K, Marillat V, Kidd T, Goodman CS, Tessier-Lavigne M, Sotelo C, Chédotal A (1999) Slit2-mediated chemorepulsion and collapse of developing forebrain axons. Neuron 22.

Bagri A, Cheng HJ, Yaron A, Pleasure SJ, Tessier-Lavigne M (2003) Stereotyped pruning of long hippocampal axon branches triggered by retraction inducers of the semaphorin family. Cell 113.

Bando T, Morikawa Y, Hisaoka T, Komori T, Miyajima A, Senba E (2012) Expression pattern of leucine-rich repeat neuronal protein 4 in adult mouse dorsal root ganglia. Neuroscience Letters 531.

Banerjee S, Riordan M, Bhat MA (2014) Genetic aspects of autism spectrum disorders: Insights from animal models. Front Cell Neurosci 8:58.

Barrios AW, Núñez G, Quinteiro PS, Salazar I (2014) Anatomy, histochemistry, and immunohistochemistry of the olfactory subsystems in mice. Frontiers in Neuroanatomy 8.

Bartsch T, Wulff P (2015) The hippocampus in aging and disease: From plasticity to vulnerability. Neuroscience 309:1–16.

Batool S, Raza H, Zaidi J, Riaz S, Hasan S, Syed NI (2019) Synapse formation: From cellular and molecular mechanisms to neurodevelopmental and neurodegenerative disorders. Journal of Neurophysiology 121:1381–1397.

Bayer SA (1980a) Development of the hippocampal region in the rat I. Neurogenesis examined with 3H-thymidine autoradiography. Journal of Comparative Neurology 190.

Bayer SA (1980b) Development of the hippocampal region in the rat II. Morphogenesis during embryonic and early postnatal life. Journal of Comparative Neurology 190.

Beaubien F, Cloutier JF (2009) Differential expression of Slitrk family members in the mouse nervous system. Developmental Dynamics 238:3285–3296.

Beaubien F, Raja R, Kennedy TE, Fournier AE, Cloutier JF (2016) Slitrk1 is localized to excitatory synapses and promotes their development. Scientific Reports 6:27343.

Bekirov IH, Nagy V, Svoronos A, Huntley GW, Benson DL (2008) Cadherin-8 and N-cadherin differentially regulate pre- and postsynaptic development of the hippocampal mossy fiber pathway. Hippocampus 18.

Bella J, Hindle KL, McEwan PA, Lovell SC (2008) The leucine-rich repeat structure. Cell Mol Life Sci 65:2307–2333.

Bellon A, Mann F (2018) Keeping up with advances in axon guidance. Curr Opin Neurobiol 53:183–191.

Biederer T, Sara Y, Mozhayeva M, Atasoy D, Liu X, Kavalali ET, Südhof TC (2002) SynCAM, a synaptic adhesion molecule that drives synapse assembly. Science 297.

Biederer T, Südhof TC (2000) Mints as adaptors. Direct binding to neurexins and recruitment of Munc18. Journal of Biological Chemistry 275.

Bishop H, Cobb MM, Kirmiz M, Parajuli LK, Mandikian D, Philp AM, Melnik M, Kuja-Panula J, Rauvala H, Shigemoto R, Murray KD, Trimmer JS (2018) Kv2 ion channels determine the expression and localization of the associated AMIGO-1 cell adhesion molecule in adult brain neurons. Frontiers in Molecular Neuroscience 11.

Blaabjerg M, Zimmer J (2007) The dentate mossy fibers: structural organization, development and plasticity. Prog Brain Res 163:85–107.

Bourgeron T (2009) A synaptic trek to autism. Curr Opin Neurobiol 19:231–234.

Bourgin C, Murai KK, Richter M, Pasquale EB (2007) The EphA4 receptor regulates dendritic spine remodeling by affecting β1-integrin signaling pathways. Journal of Cell Biology 178.

Bressel OC, Khan M, Mombaerts P (2016) Linear correlation between the number of olfactory sensory neurons expressing a given mouse odorant receptor gene and the total volume of the corresponding glomeruli in the olfactory bulb. Journal of Comparative Neurology 524:199–209.

Brigelius-Flohé R (2006) Glutathione peroxidases and redox-regulated transcription factors. In: Biological Chemistry, pp 1329–1335. Biol Chem.

Brose K, Tessier-Lavigne M (2000) Slit proteins: key regulators of axon guidance, axonal branching, and cell migration. Curr Opin Neurobiol 10:95–102.

Buck L, Axel R (1991) A novel multigene family may encode odorant receptors: A molecular basis for odor recognition. Cell 65:175–187.

Buckmaster PS (2012) Mossy Fiber Sprouting in the Dentate Gyrus. In: Jasper's Basic Mechanisms of the Epilepsies, 4th ed. (Noebels JL, Avoli M, Rogawski MA, Olsen RW, Delgado-Escueta AV, eds). Bethesda (MD): National Center for Biotechnology Information (US).

Butler CD, Schnetz SA, Yu EY, Davis JB, Temple K, Silver J, Malouf AT (2004) Keratan Sulfate Proteoglycan Phosphacan Regulates Mossy Fiber Outgrowth and Regeneration. Journal of Neuroscience 24.

Cao L, Rickenbacher GT, Rodriguez S, Moulia TW, Albers MW (2012) The precision of axon targeting of mouse olfactory sensory neurons requires the BACE1 protease. Scientific Reports 2.

Catalano SM, Messersmith EK, Goodman CS, Shatz CJ, Chédotal A (1998) Many major CNS axon projections develop normally in the absence of semaphorin III. Molecular and Cellular Neurosciences 11.

Catalano SM, Shatz CJ (1998) Activity-dependent cortical target selection by thalamic axons. Science 281.

Cavazos JE, Sutula TP (1990) Progressive neuronal loss induced by kindling: a possible mechanism for mossy fiber synaptic reorganization and hippocampal sclerosis. Brain Research 527.

Chattopadhyay K, Chatterjee K (2012) The genetic factors influencing the development of trichotillomania. J Genet 91:259–262.

Chédotal A, Rio JAD, Ruiz M, He Z, Borrell V, Castro FD, Ezan F, Goodman CS, Tessier-Lavigne M, Sotelo C, Soriano E (1998) Semaphorins III and IV repel hippocampal axons via two distinct receptors. Development 125.

Chen H, Bagri A, Zupicich JA, Zou Y, Stoeckli E, Pleasure SJ, Lowenstein DH, Skarnes WC, Chédotal A, Tessier-Lavigne M (2000) Neuropilin-2 regulates the development of select cranial and sensory nerves and hippocampal mossy fiber projections. Neuron 25.

Chen L, Gao B, Fang M, Li J, Mi X, Xu X, Wang W, Gu J, Tang B, Zhang Y, Wang Z, Zhan A, Chen G, Wang X (2017) Lentiviral Vector-Induced Overexpression of RGMa in the Hippocampus Suppresses Seizures and Mossy Fiber Sprouting. Molecular Neurobiology 54.

Chen Y, Aulia S, Li L, Tang BL (2006) AMIGO and friends: an emerging family of brain-enriched, neuronal growth modulating, type I transmembrane proteins with leucine-rich repeats (LRR) and cell adhesion molecule motifs. Brain Res Rev 51:265–274.

Chen Y, Hor HH, Tang BL (2012) AMIGO is expressed in multiple brain cell types and may regulate dendritic growth and neuronal survival. Journal of Cellular Physiology 227:2217–2229.

Chess A, Simon I, Cedar H, Axel R (1994) Allelic inactivation regulates olfactory receptor gene expression. Cell 78:823–834.

Chierzi S, Stachniak TJ, Trudel E, Bourque CW, Murai KK (2012) Activity maintains structural plasticity of mossy fiber terminals in the hippocampus. Molecular and Cellular Neuroscience 50.

Cho HJ, Lépine M, Andrews W, Parnavelas J, Cloutier JF (2007) Requirement for slit-1 and robo-2 in zonal segregation of olfactory sensory neuron axons in the main olfactory bulb. Journal of Neuroscience 27.

Cho JH, Kam JWK, Cloutier J-F (2012) Slits and Robo-2 regulate the coalescence of subsets of olfactory sensory neuron axons within the ventral region of the olfactory bulb. Developmental biology 371:269–279.

Cho JH, Prince JEA, Cloutier J-F (2009) Axon guidance events in the wiring of the mammalian olfactory system. Mol Neurobiol 39:1–9.

Cho JH, Prince JEA, Cutforth T, Cloutier JF (2011) The pattern of glomerular map formation defines responsiveness to aversive odorants in mice. Journal of Neuroscience 31.

Choi SY, Han K, Cutforth T, Chung W, Park H, Lee D, Kim R, Kim MH, Choi Y, Shen K, Kim E (2015) Mice lacking the synaptic adhesion molecule Neph2/Kirrel3 display moderate hyperactivity and defective novel object preference. Frontiers in Cellular Neuroscience 9.

Choi Y, Nam J, Whitcomb DJ, Song YS, Kim D, Jeon S, Um JW, Lee SG, Woo J, Kwon SK, Li Y, Mah W, Kim HM, Ko J, Cho K, Kim E (2016) SALM5 trans-synaptically interacts with LAR-RPTPs in a splicing-dependent manner to regulate synapse development. Scientific Reports 6.

Claiborne BJ, Amaral DG, Cowan WM (1986) A light and electron microscopic analysis of the mossy fibers of the rat dentate gyrus. Journal of Comparative Neurology 246.

Clowney EJ, Legros MA, Mosley CP, Clowney FG, Markenskoff-Papadimitriou EC, Myllys M, Barnea G, Larabell CA, Lomvardas S (2012) Nuclear aggregation of olfactory receptor genes governs their monogenic expression. Cell 151:724–737.

Coleman JLJ, Brennan K, Ngo T, Balaji P, Graham RM, Smith NJ (2015) Rapid knockout and reporter mouse line generation and breeding colony establishment using EUCOMM conditional-ready embryonic stem cells: A case study. Frontiers in Endocrinology 6.

Condomitti G, Wierda KD, Schroeder A, Rubio SE, Vennekens KM, Orlandi C, Martemyanov KA, Gounko NV, Savas JN, Wit J de (2018) An Input-Specific Orphan Receptor GPR158-HSPG Interaction Organizes Hippocampal Mossy Fiber-CA3 Synapses. Neuron 100.

Cremer H, Chazal G, Goridis C, Represa A (1997) NCAM is essential for axonal growth and fasciculation in the hippocampus. Molecular and Cellular Neurosciences 8.

Cremer H, Chazal G, Lledo PM, Rougon G, Montaron MF, Mayo W, Moal ML, Abrous DN (2000) PSA-NCAM: An important regulator of hippocampal plasticity. In: International Journal of Developmental Neuroscience.

Crusio WE, Schwegler H, Abeelen JHF van (1989) Behavioral responses to novelty and structural variation of the hippocampus in mice. II. Multivariate genetic analysis. Behavioural Brain Research 32.

Crusio WE, Schwegler H, Brust I (1993) Covariations between hippocampal mossy fibres and working and reference memory in spatial and non-spatial radial maze tasks in mice. Eur J Neurosci 5:1413–1420.

Crusio WE, Schwegler H, Lipp HP (1987) Radial-maze performance and structural variation of the hippocampus in mice: a correlation with mossy fibre distribution. Brain Res 425:182–185.

Cutforth T, Moring L, Mendelsohn M, Nemes A, Shah NM, Kim MM, Frisén J, Axel R (2003) Axonal ephrin-As and odorant receptors: Coordinate determination of the olfactory sensory map. Cell 114:311–322.

Dachtler J, Ivorra JL, Rowland TE, Lever C, Rodgers RJ, Clapcote SJ (2015) Heterozygous deletion of α-neurexin I or α-neurexin II results in behaviors relevant to autism and schizophrenia. Behavioral Neuroscience 129.

Dalton RP, Lyons DB, Lomvardas S (2013) Co-opting the unfolded protein response to elicit olfactory receptor feedback. Cell 155:321.

Danzer SC, He X, Loepke AW, McNamara JO (2009) Structural plasticity of dentate granule cell mossy fibers during the development of limbic epilepsy. Hippocampus 20.

Degl'Innocenti A, D'Errico A (2017) Regulatory Features for Odorant Receptor Genes in the Mouse Genome. Front Genet 8:19.

Demyanenko GP, Siesser PF, Wright AG, Brennaman LH, Bartsch U, Schachner M, Maness PF (2011) L1 and CHL1 cooperate in thalamocortical axon targeting. Cerebral Cortex 21.

Deng H, Le WD, Xie WJ, Jankovic J (2006) Examination of the SLITRK1 gene in Caucasian patients with Tourette syndrome. Acta neurologica Scandinavica 114:400–402.

Deng W, Aimone JB, Gage FH (2010) New neurons and new memories: how does adult hippocampal neurogenesis affect learning and memory? Nat Rev Neurosci 11:339–350.

DeWit J, O'Sullivan ML, Savas JN, Condomitti G, Caccese MC, Vennekens KM, Yates JR, Ghosh A (2013) Unbiased discovery of Glypican as a receptor for LRRTM4 in regulating excitatory synapse development. Neuron 79.

DeWit J, Sylwestrak E, O'Sullivan ML, Otto S, Tiglio K, Savas JN, Yates JR, Comoletti D, Taylor P, Ghosh A (2009) LRRTM2 interacts with Neurexin1 and regulates excitatory synapse formation. Neuron 64:799–806.

Ditlevsen DK, Køhler LB, Berezin V, Bock E (2007) Cyclic guanosine monophosphate signalling pathway plays a role in neural cell adhesion molecule-mediated neurite outgrowth and survival. Journal of Neuroscience Research 85.

Du J, Haak LL, Phillips-Tansey E, Russell JT, McBain CJ (2000) Frequency-dependent regulation of rat hippocampal somato-dendritic excitability by the K+ channel subunit Kv2.1. Journal of Physiology 522:19–31.

Dufour A, Seibt J, Passante L, Depaepe V, Ciossek T, Frisén J, Kullander K, Flanagan JG, Polleux F, Vanderhaeghen P (2003) Area specificity and topography of thalamocortical projections are controlled by ephrin/Eph genes. Neuron 39.

Durand CM et al. (2007) Mutations in the gene encoding the synaptic scaffolding protein SHANK3 are associated with autism spectrum disorders. Nature Genetics 39.

Esclassan F, Francois J, Phillips KG, Loomis S, Gilmour G (2015) Phenotypic characterization of non-social behavioral impairment in neurexin 1α knockout rats. Behavioral Neuroscience 129.

Etherton MR, Blaiss CA, Powell CM, Südhof TC (2009) Mouse neurexin-1α deletion causes correlated electrophysiological and behavioral changes consistent with cognitive impairments. Proceedings of the National Academy of Sciences of the United States of America 106.

Fiering S, Epner E, Robinson K, Zhuang Y, Telling A, Hu M, Martin DIK, Enver T, Ley TJ, Groudine M (1995) Targeted deletion of 5'HS2 of the murine β-globin LCR reveals that it is not essential for proper regulation of the β-globin locus. Genes and Development 9:2203–2213.

Fiering S, Kim CG, Epner EM, Groudine M (1993) An "in-out" strategy using gene targeting and FLP recombinase for the functional dissection of complex DNA regulatory elements:

analysis of the beta-globin locus control region. Proc Natl Acad Sci U S A 90:8469–8473.

Fogel AI, Stagi M, Arce KPD, Biederer T (2011) Lateral assembly of the immunoglobulin protein SynCAM 1 controls its adhesive function and instructs synapse formation. EMBO Journal 30.

Frazzini V, Guarnieri S, Bomba M, Navarra R, Morabito C, Mariggiò MA, Sensi SL (2016) Altered Kv2.1 functioning promotes increased excitability in hippocampal neurons of an Alzheimer's disease mouse model. Cell Death Dis 7:e2100.

Frotscher M, Zimmer J (1983) Lesion-induced mossy fibers to the molecular layer of the rat fascia dentata: Identification of postsynaptic granule cells by the Golgi-EM technique. Journal of Comparative Neurology 215.

Fuss SH, Omura M, Mombaerts P (2007) Local and cis Effects of the H Element on Expression of Odorant Receptor Genes in Mouse. Cell 130:373–384.

Gaarskjaer FB (1986) The organization and development of the hippocampal mossy fiber system.

Galimberti I, Bednarek E, Donato F, Caroni P (2010) EphA4 Signaling in Juveniles Establishes Topographic Specificity of Structural Plasticity in the Hippocampus. Neuron 65.

Galimberti I, Gogolla N, Alberi S, Santos AF, Muller D, Caroni P (2006) Long-Term Rearrangements of Hippocampal Mossy Fiber Terminal Connectivity in the Adult Regulated by Experience. Neuron 50.

Geddes MR (2006) A break near SLITRK1: A breakthrough in Tourette syndrome. Clinical genetics 69:206–208.

Giger RJ, Cloutier JF, Sahay A, Prinjha RK, Levengood DV, Moore SE, Pickering S, Simmons D, Rastan S, Walsh FS, Kolodkin AL, Ginty DD, Geppert M (2000) Neuropilin-2 is required in vivo for selective axon guidance responses to secreted semaphorins. Neuron 25.

Godfrey PA, Malnic B, Buck LB (2004) The mouse olfactory receptor gene family. Proceedings of the National Academy of Sciences of the United States of America 101:2156–2161.

Gokce O, Südhof TC (2013) Membrane-tethered monomeric neurexin LNS-domain triggers synapse formation. Journal of Neuroscience 33.

GoodSmith D, Chen X, Wang C, Kim SH, Song H, Burgalossi A, Christian KM, Knierim JJ (2017) Spatial Representations of Granule Cells and Mossy Cells of the Dentate Gyrus. Neuron 93:677-690.e5.

Graf ER, Zhang X, Jin SX, Linhoff MW, Craig AM (2004) Neurexins induce differentiation of GABA and glutamate postsynaptic specializations via neuroligins. Cell 119:1013–1026.

Grayton HM, Missler M, Collier DA, Fernandes C (2013) Altered Social Behaviours in Neurexin 1α Knockout Mice Resemble Core Symptoms in Neurodevelopmental Disorders. PLoS ONE 8.

Greenwood TA et al. (2013) Genome-wide association study of irritable vs. Elated Mania suggests genetic differences between clinical subtypes of bipolar disorder. PLoS ONE 8.

Guilmatre A, Huguet G, Delorme R, Bourgeron T (2014) The emerging role of SHANK genes in neuropsychiatric disorders. Developmental Neurobiology 74.

Hägglund M, Berghard A, Strotmann J, Bohm S (2006) Retinoic acid receptor-dependent survival of olfactory sensory neurons in postnatal and adult mice. Journal of Neuroscience 26:3281–3291.

Han KA, Jeon S, Um JW, Ko J (2016) Emergent Synapse Organizers: LAR-RPTPs and Their Companions. Int Rev Cell Mol Biol 324:39–65.

Han KA, Kim J, Kim H, Kim D, Lim D, Ko J, Um JW (2019) Slitrk2 controls excitatory synapse development via PDZ-mediated protein interactions. Scientific Reports 9:17094.

Han KA, Ko JS, Pramanik G, Kim JY, Tabuchi K, Um JW, Ko J (2018) PTPσ Drives Excitatory Presynaptic Assembly via Various Extracellular and Intracellular Mechanisms. The Journal of neuroscience : the official journal of the Society for Neuroscience 38:6700–6721.

Harris KP, Littleton JT (2015) Transmission, development, and plasticity of synapses. Genetics 201.

Hartmann S, Zheng F, Kyncl MC, Karch S, Voelkl K, Zott B, D'Avanzo C, Lomoio S, Tesco G, Kim DY, Alzheimer C, Huth T (2018) β-Secretase BACE1 promotes surface expression and function of Kv3.4 at hippocampal mossy fiber synapses. Journal of Neuroscience 38.

Hasegawa S, Hamada S, Kumode Y, Esumi S, Katori S, Fukuda E, Uchiyama Y, Hirabayashi T, Mombaerts P, Yagi T (2008) The protocadherin-α family is involved in axonal coalescence of olfactory sensory neurons into glomeruli of the olfactory bulb in mouse. Molecular and Cellular Neuroscience 38:66–79.

Hata Y, Davletov B, Petrenko AG, Jahn R, Südhof TC (1993) Interaction of synaptotagmin with the cytoplasmic domains of neurexins. Neuron 10.

Hemming ML, Elias JE, Gygi SP, Selkoe DJ (2009) Identification of β-secretase (BACE1) substrates using quantitative proteomics. PLoS ONE 4.

Henze DA, Urban NN, Barrionuevo G (2000) The multifarious hippocampal mossy fiber pathway: a review. Neuroscience 98:407–427.

Henze DA, Wittner L, Buzsáki G (2002) Single granule cells reliably discharge targets in the hippocampal CA3 network in vivo. Nature Neuroscience 5.

Heyden A, Angenstein F, Sallaz M, Seidenbecher C, Montag D (2008) Abnormal axonal guidance and brain anatomy in mouse mutants for the cell recognition molecules close homolog of L1 and NgCAM-related cell adhesion molecule. Neuroscience 155.

Hinds HL, Goussakov I, Nakazawa K, Tonegawa S, Bolshakov VY (2003) Essential function of α-calcium/calmodulin-dependent protein kinase II in neurotransmitter release at a glutamatergic central synapse. Proceedings of the National Academy of Sciences of the United States of America 100:4275–4280.

Hisaoka T, Komori T, Kitamura T, Morikawa Y (2018) Abnormal behaviours relevant to neurodevelopmental disorders in Kirrel3-knockout mice. Scientific Reports 8.

Hitt B, Riordan SM, Kukreja L, Eimer WA, Rajapaksha TW, Vassar R (2012) β-Site amyloid precursor protein (APP)-cleaving enzyme 1 (BACE1)-deficient mice exhibit a close homolog of L1 (CHL1) loss-of-function phenotype involving axon guidance defects. Journal of Biological Chemistry 287.

Hitti FL, Siegelbaum SA (2014) The hippocampal CA2 region is essential for social memory. Nature 508.

Hug BA, Wesselschmidt RL, Fiering S, Bender MA, Epner E, Groudine M, Ley TJ (1996) Analysis of mice containing a targeted deletion of beta-globin locus control region 5' hypersensitive site 3. Mol Cell Biol 16:2906–2912.

Ichtchenko K, Hata Y, Nguyen T, Ullrich B, Missler M, Moomaw C, Südhof TC (1995) Neuroligin 1: a splice site-specific ligand for beta-neurexins. Cell 81:435–443.

Ihara N, Ligao B, Ikegaya Y, Takeuchi H (2017) Differential timing of neurogenesis underlies dorsal-ventral topographic projection of olfactory sensory neurons. Neural Development 12.

Imai T, Sakano H (2009) Odorant receptor gene choice and axonal projection in the mouse olfactory system. Results and problems in cell differentiation 47:57–75.

Imai T, Sakano H (2011) Axon-axon interactions in neuronal circuit assembly: lessons from olfactory map formation. Eur J Neurosci 34:1647–1654.

Imai T, Suzuki M, Sakano H (2006) Odorant receptor-derived cAMP signals direct axonal targeting. Science 314:657–661.

Imamura K, Mataga N, Mori K (1992) Coding of odor molecules by mitral/tufted cells in rabbit olfactory bulb. I. Aliphatic compounds. Journal of Neurophysiology 68.

Ishii T, Serizawa S, Kohda A, Nakatani H, Shiroishi T, Okumura K, Iwakura Y, Nagawa F, Tsuboi A, Sakano H (2001) Monoallelic expression of the odourant receptor gene and axonal projection of olfactory sensory neurones. Genes to Cells 6:71–78.

Jamain S et al. (2003) Mutations of the X-linked genes encoding neuroligins NLGN3 and NLGN4 are associated with autism. Nature Genetics 34.

Jamot L, Bertholet JY, Crusio WE (1994) Neuroanatomical divergence between two substrains of C57BL/6J inbred mice entails differential radial-maze learning. Brain Res 644:352–356.

Jang S, Lee H, Kim E (2017) Synaptic adhesion molecules and excitatory synaptic transmission. Curr Opin Neurobiol 45:45–50.

Jessberger S, Kempermann G (2003) Adult-born hippocampal neurons mature into activity-dependent responsiveness. European Journal of Neuroscience 18.

Ji SK, Gopal P, Ji WU, Ji SS, Dongmin L, Kee HK, Gug-Young C, Giuseppe C, Ho MK, Hyun K, Joris WD, Kang-Sik P, Katsuhiko T, Jaewon K (2015) Ptpσ functions as a presynaptic receptor for the glypican-4/LRRTM4 complex and is essential for excitatory synaptic transmission. Proceedings of the National Academy of Sciences of the United States of America 112.

Jones DT, Reed RR (1989) Golf: An olfactory neuron specific-G protein involved in odorant signal transduction. Science 244.

Kaech S, Banker G (2006) Culturing hippocampal neurons. Nature Protocols 1.

Kajander T, Kuja-Panula J, Rauvala H, Goldman A (2011) Crystal structure and role of glycans and dimerization in folding of neuronal leucine-rich repeat protein AMIGO-1. Journal of Molecular Biology 413:1001–1015.

Kajiwara Y, Buxbaum JD, Grice DE (2009) SLITRK1 Binds 14-3-3 and Regulates Neurite Outgrowth in a Phosphorylation-Dependent Manner. Biological Psychiatry 66:918–925.

Kaneko-Goto T, Yoshihara S ichi, Miyazaki H, Yoshihara Y (2008) BIG-2 Mediates Olfactory Axon Convergence to Target Glomeruli. Neuron 57:834–846.

Kang H, Han K, Won SY, Kim HM, Lee YH, Ko J, Um JW (2016) Slitrk missense mutations associated with neuropsychiatric disorders distinctively impair slitrk trafficking and synapse formation. Frontiers in Molecular Neuroscience 9:104.

Karagiannidis I, Rizzo R, Tarnok Z, Wolanczyk T, Hebebrand J, Nöthen MM, Lehmkuhl G, Farkas L, Nagy P, Barta C, Szymanska U, Panteloglou G, Miranda DM, Feng Y, Sandor P, Barr C, TSGeneSEE, Paschou P (2012) Replication of association between a SLITRK1 haplotype and Tourette Syndrome in a large sample of families. Mol Psychiatry 17:665–668.

Katayama K, Yamada K, Ornthanalai VG, Inoue T, Ota M, Murphy NP, Aruga J (2010) Slitrk1-deficient mice display elevated anxiety-like behavior and noradrenergic abnormalities. Molecular Psychiatry 15:177–184.

Katayama KI, Zine A, Ota M, Matsumoto Y, Inoue T, Fritzsch B, Aruga J (2009) Disorganized innervation and neuronal loss in the inner ear of slitrk6-deficient mice. PLoS ONE 4:e7786.

Kayser MS, McClelland AC, Hughes EG, Dalva MB (2006) Intracellular and trans-synaptic regulation of glutamatergic synaptogenesis by EphB receptors. Journal of Neuroscience 26.

Kee N, Teixeira CM, Wang AH, Frankland PW (2007) Preferential incorporation of adult-generated granule cells into spatial memory networks in the dentate gyrus. Nature Neuroscience 10.

Keller F, Rimvall K, Barbe MF, Levitt P (1989) A membrane glycoprotein associated with the limbic system mediates the formation of the septo- hippocampal pathway in vitro. Neuron 3.

Kempermann G, Kuhn HG, Gage FH (1997) More hippocampal neurons in adult mice living in an enriched environment. Nature 386.

Kerr MA, Belluscio L (2006) Olfactory experience accelerates glomerular refinement in the mammalian olfactory bulb. Nature Neuroscience 9:484–486.

Khachaturian H, Watson SJ, Lewis ME, Coy D, Goldstein A, Akil H (1982) Dynorphin immunocytochemistry in the rat central nervous system. Peptides 3.

Khalaf-Nazzal R, Francis F (2013) Hippocampal development - old and new findings. Neuroscience 248:225–242.

Kim CG, Epner EM, Forrester WC, Groudine M (1992) Inactivation of the human beta-globin gene by targeted insertion into the beta-globin locus control region. Genes Dev 6:928–938.

Kim DY, Carey BW, Wang H, Ingano LAM, Binshtok AM, Wertz MH, Pettingell WH, He P, Lee VMY, Woolf CJ, Kovacs DM (2007) BACE1 regulates voltage-gated sodium channels and neuronal activity. Nature Cell Biology 9.

Kim DY, Gersbacher MT, Inquimbert P, Kovacs DM (2011) Reduced sodium channel Nav1.1 levels in BACE1-null mice. Journal of Biological Chemistry 286.

Kim JA, Koyama R, Yamada RX, Yamada MK, Nishiyama N, Matsuki N, Ikegaya Y (2004) Environmental control of the survival and differentiation of dentate granule neurons. Cerebral Cortex 14:1358–1364.

Kim JA, Yamada MK, Nishiyama N, Matsuki N, Ikegaya Y (2003) Mossy fiber pathfinding in multilayer organotypic cultures of rat hippocampal slices. Cellular and Molecular Neurobiology 23.

Kim S, Burette A, Chung HS, Kwon SK, Woo J, Lee HW, Kim K, Kim H, Weinberg RJ, Kim E (2006) NGL family PSD-95-interacting adhesion molecules regulate excitatory synapse formation. Nature Neuroscience 9.

Klein R (2009) Bidirectional modulation of synaptic functions by Eph/ephrin signaling. Nat Neurosci 12:15–20.

Knierim JJ (2015) The hippocampus. Curr Biol 25:R1116-1121.

Ko J (2012) The leucine-rich repeat superfamily of synaptic adhesion molecules: LRRTMs and Slitrks. Molecules and cells 34:335–340.

Ko J, Fuccillo MV, Malenka RC, Südhof TC (2009) LRRTM2 Functions as a Neurexin Ligand in Promoting Excitatory Synapse Formation. Neuron 64.

Ko J, Kim E (2007) Leucine-rich repeat proteins of synapses. J Neurosci Res 85:2824–2832.

Kokaia M, Ernfors P, Kokaia Z, Elmér E, Jaenisch R, Lindvall O (1995) Suppressed epileptogenesis in BDNF mutant mice. Experimental Neurology 133.

Koyama R, Ikegaya Y (2005) Mossy Fiber Sprouting as a Potential Therapeutic Target for Epilepsy. Current Neurovascular Research 1.

Koyama R, Yamada MK, Fujisawa S, Katoh-Semba R, Matsuki N, Ikegaya Y (2004a) Brain-derived neurotrophic factor induces hyperexcitable reentrant circuits in the dentate gyrus. Journal of Neuroscience 24.

Koyama R, Yamada MK, Nishiyama N, Matsuki N, Ikegaya Y (2004b) Developmental switch in axon guidance modes of hippocampal mossy fibers in vitro. Developmental Biology 267.

Kuja-Panula J, Kiiltomäki M, Yamashiro T, Rouhiainen A, Rauvala H (2003) AMIGO, a transmembrane protein implicated in axon tract development, defines a novel protein family with leucine-rich repeats. Journal of Cell Biology 160:963–973.

Kurshan PT, Shen K (2019) Synaptogenic pathways. Current Opinion in Neurobiology 57:156–162.

Laurberg S, Zimmer J (1981) Lesion-induced sprouting of hippocampal mossy fiber collaterals to the fascia dentata in developing and adult rats. Journal of Comparative Neurology 200.

Lee W, Cheng TW, Gong Q (2008) Olfactory sensory neuron-specific and sexually dimorphic expression of protocadherin 20. Journal of Comparative Neurology 507:1076–1086.

Lehnert S, Hartmann S, Hessler S, Adelsberger H, Huth T, Alzheimer C (2016) Ion channel regulation by β-secretase BACE1 - enzymatic and non-enzymatic effects beyond Alzheimer's disease. Channels (Austin) 10:365–378.

Lewcock JW, Reed RR (2004) A feedback mechanism regulates monoallelic odorant receptor expression. Proceedings of the National Academy of Sciences of the United States of America 101:1069–1074.

Li J, Han W, Pelkey KA, Duan J, Mao X, Wang YX, Craig MT, Dong L, Petralia RS, McBain CJ, Lu W (2017) Molecular Dissection of Neuroligin 2 and Slitrk3 Reveals an Essential Framework for GABAergic Synapse Development. Neuron 96:808-826.e8.

Li Y, Zhang P, Choi TY, Park SK, Park H, Lee EJ, Lee D, Roh JD, Mah W, Kim R, Kim Y, Kwon H, Bae YC, Choi SY, Craig AM, Kim E (2015) Splicing-Dependent Trans-synaptic SALM3-LAR-RPTP Interactions Regulate Excitatory Synapse Development and Locomotion. Cell Reports 12.

Linhoff MW, Laurén J, Cassidy RM, Dobie FA, Takahashi H, Nygaard HB, Airaksinen MS, Strittmatter SM, Craig AM (2009) An Unbiased Expression Screen for Synaptogenic Proteins Identifies the LRRTM Protein Family as Synaptic Organizers. Neuron 61:734–749.

Liu W, Zhang X, Deng Z, Li G, Zhang R, Yang Z, Che F, Liu S, Li H (2020) The role of SLITRK6 in the pathogenesis of Tourette syndrome: From the conclusion of a family-based study in the Chinese Han population. Journal of Gene Medicine:e3173.

Liu XB, Low LK, Jones EG, Cheng HJ (2005) Stereotyped axon pruning via plexin signaling is associated with synaptic complex elimination in the hippocampus. Journal of Neuroscience 25.

Loers G, Chen S, Grumet M, Schachner M (2005) Signal transduction pathways implicated in neural recognition molecule L1 triggered neuroprotection and neuritogenesis. Journal of Neurochemistry 92.

Login H, Butowt R, Bohm S (2015a) Activity-dependent and graded BACE1 expression in the olfactory epithelium is mediated by the retinoic acid metabolizing enzyme CYP26B1. Brain Structure and Function 220:2143–2157.

Login H, Håglin S, Berghard A, Bohm S (2015b) The stimulus-dependent gradient of Cyp26B1+ olfactory sensory neurons is necessary for the functional integrity of the olfactory sensory map. Journal of Neuroscience 35:13807–13818.

Lomvardas S, Barnea G, Pisapia DJ, Mendelsohn M, Kirkland J, Axel R (2006) Interchromosomal Interactions and Olfactory Receptor Choice. Cell 126:403–413.

Loomis C, Stephens A, Janicot R, Baqai U, Drebushenko L, Round J (2020) Identification of MAGUK scaffold proteins as intracellular binding partners of synaptic adhesion protein Slitrk2. Molecular and Cellular Neuroscience 103:103465.

Mackay-Sim A, Breipohl W, Kremer M (1988) Cell dynamics in the olfactory epithelium of the tiger salamander: a morphometric analysis. Experimental Brain Research 71:189–198.

Magklara A, Yen A, Colquitt BM, Clowney EJ, Allen W, Markenscoff-Papadimitriou E, Evans ZA, Kheradpour P, Mountoufaris G, Carey C, Barnea G, Kellis M, Lomvardas S (2011) An epigenetic signature for monoallelic olfactory receptor expression. Cell 145:555–570.

Maguire S, Estabel J, Ingham N, Pearson S, Ryder E, Carragher DM, Walker N, Sanger MGP Slc25a21 Project Team, Bussell J, Chan W-I, Keane TM, Adams DJ, Scudamore CL, Lelliott CJ, Ramírez-Solis R, Karp NA, Steel KP, White JK, Gerdin A-K (2014) Targeting of Slc25a21 is associated with orofacial defects and otitis media due to disrupted expression of a neighbouring gene. PLoS One 9:e91807.

Mah W, Ko J, Nam J, Han K, Chung WS, Kim E (2010) Selected SALM (Synaptic Adhesion-Like Molecule) family proteins regulate synapse formation. Journal of Neuroscience 30.

Malnic B (2013) Single cell RT-PCR identification of odorant receptors expressed by olfactory neurons. Methods Mol Biol 1003:123–132.

Malnic B, Hirono J, Sato T, Buck LB (1999) Combinatorial receptor codes for odors. Cell 96.

Markenscoff-Papadimitriou E, Allen WE, Colquitt BM, Goh T, Murphy KK, Monahan K, Mosley CP, Ahituv N, Lomvardas S (2014) Enhancer interaction networks as a means for singular olfactory receptor expression. Cell 159:543–557.

Martin EA, Muralidhar S, Wang Z, Cervantes DC, Basu R, Taylor MR, Hunter J, Cutforth T, Wilke SA, Ghosh A, Williams ME (2015) The intellectual disability gene Kirrel3 regulates target-specific mossy fiber synapse development in the hippocampus. eLife 4.

Martin EA, Woodruff D, Rawson RL, Williams ME (2017) Examining hippocampal mossy fiber synapses by 3D electron microscopy in wildtype and kirrel3 knockout mice. eNeuro 4.

Matsushima N, Tachi N, Kuroki Y, Enkhbayar P, Osaki M, Kamiya M, Kretsinger RH (2005) Structural analysis of leucine-rich-repeat variants in proteins associated with human diseases. Cell Mol Life Sci 62:2771–2791.

McGinty JF, Henriksen SJ, Goldstein A, Terenius L, Bloom FE (1983) Dynorphin is contained within hippocampal mossy fibers: Immunochemical alterations after kainic acid administration and colchicine-induced neurotoxicity. Proceedings of the National Academy of Sciences of the United States of America 80.

Meier ID, Bernreuther C, Tilling T, Neidhardt J, Wong YW, Schulze C, Streichert T, Schachner M (2010) Short DNA sequences inserted for gene targeting can accidentally interfere with off-target gene expression. The FASEB Journal 24:1714–1724.

Meister M, Bonhoeffer T (2001) Tuning and topography in an odor map on the rat olfactory bulb. Journal of Neuroscience 21.

Melo-Felippe FB, Fontenelle LF, Kohlrausch FB (2019) Gene variations in PBX1, LMX1A and SLITRK1 are associated with obsessive-compulsive disorder and its clinical features. Journal of Clinical Neuroscience 61:180–185.

Meshi D, Drew MR, Saxe M, Ansorge MS, David D, Santarelli L, Malapani C, Moore H, Hen R (2006) Hippocampal neurogenesis is not required for behavioral effects of environmental enrichment. Nature Neuroscience 9.

Miranda DM, Wigg K, Kabia EM, Feng Y, Sandor P, Barr CL (2009) Association of SLITRK1 to Gilles de la Tourette Syndrome. American Journal of Medical Genetics, Part B: Neuropsychiatric Genetics 150:483–486.

Misonou H, Menegola M, Mohapatra DP, Guy LK, Park KS, Trimmer JS (2006) Bidirectional activity-dependent regulation of neuronal ion channel phosphorylation. Journal of Neuroscience 26.

Misonou H, Mohapatra DP, Menegola M, Trimmer JS (2005a) Calcium- and metabolic state-dependent modulation of the voltage-dependent Kv2.1 channel regulates neuronal excitability in response to ischemia. Journal of Neuroscience 25.

Misonou H, Mohapatra DP, Park EW, Leung V, Zhen D, Misonou K, Anderson AE, Trimmer JS (2004) Regulation of ion channel localization and phosphorylation by neuronal activity. Nature Neuroscience 7.

Misonou H, Mohapatra DP, Trimmer JS (2005b) Kv2.1: A voltage-gated K+ channel critical to dynamic control of neuronal excitability. In: NeuroToxicology, pp 743–752.

Miyamichi K, Serizawa S, Kimura HM, Sakano H (2005) Continuous and overlapping expression domains of odorant receptor genes in the olfactory epithelium determine the dorsal/ventral positioning of glomeruli in the olfactory bulb. Journal of Neuroscience 25:3586–3592.

Mizuhashi S, Nishiyama N, Matsuki N, Ikegaya Y (2001) Cyclic nucleotide-mediated regulation of hippocampal mossy fiber development: A target-specific guidance. Journal of Neuroscience 21.

Mohapatra DP, Misonou H, Sheng-Jun P, Held JE, Surmeier DJ, Trimmer JS (2009) Regulation of intrinsic excitability in hippocampal neurons by activity-dependent modulation of the KV2.1 potassium channel. Channels 3:46–56.

Mombaerts P, Wang F, Dulac C, Chao SK, Nemes A, Mendelsohn M, Edmondson J, Axel R (1996) Visualizing an olfactory sensory map. Cell 87:675–686.

Monahan K, Horta A, Lomvardas S (2019) LHX2- and LDB1-mediated trans interactions regulate olfactory receptor choice. Nature 565:448–453.

Montag-Sallaz M, Schachner M, Montag D (2002) Misguided Axonal Projections, Neural Cell Adhesion Molecule 180 mRNA Upregulation, and Altered Behavior in Mice Deficient for the Close Homolog of L1. Molecular and Cellular Biology 22.

Mori K, Nagao H, Yoshihara Y (1999) The olfactory bulb: coding and processing of odor molecule information. Science 286:711–715.

Mori K, Sakano H (2011) How is the olfactory map formed and interpreted in the mammalian brain? Annual Review of Neuroscience 34.

Muller D, Stoppini L, Wang C, Kiss JZ (1994) A role for polysialylated neural cell adhesion molcule in lesion-induced sprouting in hippocampal organotypic cultures. Neuroscience 61.

Müller U (1999) Ten years of gene targeting: targeted mouse mutants, from vector design to phenotype analysis. Mech Dev 82:3–21.

Murai KK, Nguyen LN, Irie F, Yu Y, Pasquale EB (2003) Control of hippocampal dendritic spine morphology through ephrin-A3/EphA4 signaling. Nature Neuroscience 6.

Murakoshi H, Trimmer JS (1999) Identification of the Kv2.1 K+ channel as a major component of the delayed rectifier K+ current in rat hippocampal neurons. Journal of Neuroscience 19.

Muramatsu R, Nakahara S, Ichikawa J, Watanabe K, Matsuki N, Koyama R (2010) The ratio of “deleted in colorectal cancer” to “uncoordinated-5A” netrin-1 receptors on the growth cone regulates mossy fibre directionality. Brain 133.

Nakahara S, Matsumoto M, Ito H, Tajinda K (2018) Ectopic mossy fiber pathfinding in the hippocampus caused the abnormal neuronal transmission in the mouse models of psychiatric disease. Biological and Pharmaceutical Bulletin 41.

Nakahara S, Miyake S, Tajinda K, Ito H (2015) Mossy fiber mis-pathfinding and semaphorin reduction in the hippocampus of α-CaMKII hKO mice. Neuroscience Letters 598.

Nakashima A, Takeuchi H, Imai T, Saito H, Kiyonari H, Abe T, Chen M, Weinstein LS, Yu CR, Storm DR, Nishizumi H, Sakano H (2013) Agonist-independent GPCR activity regulates anterior-posterior targeting of olfactory sensory neurons. Cell 154.

Nguyen LB, Ricciardi TN, Malouf AT (1996) Reinnervation of stratum lucidum by hippocampal mossy fibers is developmentally regulated. Developmental Brain Research 95:184–193.

Niimura Y, Matsui A, Touhara K (2014) Extreme expansion of the olfactory receptor gene repertoire in African elephants and evolutionary dynamics of orthologous gene groups in 13 placental mammals. Genome Research 24:1485–1496.

Niimura Y, Nei M (2005) Evolutionary dynamics of olfactory receptor genes in fishes and tetrapods. Proceedings of the National Academy of Sciences of the United States of America 102:6039–6044.

Niimura Y, Nei M (2007) Extensive gains and losses of olfactory receptor genes in mammalian evolution. PLoS ONE 2.

Okazaki MM, Molnár P, Nadler JV (1999) Recurrent mossy fiber pathway in rat dentate gyrus: synaptic currents evoked in presence and absence of seizure-induced growth. J Neurophysiol 81:1645–1660.

Olson EN, Arnold HH, Rigby PW, Wold BJ (1996) Know your neighbors: three phenotypes in null mutants of the myogenic bHLH gene MRF4. Cell 85:1–4.

O'Roak BJ, Morgan TM, Fishman DO, Saus E, Alonso P, Gratacòs M, Estivill X, Teltsh O, Kohn Y, Kidd KK, Cho J, Lifton RP, State MW (2010) Additional support for the association of SLITRK1 var321 and Tourette syndrome. Molecular psychiatry 15:447–450.

O'Rourke JA, Scharf JM, Yu D, Pauls DL (2009) The genetics of Tourette syndrome: a review. J Psychosom Res 67:533–545.

Ou-Yang MH, Kurz JE, Nomura T, Popovic J, Rajapaksha TW, Dong H, Contractor A, Chetkovich DM, Tourtellotte WG, Vassar R (2018) Axonal organization defects in the hippocampus of adult conditional BACE1 knockout mice. Science Translational Medicine 10.

Ozomaro U, Cai G, Kajiwara Y, Yoon S, Makarov V, Delorme R, Betancur C, Ruhrmann S, Falkai P, Grabe HJ, Maier W, Wagner M, Lennertz L, Moessner R, Murphy DL, Buxbaum JD, Züchner S, Grice DE (2013) Characterization of SLITRK1 Variation in Obsessive-Compulsive Disorder. PLoS ONE 8.

Öztokatli H, Hörnberg M, Berghard A, Bohm S (2012) Retinoic acid receptor and CNGA2 channel signaling are part of a regulatory feedback loop controlling axonal convergence and survival of olfactory sensory neurons. The FASEB Journal 26:617–627.

Pak CH, Danko T, Zhang Y, Aoto J, Anderson G, Maxeiner S, Yi F, Wernig M, Südhof TC (2015) Human Neuropsychiatric Disease Modeling using Conditional Deletion Reveals Synaptic Transmission Defects Caused by Heterozygous Mutations in NRXN1. Cell Stem Cell 17.

Palacio S, Chevaleyre V, Brann DH, Murray KD, Piskorowski RA, Trimmer JS (2017) Heterogeneity in Kv2 Channel Expression Shapes Action Potential Characteristics and Firing Patterns in CA1 versus CA2 Hippocampal Pyramidal Neurons. eNeuro 4.

Pan Y, Zhang L, Liu Q, Li Y, Guo H, Peng Y, Peng H, Tang B, Hu Z, Zhao J, Xia K, Li JD (2016) Insertion of a knockout-first cassette in Ampd1 gene leads to neonatal death by disruption of neighboring genes expression. Scientific Reports 6.

Paschaki M, Cammas L, Muta Y, Matsuoka Y, Mak SS, Rataj-Baniowska M, Fraulob V, Dollé P, Ladher RK (2013) Retinoic acid regulates olfactory progenitor cell fate and differentiation. Neural Development 8.

Pasquini M, Fabbrini G, Berardelli I, Bonifati V, Biondi M, Berardelli A (2008) Psychopathological features of obsessive-compulsive disorder in an Italian family with

Gilles de la Tourette syndrome not linked to the SLITRK1 gene. Psychiatry research 161:109–111.

Pasterkamp RJ, Winter FD, Holtmaat AJGD, Verhaagen J (1998) Evidence for a role of the chemorepellent semaphorin III and its receptor neuropilin-1 in the regeneration of primary olfactory axons. Journal of Neuroscience 18.

Peltola MA, Kuja-Panula J, Lauri SE, Taira T, Rauvala H (2011) AMIGO is an auxiliary subunit of the Kv2.1 potassium channel. EMBO Reports 12:1293–1299.

Peltola MA, Kuja-Panula J, Liuhanen J, Võikar V, Piepponen P, Hiekkalinna T, Taira T, Lauri SE, Suvisaari J, Kulesskaya N, Paunio T, Rauvala H (2016) AMIGO-Kv2.1 Potassium Channel Complex Is Associated With Schizophrenia-Related Phenotypes. Schizophrenia bulletin 42:191–201.

Peluso CE, Jang W, Dräger UC, Schwob JE (2012) Differential expression of components of the retinoic acid signaling pathway in the adult mouse olfactory epithelium. Journal of Comparative Neurology 520:3707–3726.

Petrovic M, Schmucker D (2015) Axonal wiring in neural development: Target-independent mechanisms help to establish precision and complexity. Bioessays 37:996–1004.

Pham CTN, Macivor DM, Hug BA, Heusel JW, Ley TJ (1996) Long-range disruption of gene expression by a selectable marker cassette. Proceedings of the National Academy of Sciences of the United States of America 93:13090–13095.

Pimenta AF, Zhukareva V, Barbe MF, Reinoso BS, Grimley C, Henzel W, Fischer I, Levitt P (1995) The limbic system-associated membrane protein is an Ig superfamily member that mediates selective neuronal growth and axon targeting. Neuron 15:287–297.

Piton A et al. (2011) Systematic resequencing of X-chromosome synaptic genes in autism spectrum disorder and schizophrenia. Molecular Psychiatry 16:867–880.

Pleskacheva MG, Wolfer DP, Kupriyanova IF, Nikolenko DL, Scheffrahn H, Dell'Omo G, Lipp HP (2000) Hippocampal mossy fibers and swimming navigation learning in two vole species occupying different habitats. Hippocampus 10.

Price DJ, Kennedy H, Dehay C, Zhou L, Mercier M, Jossin Y, Goffinet AM, Tissir F, Blakey D, Molnár Z (2006) The development of cortical connections. Eur J Neurosci 23:910–920.

Proenca CC, Gao KP, Shmelkov SV, Rafii S, Lee FS (2011) Slitrks as emerging candidate genes involved in neuropsychiatric disorders. Trends Neurosci 34:143–153.

Pulido R, Serra-Pagè C, Tang M, Streuli M (1995) The LAR/PTPδ/PTPσ subfamily of transmembrane protein-tyrosine-phosphatases: Multiple human LAR, PTPδ, and PTPσ isoforms are expressed in a tissue-specific manner and associate with the LAR-interacting protein LIP.1. Proceedings of the National Academy of Sciences of the United States of America 92.

Qiao X, Suri C, Knusel B, Noebels JL (2001) Absence of hippocampal mossy fiber sprouting in transgenic mice overexpressing brain-derived neurotrophic factor. Journal of Neuroscience Research 64.

Qiao X, Werkman TR, Gorter JA, Wadman WJ, Vliet EAV (2013) Expression of sodium channel α subunits 1.1, 1.2 and 1.6 in rat hippocampus after kainic acid-induced epilepsy. Epilepsy Research 106.

Rajapaksha TW, Eimer WA, Bozza TC, Vassar R (2011) The Alzheimer's -secretase enzyme BACE1 is required for accurate axon guidance of olfactory sensory neurons and normal glomerulus formation in the olfactory bulb. Molecular Neurodegeneration 6.

Ramirez-Amaya V, Marrone DF, Gage FH, Worley PF, Barnes CA (2006) Integration of new neurons into functional neural networks. Journal of Neuroscience 26.

Reed RR (1992) Signaling pathways in odorant detection. Neuron 8:205–209.

Ressler KJ, Sullivan SL, Buck LB (1994a) Information coding in the olfactory system: Evidence for a stereotyped and highly organized epitope map in the olfactory bulb. Cell 79:1245–1255.

Ressler KJ, Sullivan SL, Buck LB (1994b) A molecular dissection of spatial patterning in the olfactory system. Current Opinion in Neurobiology 4.

Reznikov KY (1991) Cell proliferation and cytogenesis in the mouse hippocampus. Advances in anatomy, embryology, and cell biology 122.

Rijli FM, Dollé P, Fraulob V, LeMeur M, Chambon P (1994) Insertion of a targeting construct in a Hoxd-10 allele can influence the control of Hoxd-9 expression. Developmental Dynamics 201:366–377.

Robbins EM, Krupp AJ, Arce KP de, Ghosh AK, Fogel AI, Boucard A, Südhof TC, Stein V, Biederer T (2010) SynCAM 1 Adhesion Dynamically Regulates Synapse Number and Impacts Plasticity and Learning. Neuron 68.

Römer B, Krebs J, Overall RW, Fabel K, Babu H, Overstreet-Wadiche L, Brandt MD, Williams RW, Jessberger S, Kempermann G (2011) Adult hippocampal neurogenesis and plasticity in the infrapyramidal bundle of the mossy fiber projection: I. Co-regulation by activity. Frontiers in Neuroscience.

Roppongi RT, Dhume SH, Padmanabhan N, Silwal P, Zahra N, Karimi B, Bomkamp C, Patil CS, Champagne-Jorgensen K, Twilley RE, Zhang P, Jackson MF, Siddiqui TJ (2020) LRRTMs Organize Synapses through Differential Engagement of Neurexin and PTPσ. Neuron 106:108-125.e12.

Sachse CC, Kim YH, Agsten M, Huth T, Alzheimer C, Kovacs DM, Kim DY (2013) BACE1 and presenilin/γ-secretase regulate proteolytic processing of KCNE1 and 2, auxiliary subunits of voltage-gated potassium channels. FASEB Journal 27.

Salesse C, Charest J, Doucet-Beaupré H, Castonguay A-M, Labrecque S, Koninck PD, Lévesque M (2020) Opposite Control of Excitatory and Inhibitory Synapse Formation by Slitrk2 and Slitrk5 on Dopamine Neurons Modulates Hyperactivity Behavior. Cell reports 30:2374-2386.e5.

Sandi C, Davies HA, Cordero MI, Rodriguez JJ, Popov VI, Stewart MG (2003) Rapid reversal of stress induced loss of synapses in CA3 of rat hippocampus following water maze training. European Journal of Neuroscience 17.

Scharfman HE, Goodman JH, Sollas AL, Croll SD (2002) Spontaneous limbic seizures after intrahippocampal infusion of brain-derived neurotrophic factor. Experimental Neurology 174.

Scheibel ME, Crandall PH, Scheibel AB (1974) The Hippocampal-Dentate Complex in Temporal Lobe Epilepsy: A Golgi Study. Epilepsia 15.

Scheiffele P, Fan J, Choih J, Fetter R, Serafini T (2000) Neuroligin expressed in nonneuronal cells triggers presynaptic development in contacting axons. Cell 101:657–669.

Schroeder A, Vanderlinden J, Vints K, Ribeiro LF, Vennekens KM, Gounko NV, Wierda KD, Wit J de (2018) A Modular Organization of LRR Protein-Mediated Synaptic Adhesion Defines Synapse Identity. Neuron 99.

Schultz C, Engelhardt M (2014) Anatomy of the hippocampal formation. Front Neurol Neurosci 34:6–17.

Schwarting GA, Henion TR (2011) Regulation and function of axon guidance and adhesion molecules during olfactory map formation. Journal of Cellular Biochemistry 112.

Schwegler H, Lipp HP, Loos HVD, Buselmaier W (1981) Individual hippocampal mossy fiber distribution in mice correlates with two-way avoidance performance. Science 214.

Seki T, Arai Y (1999) Different polysialic acid-neural cell adhesion molecule expression patterns in distinct types of mossy fiber boutons in the adult hippocampus. Journal of Comparative Neurology 410.

Seki T, Rutishauser U (1998) Removal of polysialic acid-neural cell adhesion molecule induces aberrant mossy fiber innervation and ectopic synaptogenesis in the hippocampus. Journal of Neuroscience 18.

Serizawa S, Ishii T, Nakatani H, Tsuboi A, Nagawa F, Asano M, Sudo K, Sakagami J, Sakano H, Ijiri T, Matsuda Y, Suzuki M, Yamamori T, Iwakura Y, Sakano H (2000) Mutually exclusive expression of odorant receptor transgenes. Nature Neuroscience 3.

Serizawa S, Miyamichi K, Nakatani H, Suzuki M, Saito M, Yoshihara Y, Sakano H (2003) Negative Feedback Regulation Ensures the One Receptor-One Olfactory Neuron Rule in Mouse. Science 302:2088–2094.

Serizawa S, Miyamichi K, Sakano H (2004) One neuron-one receptor rule in the mouse olfactory system. Trends in genetics : TIG 20:648–653.

Serizawa S, Miyamichi K, Takeuchi H, Yamagishi Y, Suzuki M, Sakano H (2006) A Neuronal Identity Code for the Odorant Receptor-Specific and Activity-Dependent Axon Sorting. Cell 127:1057–1069.

Shibata K, Nakahara S, Shimizu E, Yamashita T, Matsuki N, Koyama R (2013) Repulsive guidance molecule a regulates hippocampal mossy fiber branching in vitro. NeuroReport 24.

Shipman SL, Nicoll RA (2012) Dimerization of postsynaptic neuroligin drives synaptic assembly via transsynaptic clustering of neurexin. Proceedings of the National Academy of Sciences of the United States of America 109.

Shmelkov SV, Hormigo A, Jing D, Proenca CC, Bath KG, Milde T, Shmelkov E, Kushner JS, Baljevic M, Dincheva I, Murphy AJ, Valenzuela DM, Gale NW, Yancopoulos GD, Ninan I, Lee FS, Rafii S (2010) Slitrk5 deficiency impairs corticostriatal circuitry and leads to obsessive-compulsive-like behaviors in mice. Nature medicine 16:598–602.

Shykind BM, Rohani SC, O'Donnell S, Nemes A, Mendelsohn M, Sun Y, Axel R, Barnea G (2004) Gene switching and the stability of odorant receptor gene choice. Cell 117:801–815.

Siddiqui TJ, Tari PK, Connor SA, Zhang P, Dobie FA, She K, Kawabe H, Wang YT, Brose N, Craig AM (2013) An LRRTM4-HSPG complex mediates excitatory synapse development on dentate gyrus granule cells. Neuron 79.

Skutella T (1999) Semaphorin D acts as a repulsive factor for entorhinal and hippocampal neurons. European Journal of Neuroscience 11.

Skutella T, Nitsch R (2001) New molecules for hippocampal development. Trends Neurosci 24:107–113.

Sloviter RS (1982) A simplified Timm stain procedure compatible with formaldehyde fixation and routine paraffin embedding of rat brain. Brain Res Bull 8:771–774.

Smith EN et al. (2009) Genome-wide association study of bipolar disorder in European American and African American individuals. Molecular Psychiatry 14.

Song H, Poo M (2001) The cell biology of neuronal navigation. Nat Cell Biol 3:E81-88.

Song M, Giza J, Proenca CC, Jing D, Elliott M, Dincheva I, Shmelkov SV, Kim J, Schreiner R, Huang SH, Castrén E, Prekeris R, Hempstead BL, Chao MV, Dictenberg JB, Rafii S, Chen ZY, Rodriguez-Boulan E, Lee FS (2015a) Slitrk5 Mediates BDNF-Dependent TrkB Receptor Trafficking and Signaling. Developmental Cell 33:690–702.

Song M, Mathews CA, Stewart SE, Shmelkov SV, Mezey JG, Rodriguez-Flores JL, Rasmussen SA, Britton JC, Oh YS, Walkup JT, Lee FS, Glatt CE (2017) Rare synaptogenesis-impairing mutations in SLITRK5 are associated with obsessive compulsive disorder. PLoS ONE 12.

Song M, Tian F, Xia H, Xie Y (2019) Repulsive guidance molecule a suppresses seizures and mossy fiber sprouting via the FAK-p120RasGAP-Ras signaling pathway. Molecular Medicine Reports 19.

Song MY, Tian FF, Wang YZ, Huang X, Guo JL, Ding DX (2015b) Potential roles of the RGMa-FAK-Ras pathway in hippocampal mossy fiber sprouting in the pentylenetetrazole kindling model. Molecular Medicine Reports 11.

Spangler SA, Schmitz SK, Kevenaar JT, Graaff ED, Wit HD, Demmers J, Toonen RF, Hoogenraad CC (2013) Liprin-α2 promotes the presynaptic recruitment and turnover of RIM1/CASK to facilitate synaptic transmission. Journal of Cell Biology 201.

Speca DJ, Ogata G, Mandikian D, Bishop HI, Wiler SW, Eum K, Wenzel HJ, Doisy ET, Matt L, Campi KL, Golub MS, Nerbonne JM, Hell JW, Trainor BC, Sack JT, Schwartzkroin PA, Trimmer JS (2014) Deletion of the Kv2.1 delayed rectifier potassium channel leads to neuronal and behavioral hyperexcitability. Genes, Brain and Behavior 13:394–408.

Speed WC, O'Roak BJ, Tárnok Z, Barta C, Pakstis AJ, State MW, Kidd KK (2008) Haplotype evolution of SLITRK1, a candidate gene for Gilles de la Tourette syndrome. American journal of medical genetics Part B, Neuropsychiatric genetics : the official publication of the International Society of Psychiatric Genetics 147B:463–466.

St John JA, Clarris HJ, McKeown S, Royal S, Key B (2003) Sorting and convergence of primary olfactory axons are independent of the olfactory bulb. J Comp Neurol 464:131–140.

Stanfield BB, Cowan WM (1979) The development of the hippocampus and dentate gyrus in normal and reeler mice. Journal of Comparative Neurology 185.

Steup A, Lohrum M, Hamscho N, Savaskan NE, Ninnemann O, Nitsch R, Fujisawa H, Püschel AW, Skutella T (2000) Sema3C and Netrin-1 differentially affect axon growth in the hippocampal formation. Molecular and Cellular Neurosciences 15.

Stillman AA, Krsnik Ž, Sun J, Rašin MR, State MW, Şestan N, Louvi A (2009) Developmentally regulated and evolutionarily conserved expression of SLITRK1 in brain circuits implicated in Tourette syndrome. Journal of Comparative Neurology 513:21–37.

Stoeckli ET (2018) Understanding axon guidance: are we nearly there yet? Development 145.

Südhof TC (2017) Synaptic Neurexin Complexes: A Molecular Code for the Logic of Neural Circuits. Cell 171:745–769.

Sullivan SL, Adamson MC, Ressler KJ, Kozak CA, Buck LB (1996) The chromosomal distribution of mouse odorant receptor genes. Proceedings of the National Academy of Sciences of the United States of America 93:884–888.

Surmeier DJ, Foehring R (2004) A mechanism for homeostatic plasticity. Nat Neurosci 7:691–692.

Suto F, Tsuboi M, Kamiya H, Mizuno H, Kiyama Y, Komai S, Shimizu M, Sanbo M, Yagi T, Hiromi Y, Chédotal A, Mitchell KJ, Manabe T, Fujisawa H (2007) Interactions between Plexin-A2, Plexin-A4, and Semaphorin 6A Control Lamina-Restricted Projection of Hippocampal Mossy Fibers. Neuron 53.

Sutula T, Xiao-Xian H, Cavazos J, Scott G (1988) Synaptic reorganization in the hippocampus induced by abnormal functional activity. Science 239.

Takahashi H, Katayama K-I, Sohya K, Miyamoto H, Prasad T, Matsumoto Y, Ota M, Yasuda H, Tsumoto T, Aruga J, Craig AM (2012) Selective control of inhibitory synapse development by Slitrk3-PTPd trans-synaptic interaction. 15.

Takeuchi H, Inokuchi K, Aoki M, Suto F, Tsuboi A, Matsuda I, Suzuki M, Aiba A, Serizawa S, Yoshihara Y, Fujisawa H, Sakano H (2010) Sequential arrival and graded secretion of Sema3F by olfactory neuron axons specify map topography at the bulb. Cell 141.

Tamminga CA, Stan AD, Wagner AD (2010) The hippocampal formation in schizophrenia. Am J Psychiatry 167:1178–1193.

Tawarayama H, Yamada H, Shinmyo Y, Tanaka H, Ikawa S (2018) The chemorepellent draxin is involved in hippocampal mossy fiber projection. Biochemical and Biophysical Research Communications 500:217–223.

Tawarayama H, Yoshida Y, Suto F, Mitchell KJ, Fujisawa H (2010) Roles of semaphorin-6B and plexin-A2 in lamina-restricted projection of hippocampal mossy fibers. Journal of Neuroscience 30.

Taylor MR, Martin EA, Sinnen B, Trilokekar R, Ranza E, Antonarakis SE, Williams ME (2020) Kirrel3-Mediated Synapse Formation Is Attenuated by Disease-Associated Missense Variants. Journal of Neuroscience 40.

Tekin M et al. (2013) SLITRK6 mutations cause myopia and deafness in humans and mice. Journal of Clinical Investigation 123.

Torborg CL, Nakashiba T, Tonegawa S, McBain CJ (2010) Control of CA3 output by feedforward inhibition despite developmental changes in the excitation-inhibition balance. Journal of Neuroscience 30.

Toro R, Konyukh M, Delorme R, Leblond C, Chaste P, Fauchereau F, Coleman M, Leboyer M, Gillberg C, Bourgeron T (2010) Key role for gene dosage and synaptic homeostasis in autism spectrum disorders. Trends Genet 26:363–372.

Trouche S, Bontempi B, Roullet P, Rampon C (2009) Recruitment of adult-generated neurons into functional hippocampal networks contributes to updating and strengthening of spatial memory. Proceedings of the National Academy of Sciences of the United States of America 106.

Tsuboi A, Miyazaki T, Imai T, Sakano H (2006) Olfactory sensory neurons expressing class I odorant receptors converge their axons on an antero-dorsal domain of the olfactory bulb in the mouse. European Journal of Neuroscience 23:1436–1444.

Tuerdi A, Kikuta S, Kinoshita M, Kamogashira T, Kondo K, Iwasaki S, Yamasoba T (2018) Dorsal-zone-specific reduction of sensory neuron density in the olfactory epithelium following long-term exercise or caloric restriction. Scientific Reports 8.

Um JW, Kim KH, Park BS, Choi Y, Kim D, Kim CY, Kim SJ, Kim M, Ko JS, Lee SG, Choii G, Nam J, Heo WD, Kim E, Lee JO, Ko J, Kim HM (2014) Structural basis for LAR-RPTP/Slitrk complex-mediated synaptic adhesion. Nature Communications 5:5423.

Um JW, Ko J (2013) LAR-RPTPs: synaptic adhesion molecules that shape synapse development. Trends Cell Biol 23:465–475.

Vaddadi N, Iversen K, Raja R, Phen A, Brignall A, Dumontier E, Cloutier JF (2019) Kirrel2 is differentially required in populations of olfactory sensory neurons for the targeting of axons in the olfactory bulb. Development (Cambridge, England) 146.

Vago DR, Wallenstein GV (2014) Hippocampus. Encyclopedia of Neurological Sciences.

Vaidya VA, Siuciak JA, Du F, Duman RS (1999) Hippocampal mossy fiber sprouting induced by chronic electroconvulsive seizures. Neuroscience 89.

Vaishnav RA, Getchell ML, Poon HF, Barnett KR, Hunter SA, Pierce WM, Klein JB, Butterfield DA, Getchell TV (2007) Oxidative stress in the aging murine olfactory bulb: Redox proteomics and cellular localization. Journal of Neuroscience Research 85:373–385.

van Praag H, Kempermann G, Gage FH (1999) Running increases cell proliferation and neurogenesis in the adult mouse dentate gyrus. Nat Neurosci 2:266–270.

Vassar R, Chao SK, Sitcheran R, Nuñez JM, Vosshall LB, Axel R (1994) Topographic organization of sensory projections to the olfactory bulb. Cell 79:981–991.

Vedin V, Molander M, Bohm S, Berghard A (2009) Regional differences in olfactory epithelial homeostasis in the adult mouse. Journal of Comparative Neurology 513:375–384.

Völker LA, Maar BA, Guevara BAP, Bilkei-Gorzo A, Zimmer A, Brönneke H, Dafinger C, Bertsch S, Wagener JR, Schweizer H, Schermer B, Benzing T, Hoehne M (2018) Neph2/Kirrel3 regulates sensory input, motor coordination, and home-cage activity in rodents. Genes, Brain and Behavior 17.

Walz A, Mombaerts P, Greer CA, Treloar HB (2006) Disrupted compartmental organization of axons and dendrites within olfactory glomeruli of mice deficient in the olfactory cell adhesion molecule, OCAM. Molecular and Cellular Neuroscience 32.

Wang K et al. (2009) Common genetic variants on 5p14.1 associate with autism spectrum disorders. Nature 459.

Wang PY, Seabold GK, Wenthold RJ (2008) Synaptic adhesion-like molecules (SALMs) promote neurite outgrowth. Molecular and Cellular Neuroscience 39.

Weber M, Wu T, Meilandt WJ, Dominguez SL, Solanoy HO, Maloney JA, Ngu H, Baca M, Kung C, Lima L, Earr TK, Fleck D, Shields SD, Forrest WF, Foreman O, Warming S, Watts RJ, Scearce-Levie K (2017) BACE1 across species: A comparison of the in vivo consequences of BACE1 deletion in mice and rats. Scientific Reports 7.

West DB, Engelhard EK, Adkisson M, Nava AJ, Kirov JV, Cipollone A, Willis B, Rapp J, de Jong PJ, Lloyd KC (2016) Transcriptome Analysis of Targeted Mouse Mutations Reveals the Topography of Local Changes in Gene Expression. PLoS Genet 12:e1005691.

West JR, Hoesen GWV, Kosel KC (1982) A Demonstration of hippocampal mossy fiber axon morphology using the anterograde transport of horseradish peroxidase. Experimental Brain Research 48.

Willem M, Garratt AN, Novak B, Citron M, Kaufmann S, Rittger A, DeStrooper B, Saftig P, Birchmeier C, Haass C (2006) Control of peripheral nerve myelination by the β-secretase BACE1. Science 314.

Williams ME, Wilke SA, Daggett A, Davis E, Otto S, Ravi D, Ripley B, Bushong EA, Ellisman MH, Klein G, Ghosh A (2011) Cadherin-9 regulates synapse-specific differentiation in the developing hippocampus. Neuron 71.

Winther M, Walmod PS (2014) Neural Cell Adhesion Molecules Belonging to the Family of Leucine-Rich Repeat Proteins. In: Cell Adhesion Molecules: Implications in Neurological Diseases (Berezin V, Walmod PS, eds), pp 315–395 Advances in Neurobiology. New York, NY: Springer.

Wolman MA, Regnery AM, Becker T, Becker CG, Halloran MC (2007) Semaphorin3D regulates axon-axon interactions by modulating levels of L1 cell adhesion molecule. Journal of Neuroscience 27.

Won SY, Kim CY, Kim D, Ko J, Um JW, Lee SB, Buck M, Kim E, Heo WD, Lee J-O, Kim HM (2017) LAR-RPTP Clustering Is Modulated by Competitive Binding between Synaptic Adhesion Partners and Heparan Sulfate. Front Mol Neurosci 10:327.

Won SY, Kim HM (2018) Structural Basis for LAR-RPTP-Mediated Synaptogenesis. Mol Cells 41:622–630.

Won SY, Lee P, Kim HM (2019) Synaptic organizer: Slitrks and type IIa receptor protein tyrosine phosphatases. Curr Opin Struct Biol 54:95–103.

Wright GJ, Washbourne P (2011) Neurexins, neuroligins and LRRTMs: synaptic adhesion getting fishy. J Neurochem 117:765–778.

Yamagata A, Fukai S (2019) Structural insights into leucine-rich repeat-containing synaptic cleft molecules. Current Opinion in Structural Biology 54:68–77.

Yamagata A, Sato Y, Goto-Ito S, Uemura T, Maeda A, Shiroshima T, Yoshida T, Fukai S (2015) Structure of Slitrk2-PTP complex reveals mechanisms for splicing-dependent trans-synaptic adhesion. Scientific Reports 5:1–6.

Yamagishi S, Hampel F, Hata K, Toro DD, Schwark M, Kvachnina E, Bastmeyer M, Yamashita T, Tarabykin V, Klein R, Egea J (2011) FLRT2 and FLRT3 act as repulsive guidance cues for Unc5-positive neurons. EMBO Journal 30.

Yamasaki N et al. (2008) Alpha-CaMKII deficiency causes immature dentate gyrus, a novel candidate endophenotype of psychiatric disorders. Molecular brain 1:6.

Yim YS, Kwon Y, Nam J, Yoon HI, Lee K, Kim DG, Kim E, Kim CH, Ko J (2013) Slitrks control excitatory and inhibitory synapse formation with LAR receptor protein tyrosine phosphatases. Proceedings of the National Academy of Sciences of the United States of America 110:4057–4062.

Young JM, Luche RM, Trask BJ (2011) Rigorous and thorough bioinformatic analyses of olfactory receptor promoters confirm enrichment of O/E and homeodomain binding sites but reveal no new common motifs. BMC Genomics 12.

Yu CR, Power J, Barnea G, O'Donnell S, Brown HEV, Osborne J, Axel R, Gogos JA (2004) Spontaneous neural activity is required for the establishment and maintenance of the olfactory sensory map. Neuron 42:553–566.

Zacco A, Cooper V, Chantler PD, Fisher-Hyland S, Horton HL, Levitt P (1990) Isolation, biochemical characterization and ultrastructural analysis of the limbic system-associated membrane protein (LAMP), a protein expressed by neurons comprising functional neural circuits. Journal of Neuroscience 10.

Zapiec B, Mombaerts P (2020) The Zonal Organization of Odorant Receptor Gene Choice in the Main Olfactory Epithelium of the Mouse. Cell Reports 30:4220-4234.e5.

Zhang K, Feng Y, Wigg KG, Sandor P, Barr CL (2015) Association study of the SLITRK5 gene and Tourette syndrome. Psychiatric Genetics 25:31–34.

Zhang S, Su Y, Shinmyo Y, Islam SM, Naser IB, Ahmed G, Tamamaki N, Tanaka H (2010) Draxin, a repulsive axon guidance protein, is involved in hippocampal development. Neuroscience Research 66.

Zhang X, Firestein S (2002) The olfactory receptor gene superfamily of the mouse. Nature Neuroscience 5:124–133.

Zhang X, Rogers M, Tian H, Zhang X, Zou DJ, Liu J, Ma M, Shepherd GM, Firestein SJ (2004) High-throughput microarray detection of olfactory receptor gene expression in the mouse. Proceedings of the National Academy of Sciences of the United States of America 101:14168–14173.

Zhao X, Kuja-Panula J, Sundvik M, Chen YC, Aho V, Peltola MA, Porkka-Heiskanen T, Panula P, Rauvala H (2014) Amigo adhesion protein regulates development of neural circuits in zebrafish brain. Journal of Biological Chemistry 289:19958–19975.

Zhiling Y, Fujita E, Tanabe Y, Yamagata T, Momoi T, Momoi MY (2008) Mutations in the gene encoding CADM1 are associated with autism spectrum disorder. Biochemical and Biophysical Research Communications 377.

Zhou L, Barão S, Laga M, Bockstael K, Borgers M, Gijsen H, Annaert W, Moechars D, Mercken M, Gevaer K, Strooper BD (2012) The neural cell adhesion molecules L1 and CHL1 are cleaved by BACE1 protease in vivo. Journal of Biological Chemistry 287.

Zimprich A, Hatala K, Riederer F, Stogmann E, Aschauer HN, Stamenkovic M (2008) Sequence analysis of the complete SLITRK1 gene in Austrian patients with Tourette's disorder. Psychiatric Genetics 18:308–309.

Zou DJ, Feinstein P, Rivers AL, Mathews GA, Kim A, Greer CA, Mombaerts P, Firestein S (2004) Postnatal refinement of peripheral olfactory projections. Science 304:1976–1979.

Züchner S, Cuccaro ML, Tran-Viet KN, Cope H, Krishnan RR, Pericak-Vance MA, Wright HH, Ashley-Koch A (2006) SLITRK1 mutations in trichotillomania. Molecular Psychiatry 11:887.